ISSN 2686-7575 (Online)

ТОНКИЕ ХИМИЧЕСКИЕ ТЕХНОЛОГИИ

Fine Chemical Technologies

- Theoretical Basis of Chemical Technology
- Chemistry and Technology of Organic Substances
- Chemistry and Technology of Medicinal Compounds and Biologically Active Substances
- Biochemistry and Biotechnology
- Synthesis and Processing of Polymers and Polymeric Composites
- Chemistry and Technology of Inorganic Materials
- Analytical Methods in Chemistry and Chemical Technology
- Mathematical Methods and Information Systems in Chemical Technology

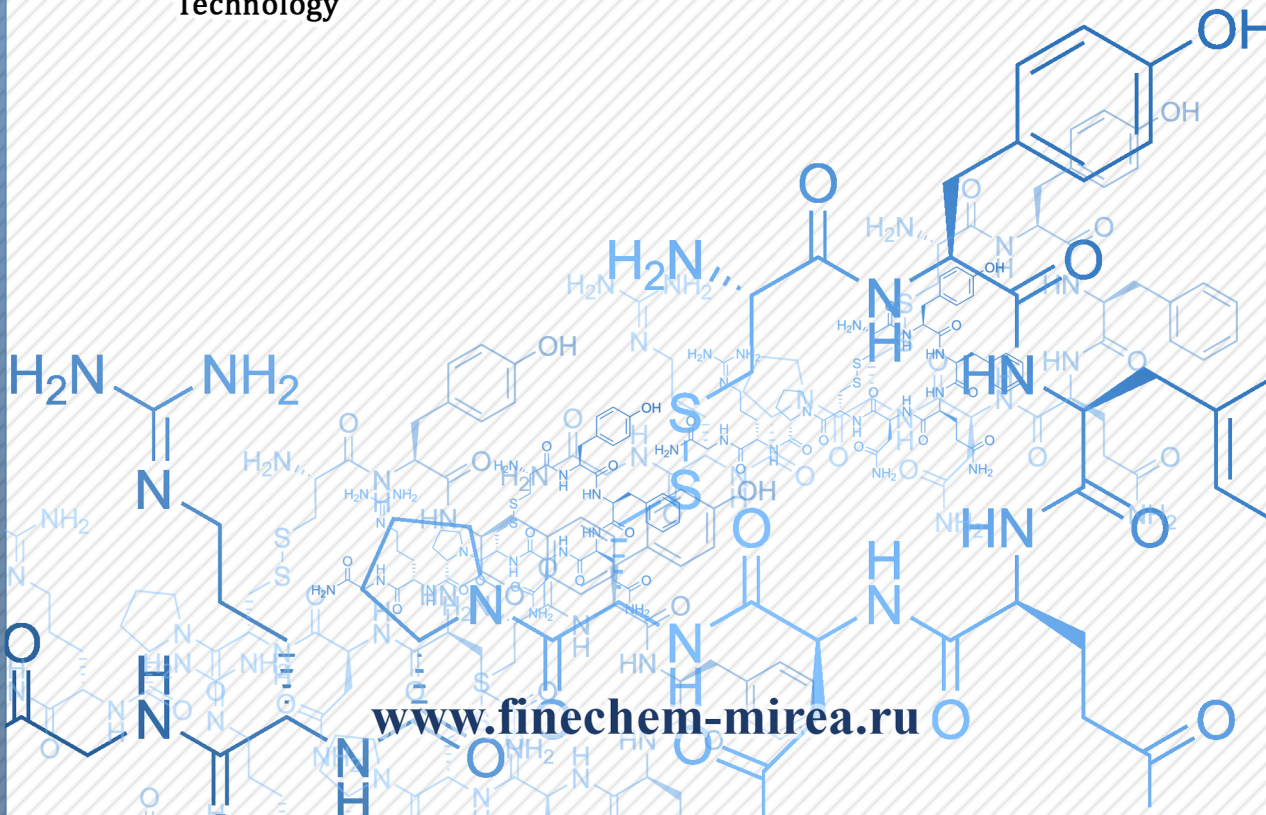

20(5)
2025

www.finechem-mirea.ru

ISSN 2686-7575 (Online)

ТОНКИЕ ХИМИЧЕСКИЕ ТЕХНОЛОГИИ

Fine Chemical Technologies

- Theoretical Basis of Chemical Technology
- Chemistry and Technology of Organic Substances
- Chemistry and Technology of Medicinal Compounds and Biologically Active Substances
- Biochemistry and Biotechnology
- Synthesis and Processing of Polymers and Polymeric Composites
- Chemistry and Technology of Inorganic Materials
- Analytical Methods in Chemistry and Chemical Technology
- Mathematical Methods and Information Systems in Chemical Technology

Tonkie Khimicheskie Tekhnologii = Fine Chemical Technologies.
Vol. 20, No. 5, 2025

Тонкие химические технологии = Fine Chemical Technologies.
Том 20, № 5, 2025

https://doi.org/10.32362/2410-6593-2025-20-5
www.finechem-mirea.ru

https://doi.org/10.32362/2410-6593-2025-20-5
www.finechem-mirea.ru ISSN 2686-7575 (Online)

**Tonkie Khimicheskie Tekhnologii =
Fine Chemical Technologies
2025, Vol. 20, No. 5**

The peer-reviewed scientific and technical journal Fine Chemical Technologies highlights the modern achievements of fundamental and applied research in the field of fine chemical technologies, including the theoretical basis of chemical technology, chemistry and technology of medicinal compounds and biologically active substances, organic substances and inorganic materials, biochemistry and biotechnology, synthesis and processing of polymers and polymeric composites, analytical and mathematical methods and information systems in chemistry and chemical technology.

Founder and Publisher

Federal State Budget
Educational Institution of Higher Education
"MIREA – Russian Technological University"
78, Vernadskogo pr., Moscow, 119454, Russian Federation.
Publication frequency: bimonthly.
The journal was founded in 2006. The name was Vestnik MITHT until 2015 (ISSN 1819-1487).

The journal is included into the List of peer-reviewed science press of the State Commission for Academic Degrees and Titles of the Russian Federation; the Unified State List of Scientific Publications – White List (K1).

The journal is indexed: SCOPUS, DOAJ, Chemical Abstracts, Science Index, RSCI, Ulrich's International Periodicals Directory

86, Vernadskogo pr., Moscow, 119571, Russian Federation.
Phone: +7 (499) 600-80-80 (#31288)
E-mail: *seredina@mirea.ru*

The registration number ПИ № ФС 77-74580 was issued in December 14, 2018 by the Federal Service for Supervision of Communications, Information Technology, and Mass Media of Russia

The subscription index of *Pressa Rossii*: **36924**

Publication date 31.10.2025

**Тонкие химические технологии =
Fine Chemical Technologies
2025, том 20, № 5**

Научно-технический рецензируемый журнал «Тонкие химические технологии» освещает современные достижения фундаментальных и прикладных исследований в области тонких химических технологий, включая теоретические основы химической технологии, химию и технологию лекарственных препаратов и биологически активных соединений, органических веществ и неорганических материалов, биохимию и биотехнологию, синтез и переработку полимеров и композитов на их основе, аналитические и математические методы и информационные системы в химии и химической технологии.

Учредитель и издатель

федеральное государственное бюджетное
образовательное учреждение высшего образования
«МИРЭА – Российский технологический университет»
119454, РФ, Москва, пр-т Вернадского, д. 78.
Периодичность: один раз в два месяца.
Журнал основан в 2006 году. До 2015 года издавался под названием «Вестник МИТХТ» (ISSN 1819-1487).

Журнал входит в Перечень ведущих рецензируемых научных журналов ВАК РФ, в Единый государственный перечень научных изданий – Белый список (К1).

Индексируется: SCOPUS, DOAJ, Chemical Abstracts, РИНЦ (Science Index), RSCI, Ulrich's International Periodicals Directory

РФ, 119571, Москва, пр. Вернадского, 86, оф. Р-108.
Тел.: +7 (499) 600-80-80 (#31288)
E-mail: *seredina@mirea.ru*

Регистрационный номер и дата принятия решения о регистрации СМИ: ПИ № ФС 77-74580 от 14.12.2018 г. СМИ зарегистрировано Федеральной службой по надзору в сфере связи, информационных технологий и массовых коммуникаций (Роскомнадзор)

Индекс по Объединенному каталогу «Пресса России»: **36924**

Дата опубликования 31.10.2025 г.

EDITORIAL BOARD

РЕДАКЦИОННАЯ КОЛЛЕГИЯ

20(5) 2025 | Tonkie Khimicheskie Tekhnologii
Fine Chemical Technologies

Contents

СОДЕРЖАНИЕ

Tonkie Khimicheskie Tekhnologii = Fine Chemical Technologies.
2025;20(5):405–406
ISSN 2686-7575 (Online)

Anniversaries

Юбилеи

https://doi.org/10.32362/2410-6593-2025-20-5-405-406
EDN GROMJM

EDITORIAL ARTICLE

M.V. Lomonosov Institute of Fine Chemical Technologies celebrates its 125th anniversary

РЕДАКЦИОННАЯ СТАТЬЯ

Институту тонких химических технологий имени М.В. Ломоносова — 125 лет

The Editorial Board of *Fine Chemical Technologies* congratulates the M.V. Lomonosov Institute of Fine Chemical Technologies on its glorious anniversary that commemorates 125 years since of its founding!

Few Moscow universities can boast a history spanning more than a century. The Institute dates back to July 1, 1900, when, by the Highest Decree of Tsar Nicholas II, the Moscow Higher Courses for Women were established in Moscow as a university-level institution to train women for teaching, scientific, and practical activities in the field of natural sciences. The courses were offered at two faculties: Physics and Mathematics, History and Philosophy. The first female students graduated the Higher Courses in 1904.

In 1918, by decision of the Collegium of the People's Commissariat for Education, the Higher Courses for Women was transformed into the Second Moscow State University, and in 1931, by Decree of the Council of People's Commissars of the USSR, the Moscow Institute of Fine Chemical Technology (MITHT) was approved as an independent university. In 1940, MITHT was named after the great Russian scientist Mikhail Lomonosov in recognition of its scientific achievements in training highly qualified specialists.

During the Great Patriotic War, teachers, scientists, and employees of the Lomonosov Moscow State University made a significant contribution to the Victory. N.I. Gelperin's high-powered bombs, K.A. Bolshakov's super-strong armor, N.A. Preobrazhenskiy's unique medicines, and B.A. Dogadkin's new elastomeric materials were recognized with a total of seven Stalin Prizes.

In 1993, by Order of the State Committee for Higher Education, MITHT was renamed the Lomonosov Moscow State Academy of Fine Chemical Technology; in 2011, it received the status of a state university.

In 2015, the MITHT was merged with Moscow State University of Radio Engineering, Electronics and Automation (MIREA), and Moscow State University of Instrument Engineering and Computer Science to form the Moscow Technological University. This merged institution was later renamed as MIREA – Russian Technological University (RTU MIREA). From that moment on, a new chapter began in the development of the M.V. Lomonosov Institute of Fine Chemical Technologies. Currently, 10 mega-laboratories and research centers have been created, while 18 departments of the institute are undergoing major re-equipment, opening up new opportunities for training and scientific and technical creativity for students of all chemical and technological disciplines at RTU MIREA.

Scientific schools established by a group of outstanding scientists and organizers of Russian science who taught at the Moscow Higher Chemical Engineering School or the Moscow Institute of Chemical Technology at various times (including academicians N.D. Zelinsky, A.N. Nesmeyanov, Ya.K. Syrkin, K.A. Andrianov, G.G. Nametkin, G.G. Urazov, S.S. Medvedev, I.N. Nazarov, I.L. Knunyants, I.P. Alimarin, N.P. Fedorenko, and V.I. Shvets) continue to be successfully developed by their followers, the scientists of our present generation.

Many graduates of MITHT have been recognized as the cream of the Russian scientific crop in the field of fundamental chemistry and chemical technologies. More than thirty graduates have received the titles of corresponding members and academicians of the Russian Academy of Sciences, going on to establish leading scientific schools or head scientific institutes and large departments in various educational and industrial organizations.

A tremendous amount of progress has been made in the field of education and science. In addition to its indisputable achievements in the field of chemistry and chemical technology, MITHT has always been a university with a "human face." Even during difficult years of persecution on certain issues related to the development of science, its steadfast position was exercised to support scientists that promoted modern trends in fundamental and applied chemistry. Subsequent history has vindicated the leading position of the MITHT, which continues to maintain a tradition of friendly treatment of students and respectful communication between colleagues.

Since the Higher Women's Courses were the original the source from which so much else flowed, it is fitting to remember the outstanding women who graduated from them. These include Ekaterina Alekseyevna Furtseva, Minister of Culture of the USSR; Mother Seraphima (Doctor of Technical Sciences, Professor Varvara Vasilyevna Chernaya-Chichagova), the first abbess of the Novodevichy Convent, who restored it in 1994; mountaineer Lyubov Georgievna Korotaeva, who hoisted the Soviet flag on Mount Elbrus during the Great Patriotic War; mathematician Olga Nikolaevna Tsuberbiller, who created a unique textbook on analytical geometry; corresponding member of the USSR Academy of Sciences Rimma Porfiryevna Evstigneeva; rector MITHT (2005–2015), Doctor of Technical Sciences, Professor Alla Konstantinovna Frolkova.

Key milestones in the history of the MITHT, numerous achievements, brief biographical notes on all outstanding scientists who taught at the institute, as well as on famous graduates who have achieved high positions in the organization of Russian science, have been carefully and respectfully collected and presented on the RTU MIREA website at mitht.site.

We wish the staff of the M.V. Lomonosov Institute of Fine Chemical Technologies many more significant achievements in science to come and every success in training high-class specialists for the prosperity of Russia.

Editor-in-Chief
of *Fine Chemical Technologies* journal

Andrey V. Timoshenko

Tonkie Khimicheskie Tekhnologii = Fine Chemical Technologies.
2025;20(5):407–429 ISSN 2686-7575 (Online)

Theoretical basis of chemical technology

Теоретические основы химической технологии

UDC 66.048:66.061
https://doi.org/10.32362/2410-6593-2025-20-5-407-429
EDN AEQBMZ

REVIEW ARTICLE

Comparative analysis of liquid mixture separation flowsheets

Anastasiya V. Frolkova✉, Albina N. Novruzova

MIREA – Russian Technological University (Lomonosov Institute of Fine Chemical Technologies), Moscow, 119454 Russia

✉ *Corresponding author, e-mail: frolkova_nastya@mail.ru*

Abstract

Objectives. When developing separation flowsheets for liquid mixtures, preference is often given to a specific process or flowsheet. Although alternative separation variants are sometimes considered, these tend to be based on a single-phase process, usually distillation. And while review papers on the specifics of implementing a particular separation technique exist, these mainly focus on the specific process of extractive distillation, combination of distillation and splitting processes, and extraction. Moreover, studies comparing the separation flowsheets of mixtures of different physicochemical nature based on different processes and special methods are fragmentary. This study presents a comparative analysis of the processes and methods of liquid mixtures separation based on a critical review of the literature and the authors' own research results.

Methods. The study is based on the critical analysis of literature and mathematical modeling of phase equilibria using local composition equations via freely distributed software packages.

Results. Specific liquid mixture separation methods, including combining various processes in one flowsheet (including hybrid technologies), are compared in terms of their advantages and disadvantages.

Conclusions. Promising areas of further research in the field of synthesis of organic mixtures separation flowsheets through the use of various separation processes and methods are identified. The effectiveness of the various processes (extraction, splitting, special distillation techniques) is estimated at different stages of different number of components mixtures separation. A comparative analysis of extractive and heteroazeotropic distillation processes when separating mixtures of different initial composition highlights the areas of energy advantage of each process. The effectiveness of the flowsheets is estimated by combining extraction with other processes, depending on the stage of extractant regeneration.

Keywords

separation flowsheet, phase equilibria, distillation, splitting, pressure swing-distillation, extraction, separating agents, energy consumption

Submitted: 23.01.2025
Revised: 05.02.2025
Accepted: 03.09.2025

For citation

Frolkova A.V., Novruzova A.N. Comparative analysis of liquid mixture separation flowsheets. *Tonk. Khim. Tekhnol. = Fine Chem. Technol.* 2025;20(5):407–429. https://doi.org/10.32362/2410-6593-2025-20-5-407-429

ОБЗОРНАЯ СТАТЬЯ

Сравнительный анализ схем разделения жидких смесей, основанных на различных процессах и методах

А.В. Фролкова✉, А.Н. Новрузова

МИРЭА – Российский технологический университет (Институт тонких химических технологий им. М.В. Ломоносова), Москва, 119454 Россия

✉ *Автор для переписки, e-mail: frolkova_nastya@mail.ru*

Аннотация

Цели. При разработке схем разделения жидких смесей часто отдается предпочтение конкретному процессу или схеме. В редких случаях рассматривается не один, а несколько альтернативных вариантов разделения, чаще основанных на одном фазовом процессе, как правило, ректификации. Имеющиеся на сегодня обзорные работы по особенностям реализации того или иного приема разделения сконцентрированы на конкретном процессе: экстрактивная ректификация, сочетание ректификации и расслаивания, экстракция. Комплексные исследования по сравнению схем разделения смесей разной физико-химической природы, базирующихся на разных процессах и специальных методах, не проводились. Научные публикации в данной области представлены фрагментарно и относятся к определенным объектам исследования. Целью настоящей работы является сравнительный анализ процессов и методов разделения жидких смесей на основе критического обзора литературы и результатов собственных исследований.

Методы. Работа базируется на критическом анализе литературы и математическом моделировании фазовых равновесий на основе уравнений локальных составов с использованием свободно распространяемых программных комплексов.

Результаты. Проведен обзор научной литературы, на основе которого показаны достоинства и недостатки конкретных приемов разделения жидких смесей, преимущества и ограничения на сочетание в одной схеме различных процессов (в том числе в гибридных технологиях).

Выводы. Перспективными направлениями дальнейших исследований в области синтеза и сравнения схем разделения смесей органических продуктов за счет использования различных методов и процессов разделения являются: оценка эффективности применения различных процессов (экстракции, расслаивания, специальных приемов ректификации) на разных этапах разделения смеси различной компонентности; сравнительный анализ процессов экстрактивной и гетероазеотропной ректификации при разделении смесей разного исходного состава (выделение областей энергетического преимущества каждого процесса); оценка эффективности реализации схем, основанных на сочетании экстракции с другими процессами, в зависимости от стадии регенерации экстрагента.

Ключевые слова

схема разделения, фазовые равновесия, ректификация, расслаивание, варьирование давления, экстракция, экстрактивные агенты, энергозатраты

Поступила: 23.01.2025
Доработана: 05.02.2025
Принята в печать: 03.09.2025

Для цитирования

Фролкова А.В., Новрузова А.Н. Сравнительный анализ схем разделения жидких смесей, основанных на различных процессах и методах. *Тонкие химические технологии*. 2025;20(5):407–429. https://doi.org/10.32362/2410-6593-2025-20-5-407-429

INTRODUCTION

A basis for the development of technological separation flowsheets is provided by information about the phase behavior of the system, including under changing external conditions (pressure, temperature), as well as in the presence of additional substances. The diversity of manifestations of phase behavior forms a basis for separation process flowsheets having different structures based on specific phase processes or their combinations. As such, each process has its own limitations related to the peculiarities of the phase equilibrium of the systems: for distillation process, such limitations include azeotropes, separatrix varieties and the proximity of component volatilities; for phase-separation processes, the presence of isopycnics (when implemented in a liquid separator); for extraction, the presence of solutropes; for crystallization, eutectic points, etc.

The separation techniques can be conditionally divided into two groups: the first being based on the use of the internal reserves of the system (the addition of a new component into the system is excluded), while the second always involves the addition of new substances. Here, by internal reserves, we refer to the specifics of phase behavior manifestation, which are influenced by the shift of the azeotrope under pressure (separation in a complex of columns operating at different pressures), the belonging of the azeotrope to the splitting region (a combination of distillation and splitting process), the effect of one of the components present in the mixture on the relative volatility of other components pairs (autoextractive distillation (AED)), different compositions of azeotropic and eutectic points (a combination of distillation and crystallization), and the curvature of separatrix manifolds. Such reserves represent possibilities for overcoming the limitations imposed by the nature of the mixture itself. The second group involves the addition of one or more new substances whose task is to transform the phase space and dynamic system of the separation process. These include processes such as extractive distillation (ED), re-extractive distillation (RED), (hetero)azeotropic distillation (HAD), as well as extraction and separation in the presence of an inert gas.

The peculiarities of the phase behavior of systems with different component compositions (primarily binary and ternary) have been fairly well studied along with the general patterns of their separation processes [1–3]. A large number of publications are dedicated to the study of various separation processes of specific mixtures, the vast majority of them pertaining to the ED process. This process has clear advantages over alternative separation methods: it is universal in terms of the properties of the initial mixture, has virtually no limitations, and is considered an energy-efficient separation technique. The main disadvantages of the process include the necessity for adding a new substance, which can negatively affect the quality of the obtained products, and the requirement of an additional column for agent regeneration. Summaries of the experience of using the ED process for the separation of mixtures of different physicochemical natures are presented in the previous studies [4–8].

Some energy-efficient separation methods combine distillation and splitting processes. Due to the common presence in reaction mixtures for the production of organic substances of components having limited mutual solubility (organic and water-organic mixtures), such separation methods are used quite frequently. A summary of the features of implementing this method for combining two processes and the effectiveness of its application for separating liquid mixtures is provided in studies [9, 10]. The authors discuss possible ways to reduce energy consumption in such flowsheets by using additional liquid separators (changing the qualitative composition of the reflux flow) and external decanters, as well as by reorganizing the flow structure of the flowsheet.

There are a few review articles dedicated to the efficiency of using extraction and various extractants (classical solvents, ionic liquids, deep eutectic solvents) for the separation of liquid mixtures [11–13]. Other studies discuss the effectiveness of applying the crystallization process [14–16]. However, while there are plenty of articles focused on developing separation technologies for specific mixtures, the scientific literature lacks studies on the broader use or combination of these methods.

The present article is dedicated to the analysis of literary sources that compare various separation methods: the combination of processes (extraction / distillation / phase separation), the use of special distillation methods (pressure-swing distillation (PSD), HAD, ED, AED, RED, (auto)extractive-heteroazeotropic distillation (AEHAD)). To identify the characteristics and conditions for the implementation of a particular process, a computational experiment is conducted using the Non-Random Two-Liquid model, whose parameters are taken from the database of the software package or the corresponding scientific article. All sets of parameters reproduce the features of the phase behavior of the systems with an error not exceeding 3%.

The presentation of the material requires the systematization and structuring of such basic concepts as process, method, technique, and separation mode. The processes discussed in the article include distillation, extraction and splitting (based on first-order phase transitions), as well as pervaporation (separation through a membrane). Here method refers to the way to achieve the required qualitative separation of a mixture (for

example, ED, PSD, etc.), while techniques involve the combination of one (homogeneous flowsheets) or several (heterogeneous or hybrid flowsheets) methods within a single technological flowsheet (for example, the combination of distillation and extraction), fractionation, or pre-concentration of a multi-component mixture (through the use of a specific method or process). The mode of operation determines the nature of the equipment's functioning (periodic, continuous, stationary, dynamic), as well as the set of technological parameters that ensure a certain separation result (for example, pressure in the columns, reflux ratio, solvent flow rate, number of separation stages, etc.).

The structure of the separation technological flowsheet is determined by the specifics of the organization and direction of recycle flows. In the absence of the latter, the flowsheet has a linear appearance; if all the apparatuses of the flowsheet are covered by feedback (recycle flow), it represents a separation complex. The flowsheet can consist of a linear part and one or several complexes; the most complicated structure of the flowsheet is a "complex within a complex."

THEORETICAL ANALYSIS

The physicochemical principles of separation processes are well known and thoroughly covered in the studies [1–3, 11–13, 17]. Each of the processes, methods and separation techniques is characterized by its own limitations and possesses its own advantages and disadvantages, as mentioned above.

The first stage of the synthesis of separation flowsheet involves the study of phase behavior (thermodynamic-topological analysis of the phase equilibrium diagram structure) [2, 17]. This analysis comprises the following stages:

1) determine the structure of the phase portrait (the diversity of types of singular points formed not only by pure components but also by their mixtures is manifested on phase diagrams of liquid–vapor and liquid–solid equilibrium; splitting phase diagrams (containing different numbers of liquid phases) are characterized by the presence of various varieties of different dimensionalities (binoidal/critical), splitting phase simplices);
2) establish the presence of phase equilibrium constraints on specific processes;
3) determine the limiting capabilities (maximum achievable compositions) of processes (for example, by determining the boundaries of areas and sub-areas of distillation or crystallization, the boundaries of the splitting area);
4) determine the characteristics of the change in the structure of the diagram of a specific type of equilibrium (including the possibility of lifting constraints) when conditions (pressure, temperature) change;
5) assess the feasibility and prospects of combining different processes through comparative analysis of the structures of diagrams related to different types of equilibrium (for example, by superimposing one diagram onto another) or to one type under various conditions;
6) determine the qualitative compositions of impurity components (for example, when isolating pure substances in the distillate or the bottom of a distillation column based on the analysis of the arrangement features of distillation line bundles or when separating a mixture in a liquid separator, when one or both layers may potentially represent the product flow);
7) identify the mutual influence of the components of the base mixture on each other (changes in relative volatility, formation of (hetero)azeotropes with minimum boiling point, etc.) to assess the feasibility of using so-called "auto" processes (AED, autoheteroazeotropic distillation);
8) determine the behavior of the system in the presence of specially selected substances for processes such as ED and RED (change in relative volatility), HAD (formation of a new azeotrope with the lowest boiling point), distillation with a medium-boiling agent (separation of the mixture through conventional distillation by correctly selecting the desired distillation type), and extraction (formation of a two-phase splitting region).

Even at the stage of studying the phase behavior of the system, it is possible to discriminate some processes, methods of mixture separation, as well as the possibilities of their combination (approaches). Exclusion of variants is related not only to the principled impossibility of implementing a particular process but also to the feasibility of its implementation (for example, separation of a mixture in a column complex under different pressures with a small azeotrope shift, in an ED complex with a low-selectivity agent, in a hybrid flowsheet combining distillation and crystallization, with similar azeotrope and eutectic points compositions, etc.).

The variants for a multitude of synthesized separation flowsheets can further be discriminated based on certain qualitative or quantitative criteria: by the number of apparatuses, the amount of material flows (when the number of degrees of freedom in the separation flowsheets is greater than zero and part of the parameters should be arbitrarily set for material balance calculations), etc. The selected flowsheets after discrimination can be modified (structural optimization) by coupling material and thermal flows, using additional equipment (for example, separators, heat pumps), using

complex dividing wall columns (with side section flows, with internal walls), etc.

The set of separation flowsheets formed at the final stage of structural optimization is subject to parametric optimization. The criteria for selecting optimal parameters (while achieving the required quality of product fractions) can include the total duty of column reboilers (for distillation separation flowsheets), total operating costs, total annual costs (TAC), environmental indicators (carbon dioxide emissions, water consumption, wastewater generation), as well as the criterion of best available technologies as a whole. It is important to note that, regardless of the choice of criterion, the comparison of variants should be considered correct, for which not only the required product quality is achieved, but also the adequacy (optimality) of the selected conditions and parameters, as well as selectivity of the chosen solvents are taken into account. For example, it would be incorrect to compare processes based on the addition of a new substance, one of which is low-selective, since in this case, one of the processes or flowsheets is placed in a priori unfavorable conditions.

(Auto)ED and (auto)HAD

Both methods involve the addition of a new substance, except for auto processes. ED and HAD are considered as energy-efficient separation techniques. For example, in the ED process, separation efficiency is enhanced by the multi-level feeding of the agent and the initial mixture. It creates an additional counterflow in the column and forms an area of maximum agent concentration in the middle part of the column since the work expended on separating the mixture is partially compensated by the work of mixing the two feed flows. The addition of a new substance in the HAD process leads to the formation of an unstable node type azeotrope, which favorably affects the reduction of temperature along the height of the column.

A brief description of the processes and separation flowsheets for specific mixtures is provided in Table 1.

Table 1. Brief characterization of mixtures and their separation processes using (auto)extractive distillation ((A)ED) and (auto) heteroazeotropic distillation ((A)HAD)

System	Specifics of vapor–liquid equilibrium (VLE)*, process separating agent (SA)	Comparison indicators	(A)HAD	(A)ED
Ethanol–water [18]	Positive azeotrope; for HAD—pentane for ED—ethylene glycol	Equipment Σ*N* Σ*Q*	2C+S 54 6942.8	2C 33 2007.8
		Equipment Σ*N* Σ*Q*	DWC 1C+S 60 5538.1	DWC 1C 36 1819.5
Propionic acid–water [19]	Positive azeotrope; for HAD—cyclohexanol for ED—*N*-MP	Equipment Σ*N* Σ*Q*	1C+S 18 376.8	2C 40 1816.4
Acetic acid–water [19]	– for HAD—vinyl acetate for ED—*N*-methylacetamide	Equipment Σ*N* Σ*Q*	1C+S 18 1070.0	2C 88 1832.3
1-Methoxy-2-propanol–water [19]	Positive azeotrope; for HAD—isopropyl acetate for ED—sulfolane	Equipment Σ*N* Σ*Q*	2C+S 36 1795.9	2C 52 2271.3
1-Methoxy-2-propanol–water [20]	Positive azeotrope; for HAD—isopropyl acetate; for ED—sulfolane / *N*-MP	Equipment Σ*N* Σ*Q* TAC × 10^6	2C+S 37 11870 34.5	2C / 2C 35 / 72 6600 / 9040 23.2 / 33.0
Ethanol–toluene–water [21]	3.3.1-2; for HAD—toluene for ED—glycerol	Equipment Σ*N* Σ*Q* TAC × 10^6	3C+S 92 1017.6 3.66	2C+S 42 455.2 1.96
		PCHMF flowsheet Σ*N* Σ*Q* TAC × 10^6	 92 735.8 3.23	 –

Table 1. Continued

System	Specifics of vapor–liquid equilibrium (VLE)*, process separating agent (SA)	Comparison indicators	(A)HAD	(A)ED
Methanol–water–methyl methacrylate [22]	3.2.0-2b; for AED—water for ED—phenol / DMSO and phenol	Equipment Σ*N* Σ*Q*	3C+S 58 2369.7	3C / 4C 89 / 107 4395.6 / 4477.4

Note: * azeotrope type or VLE diagram class according to L.A. Serafimov's classification [23]; *N*-MP is *N*-methyl-2-pyrrolidone; DMSO is dimethyl sulfoxide; *N* is a number of theoretical stages; *Q* is reboiler duty, kW; C — column, S — liquid separator; DWC is a divided-wall column—indicated for flowsheets that consider the same technology, but with the replacement of a conventional column with a complex one; PCHMF are partially coupled heat and material flows; HAD — heteroazeotropic distillation; ED — extractive distillation; TAC — total annual costs, USD/year.

A comparison of the separation flowsheets of the ethanol–water mixture showed that ED with ethylene glycol is a less energy-intensive separation variant (approximately 70% savings compared to HAD) [18]. Such a significant difference in energy consumption is due to the selection of a low-selectivity solvent (pentane) for the HAD process, which affected its consumption (for HAD 751.6 kmol/h, for ED 190 kmol/h per 100 kmol/h of the initial mixture) (Fig. 1, the ratio of the amounts of the pentane and aqueous phases is above 12). Moreover, pentane needs to be evaporated in the HAD process. Increasing the efficiency of this process is possible by using another agent (for example, benzene, cyclohexane [1]). Conversely, ethylene glycol is claimed to be a selective solvent for the ED process [24]. However, the comparison provided by the authors appears to be biased since the HAD process is placed in an a priori disadvantageous position.

The use of complex dividing wall columns allowed for a reduction in energy consumption for both HAD (by 20%) and ED (by 9.5%), which did not affect the cost ratio between the flowsheets. The difference in the placement of the dividing wall (at the top for HAD and at the bottom of the column for ED) is related to the implementation specifics of the process.

The study [19] shows that when separating mixtures of high-boiling components, HAD can be more energy-efficient than ED due to the reduction in process temperature through the formation of azeotropes with a minimum boiling point and the possibility of eliminating one of the columns (one of the layers leaving the separator represents the product flow). As the boiling point of the components in the base mixture increases, the efficiency of the ED process decreases. When selecting an extractive agent (EA) for the HAD process, it is necessary to comprehensively evaluate the characteristics of the liquid–liquid equilibrium (under separator operating conditions) and the liquid–liquid–vapor equilibrium due to the latter affecting the amount of the recycle flow [19]. It should be noted that for both processes, the present authors selected the most selective agents on the basis of literature analysis and their own research results to inform the comparison correctly.

When separating the 1-methoxy-2-propanol-water mixture of composition F (Fig. 2) in a two-column flowsheet, the HAD process is carried out in the second

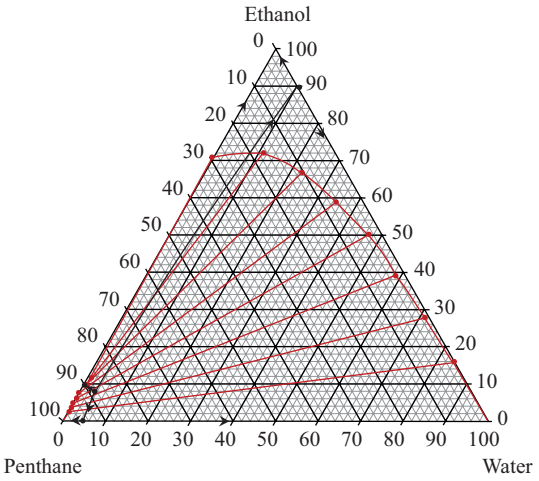

Fig. 1. Structure of the ethanol–water–pentane system phase diagram

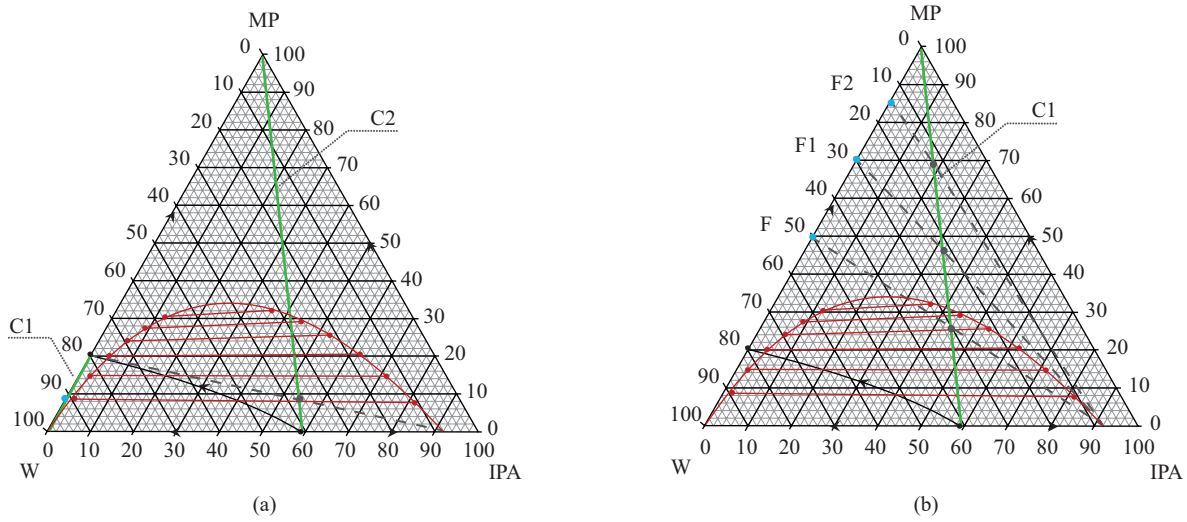

Fig. 2. Balance lines of the heteroazeotropic distillation (HAD) flowsheet of the mixture 1-methoxy-2-propanol (MP)–water (W) in the presence of isopropylacetate (IPA): (a) HAD is realized in the second column C2, (b) HAD is realized in the first column C1

column [20]. The first column (C1) is intended for the partial separation of water to subsequently reduce the load on the azeotropic distillation column. In the second column (C2), the flows of distillate from the first column and the organic layer leaving the liquid separator are mixed, followed by separation into pure 1-methoxy-2-propanol and a mixture of the azeotropic composition of water–isopropyl acetate. The balance lines are shown in Fig. 2a. Due to the low solubility of isopropyl acetate in water, residual water can be separated in the form of a product flow (if necessary, this flow can be further purified in an additional distillation column). Comparing the structure of flowsheets that differ in the organization of the HAD in column C2 or C1, the possibility of reducing the ratio of distillate and bottom flows in the HAD column (the balance green line of column C2 in Fig. 2a) compared to the same ratio in the HAD column in column C1 (the balance green line of column C1 in Fig. 2b) should be noted. However, if the water concentration in the aqueous layer of the separator meets the specified requirements, the second column in the classical HAD flowsheet will be absent.

For the ED process of the considered binary mixture, two selective solvents were chosen: sulfolane and *N*-methyl-2-pyrrolidone (*N*-MP), with the selectivity of the former being 1.5 times higher, which resulted in lower agent consumption and lower energy costs for the complex compared to *N*-MP. The energy costs of the ED flowsheets with *N*-MP and HAD are comparable (a difference of 4% in favor of ED), while for ED with sulfolane they are significantly lower (by more than 30%). This example clearly illustrates how significantly the separation results in terms of energy costs can differ when comparing ED and HAD flowsheets with effective solvents.

Comparing the results of studies [19] and [20], in which the same mixture is subject to separation but with different compositions, it can be noted that with an increase in the concentration of 1-methoxy-2-propanol in the initial mixture (compositions F1 and F2 in Fig. 2b), the efficiency of applying the HAD process with isopropyl acetate increases, while the ED process with sulfolane decreases. This is explained by the decrease in isopropyl acetate consumption and consequent distillate- bottom ratio in the HAD column (Fig. 2b) (the product flows are represented in the column's bottom). Thus, when comparing the ED and HAD processes, it is important to consider not only the boiling points of the components of the base mixture (light or heavy boiling) [19], but also its composition, which will directly affect the solvent consumption in HAD.

For the separation of the ethanol–toluene–water mixture, two methods have been proposed: HAD, including with partially coupled heat and material flows (PCHMF), and ED [21]. The first method is called HAD by the authors, as the material flows of the flowsheet are organized in such a way that a ternary heteroazeotrope is separated in the distillate of the first column (ethanol in the bottom) (however, no new agent is added into the system). ED turned out to be the more advantageous variant (lower energy and TAC). This is due to the necessity of using only two distillation columns; a liquid separator was used to separate the water–toluene pair (a combination of ED and liquid phase splitting). However, the cost calculations for this process did not take into account the necessity of using expensive refrigerants for condensing the vapors of the distillate from the regeneration column (the top temperature of the column is 8°C). It should be noted that the initial structure of the phase equilibrium diagram of the ternary system is unfavorable for the implementation

of the method based on the combination of distillation and phase splitting: near the ternary azeotrope in the region with a stable node—ethanol, there is a touching of the separatrix (Fig. 3), which ultimately leads to the difficulty of isolating this alcohol and achieving the azeotropic composition (the column efficiency was 75 theoretical stages). The ethanol separation column in the HAD flowsheet is also characterized by the highest energy costs (more than twice compared to the other columns in both flowsheets), i.e., this method is placed in an a priori disadvantageous position. The application of PCHMF allowed for a reduction in energy costs for the HAD flowsheet, but it did not make it competitive with the ED process.

When separating the methanol–methyl methacrylate–water mixture, separation flowsheets based on the use of additional substances were compared: ED, AED, extraction [22]. The use of water in the first stage of the extraction process is ineffective due to the extract flow consisting of a ternary mixture with a predominant content of water and methanol (with an impurity of about 1% methyl methacrylate), while the raffinate flow is binary (methyl methacrylate with an impurity of about 5% water). To isolate all components in pure form, additional methods will need to be employed, which will negatively impact energy costs. The lowest energy costs are observed for the AED flowsheet with water. Water not only increases the volatility of methyl methacrylate, but also lowers the process temperature due to the formation of a positive azeotrope, which positively affects energy consumption. The latter for the AED column is four times lower compared to the ED column with phenol or dimethyl sulfoxide (DMSO). Concerning the temperature profile of the AED column between the levels of the feed mixture and EA, a decrease in process temperature is observed, averaging around 56°C, with; here, the distillate temperature is approximately 80°C, while the bottom temperature is about 85°C. With the temperature profile of the ED column with DMSO, on the contrary, an increase in temperature averaging up to 100°C is observed.

Despite AED being more advantageous overall, it is necessary to pay attention to the flowsheet with phenol, as it acts as a stabilizer for methyl methacrylate to prevent its polymerization. The higher quality of the target product in these flowsheets should additionally be noted.

The combination of the two methods discussed, provided that EA is a component of the base mixture (AEHAD in one apparatus), is generally the most efficient option in terms of energy consumption for separation [22, 25, 26].

ED and PSD

The characteristics of the processes and separation flowsheets of specific mixtures are presented in Table 2.

For almost all the mixtures in Table 2, whose separation is planned in the ED or PSD complex, an economic analysis is conducted with the determination of annual costs. The correlation between the ratio of energy costs for the separation of these processes and the TAC criterion is quite justified considering the fact that operating costs generally contribute more to the annual totals. An exception is the mixture of dipropyl ether–*n*-propanol [28] for which the ED process shows lower energy costs for column reboilers, but higher TAC. Such a difference is due to the contribution of capital costs to the TAC indicator (to achieve the required product quality, the ED complex requires a greater total number of theoretical separation stages, 67 *vs* 24). The authors [28] note that the difference in annual costs will decrease with an increase in production volume due to the increased load on the column reboilers.

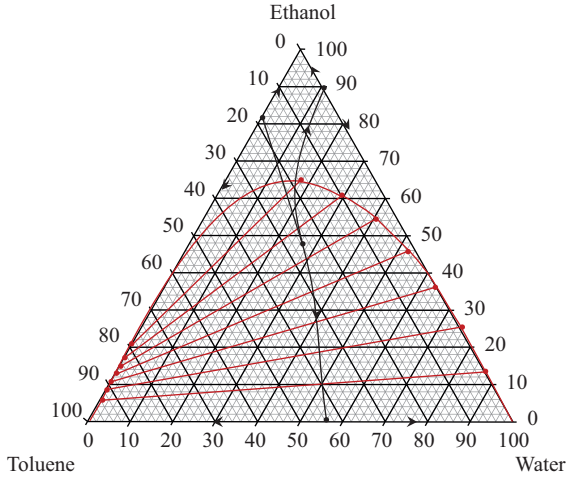

Fig. 3. Structure of the ethanol–toluene–water system phase equilibrium diagram

Table 2. Brief characterization of mixtures and their separation processes using ED and PSD

System	Specifics of VLE*	Comparison indicators	PSD	ED
Isopropanol–diisopropyl ether [27]	Positive azeotrope; for ED—2-methoxyethanol	Equipment Σ*N* Σ*Q* TAC × 10^6	2C 56 4293.6 –	2C 106 3027.1 1.964
		PCHMF flowsheet Σ*N* Σ*Q* TAC × 10^6	 56 4085.2 1.851	 120 2677.1 2.149
Dipropyl ether–*n*-propanol [28]	Positive azeotrope; for ED—2-methoxyethanol	Equipment Σ*N* Σ*Q* TAC × 10^6 Capital expenses × 10^6	2C 24 1058.3 0.632 1.479	2C 67 816.7 0.896 2.364
Acetonitrile–*n*-propanol [29]	Positive azeotrope; for ED—*N*-MP	Equipment Σ*N* Σ*Q* TAC × 10^6	2C (PCHMF) 41 2133.3 0.920	1C (DWC) 38 2716.7 1.18
Tetrahydrofuran–water [30]	Positive azeotrope; for ED—DMSO	Equipment Σ*N* Σ*Q* Capital expenses × 10^6 TAC × 10^6	2C 29 1985.9 0.430 0.600	2C 35 1391.7 0.473 0.469
		PCHMF flowsheet Σ*N* Σ*Q* Capital expenses × 10^6 TAC × 10^6	 29 1450.4 0.426 0.479	 35 1324.9 0.470 0.454
		FCHMF flowsheet Σ*N* Σ*Q* Capital expenses × 10^6 TAC × 10^6	 29 1414.16 0.458 0.487	 –
Isobutanol–isobutyl acetate [31]	Positive azeotrope; for ED—*n*-butylpropionate	Equipment Σ*N* Σ*Q* Capital expenses × 10^6 TAC × 10^6	2C 46 1275.0 2.79 1.26	2C 80 930.6 4.62 1.69
Methanol–chloroform [32]	Positive azeotrope; for ED—*n*-propanol	Equipment Σ*N* Σ*Q* Capital expenses × 10^6 Energy expenses × 10^6 TAC × 10^6	2C 49 3220.0 1.61 0.737 1.27	2C 156 10270.0 7.34 2.29 4.73
		Including VDC Capital expenses × 10^6 Energy expenses × 10^6 TAC × 10^6 Savings when using the VDC column	 1.48 0.737 1.23 10.36%	 7.27 2.29 4.71 1.01%

Table 2. Continued

System	Specifics of VLE*	Comparison indicators	PSD	ED
Acetone–methanol [32]	Positive azeotrope; for ED—water	Savings when using the VDC column	4.18%	1.85%
Acetone–chloroform [32]	Negative azeotrope	Savings when using the VDC column	2.57%	1.07%
Benzene–cyclohexane [32]	Positive azeotrope	Savings when using the VDC column	0.57%	0.36%
Isopropanol–diisopropyl ether [32]	Positive azeotrope	Savings when using the VDC column	7.96%	0.00%
Methanol–isopentane–*n*-pentane–1-pentene–2-pentene [33]	Positive azeotropes in binary subsystems; for ED—water	Equipment Σ*N* Σ*Q* Capital expenses × 10^6 Energy expenses × 10^6 TAC × 10^6	2C 20 46700.0 4.25 6.92 8.34	2C 44 14730.0 2.44 2.22 3.04
Acetone–methanol [34]	Positive azeotrope; for ED—water	Equipment Σ*N* Σ*Q* Capital expenses × 10^6 Energy expenses × 10^6 TAC × 10^6	3C 79 2733.3 0.327 1.77 −8.52**	2C 62 1197.2 0.175 0.776 −9.34**
		Including PCHMF Capital expenses × 10^6 Energy expenses × 10^6 TAC × 10^6	 0.327 1.37 −8.92**	–
Acetone–methanol [35]	Positive azeotrope; for ED—water	Equipment Σ*N* Σ*Q* Capital expenses × 10^6 Energy expenses × 10^6 TAC × 10^6	2C 114 23220.0 3.51 3.35 4.52	2C 83 18510.0 3.03 2.72 3.75
		Including PCHMF Capital expenses × 10^6 Energy expenses × 10^6 TAC × 10^6	 2.65 2.45 3.33	 3.00 1.98 2.98
Acetone–chloroform [36]	Positive azeotrope; for ED—DMSO	Equipment Σ*N* Σ*Q* Capital expenses × 10^6 Energy expenses × 10^6 TAC × 10^6	2C 78 21508.0 3.65 3.11 4.33	2C 34 2628.0 0.65 0.74 0.95
Methanol–chloroform [37]	Positive azeotrope; for ED—1-propanol	Equipment Σ*N* Σ*Q* Capital expenses × 10^6 Energy expenses × 10^6 TAC × 10^6	2C 49 3350.0 0.89 0.43 0.73	2C 156 9070.0 2.62 1.34 2.22
		Including PCHMF Capital expenses × 10^6 Energy expenses × 10^6 TAC × 10^6	 0.76 0.31 0.56	–

Table 2. Continued

System	Specifics of VLE*	Comparison indicators	PSD	ED
Methyl acetate–methanol–acetic acid–acetic anhydride [38]	Positive azeotrope: methylacetate–methanol for ED—ethylene glycol	Equipment ΣQ	4C 67000.0	4C 24500.0
Isopropanol–water [39]	Positive azeotrope; for PSD—tetrahydrofuran for ED—DMSO	Equipment ΣN ΣQ Capital expenses × 10^6 Energy expenses × 10^6 TAC × 10^6	2C 75 7916.2 1.94 1.77 2.42	2C 75 2097.5 0.78 0.54 0.80
		Including PCHMF Capital expenses × 10^6 Energy expenses × 10^6 TAC × 10^6	 1.65 1.10 1.65	–

Note: * azeotrope type is indicated; N is a number of theoretical stages; Q is reboiler duty, kW; C — column, S — liquid separator, DWC is a divided-wall column, VDC is a variable diameter column; P(F)CHMF are partially (fully) coupled heat and material flows; economic indicators are presented in USD/year; ** authors indicate profit.

Comparison of separation flowsheets (based on ED or PSD) of binary mixtures with different physicochemical properties (with positive or negative deviations from ideality) (Table 2) showed a nearly uniform distribution between variants where PSD [29, 31, 32, 39] or ED [33–36, 38] is more advantageous. The costs of separation flowsheets for the tetrahydrofuran-water mixture (ED with DMSO and PSD) turned out to be comparable [30].

It should be noted that such a comparison is not always correct. For example, when separating a methanol–chloroform mixture in an ED complex, a low-efficiency (low-selectivity) *n*-propanol [32, 37] EA was chosen, which affected the process indicators and equipment parameters: the total number of theoretical trays (N) in the ED flowsheet was 156 stages, while the reflux ratios in the columns were 7.64 and 7.9, respectively; here, the agent consumption was 600 kmol/h per 100 kmol/h of the initial mixture. The conducted own calculation of the vapor-liquid equilibrium in the derivative ternary system methanol–chloroform–*n*-propanol showed that the composition simplex of the base binary system is divided into composition areas for which the relative volatility of the mixture components changes differently with increasing EA consumption. In the range of 0 to 0.5 mole fractions of chloroform, the relative volatility of the chloroform–methanol pair decreases with increasing propanol concentration: in the range of 0.50–0.56 mole fractions, it passes through an extremum, while in the range of 0.56–0.66 mole fractions (azeotropic composition), it increases (Fig. 4). The patterns of change in the relative volatility of binary mixtures in the presence of EAs are presented in study [40]. The authors of study [32] consider an equimolar composition as the initial one, for which the change in relative volatility is insignificant, which explains the result of the ED process calculation.

It is possible that the choice of a more selective solvent may change the cost ratio picture of the considered flowsheets.

This study discusses the efficiency of using varied-diameter columns (VDC) when the flow of liquid and vapor in different sections of the column significantly differs. This is illustrated by the example of five binary systems (considering different diameters of the rectifying and stripping sections in several cases allows for a reduction in capital costs and achieving an overall economic effect when comparing TAC in the range of 0–10%). Similar research was conducted in study [37].

In the study [36], the PSD separation flowsheet of the acetone-chloroform mixture turned out to be significantly more energy-intensive due to the low sensitivity of the azeotrope composition to pressure changes (about 0.02 mole fractions with a pressure difference in the columns exceeding 9 atm).

While the transformation of ED and PSD flowsheets to structures with PCHMF generally leads to reduced separation costs, this does not affect the ratio of operational to annual costs between separation variants. However, if the difference in separation

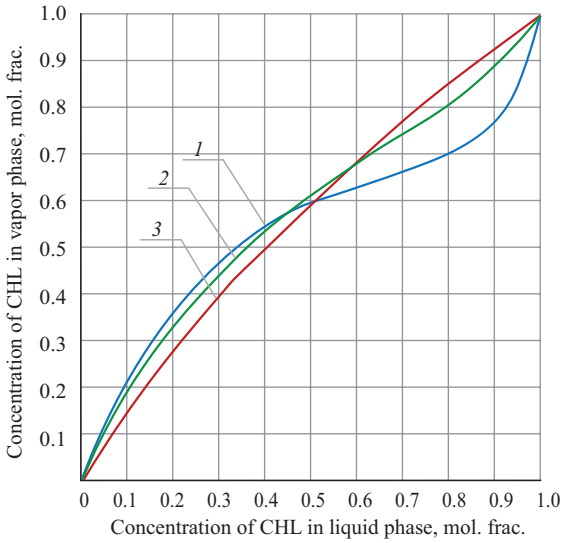

Fig. 4. Phase equilibrium curve of binary and pseudo-binary chloroform–methanol system at different amounts of *n*-propanol, mol %: (*1*) 0, (*2*) 30, (*3*) 80

costs in the initial flowsheets is significant, then using PCHMF reduces it; moreover, the effect of such structural optimization is generally more pronounced for a more energy-intensive flowsheet [35]. In the study [30], partial flow coupling for both flowsheets allowed for a reduction in operational (annual) costs by 4.8% (3.4%) and 26% (20%) for ED and PSD, respectively. Full heat integration for the flowsheet based on pressure variation led to a reduction in operational (annual) costs by 27% (18.7%). The lesser effect of full heat integration for the PSD flowsheet is associated with the need to use additional equipment and the increase in capital costs by 6.4% compared to the classical flowsheet.

In the study [29], structural optimization of flowsheets was carried out by using a dividing wall column (DWC) for the ED flowsheet of the acetonitrile–*n*-propanol mixture and partial flow coupling for the PSD complex. The application of a complex column compared to the classical ED complex allowed for a 7.94% reduction in TAC and a 12.8% reduction in PCHMF for the PSD complex. The optimization of the flowsheet structure did not change the cost ratio of the flowsheets, which is higher for the ED process. Dynamic process modeling (in nonstationary and transitional modes) showed greater resistance to disturbances (changes in flow rate and feed composition) of the PSD flowsheet with PCHMF compared to ED (DWC).

When purifying methanol from C5 fraction components (during the production of *tert*-amyl ether), the process of extractive heteroazeotropic distillation with water [33] serves as an alternative to the PSD process. Water is not only an extractive heteroazeotropic agent, which serves to lower the overall temperature of the process in the column by forming azeotropes with a boiling point minimum, but also possesses the properties of an extractant (elements of extraction are present), which ensures greater energy efficiency of this process.

The phase diagram of the methyl acetate–methanol–acetic acid–acetic anhydride mixture is characterized by a simple structure of the phase equilibrium diagram: there is a single azeotrope having a minimum boiling point, whose composition changes with varying pressure. Considering two main PSD and ED separation methods, the authors [38] synthesized 12 flowsheets of different structures. The latter differ in the use of ED, varying pressure, and the column of conventional distillation at different stages of separation. Such a comprehensive study not only allowed for the comparison of different separation methods, but also determined the effectiveness of their application in separating mixtures of varying component compositions: quaternary, ternary, binary. As a rule, the latter decreases with an increase in the number of components in the mixture being separated. When using ED (PSD), the total columns reboiler duty was: binary mixture, 24.5 MW (67.0 MW); ternary, 37.4 MW (70.3 MW); quaternary, 37.6 MW (92.5 MW) [38].

Special attention should be given to the results of the authors [39] on the separation of the isopropanol–water mixture. Since the composition of the azeotrope is practically independent of pressure, the authors add a new substance (tetrahydrofuran) into the system

in order to use PSD. This forms new azeotropes (tetrahydrofuran–water at 0.1 and 0.6 MPa and tetrahydrofuran–isopropanol at 0.6 MPa), whose composition is sensitive to changes in external conditions. In place of pure ether, a mixture of ether with water in a composition close to azeotropic is added in the initial mixture. The separation of the mixture occurs in a two-column complex. A comparison with the classical ED flowsheet using DMSO demonstrated the inefficiency of this method even with partial flow coupling. The amount of agent in the PSD process (95 kmol/h per 100 kmol/h of the initial mixture) is twice that of the solvent in the ED process (45 kmol/h), while tetrahydrofuran is always present in the distillate flow, which negatively affects energy costs. Furthermore, water must also be present in the recycle flow (163 kmol/h).

Comparison of flowsheets based on the combination of various processes and separation methods

The article [41] compares two separation variants for the diisopropyl ether–isopropanol–water mixture: PSD and a combination of distillation and splitting, including the use of partial heat and material flow integration. The comparison of classical flowsheets without heat integration demonstrated the advantages of the flowsheet based on pressure variation over the second variant (reduction of energy, capital, and TAC by 5.3%, 6.3%, and 5.5%, respectively) in terms of a smaller recycle flow, lower reflux ratios, and a total number of theoretical stages. The application of partial heat integration for the PSD flowsheet further reduced energy consumption by 15% and TAC by 11%.

For the separation of the ternary mixture water–benzene–isopropanol, two flowsheets have been considered: the first is based on varying the pressure in the columns (PSD), while the second is a combination of (preliminary) phase separation, conventional distillation, and pressure variation [42]. For both flowsheets, the possibility and efficiency of using partial heat integration are considered. The amount of the recycle flow formed from the distillate flows of the distillation columns for the flowsheet with phase splitting is significantly higher (179.42 *vs* 95.45 kmol/h per 100 kmol/h of the feed mixture), which ultimately had a negative impact on the energy costs of the flowsheet (the latter being 20% higher when compared to flowsheets without heat integration). An analysis of the phase equilibrium diagram structure and the position of the balance lines shows the inefficiency of the method based on preliminary phase separation. An increase in the values of reflux ratios and the number of theoretical stages in distillation columns (101 compared to 74 theoretical plates in the PSD flowsheet) is achieved using large distillate and bottom flow ratios in columns. This is due to the need to reach the boundaries of separation areas to ensure the possibility of transitioning to the required distillation area. At the same time, capital costs are more than 40% higher. Already at the stage of studying the phase diagram, it was possible to abandon the method based on the combination of different processes. The use of preliminary phase separation is generally not an effective separation technique if all components are present in the equilibrium liquid layers in the separator [9]. This example also shows that the use of partial heat integration does not yield a significant effect in any cases: for PSD flowsheets, this effect is around 2.8%, while for the flowsheet based on preliminary phase separation the corresponding figure is about 6%.

In the study [43], a comparison of two methods for dehydrating acetonitrile obtained through the ammoxidation of ethanol is presented: varying pressure in distillation columns (1–7 bar and 1–10 bar) and a combination of extraction (with dichloromethane) and distillation. As the calculation results showed, the lowest capital costs at comparable operating costs are observed for the PSD flowsheet (1–10 bar), while the highest are for the extraction flowsheet; however, in the hybrid flowsheet, the required quality of acetonitrile (99.99 wt %) is not achieved. It should be noted that the extractant is not used in its pure form, but with a certain amount of acetonitrile due to its low selectivity, which reduces the efficiency of the extraction process and increases the recycle flow (the extractant in the ternary mixture is separated in the bottom of the distillation column).

Different separation flowsheet structures for the toluene–methanol–water mixture based on the use of the ED single separation method are associated with varying effects of the selected solvents on the relative volatility of the components: in the presence of *N*-methyl-2-pyrrolidone, the volatility of methanol increases relative to the other components, while in the presence of ethylene glycol, it is toluene that demonstrates the highest relative increase in volatility [44]. As a result of the separation of methanol after the agent regeneration column due to their low mutual solubility, the separation of the toluene–water mixture occurs in the liquid separator (the flowsheet includes two columns and a separator). If toluene is separated in the distillate of the column, an additional distillation column will be required for the subsequent separation of the water–methanol mixture, which will negatively impact both the energy costs of the flowsheet

and the total number of theoretical stages N (the flowsheet contains three distillation columns). This is confirmed by a computational experiment in the study: for the flowsheets with *N*-MP and ethylene glycol, the $\Sigma N/\Sigma Q$ was 91/4.15 and 137/4.47, respectively. The TAC were also higher for the flowsheet with ethylene glycol.

The problem of purifying components that are present in trace amounts, especially when dealing with a multicomponent mixture, can be addressed by using ED (RED) or RED processes. In the study [45], two separation flowsheets based on the combination of ED or RED and single extraction are proposed for the separation of a six-component mixture of water–hydroxyacetone–isopropylbenzene–alpha-methylstyrene–phenol–2-methylbenzofuran. The structures of the flowsheets are almost identical except for the method of introducing the agent into the first column (diethylene glycol as a high-boiling or acetone as a low-boiling solvent) and its regeneration (diethylene glycol in the bottom, acetone in the column distillate). The flowsheet with acetone was found to be significantly inferior to the flowsheet with diethylene glycol with double the energy costs. However, the authors state that the competitiveness of the flowsheet may be due to the repeated use of the excess acetone generated during the cumene method of phenol production in the technological chain.

A large amount of experimental data on liquid–liquid equilibrium in ternary and quaternary systems is presented in both the Russian and foreign scientific literature (as a rule, a basic binary mixture is considered in the presence of one or two potential extractants for the extraction process). Conclusions about the feasibility of using a particular solvent—and consequently the implementation of the extraction process—are based solely on known separation criteria (distribution and separation coefficients). The articles do not evaluate the feasibility of implementing such a separation option considering the solvent regeneration unit. Considering that the energy-intensive distillation process is typically used for solvent regeneration, the efficiency of the combination of these two processes can be significantly reduced due to the presence of thermodynamic equilibrium constraints of the liquid–vapor (liquid–liquid–vapor) mixture representing the extract.

The separation of the acetonitrile–water mixture in a flowsheet based on a combination of extraction (chloroform as the extractant) and distillation turned out to be a less energy-efficient process compared to the ED flowsheet with DMSO (by more than 30%) and comparable to the PSD flowsheet (a difference of 1.7%) [46]. The high-energy costs are due to the need to separate (evaporate) chloroform in the distillate of the extractor regeneration column.

Another variant for separating this mixture [47] involves a pre-concentration column for the mixture (partial separation of water) followed by its separation in an ED complex with ethylene glycol (the total duty on the column reboilers was 4556 kW, TAC was $1.56 \cdot 10^6$ USD/year). Due to the restructuring of material flows, the flowsheet was transformed into a two-column complex by combining the concentration column and the EA regeneration column, which allowed for a 16% reduction in heat duty and a 13% reduction in TAC compared to the initial version. The extraction flowsheet for this mixture with *n*-propyl chloride (with some amount of acetonitrile) includes 4 units: an extractor, a liquid separator, and two distillation columns. The regeneration of the extractant is carried out by a combination of distillation and liquid phase splitting. This flowsheet turned out to be more advantageous both in terms of energy consumption (2972 kW) and annual costs ($1.02 \cdot 10^6$ USD/year).

Comparing the results of the studies [46, 47], it can be assumed that the ratio between the considered separation options may be changed by abandoning the mixture concentration column and selecting a more selective agent for the ED process.

When investigating the possibilities of the extraction process of ethanol mixtures with hydrocarbons (hexane and heptane) using ionic liquids, the authors of study [11] indicate a positive economic effect when organizing a combination of extraction and distillation compared to classical separation ED or HAD methods (more detailed information is not provided in the article).

Another example of the use of hybrid technologies consists in the combination of distillation and membrane separation (in particular, pervaporation). The principle of membrane separation differs from the previously discussed phase processes; it is based on the selective extraction of substances as they pass through the membrane. The processes occur in different apparatuses arranged sequentially (in any order) or using an external pervaporation unit [48]. The authors of study [48] discuss the efficiency of hybridization flowsheets through the combination or integration of membrane and distillation separation processes, which can provide a significant positive economic effect compared to previously considered methods. These conclusions are also supported by the results of studies [49–58] on the example of systems: methanol–methyl *tert*-butyl ether [49], isopropanol–water and propylene–propane [50], isopropanol–water (24% savings compared to azeotropic distillation) [52], ethanol–water [53], ethanol–water

(66% savings compared to heteroazeotropic distillation) [54], dimethylformamide–water [55], isobutanol–water [56], and methyl acetate–methanol (24% savings compared to ED and PSD, 31.7% compared to PSD with CSM) [57].

The diversity of phase behavior in liquid mixtures [1–3, 9, 14, 59], including in the presence of specially selected substances, determines the polyvariance of the choice of processes and methods, as well as the structures of separation technological flowsheets. The development of qualitative and quantitative criteria for the discrimination of processes, methods, and flowsheets at various stages of structural and parametric optimization remains an urgent objective. These include: analysis of physicochemical information about the properties of mixture components; the structure of the phase diagram (including the construction and analysis of the balance lines); assessment of the selectivity and feasibility of introducing EA; selection of separation processes and methods; determination of material flow rates when solving the balance problem (correct assignment of free variables); synthesis of separation flowsheets based on a specific process or the application of hybrid technologies, analysis of the operational equipment (meeting specific criteria: energy, economic, environmental) and separation results parameters; evaluation of the effectiveness of process or flowsheet management.

To minimize heat losses and reduce energy costs, many efforts are directed towards various types of heat integration, such as partial [21, 30, 35, 37, 39–42, 60–63], full [30, 64], internal [65], or external [66, 67]. An effective energy-saving measure consists in the use of complex columns (with side flows, DWC) [18, 29, 63] and heat pumps [68, 69]. The cost ratio (operational and annual) between separation options is not affected by restructuring the flows of the flowsheet or using complex columns; if the difference in separation costs in the initial flowsheets is significant, it can be reduced by one of the structural optimization options (the more optimal the structure and operating conditions of the initial flowsheet, the less effective the methods related to structural restructuring).

It is necessary to separately highlight the study of dynamic modes (control and stability to perturbations) of various processes [28, 70–75], which also influence the final choice of separation technology for a specific mixture.

CONCLUSIONS

The presented analysis of the scientific literature confirms that when developing separation flowsheets for specific mixtures, authors generally prefer a specific method, with ED being more frequently considered as the universal and energy-efficient separation method. The number of studies comparing alternative methods is significantly smaller; moreover, these are typically techniques based on a specific process (usually distillation). Flowsheets based on various mass transfer processes (hybrid technologies) are rarely considered. The criterion for comparing alternative separation variants is the total heat duty on the column reboilers and the TAC. As a rule, there is a complete correlation between these criteria. In rare cases, the contribution of capital costs to annual totals can be decisive, leading to different ratios of energy costs and TAC. Such a situation is observed if the flowsheets differ significantly in the total number of stages.

As confirmed by one of the processes (flowsheets) being placed in an a priori disadvantageous position (nonselective agents are chosen; the geometry of the phase diagram elements does not favor the use of the chosen method; the azeotrope shifts slightly when the pressure changes; etc.), the comparison of flowsheets is not always objective. Such variants can be excluded from consideration at the stage of studying the structure of the phase equilibrium diagram, synthesizing separation flowsheets, and calculating the material balance (up to the stage of parametric optimization).

In certain cases, the authors may reasonably prefer flowsheets characterized by higher energy consumption, which may be due to the physicochemical properties of the components of the base mixture or the newly added substances, as well as the specifics of the separation technology implementation.

The presented comparison of effective separation methods (cases where nonselective agents are chosen or the phase diagram structure is unfavorable for the chosen method are excluded) confirms that ED remains the most energy-efficient separation method. However, in some cases, its competitiveness significantly decreases compared to alternative methods, particularly HAD. The latter should be preferred for the separation of mixtures containing high-boiling components. The ratio of energy costs for the HAD and ED flowsheets will be significantly influenced by the composition of the initial mixture, which directly affects the solvent consumption, especially in the HAD process (agent is present in the azeotropic mixture in the column distillate). The latter process will be more advantageous if the content of the component in the initial mixture with which the solvent forms a heteroazeotrope exceeds the concentration of the second component. It is likely that the composition simplex of a binary system can

be conditionally divided into composition regions for which the cost ratio of the processes of HAD and ED (with the same agents) will be different. The significant reduction in energy consumption of the flowsheets by organizing ED and HAD in auto mode—and even more so by combining them—is due to the absence of the need to use an additional column for agent regeneration, as well as the lowering of the separation process temperature inside the column due to the formation of positive azeotropes.

Another effective separation technique is the combination of distillation and splitting process. The feasibility and practicality of implementing this method are significantly influenced by the specific arrangement of azeotropes, separatrix manifolds, and splitting simplices. The unfavorable arrangement of the latter when solving the balance problem leads to inflated values of columns distillate flows and difficulties in achieving certain compositions (for example, when touching the separatrix). If this technique can be effectively implemented independently (without the involvement of other specialized methods) then comparisons with other methods are not conducted since any other method is likely to be less effective.

A reduction in energy costs can be achieved by using a liquid separator (splitting) in complex flowsheets that combine different methods and processes. This is explained by the fact that phase separation is a spontaneous process; moreover, in some cases, one or both flows leaving the separator can represent product flows due to the almost complete insolubility of the components in each other.

When separating multicomponent mixtures, a question arises about the feasibility of using a particular method or process at different stages of separation (when separating mixtures with different numbers of components). The analyzed sources do not fully answer this question: a detailed study has been conducted only for one system and two methods (ED and PSD). The efficiency of these processes in separating a mixture of specific composition decreases with the increase in the number of components in the mixture being separated.

The comparison of extraction-based flowsheets with other separation variants is scarcely mentioned in other studies. When assessing the feasibility of combining extraction and distillation processes, it is important to consider the possibility of regenerating the extractant in the bottom of the column, especially in cases where the ratio of the amounts of the initial mixture to the extractant is ≤1.

Based on the conducted review of scientific literature, the following promising directions for further research in the synthesis of separation flowsheets for organic product mixtures through the use of various separation methods and processes can be formulated:

(1) evaluation of the effectiveness of applying different processes (extraction, liquid phase splitting, distillation, special distillation methods) at different stages of separation;
(2) comparative analysis of ED and HAD methods in the separation of mixtures with different initial compositions (identification of areas of energy advantage for each method);
(3) evaluation of the effectiveness of implementing flowsheets based on the combination of extraction with other processes, depending on the stage of extractant regeneration.

Acknowledgments

The work was conducted within the framework of the State Assignment of the Russian Federation, grant No. FSFZ-2023-0003.

Authors' contributions

A.V. Frolkova—management, formulation of the scientific concept of the study, critical literature review, and writing the text of the article.

A.N. Novruzova—collecting and processing the scientific literature, mathematical modeling the phase equilibria, and preparing illustrations and tables for the article.

The authors declare no conflicts of interest.

REFERENCES

1. Timofeev V.S., Serafimov L.A., Timoshenko A.V. *Printsipy tekhnologii osnovnogo organicheskogo i neftekhimicheskogo sinteza* (*The Principles of the Technology of Basic Organic and Petrochemical Synthesis*). Moscow: Vysshaya shkola; 2010. 408 p. (in Russ.). ISBN 978-5-06-006067-6
2. Zharov V.T., Serafimov L.A. *Fiziko-khimicheskie osnovy distillyatsii i rektifikatsii Physicochemical Principles of Distillation and Rectification*). Leningrad: Khimiya; 1975. 240 p. (in Russ.).
3. Frolkova A.K. *Razdelenie azeotropnykh smesei. Fiziko-khimicheskie osnovy i tekhnologicheskie priemy* (*Separation of Azeotropic Mixtures. Physicochemical Fundamentals and Technological Methods*). Moscow: VLADOS; 2010. 192 p. (in Russ.). ISBN 978-5-691-01743-8
4. Zhigang L., Chengyue L., Biaohua C. Extractive Distillation: A Review. *Sep. Purif. Rev*. 2003;32(2):121–213. https://doi.org/10.1081/SPM-120026627
5. Gerbaud V., Rodriguez-donis I., Hegely L., Lang P., Denes F., You X. Review of Extractive Distillation. Process design, operation, optimization and control. *Chem. Eng. Res. Des*. 2019;141:229–271. https://doi.org/10.1016/j.cherd.2018.09.020
6. Hilal N., Yousef G., Langston P. The reduction of extractive agent in extractive distillation and auto-extractive distillation. *Chemical Engineering and Processing: Process Intensification*. 2002;41(8):673–679. https://doi.org/10.1016/S0255-2701(01)00187-8
7. Anokhina E.A. Energy saving in extractive distillation. *Fine Chem. Technol*. 2013;8(5):3–19 (in Russ.).
8. Raeva V.M., Sazonova A.Yu., Sebyakin A.Yu., Kudryavtseva D.Yu. Criterion of choosing potential entrainers for extractive distillation. *Fine Chem. Technol*. 2011;6(4):20–27 (in Russ.).
9. Frolkova A.V., Merkulyeva A.D., Gaganov I.S. Synthesis of flowsheets for separation of multiphase mixtures: state of the art. *Fine Chem. Technol*. 2018;13(3):5–22 (in Russ.). https://doi.org/10.32362/24106593-2018-13-3-5-22
10. Frolkova A.V., Frolkova A.K., Podtiagina A.V., *et al.* Energy savings in flowsheets based on combination of distillation and splitting processes. *Theor. Found. Chem. Eng*. 2018;52(5):771–778. https://doi.org/10.1134/S0040579518050329 [Original Russian Text: Frolkova A.V., Frolkova A.K., Podtiagina A.V., Spiriakova V.V. Energy savings in flowsheets based on combination of distillation and splitting processes. *Teoreticheskie osnovy khimicheskoi tekhnologii.* 2018;52(5):489–496 (in Russ.). https://doi.org/10.1134/S0040357118050032]
11. Sosa J.E., Araújo J.M.M., Amado-González E., Pereiro A.B. Separation of azeotropic mixtures using protic ionic liquids as extraction solvents. *J. Mol. Liquids*. 2019;297:111733. https://doi.org/10.1016/j.molliq.2019.111733
12. Patel K., Panchal N., Ingle Dr.Pr. Review of Extraction Techniques Extraction Methods: Microwave, Ultrasonic, Pressurized Fluid, Soxhlet Extraction, Etc. *International Journal of Advanced Research in Chemical Science* (*IJARCS*). 2018;6(3):6–21. http://doi.org/10.20431/2349-0403.0603002
13. Silvestre Cr.I.C., Santos J.L.M., Lima J.L.F.C., Zagatto E.A.G. Liquid–liquid extraction in flow analysis: A critical review. *Anal. Chim. Acta*. 2009;652(1–2):54–65. https://doi.org/10.1016/j.aca.2009.05.042
14. Nosov G.A., Mikhailov M.V., Absattarov A.I. Separation of mixtures by combining rectification and fractional crystallization processes. *Fine Chem. Technol*. 2017;12(3):44–51 (in Russ.). https://doi.org/10.32362/2410-6593-2017-12-3-44-51

СПИСОК ЛИТЕРАТУРЫ

1. Тимофеев В.С., Серафимов Л.А., Тимошенко А.В. *Принципы технологии основного органического и нефтехимического синтеза*. М.: Высшая школа; 2010. 408 с. ISBN 978-5-06-006067-6
2. Жаров В.Т., Серафимов Л.А. *Физико-химические основы дистилляции и ректификации*. Л.: Химия; 1975. 240 с.
3. Фролкова А.К. *Разделение азеотропных смесей. Физико-химические основы и технологические приемы: монография*. М.: ВЛАДОС; 2010. 192 с. ISBN 978-5-691-01743-8
4. Zhigang L., Chengyue L., Biaohua C. Extractive Distillation: A Review. *Sep. Purif. Rev*. 2003;32(2):121–213. https://doi.org/10.1081/SPM-120026627
5. Gerbaud V., Rodriguez-Donis I., Hegely L., Lang P., Denes F., You X. Review of Extractive Distillation. Process design, operation, optimization and control. *Chem. Eng. Res. Des.* 2019;141:229–271. https://doi.org/10.1016/j.cherd.2018.09.020
6. Hilal N., Yousef G., Langston P. The reduction of extractive agent in extractive distillation and auto-extractive distillation. *Chemical Engineering and Processing: Process Intensification*. 2002;41(8):673–679. https://doi.org/10.1016/S0255-2701(01)00187-8
7. Анохина Е.А. Энергосбережение в процессах экстрактивной ректификации. *Тонкие химические технологии.* 2013;8(5):3–19.
8. Раева В.М., Сазонова А.Ю., Себякин А.Ю., Кудрявцева Д.Ю. Критерий выбора потенциальных разделяющих агентов экстрактивной дистилляции. *Тонкие химические технологии*. 2011;6(4):20–27.
9. Фролкова А.В., Меркульева А.Д., Гаганов И.С. Синтез схем разделения расслаивающихся смесей: современное состояние проблемы. *Тонкие химические технологии*. 2018;13(3):5–22. https://doi.org/10.32362/24106593-2018-13-3-5-22
10. Фролкова А.В., Фролкова А.К., Подтягина А.В., Спирякова В.В. Энергосбережение в схемах, основанных на сочетании ректификации и расслаивания. *Теор. основы хим. технологии*. 2018;52(5):489–496. https://doi.org/10.1134/S0040357118050032
11. Sosa J.E., Araújo J.M.M., Amado-González E., Pereiro A.B. Separation of azeotropic mixtures using protic ionic liquids as extraction solvents. *J. Mol. Liquids*. 2019;297:111733. https://doi.org/10.1016/j.molliq.2019.111733
12. Patel K., Panchal N., Ingle Dr.Pr. Review of Extraction Techniques Extraction Methods: Microwave, Ultrasonic, Pressurized Fluid, Soxhlet Extraction, Etc. *International Journal of Advanced Research in Chemical Science* (*IJARCS*). 2018;6(3):6–21. http://doi.org/10.20431/2349-0403.0603002
13. Silvestre Cr.I.C., Santos J.L.M., Lima J.L.F.C., Zagatto E.A.G. Liquid–liquid extraction in flow analysis: A critical review. *Anal. Chim. Acta.* 2009;652(1–2):54–65. https://doi.org/10.1016/j.aca.2009.05.042
14. Носов Г.А., Михайлов М.В., Абсаттаров А.И. Разделение смесей путем сочетания процессов ректификации и фракционной кристаллизации. *Тонкие химические технологии.* 2017;12(3):44–51. https://doi.org/10.32362/2410-6593-2017-12-3-44-51
15. Berry D.A, Ng K.M. Synthesis of crystallization-distillation hybrid separation processes. *AIChE J*. 1997;43(7):1751–1762. https://doi.org/10.1002/aic.690430712
16. Cisternas L.A., Vasquez C.M., Swaney R.E. On the Design of Crystallization-Based Separation Processes: Review and Extension. *AIChE J*. 2006;52(5):1754–1769. https://doi.org/10.1002/aic.10768
17. Серафимов Л.А. Современное состояние термодинамико-топологического анализа фазовых диаграмм. *Теор. основы хим. технологии.* 2009;43(3):284–294.

15. Berry D.A, Ng K.M. Synthesis of crystallization-distillation hybrid separation processes. *AIChE J*. 1997;43(7):1751–1762. https://doi.org/10.1002/aic.690430712
16. Cisternas L.A., Vasquez C.M., Swaney R.E. On the Design of Crystallization-Based Separation Processes: Review and Extension. *AIChE J*. 2006;52(5):1754–1769. https://doi.org/10.1002/aic.10768
17. Serafimov L.A. State of the art in the thermodynamic and topological analysis of phase diagrams. *Theor. Found. Chem. Eng.* 2009;43(3):268–278. https://doi.org/10.1134/S0040579509030051 [Original Russian Text: Serafimov L.A. State of the art in the thermodynamic and topological analysis of phase diagrams. *Teoreticheskie osnovy khimicheskoi tekhnologii.* 2009;43(3):284–294 (in Russ.).]
18. Kiss A.A., Suszwalak D. J-.P.C. Enhanced bioethanol dehydration by extractive and azeotropic distillation in dividing-wall columns. *Sep. Purif. Technol*. 2012;86:70–78. https://doi.org/10.1016/j.seppur.2011.10.022
19. Frolkova A.V., Frolkova A.K., Gaganov I.S. Comparison of Extractive and Heteroazeotropic Distillation of High-Boiling Aqueous Mixtures. *ChemEngineering* 2022;6(5):83. https://doi.org/10.3390/chemengineering6050083
20. Chen Y.-Ch., Yu B.-Y., Hsu Ch.-Ch., Chien I-L. Comparison of heteroazeotropic and extractive distillation for the dehydration of propylene glycol methyl ether. *Chem. Eng. Res. Des*. 2016;111:184–195. https://doi.org/10.1016/j.cherd.2016.05.003
21. Zhao L., Lyu X., Wang W., Shan J., Qiu T. Comparison of heterogeneous azeotropic distillation and extractive distillation methods for ternary azeotrope ethanol/toluene/water separation. *Comput. Chem. Eng*. 2017;100:27–37 https://doi.org/10.1016/j.compchemeng.2017.02.007
22. Frolkova A.V., Frolkova A.K., Gaganov I.S. Combination special techniques in development of separation schemes for mixture of methanol + water + methyl methacrylate. *Khimicheskaya Tekhnologiya*. 2023;24(8):314–320 (in Russ.). https://doi.org/10.31044/1684-5811-2023-24-8-314-320
23. Serafimov L.A. The azeotropic rule and the classification of multicomponent mixtures: VII. Diagrams for ternary systems mixtures. *Russ. J. Phys. Chem*. 1970;44(4):567–571. [Original Russian Text: Serafimov L.A. The azeotropic rule and the classification of multicomponent mixtures: VII. Diagrams for ternary systems mixtures. *Zhurnal fizicheskoi khimii.* 1970;44(4):1021–1027 (in Russ.).]
24. Klinov A.V., Fazlyev A.R., Khairullina A.R., Alekseev K.A., Latypov D.R. Extractive rectification of ethanol-water mixture using ethylene glycol. *Vestnik tekhnologicheskogo universiteta = Herald of Technological University*. 2023;26(1):44–47 (in Russ.). https://doi.org/10.55421/1998-7072_2023_26_1_44
25. Frolkova A.K., Frolkova A.V., Raeva V.M., Zhuchkov V.I. Features of distillation separation of multicomponent mixtures. *Fine Chem. Technol*. 2022;17(3):87–106. https://doi.org/10.32362/2410-6593-2022-17-2-87-106
26. Frolkova A., Frolkova A., Gaganov I. Extractive and Auto-Extractive Distillation of Azeotropic Mixtures. *Chem. Eng. Technol*. 2021;44(8):1397–1402. https://doi.org/10.1002/ceat.202100024
27. Luo H., Liang K., Li W., Ming Xia Y., Xu C. Comparison of PressureSwing Distillation and Extractive Distillation Methods for Isopropyl Alcohol/Diisopropyl Ether Separation. *Ind. Eng. Chem. Res.* 2014;53(39):15167–15182. https://doi.org/10.1021/ie502735g
28. Lladosa E., Montón J.B., Burguet M. Separation of di-*n*-propyl ether and *n*-propyl alcohol by extractive distillation and pressure-swing distillation: Computer simulation and economic optimization. *Chem. Eng. Process.: Process Intensif*. 2011;50(11–12):1266–1274. https://doi.org/10.1016/j.cep.2011.07.010
18. Kiss A.A., Suszwalak D. J-.P.C. Enhanced bioethanol dehydration by extractive and azeotropic distillation in dividing-wall columns. *Sep. Purif. Technol*. 2012;86:70–78. https://doi.org/10.1016/j.seppur.2011.10.022
19. Frolkova A.V., Frolkova A.K., Gaganov I.S. Comparison of Extractive and Heteroazeotropic Distillation of High-Boiling Aqueous Mixtures. *ChemEngineering* 2022;6(5):83. https://doi.org/10.3390/chemengineering6050083
20. Chen Y.-Ch., Yu B.-Y., Hsu Ch.-Ch., Chien I-L. Comparison of heteroazeotropic and extractive distillation for the dehydration of propylene glycol methyl ether. *Chem. Eng. Res. Des*. 2016;111:184–195. https://doi.org/10.1016/j.cherd.2016.05.003
21. Zhao L., Lyu X., Wang W., Shan J., Qiu T. Comparison of heterogeneous azeotropic distillation and extractive distillation methods for ternary azeotrope ethanol/toluene/water separation. *Comput. Chem. Eng*. 2017;100:27–37 https://doi.org/10.1016/j.compchemeng.2017.02.007
22. Фролкова А.В., Фролкова А.К., Гаганов И.С. Комбинирование специальных приемов при разработке схем разделения смеси метанол + вода + метилметакрилат. *Химическая технология*. 2023;24(8):314–320. https://doi.org/10.31044/1684-5811-2023-24-8-314-320
23. Серафимов Л.А. Правило азеотропии и классификация многокомпонентных смесей VII. Диаграммы трехкомпонентных смесей. *Журн. физ. химии*. 1970;44(4):1021–1027.
24. Клинов А.В., Фазлыев А.Р., Хайруллина А.Р., Алексеев К.А., Латыпов Д.Р. Экстрактивная ректификация смеси этанол – вода с использованием этиленгликоля. *Вестник технологического университета*. 2023;26(1):44–47. https://doi.org/10.55421/1998-7072_2023_26_1_44
25. Фролкова А.К., Фролкова А.В., Раева В.М., Жучков В.И. Особенности дистилляционного разделения многокомпонентных смесей. *Тонкие химические технологии*. 2022;17(3):87–106. https://doi.org/10.32362/2410-6593-2022-17-2-87-106
26. Frolkova A., Frolkova A., Gaganov I. Extractive and Auto-Extractive Distillation of Azeotropic Mixtures. *Chem. Eng. Technol*. 2021;44(8):1397–1402. https://doi.org/10.1002/ceat.202100024
27. Luo H., Liang K., Li W., Ming Xia Y., Xu C. Comparison of PressureSwing Distillation and Extractive Distillation Methods for Isopropyl Alcohol/Diisopropyl Ether Separation. *Ind. Eng. Chem. Res.* 2014;53(39):15167–15182. https://doi.org/10.1021/ie502735g
28. Lladosa E., Montón J.B., Burguet M. Separation of di-*n*-propyl ether and *n*-propyl alcohol by extractive distillation and pressure-swing distillation: Computer simulation and economic optimization. *Chem. Eng. Process.: Process Intensif*. 2011;50(11–12):1266–1274. https://doi.org/10.1016/j.cep.2011.07.010
29. Wang X., Xie L., Tian P., Tian G. Design and control of extractive dividing wall column and pressure-swing distillation for separating azeotropic mixture of acetonitrile/*N*-propanol. *Chem. Eng. Process.: Process Intensif*. 2016;110:172–187. https://doi.org/10.1016/j.cep.2016.10.009
30. Ghuge Pr.D., Mali N.A., Joshi S.S. Comparative Analysis of Extractive and Pressure Swing Distillation for Separation of THF-Water Separation. *Comput. Chem. Eng*. 2017;103:188–200. http://dx.doi.org/10.1016/j.compchemeng.2017.03.019
31. Muñoz R., Montón J.B., Burguet M.C., de la Torre J. Separation of isobutyl alcohol and isobutyl acetate by extractive distillation and pressure-swing distillation: Simulation and optimization. *Sep. Purif. Technol*. 2006;50(2):175–183. https://doi.org/10.1016/j.seppur.2005.11.022
32. Cao Y., Hu J., Jia H., Bu G., Zhu Zh., Wang Y. Comparison of pressure-swing distillation and extractive distillation with varied-diameter column in economics and dynamic control. *J. Process Control*. 2017;49:9–25. https://doi.org/10.1016/j.jprocont.2016.11.005

29. Wang X., Xie L., Tian P., Tian G. Design and control of extractive dividing wall column and pressure-swing distillation for separating azeotropic mixture of acetonitrile/*N*-propanol. *Chem. Eng. Process.: Process Intensif.* 2016;110:172–187. https://doi.org/10.1016/j.cep.2016.10.009
30. Ghuge Pr.D., Mali N.A., Joshi S.S. Comparative Analysis of Extractive and Pressure Swing Distillation for Separation of THF-Water Separation. *Comput. Chem. Eng*. 2017;103: 188–200. http://doi.org/10.1016/j.compchemeng.2017.03.019
31. Muñoz R., Montón J.B., Burguet M.C., de la Torre J. Separation of isobutyl alcohol and isobutyl acetate by extractive distillation and pressure-swing distillation: Simulation and optimization. *Sep. Purif. Technol*. 2006;50(2):175–183. https://doi.org/10.1016/j.seppur.2005.11.022
32. Cao Y., Hu J., Jia H., Bu G., Zhu Zh., Wang Y. Comparison of pressure-swing distillation and extractive distillation with varied-diameter column in economics and dynamic control. *J. Process Control*. 2017;49:9–25. https://doi.org/10.1016/j.jprocont.2016.11.005
33. Luyben W.L. Comparison of pressure-swing and extractive-distillation methods for methanol-recovery systems in the TAME reactive-distillation process. *Ind. Eng. Chem. Res.* 2005;44(15):5715–5725. https://doi.org/10.1021/ie058006q
34. Modla G., Lang P. Removal and Recovery of Organic Solvents from Aqueous Waste Mixtures by Extractive and Pressure Swing Distillation. *Ind. Eng. Chem. Res.* 2012;51(35): 11473–11481. https://doi.org/10.1021/ie300331d
35. Luyben W.L. Comparison of extractive distillation and pressure swing distillation for acetone-methanol separation. *Ind. Eng. Chem. Res*. 2008;47(8):2696−2707. https://doi.org/10.1021/ie701695u
36. Luyben W.L. Comparison of extractive distillation and pressure-swing distillation for acetone/chloroform separation. *Comput. Chem. Eng*. 2013;50:1–7. https://doi.org/10.1016/j.compchemeng.2012.10.014
37. Hosgor E., Kucuk T., Oksal I.N., Kaymak D.B. Design and control of distillation processes for methanol–chloroform separation. *Comput. Chem. Eng*. 2014;67:166–177. https://doi.org/10.1016/j.compchemeng.2014.03.026
38. Frolkova A.V., Shashkova Y.I., Frolkova A.K., Mayevskiy M.A. Comparison of alternative methods for methyl acetate + methanol + acetic acid + acetic anhydride mixture separation. *Fine Chem. Technol*. 2019;14(5):51–60. https://doi.org/10.32362/2410-6593-2019-14-5-51-60
39. Qin Y., Zhuang Y., Wang Ch., Dong Y., Zhang L., Liu L., Du J. Comparison of Pressure-Swing Distillation and Extractive Distillation for the Separation of the Non-Pressure-Sensitive Azeotropes. In: *Proceedings of the 24th Conference on Process Integration, Modelling and Optimisation for Energy Saving and Pollution Reduction*. 2021. URL: Comparison of Pressure-Swing Distillation and Extractive Distillation for the Separation of the Non-Pressure-Sensitive Azeotropes. Accessed September 08, 2025.
40. Raeva V.M., Kapranova A.S. Comparison efficiency of extractive agents at the separation of mixture acetone–methanol. *Khimicheskaya promyshlennost' segodnya = Chemical Industry Developments.* 2015;3:33–46 (in Russ.).
41. Guang C., Shi X., Zhang Z., Wang C., Wang C., Gao J. Comparison of heterogeneous azeotropic and pressure-swing distillations for separating the diisopropylether/isopropanol/water mixtures. *Chem. Eng. Res. Design*. 2019;143:249–260. https://doi.org/10.1016/j.cherd.2019.01.021
42. Cui Y., Shi X., Guang C., Zhang Z., Wang C., Wang C. Comparison of pressure-swing distillation and heterogeneous azeotropic distillation for recovering benzene and isopropanol from wastewater. *Process Saf. Environ. Protection*. 2018;122:1–12. https://doi.org/10.1016/j.psep.2018.11.017
33. Luyben W.L. Comparison of pressure-swing and extractive-distillation methods for methanol-recovery systems in the TAME reactive-distillation process. *Ind. Eng. Chem. Res.* 2005;44(15):5715–5725. https://doi.org/10.1021/ie058006q
34. Modla G., Lang P. Removal and Recovery of Organic Solvents from Aqueous Waste Mixtures by Extractive and Pressure Swing Distillation. *Ind. Eng. Chem. Res.* 2012;51(35): 11473–11481. https://doi.org/10.1021/ie300331d
35. Luyben W.L. Comparison of extractive distillation and pressure swing distillation for acetone-methanol separation. *Ind. Eng. Chem. Res*. 2008;47(8):2696−2707. https://doi.org/10.1021/ie701695u
36. Luyben W.L. Comparison of extractive distillation and pressure-swing distillation for acetone/chloroform separation. *Comput. Chem. Eng*. 2013;50:1–7. https://doi.org/10.1016/j.compchemeng.2012.10.014
37. Hosgor E., Kucuk T., Oksal I.N., Kaymak D.B. Design and control of distillation processes for methanol–chloroform separation. *Comput. Chem. Eng*. 2014;67:166–177. https://doi.org/10.1016/j.compchemeng.2014.03.026
38. Фролкова А.В., Шашкова Ю.И., Фролкова А.К., Маевский М.А. Сравнение альтернативных методов разделения смеси метилацетат – метанол – уксусная кислота – уксусный ангидрид. *Тонкие химические технологии*. 2019;14(5): 51–60. https://doi.org/10.32362/2410-6593-2019-14-5-51-60
39. Qin Y., Zhuang Y., Wang Ch., Dong Y., Zhang L., Liu L., Du J. Comparison of Pressure-Swing Distillation and Extractive Distillation for the Separation of the Non-Pressure-Sensitive Azeotropes. In: *Proceedings of the 24th Conference on Process Integration, Modelling and Optimisation for Energy Saving and Pollution Reduction*. 2021. URL: Comparison of Pressure-Swing Distillation and Extractive Distillation for the Separation of the Non-Pressure-Sensitive Azeotropes. Accessed September 08, 2025.
40. Раева В.М., Капранова А.С. Сравнение эффективности экстрактивных агентов при разделении смеси ацетон – метанол. *Химическая промышленность сегодня.* 2015;3:33–46.
41. Guang C., Shi X., Zhang Z., Wang C., Wang C., Gao J. Comparison of heterogeneous azeotropic and pressure-swing distillations for separating the diisopropylether/isopropanol/water mixtures. *Chem. Eng. Res. Design*. 2019;143:249–260. https://doi.org/10.1016/j.cherd.2019.01.021
42. Cui Y., Shi X., Guang C., Zhang Z., Wang C., Wang C. Comparison of pressure-swing distillation and heterogeneous azeotropic distillation for recovering benzene and isopropanol from wastewater. *Process Saf. Environ. Protection*. 2018;122:1–12. https://doi.org/10.1016/j.psep.2018.11.017
43. Tripodi A., Compagnoni M., Ramis G., Rossetti I. Pressure-swing or extraction-distillation for the recovery of pure acetonitrile from ethanol ammoxidation process: A comparison of efficiency and cost. *Chem. Eng. Res. Design*. 2017;127: 92–102. https://doi.org/10.1016/j.cherd.2017.09.018
44. Zhu Z., Wang Y., Hu J., Qi X., Wang Y. Extractive distillation process combined with decanter for separating ternary azeotropic mixture of toluene-methanol-water. *Chem. Eng. Trans*. 2017;61:763–768. https://doi.org/10.3303/CET1761125
45. Гаганов И.С., Белим С.С., Фролкова А.В., Фролкова А.К. Разработка схем разделения смеси получения фенола на основе анализа диаграмм фазового равновесия. *Теор. основы хим. технологии*. 2023;57(1):38–47. https://doi.org/10.31857/S0040357123010049
46. Новрузова А.Н., Фролкова А.В. Сравнение технологических схем разделения смеси ацетонитрил – вода, основанных на разных массообменных процессах. В сб.: *Химия и химическая технология: достижения и перспективы:* Сборник тезисов I Международной VII Всероссийской конференции. 2024. С. 0234.1–0234.6.

43. Tripodi A., Compagnoni M., Ramis G., Rossetti I. Pressure-swing or extraction-distillation for the recovery of pure acetonitrile from ethanol ammoxidation process: A comparison of efficiency and cost. *Chem. Eng. Res. Design*. 2017;127: 92–102. https://doi.org/10.1016/j.cherd.2017.09.018
44. Zhu Z., Wang Y., Hu J., Qi X., Wang Y. Extractive distillation process combined with decanter for separating ternary azeotropic mixture of toluene-methanol-water. *Chem. Eng. Trans*. 2017;61:763–768. https://doi.org/10.3303/CET1761125
45. Gaganov I.S., Belim S.S., Frolkova A.V., Frolkova A.K. Development of Flowsheet of Separation of a Phenol Production Mixture Based on the Analysis of Phase Equilibrium Diagrams. *Theor. Found. Chem. Eng*. 2023;57(1):35–44. https://doi.org/10.1134/S0040579523010049
[Original Russian Text: Gaganov I.S., Belim S.S., Frolkova A.V., Frolkova A.K. Development of Flowsheet of Separation of a Phenol Production Mixture Based on the Analysis of Phase Equilibrium Diagrams. *Teoreticheskie osnovy khimicheskoi tekhnologii.* 2023;57(1):38–47 (in Russ.). https://doi.org/10.31857/S0040357123010049]
46. Novruzova A.N., Frolkova A.V. Comparison of technological schemes of separation of the mixture acetonitrile – water, based on different mass transfer processes. In: *Chemistry and Chemical Technology: Achievements and Prospects:* Thesis Collection I of the 7th International All-Russian Conference. 2024. P. 0234.1-0234.6 (in Russ.).
47. Yu B.-Y., Huang R., Zhong X.-Y., Lee M.-J., Chien I.-L. Energy-Efficient Extraction-Distillation Process for Separating Diluted Acetonitrile-Water Mixture: Rigorous Design with Experimental Verification from Ternary Liquid-Liquid Equilibrium Data. *Ind. Eng. Chem. Res*. 2017;56(51): 15112–15121. https://doi.org/10.1021/acs.iecr.7b04408
48. Mahdi T., Ahmad A. Nasef M.M., Ripin A. State-of-the-Art Technologies for Separation of Azeotropic Mixtures. *Sep. Purif. Rev*. 2015;44(4):308–330. https://doi.org/10.1080/154 22119.2014.963607
49. Daviou M.C., Hoch P.M., Eliceche A.M. Design of membrane modules used in hybrid distillation/pervaporation systems. *Ind. Eng. Chem. Res*. 2004;43(13):3403–3412. https://doi.org/10.1021/ie034259c
50. Naidu Y., Malik R.K. A generalized methodology for optimal configurations of hybrid distillation–pervaporation processes. *Chem. Eng. Res. Design*. 2011;89(8):1348–1361. https://doi.org/10.1016/j.cherd.2011.02.025
51. Kookos I.K. Optimal design of membrane/distillation column hybrid processes. *Ind. Eng. Chem. Res*. 2003;42(8): 1731–1738. https://doi.org/10.1021/ie020616s
52. Hoof V.V., Van den Abeele L., Buekenhoudt A., Dotremont C., Leysen R. Economic comparison between azeotropic distillation and different hybrid systems combining distillation with pervaporation for the dehydration of isopropanol. *Sep. Purif. Technol*. 2004;37(1):33–49. https://doi.org/10.1016/j. seppur.2003.08.003
53. Nangare D.M., Suseeladevi M. Hybrid pervaporation/ distillation process for ethanol – water separation effect of distillation column side stream. *Asian J. Sci. Technol*. 2017;8(11):6522–6525.
54. Koczka K., Mizsey P., Fonyo Zs. Rigorous modelling and optimization of hybrid separation processes based on pervaporation. *Open Chemistry.* 2005;5(4):1124–1147. https://doi.org/10.2478/s11532-007-0050-8
55. Han G.L., Zhang Q., Zhong J., Shao H. Separation of Dimethylformamide/H_2O Mixtures Using Pervaporation-distillation Hybrid Process. *Adv. Mater. Res.* 2011;233–235:866–869. https://doi.org/10.4028/www.scientific.net/AMR.233-235.866
47. Yu B.-Y., Huang R., Zhong X.-Y., Lee M.-J., Chien I.-L. Energy-Efficient Extraction-Distillation Process for Separating Diluted Acetonitrile-Water Mixture: Rigorous Design with Experimental Verification from Ternary Liquid-Liquid Equilibrium Data. *Ind. Eng. Chem. Res*. 2017;56(51):15112–15121. https://doi.org/10.1021/acs.iecr.7b04408
48. Mahdi T., Ahmad A. Nasef M.M., Ripin A. State-of-the-Art Technologies for Separation of Azeotropic Mixtures. *Sep. Purif. Rev*. 2015;44(4):308–330. https://doi.org/10.1080/ 15422119.2014.963607
49. Daviou M.C., Hoch P.M., Eliceche A.M. Design of membrane modules used in hybrid distillation/pervaporation systems. *Ind. Eng. Chem. Res*. 2004;43(13):3403–3412. https://doi.org/10.1021/ie034259c
50. Naidu Y., Malik R.K. A generalized methodology for optimal configurations of hybrid distillation–pervaporation processes. *Chem. Eng. Res. Design*. 2011;89(8):1348–1361. https://doi.org/10.1016/j.cherd.2011.02.025
51. Kookos I.K. Optimal design of membrane/distillation column hybrid processes. *Ind. Eng. Chem. Res*. 2003;42(8): 1731–1738. https://doi.org/10.1021/ie020616s
52. Hoof V.V., Van den Abeele L., Buekenhoudt A., Dotremont C., Leysen R. Economic comparison between azeotropic distillation and different hybrid systems combining distillation with pervaporation for the dehydration of isopropanol. *Sep. Purif. Technol*. 2004;37(1):33–49. https://doi.org/10.1016/j. seppur.2003.08.003
53. Nangare D.M., Suseeladevi M. Hybrid pervaporation/ distillation process for ethanol – water separation effect of distillation column side stream. *Asian J. Sci. Technol*. 2017;8(11):6522–6525.
54. Koczka K., Mizsey P., Fonyo Zs. Rigorous modelling and optimization of hybrid separation processes based on pervaporation. *Open Chemistry.* 2005;5(4):1124–1147. https://doi.org/10.2478/s11532-007-0050-8
55. Han G.L., Zhang Q., Zhong J., Shao H. Separation of Dimethylformamide/H_2O Mixtures Using Pervaporation-distillation Hybrid Process. *Adv. Mater. Res.* 2011;233–235:866–869. https://doi.org/10.4028/www.scientific.net/AMR.233-235.866
56. Hassankhan B., Raisi A. Separation of isobutanol/water mixtures by hybrid distillationpervaporation process: Modeling, simulation and economic comparison. *Chem. Eng. Process.: Process Intensif.* 2020;155:108071. https://doi.org/10.1016/j.cep.2020.108071
57. Zong Ch., Guo Q., Shen B., Yang X., Zhou H., Jin W. Heat-Integrated Pervaporation−Distillation Hybrid System for the Separation of Methyl Acetate−Methanol Azeotropes. *Ind. Eng. Chem. Res*. 2021;60(28):10327–10337. https://doi.org/10.1021/acs.iecr.1c01513
58. Penkova A.V., Polotskaya G.A., Toikka A.M. Separation of acetic acid–methanol–methyl acetate–water reactive mixture. *Chem. Eng. Sci.* 2013;101:586–592. https://doi.org/10.1016/j.ces.2013.05.055
59. Тойкка А.М., Самаров А.А., Тойкка М.А. Фазовое и химическое равновесие в многокомпонентных флюидных системах с химической реакцией. *Успехи химии*. 2015;84(4):378–392. https://doi.org/10.1070/RCR4515
60. Wang Y., Zhang Z., Zhang H., Zhang Q. Control of heat integrated pressure-swing-distillation process for separating azeotropic mixture of tetrahydrofuran and methanol. *Ind. Eng. Chem. Res*. 2015;54(5):1646–1655. https://doi.org/10.1021/ie505024q
61. Zhu Z., Wang L., Ma Y., Wang W., Wang Y. Separating an azeotropic mixture of toluene and ethanol via heat integration pressure swing distillation. *Comput. Chem. Eng*. 2015;76: 137–149. https://doi.org/10.1016/j.compchemeng.2015.02.016

56. Hassankhan B., Raisi A. Separation of isobutanol/water mixtures by hybrid distillationpervaporation process: Modeling, simulation and economic comparison. *Chem. Eng. Process.: Process Intensif.* 2020;155:108071. https://doi.org/10.1016/j.cep.2020.108071
57. Zong Ch., Guo Q., Shen B., Yang X., Zhou H., Jin W. Heat-Integrated Pervaporation−Distillation Hybrid System for the Separation of Methyl Acetate−Methanol Azeotropes. *Ind, Eng. Chem. Res*. 2021;60(28):10327–10337. https://doi.org/10.1021/acs.iecr.1c01513
58. Penkova A.V., Polotskaya G.A., Toikka A.M. Separation of acetic acid–methanol–methyl acetate–water reactive mixture. *Chem. Eng. Sci.* 2013;101:586–592. https://doi.org/10.1016/j.ces.2013.05.055
59. Toikka A.M., Samarov A.A., Toikka M.A. Phase and chemical equilibria in multicomponent fluid systems with a chemical reaction. *Russ. Chem. Rew.* 2015;84(4):378–392. https://doi.org/10.1070/RCR4515
[Original Russian Text: Toikka A.M., Samarov A.A., Toikka M.A. Phase and chemical equilibria in multicomponent fluid systems with a chemical reaction. *Uspekhi khimii.* 2015;84(4):378–392 (in Russ.). https://doi.org/10.1070/RCR4515]
60. Wang Y., Zhang Z., Zhang H., Zhang Q. Control of heat integrated pressure-swing-distillation process for separating azeotropic mixture of tetrahydrofuran and methanol. *Ind. Eng. Chem. Res*. 2015;54(5):1646–1655. https://doi.org/10.1021/ie505024q
61. Zhu Z., Wang L., Ma Y., Wang W., Wang Y. Separating an azeotropic mixture of toluene and ethanol via heat integration pressure swing distillation. *Comput. Chem. Eng*. 2015;76: 137–149. https://doi.org/10.1016/j.compchemeng.2015.02.016
62. Anokhina E.A., Timoshenko A.V. Synthesis of the thermally coupled distillation sequences. *Fine Chem. Technol*. 2017;12(6):46–70 (in Russ.). https://doi.org/10.32362/2410-6593-2017-12-6-46-70
63. Anokhina E.A., Timoshenko A.V. Effect of the Side-Stream Location and the Side-Stream Value on the Optimal Entrainer Flowrate in Thermally Coupled Extractive Distillation Columns. *Theor. Found. Chem. Eng*. 2023;57(2):165–175. https://doi.org/10.1134/s0040579523010013
[Original Russian Text: Anokhina E.A., Timoshenko A.V. Effect of the Side-Stream Location and the Side-Stream Value on the Optimal Entrainer Flowrate in Thermally Coupled Extractive Distillation Columns. *Teoreticheskie osnovy khimicheskoi tekhnologii.* 2023;57(2)165–175 (in Russ.). https://doi.org/10.1134/S0040579523010013]
64. Yu B., Wang Q., Xu C. Design and control of distillation system for methylal/methanol separation. Part 2: pressure swing distillation with full heat integration. *Ind. Eng. Chem. Res*. 2012;51(3):1293–1310. https://doi.org/10.1021/ie201949q
65. Shirsat S.P. Modeling, simulation and control of an internally heat integrated pressure swing distillation process for bioethanol separation. *Comput. Chem. Eng*. 2013;53:201–202. https://doi.org/10.1016/j.compchemeng.2013.01.009
66. Liu G., Chen Z., Huang K., Shi Z., Chen H., Wang S. Studies of the externally heat-integrated double distillation columns (EHIDDiC). *Asia-Pacific J. Chem. Eng*. 2011;6(3):327–337. https://doi.org/10.1002/apj.566
67. Huang K., Liu W., Ma J., Wang S. Externally heat-integrated double distillation column (EHIDDiC): basic concept and general characteristics. *Ind. Eng. Chem. Res*. 2010;49(3): 1333–1350. https://doi.org/10.1021/ie901307j
68. Rudakov D.G., Klauzner P.S., Ramochnikov D.A., Anokhina E.A., Timoshenko A.V. Efficiency of Using Heat Pumps in the Extractive Rectification of an Allyl Alcohol–Allyl Acetate Mixture Depending on the Composition of the Feed. Part 2. Application of Heat Pumps in Column Complexes with Partially Coupled Heat and Material Flows. *Theor. Found. Chem. Eng*. 2024;58(1):192–201. https://doi.org/10.1134/S0040579524700337
62. Анохина Е.А., Тимошенко А.В. Синтез схем ректификации со связанными тепловыми и материальными потоками. *Тонкие химические технологии*. 2017;12(6):46–70. https://doi.org/10.32362/2410-6593-2017-12-6-46-70
63. Анохина Е.А., Тимошенко А.В. Влияние количества и уровня бокового отбора на расход экстрактивного агента в комплексах экстрактивной ректификации с частично связанными тепловыми и материальными потоками. *Теор. основы хим. технологии*. 2023;57(2):177–187. https://doi.org/10.31857/S0040357123010013
64. Yu B., Wang Q., Xu C. Design and control of distillation system for methylal/methanol separation. Part 2: pressure swing distillation with full heat integration. *Ind. Eng. Chem. Res*. 2012;51(3):1293–1310. https://doi.org/10.1021/ie201949q
65. Shirsat S.P. Modeling, simulation and control of an internally heat integrated pressure swing distillation process for bioethanol separation. *Comput. Chem. Eng*. 2013;53:201–202. https://doi.org/10.1016/j.compchemeng.2013.01.009
66. Liu G., Chen Z., Huang K., Shi Z., Chen H., Wang S. Studies of the externally heat-integrated double distillation columns (EHIDDiC). *Asia-Pacific J. Chem. Eng*. 2011;6(3):327–337. https://doi.org/10.1002/apj.566
67. Huang K., Liu W., Ma J., Wang S. Externally heat-integrated double distillation column (EHIDDiC): basic concept and general characteristics. *Ind. Eng. Chem. Res*. 2010;49(3): 1333–1350. https://doi.org/10.1021/ie901307j
68. Rudakov D.G., Klauzner P.S., Ramochnikov D.A., Anokhina E.A., Timoshenko A.V. Efficiency of Using Heat Pumps in the Extractive Rectification of an Allyl Alcohol–Allyl Acetate Mixture Depending on the Composition of the Feed. Part 2. Application of Heat Pumps in Column Complexes with Partially Coupled Heat and Material Flows. *Theor. Found. Chem. Eng*. 2024;58(1):192–201. https://doi.org/10.1134/S0040579524700337
69. Клаузнер П.С., Рудаков Д.Г., Анохина Е.А., Тимошенко А.В. Закономерности применения тепловых насосов в экстрактивной ректификации. *Теор. основы хим. технологии*. 2022;56(3):313–325. https://doi.org/10.31857/S0040357122030071
70. Wang Y., Zhang Z., Xu D., Liu W., Zhu Z. Design and control of pressure-swing distillation for azeotropes with different types of boiling behavior at different pressures. *J. Process. Control.* 2016;42:59–76. https://doi.org/10.1016/j.jprocont.2016.04.006
71. Luyben W.L. Control comparison of conventional and thermally coupled ternary extractive distillation processes. *Chem. Eng. Res. Des*. 2016;106:253–262. https://doi.org/10.1016/j.cherd.2015.11.021
72. Gil I.D., Gómez J.M., Rodríguez G. Control of an extractive distillation process to dehydrate ethanol using glycerol as entrainer. *Comput. Chem. Eng*. 2012;39:129–142. https://doi.org/10.1016/j.compchemeng.2012.01.006
73. Qin J., Ye Q., Xiong X., Li N. Control of benzene-cyclohexane separation system via extractive distillation using sulfolane as entrainer. *Ind. Eng. Chem. Res*. 2013;52(31):10754–10766. https://doi.org/10.1021/ie401101c
74. Wei H.-M., Wang F., Zhang J.-L., Liao B., Zhao N., Xiao F., Wei W., Sun Y. Design and control of dimethyl carbonate-methanol separation via pressure-swing distillation. *Ind. Eng. Chem. Res*. 2013;52(33):11463–11478. https://doi.org/10.1021/ie3034976
75. Fan Z., Zhang X., Cai W., Wang F. Design and control of extraction distillation for dehydration of tetrahydrofuran. *Chem. Eng. Technol*. 2013;36(5):829–839. https://doi.org/10.1002/ceat.201200611

69. Klauzner P.S., Rudakov D.G., Anokhina E.A., Timoshenko A.V. Application Regularities of Heat Pumps in Extractive Distillation. *Theor. Found. Chem. Eng*. 2022;56(3):308–320. https://doi.org/10.1134/S0040579522030071 [Original Russian Text: Klauzner P.S., Rudakov D.G., Anokhina E.A., Timoshenko A.V. Application Regularities of Heat Pumps in Extractive Distillation. *Teoreticheskie osnovy khimicheskoi tekhnologii.* 2022;56(3):313–325 (in Russ.). https://doi.org/10.31857/S0040357122030071]
70. Wang Y., Zhang Z., Xu D., Liu W., Zhu Z. Design and control of pressure-swing distillation for azeotropes with different types of boiling behavior at different pressures. *J. Process. Control.* 2016;42:59–76. https://doi.org/10.1016/j.jprocont.2016.04.006
71. Luyben W.L. Control comparison of conventional and thermally coupled ternary extractive distillation processes. *Chem. Eng. Res. Des*. 2016;106:253–262. https://doi.org/10.1016/j.cherd.2015.11.021
72. Gil I.D., Gómez J.M., Rodríguez G. Control of an extractive distillation process to dehydrate ethanol using glycerol as entrainer. *Comput. Chem. Eng*. 2012;39:129–142. https://doi.org/10.1016/j.compchemeng.2012.01.006
73. Qin J., Ye Q., Xiong X., Li N. Control of benzene-cyclohexane separation system via extractive distillation using sulfolane as entrainer. *Ind. Eng. Chem. Res*. 2013;52(31):10754–10766. https://doi.org/10.1021/ie401101c
74. Wei H.-M., Wang F., Zhang J.-L., Liao B., Zhao N., Xiao F., Wei W., Sun Y. Design and control of dimethyl carbonate-methanol separation via pressure-swing distillation. *Ind. Eng. Chem. Res*. 2013;52(33):11463–11478. https://doi.org/10.1021/ie3034976
75. Fan Z., Zhang X., Cai W., Wang F. Design and control of extraction distillation for dehydration of tetrahydrofuran. *Chem. Eng. Technol*. 2013;36(5):829–839. https://doi.org/10.1002/ceat.201200611

About the Authors

Anastasiya V. Frolkova, Dr. Sci. (Eng.), Professor, Department of Chemistry and Technology of Basic Organic Synthesis, M.V. Lomonosov Institute of Fine Chemical Technologies, MIREA – Russian Technological University (78, Vernadskogo pr., Moscow, 119454, Russia). E-mail: frolkova_nastya@mail.ru. Scopus Author ID 12782832700, ResearcherID N-4517-2014, RSCI SPIN-code 4504-2591, https://orcid.org/0000-0001-5675-5777

Albina N. Novruzova, Postgraduate Student, Department of Chemistry and Technology of Basic Organic Synthesis, M.V. Lomonosov Institute of Fine Chemical Technologies, MIREA – Russian Technological University (78, Vernadskogo pr., Moscow, 119454, Russia). E-mail: albina.novruzova2018@yandex.ru. RSCI SPIN-code 5681-8304, https://orcid.org/0009-0008-1637-8266

Об авторах

Фролкова Анастасия Валериевна, д.т.н., доцент, профессор кафедры химии и технологии основного органического синтеза, Институт тонких химических технологий им. М.В. Ломоносова, ФГБОУ ВО «МИРЭА – Российский технологический университет» (119454, Россия, Москва, пр-т Вернадского, д. 78). E-mail: frolkova_nastya@mail.ru. Scopus Author ID 12782832700, ResearcherID N-4517-2014, SPIN-код РИНЦ 4504-2591, https://orcid.org/0000-0001-5675-5777

Новрузова Альбина Назимовна, аспирант, кафедра химии и технологии основного органического синтеза, Институт тонких химических технологий им. М.В. Ломоносова, ФГБОУ ВО «МИРЭА – Российский технологический университет» (119454, Россия, Москва, пр-т Вернадского, д. 78). E-mail: albina.novruzova2018@yandex.ru. SPIN-код РИНЦ 5681-8304, https://orcid.org/0009-0008-1637-8266

Translated from Russian into English by H. Moshkov
Edited for English language and spelling by Thomas A. Beavitt

Tonkie Khimicheskie Tekhnologii = Fine Chemical Technologies.
2025;20(5):430–440
ISSN 2686-7575 (Online)

Chemistry and technology of medicinal compounds
and biologically active substances

Химия и технология лекарственных препаратов
и биологически активных соединений

UDC 57:615.1
https://doi.org/10.32362/2410-6593-2025-20-5-430-440
EDN AHUIDO

RESEARCH ARTICLE

Enhanced ibuprofen loading capacity of chitosan nanoparticles for prolonged release: A comprehensive study

Nga H.N. Do[1,2], Phuong Khanh Thy Vo[1,2], Thanh V.N. Le[1,2], Hung D. Vuong[1,2], Trang P.T. Nguyen[1,2], Phung K. Le[3], Anh C. Ha[1,2]✉

[1] *Faculty of Chemical Engineering, Ho Chi Minh City University of Technology (HCMUT), 268 Ly Thuong Kiet Street, Dien Hong Ward, Ho Chi Minh City, Viet Nam*

[2] *Vietnam National University Ho Chi Minh City, Linh Trung Ward, Thu Duc City, Ho Chi Minh City, Viet Nam*

[3] *CIRTech Institute, HUTECH University, Ho Chi Minh City, Viet Nam*

✉ *Corresponding author, e-mail: hcanh@hcmut.edu.vn*

Abstract

Objectives. Oral administration of ibuprofen often requires much higher doses than the necessary therapeutic dose due to the low solubility and first-pass metabolism of this anti-inflammatory drug. In order to improve its solubility and bioavailability, orally administered ibuprofen can be encapsulated into chitosan nanoparticles. The release of ibuprofen from chitosan nanoparticles can be pH-controlled to increase drug delivery efficiency when passing through the gastrointestinal tract. While ionic gelation provides versatile nanochitosan synthesis, the impact of the chitosan-to-tripolyphosphate (CS/TPP) ratio on encapsulation efficiency (EE) and loading capacity (LC) of the ibuprofen-loaded chitosan nanoparticles (IBU-CSNPs), as well as their release behavior under various pH conditions, remains unexplored. The study aims to determine the appropriate CS/TPP ratio for the highest EE and LC, as well as to evaluate the morphology, release behavior, and degradability of the IBU-CSNPs under optimal conditions.

Methods. The effect of CS/TPP ratio on the EE and LC of nanoparticle-loaded ibuprofen is studied by comparing the total and free concentrations of the drug and the weights of the CSNPs and IBU-CSNPs. To elucidate the characteristic properties of the IBU-CSNPs prepared at the optimal CS/TPP ratio, in-depth characterization was performed, including their morphology, chemical structure, crystallinity profile, *in vitro* degradation, and release behavior. The release profile of the IBU-CSNPs is studied under simulated gastric fluid (SGF), intestinal fluid (SIF), and sequential conditions of SGF and SIF.

Results. EE and LC were found to be significantly enhanced by an appropriate 1 : 1 mg/mg ratio, reaching 77.70 ± 0.65% and 46.62 ± 0.39%, respectively. The fabricated IBU-CSNPs exhibit a spherical shape with a uniform size distribution of approximately 50–60 nm and accelerated degradation compared to the unadulterated chitosan nanoparticles under simulated gastrointestinal conditions. The synthesized IBU-CSNPs demonstrate remarkable acid resistance by a minimal drug release of 9.44% in SGF after 3 h. However, a sustained release pattern in SIF achieves an equilibrium cumulative release of 94.51% over 5 days. The elaboration of drug release kinetics using the Kopcha and Korsmeyer–Peppas models suggests erosion-controlled release in SGF and diffusion-controlled release with swellable ability in SIF.

Conclusions. The results represent valuable insights into the formulation of pH-responsive IBU-CSNPs for the controlled delivery of ibuprofen via oral administration.

Keywords

chitosan nanoparticles, ibuprofen, pH-controlled release, encapsulation efficiency, loading capacity

Submitted: 12.01. 2025
Revised: 08.07.2025
Accepted: 01.09.2025

For citation

Do N.H.N., Vo P.K.T., Le T.V.N., Vuong H.D., Nguyen T.P.T., Le P.K., Ha A.C. Enhanced ibuprofen loading capacity of chitosan nanoparticles for prolonged release: A comprehensive study. *Tonk. Khim. Tekhnol. = Fine Chem. Technol*. 2025;20(5):430–440. https://doi.org/10.32362/2410-6593-2025-20-5-430-440

НАУЧНАЯ СТАТЬЯ

Комплексное исследование способности наночастиц хитозана к пролонгированному высвобождению ибупрофена

Nga H.N. Do[1,2], Phuong Khanh Thy Vo[1,2], Thanh V.N. Le[1,2], Hung D. Vuong[1,2], Trang P.T. Nguyen[1,2], Phung K. Le[3], Anh C. Ha[1,2,✉]

[1] *Faculty of Chemical Engineering, Ho Chi Minh City University of Technology (HCMUT), 268 Ly Thuong Kiet Street, Dien Hong Ward, Ho Chi Minh City, Viet Nam*

[2] *Vietnam National University Ho Chi Minh City, Linh Trung Ward, Thu Duc City, Ho Chi Minh City, Viet Nam*

[3] *CIRTech Institute, HUTECH University, Ho Chi Minh City, Viet Nam*

✉ *Автор для переписки, e-mail: hcanh@hcmut.edu.vn*

Аннотация

Цели. Пероральное применение ибупрофена часто требует значительно более высоких доз, чем необходимая терапевтическая доза, из-за низкой растворимости и быстрого метаболизма этого противовоспалительного препарата. Чтобы улучшить его растворимость и биодоступность, ибупрофен, вводимый перорально, может быть инкапсулирован в наночастицы хитозана. Для того, чтобы повысить эффективность доставки лекарства при прохождении через желудочно-кишечный тракт, можно регулировать высвобождение ибупрофена из наночастиц хитозана, контролируя pH. В то время как ионное гелеобразование обеспечивает универсальный синтез нанохитозана, влияние соотношения хитозана и триполифосфата (CS/TPP) на эффективность инкапсуляции и загрузочную способность наночастиц хитозана, содержащих ибупрофен (IBU-CSNPS), а также на их высвобождение при различных значениях pH, остается неизученным. Цель исследования — определить подходящее соотношение CS/TPP для получения наивысших значений инкапсуляции и загрузочной способности, а также оценить морфологию, характеристики высвобождения и способность к разложению IBU-CSNPS в оптимальных условиях.

Методы. Влияние соотношения CS/TPP на инкапсуляцию и загрузочную способность ибупрофена, содержащего наночастицы, изучают путем сравнения общей и свободной концентраций препарата и масс CSNP и IBU-CSNP. Для выяснения характерных свойств IBU-CSNPs, приготовленных при оптимальном соотношении CS/TPP, был проведен углубленный анализ, включающий их морфологию, химическую структуру, профиль кристалличности, разложение *in vitro* и поведение при высвобождении. Профиль высвобождения IBU-CSNPs изучался с помощью моделирования поведения IBU-CSNPs в желудочной и кишечной жидкостях, а также при последовательном введении в желудочную и кишечную жидкости.

Результаты. Найдено, что инкапсуляция и загрузочная способность IBU-CSNPs значительно повышаются при соотношении CS/TPP = 1 : 1 мг/мг, достигая 77.70 ± 0.65% и 46.62 ± 0.39% соответственно. Модельные наночастицы IBU-CSNPs имеют сферическую форму с равномерным распределением по размерам (приблизительно 50–60 нм) и ускоренным разложением по сравнению с наночастицами чистого хитозана в условиях, имитирующих желудочно-кишечный тракт. Синтезированные IBU-CSNPs демонстрируют значительную кислотоустойчивость благодаря минимальному высвобождению лекарственного средства — 9.44% в желудочной жидкости через 3 часа. Однако при длительном нахождении в кишечной жидкости достигается равновесное кумулятивное высвобождение в размере 94.51% в течение 5 дней. Кинетика высвобождения лекарственного средства с использованием моделей Копча и Корсмейера–Пеппаса предполагает высвобождение с контролем эрозии в желудочной жидкости и высвобождение со способностью к набуханию и контролем диффузии в кишечной жидкости.

Выводы. Полученные результаты представляют значительную ценность в разработке PH-чувствительных IBU-CSNPs для контролируемой доставки ибупрофена при пероральном приеме.

Ключевые слова

наночастицы хитозана, ибупрофен, высвобождение с регулируемым pH, эффективность инкапсуляции, несущая способность

Поступила: 12.01. 2025
Доработана: 08.07.2025
Принята в печать: 01.09.2025

Для цитирования

Do N.H.N., Vo P.K.T., Le T.V.N., Vuong H.D., Nguyen T.P.T., Le P.K., Ha A.C. Enhanced ibuprofen loading capacity of chitosan nanoparticles for prolonged release: A comprehensive study. *Tonk. Khim. Tekhnol. = Fine Chem. Technol*. 2025;20(5):430–440. https://doi.org/10.32362/2410-6593-2025-20-5-430-440

INTRODUCTION

Ibuprofen is a nonsteroidal anti-inflammatory drug that exerts nonselective inhibition on cyclo-oxygenase-1 and cyclo-oxygenase-2 to hinder the transformation of arachidonic acid into prostaglandins, which play a key role in pyrexia, inflammation, and pain sensation. Ibuprofen is predominantly administered orally at a dosage of 200–600 mg every 6 hours. However, the required dose for therapeutic effect is only about 20–30 mg/kg, which means that the oral dosage of ibuprofen is 10–20 times higher than the necessary therapeutic dose [1]. This is a drawback of oral ibuprofen usage owing to the low solubility (0.685 mg/mL at 37°C) [2] and the first-pass metabolism of the drug. Ibuprofen overdosage may result in some reported adverse effects, including gastrointestinal problems (heartburn, indigestion, nausea, and vomiting), uncommon metabolic acidosis, as well as rarely experienced effects on the central nervous system [3]. The low dissolution rate of ibuprofen contributes to its low bioavailability, even when administered at high oral doses. Many attempts have been made to formulate ibuprofen into topical products such as creams and gels as an alternative to oral administration. However, these alternatives also exhibit limited therapeutic concentration of ibuprofen because of its poor skin permeability [4].

An alternative strategy for enhancing the solubility of ibuprofen for oral administration is to encapsulate it into a nanoscale drug delivery system. By protecting the drug from bio-metabolism, the encapsulation of ibuprofen into nanoparticles improves absorption, as well as decreasing the frequency and dose of administration [5]. In general, nano-sized carrier systems having a large surface area have a significant advantage in improving the solubility of hydrophobic drugs. In order for the nanoparticles to be considered as suitable delivery systems, they must demonstrate suitable properties such as biodegradability, biocompatibility, and non-toxicity. For this reason, naturally derived polymers emerge as promising materials for the synthesis of ibuprofen-encapsulated nanoparticles. In recent years, chitosan has become a widely used bio-based polymer for the fabrication of nano-sized drug delivery systems. This is attributed to its distinctive chemical structure containing functional groups of the amino ($–NH_2$) and hydroxyl (–OH), as well as biocompatibility, mucoadhesion, and low toxicity. Under appropriate conditions, ibuprofen with the carboxylic group interacts with the chitosan chains through electrostatic interactions and hydrogen bonding between the functional groups of chitosan and ibuprofen, resulting in the entrapment of the drug within the polymeric matrix [6]. During the synthesis of ibuprofen-loaded chitosan nanoparticles (IBU-CSNPs), cross-linking agents are utilized in association with mechanical methods like ultra-sonication or homogenization to facilitate the formation of the nano-sized particles. In the case of chitosan nanoparticles, tripolyphosphate (TPP) is applied to promote the ionic gelation process via ionic interactions between the negatively charged TPP and positively charged chitosan groups in combination with mechanical stirring or homogenization-ultrasonication. IBU-CSNPs were successfully synthesized by following the ionic gelation method with TPP as the cross-linker and *in situ* loading of ibuprofen, achieving an encapsulation efficiency (EE) and loading capacity (LC) of 68.94 ± 1.61% and 28 ± 1.18%, respectively. The release of ibuprofen from the fabricated IBU-CSNPs reached an equilibrium state after 15 h with cumulative drug release (CDR) of 86.79 ± 1.02% and 77.27 ± 1.48% in simulated gastric fluid (SGF) and simulated intestinal fluid (SIF), respectively. The IBU release mechanism from the IBU-CSNPs is mainly driven by Fickian diffusion according to the Ritger–Peppas model [7]. Another study conducted by Olvera Rodríguez *et al*., which is focused on synthesizing IBU-CSNPs for pulmonary therapy, uses the same ionic crosslinking method with TPP but incorporating a post-loading approach for ibuprofen. After the formation of chitosan nanoparticles, these particles were dispersed in an ibuprofen solution, allowing the drug to diffuse into and anchor onto the chitosan nanoparticles via surface adsorption. This incubation method achieved a high EE of 80% across all tested drug concentrations (1000 mg/mL, 500 mg/mL, and 250 mg/mL). The particle size of IBU-CSNPs was found to range from 5 to 20 nm [8].

One key benefit of the ionic gelation for the synthesis of chitosan nanoparticles is the ease with which their characteristics, including particle size, EE, LC, and release behavior, may be adjusted by manipulating technological parameters such as chitosan-to-TPP (CS/TPP) ratio, pH, temperature, and velocity of chitosan and TPP mixing [9]. However, to the best of our knowledge, no study has evaluated the influence of the CS/TPP ratio on the EE and LC of IBU-CSNPs to suggest the appropriate IBU-CSNPs synthesis condition for enhanced drug encapsulation. Moreover, the existing works have only investigated the release kinetics of IBU-CSNPs in batches of SGF and SIF without examining the release profile under conditions of sequential pH change.

In the present study, batch experiments are performed to fabricate IBU-CSNPs with varying CS/TPP ratios from 1 : 0.25 to 1 : 3 (mg/mg) to assess the impact of this parameter on the drug LC of the nanoparticles and figure out the appropriate synthesis condition. Additionally,

various properties of morphology, chemical structure, crystallinity, and degradability of the IBU-CSNPs under the determined synthesis condition are comprehensively analyzed. The *in vitro* drug release profile of the IBU-CSNPs in different simulated environments is investigated by employing diverse mathematical models of zero order, first order, Higuchi, Kormeyer–Peppas, and Kopcha.

2. MATERIALS AND METHOD

2.1. Materials

Chitosan with a molecular weight of 158 kDa and a degree of deacetylation of above 80% was supplied by *Vietnam Food* (Vietnam). Ibuprofen (IBU, ≥98%) and phosphate-buffered saline (PBS) were obtained from *Sigma-Aldrich*, USA. Dialysis Flat Tubing with a molecular weight cut-off of 14000 kDa was supplied by *Frey Scientific*, USA. Acetic acid (CH_3COOH, 99.5%), lactic acid (85.5–90%), hydrochloric acid (HCl, 36%), sodium tripolyphosphate (TPP, 56–60%), and ethanol (99.5%) were purchased from *Xilong*, China. In order to prepare solutions, distilled water was utilized.

2.2. Preparation of chitosan nanoparticles loaded with ibuprofen (IBU-CSNPs)

Chitosan is firstly dissolved in 1% acetic acid solution under continuous stirring to prepare a chitosan solution of 3.75 mg/mL. An ibuprofen solution of 1.25 mg/mL is also prepared by dissolving ibuprofen in 70% ethanol. Next, 1 mL of ibuprofen solution is added to the chitosan solution and a mixture is stirred in 15 min at 800 rpm. Finally, an aqueous TPP solution is added dropwise to the CS/IBU mixture under stirring at 800 rpm for 1.5 h until an opalescent suspension is obtained. The formulation of IBU-CSNPs with varying TPP concentrations is presented in Table 1. The CSNPs without loading ibuprofen are prepared by following the same procedure.

Table 1. Experimental design of synthesizing IBU-CSNPs

CS/TPP ratio, mg/mg	Final concentration		
	Chitosan, mg/mL	TPP, mg/mL	Ibuprofen, mg/mL
1 : 0.25	3.00	0.75	1.00
1 : 0.5		1.50	
1 : 1		3.00	
1 : 2		6.00	
1 : 3		9.00	

2.3. Characterization

Following synthesis, both CSNPs and IBU-CSNPs were evaluated for their morphologies using field emission scanning electron microscopy (FE-SEM, *Hitachi*, S-4800, Japan). The samples were coated with thin Pt layers before measurement. Chemical structure of ingredients (chitosan, ibuprofen, TPP) and synthesized nanoparticles (CSNPs and IBU-CSNPs) were studied by Fourier-transform infrared spectroscopy (FTIR, Alpha II, *Bruker*, Germany). FTIR spectra were plotted in the wavenumber range of 600–4000 cm^{-1} at a resolution of 4 cm^{-1}. The crystallinity profile of the individual ingredients, CSNPs, and IBU-CSNPs was obtained by utilizing X-ray diffraction (XRD, *Bruker*, D8 Advance). The specimens are ground into fine powder and investigated for their XRD spectra in the range of 5°–80° (2θ).

2.4. EE and LC of chitosan nanoparticles

The opalescent suspensions of the chitosan nanoparticles with increasing TPP concentration were centrifuged at 13000 rpm (16058g) for 30 min. The precipitated IBU-CSNPs were then resuspended in 70% ethanol to solubilize the nanoparticles and remove unbound ibuprofen. The suspensions were further centrifuged at 13000 rpm (16058g) for another 30 min. Finally, the collected IBU-CSNPs were washed with water and dissolved in an HCl solution of 0.02 M for more than 1 day to completely release ibuprofen from the nanoparticles. The ibuprofen concentration in the media was analyzed using a UV–Vis spectrophotometer (UV–Vis, Model 754, *Stech International*, United Kingdom) at 222 nm. The EE and LC of the IBU-CSNPs are determined by Eqs. (1) and (2):

$$\mathrm{EE}(\%) = \frac{C_\mathrm{T} - C_\mathrm{F}}{C_\mathrm{T}} \times 100\%, \quad (1)$$

$$\mathrm{LC}(\%) = \frac{W_\mathrm{L}}{W_\mathrm{N}} \times 100\%, \quad (2)$$

where C_T and C_F (mg/mL) are total and free concentrations of ibuprofen in the CSNPs suspensions, respectively; W_L and W_N (g) are weight of ibuprofen loaded in CSNPs and the weight of nanoparticles, respectively.

2.5. *In vitro* ibuprofen release kinetics of the IBU-CSNPs

The IBU-CSNPs were studied *in vitro* release profile under different pH conditions by applying the analysis membrane method [10]. In particular, 1.5 mL of the IBU-CSNPs suspension was added into the tied dialysis

tube. For the drug release, three mediums of simulated gastric fluid (SGF, pH 1.2), simulated intestinal fluid (SIF, pH 6.8), and simulated biological fluid (SBF, pH 7.4) were prepared. Furthermore, ibuprofen release capacity from nanoparticles was evaluated in sequential release with a medium of pH 1.2 for the first 3 h [11, 12] and then moved to pH 6.8 for the next 12 days [13]. The equipped dialysis tube is immersed into 25 mL of each media to release the drug from the nanoparticles into the environment through the membrane. The CDR is calculated at different time intervals using a UV–Vis Spectrophotometer at 222 nm. The release kinetics of the IBU-CSNPs are studied by using mathematical models of zero order (Z-O), first order (F-O), Higuchi (H), and Korsmeyer–Peppas (K–P) as presented in Eqs. (3)–(7) [14]. In order to determine the appropriate release mechanism, the most suitable model for the release behavior of the IBU-CSNPs was identified.

Zero-order model (Z-O):

$$\frac{M_t}{M_\infty} = k_0 t\,, \tag{3}$$

First-order model (F-O):

$$\ln\left(\frac{M_t}{M_\infty}\right) = k_1 t\,, \tag{4}$$

Higuchi model (H):

$$\frac{M_t}{M_\infty} = k_H \sqrt{t}\,, \tag{5}$$

Korsmeyer–Peppas model (K–P):

$$\frac{M_t}{M_\infty} = k_{KP} t^n\,, \tag{6}$$

Kopcha model:

$$\frac{M_t}{M_\infty} = A\sqrt{t} + Bt\,, \tag{7}$$

where $\frac{M_t}{M_\infty}$ is the fractional amount of the drug released at time t (h); k_0, k_1, k_H, k_{KP}, A, and B are constants of the corresponding models. Besides, n is the diffusion exponent indicating the release mechanism (K–P model).

2.6. Degradability of the CSNPs and IBU-CSNPs

The degradability of the nanoparticles with and without ibuprofen was evaluated in a sequentially pH-changing experiment. In particular, the particles were incubated in the SGF solution (pH 1.2) for 3 h and then transferred to the SIF environment (pH 6.8) during the remaining period. The degradability of the nanoparticles is determined by their dry weight difference before and after incubation as described in Eq. (8).

$$\text{Degradability}(\%) = \frac{W_0 - W_t}{W_0} \times 100\%\,, \tag{8}$$

where W_0 and W_t are respectively the weight of the IBU-CSNPs initially and at the time t (h).

3. RESULTS AND DISCUSSION

3.1. EE and LC of the IBU-CSNPs

Following the synthesis process, IBU-CSNPs were successfully fabricated and homogenously suspended as a milky suspension (Fig. 1). The opacity of the samples was observed to progressively increase with a decrease in the CS/TPP ratio: in particular, the suspensions with the CS/TPP ratios of 1 : 2 and 1 : 3 (mg/mg) show particle aggregation at the bottom of the beaker. As the TPP concentration increases, the extent of the repulsive electrostatic interactions between the IBU-CSNPs reduces, resulting in the compression of the double electrical layer and a reduction in the zeta potential of the nanoparticles [15]. Consequently, aggregation is promoted, leading to a declined colloidal stability of the IBU-CSNPs. Previous studies have also shown that forming weak bonds between chitosan and TPP by adjusting the CS/TPP ratio helps prevent aggregation [16, 17].

Figure 2 illustrates the EE and LC of the IBU-CSNPs with decreasing CS/TPP ratio from 1 : 0.25 to 1 : 3 mg/mg; in other words, increasing TPP concentration from 0.75 to 9.00 mg/mL. Overall, both EE and LC of the IBU-CSNPs tend to grow as the CS/TPP ratio declines from 1 : 0.25 to 1 : 1 (mg/mg), followed by a decrease in both criteria with a further reduction in the CS/TPP ratio

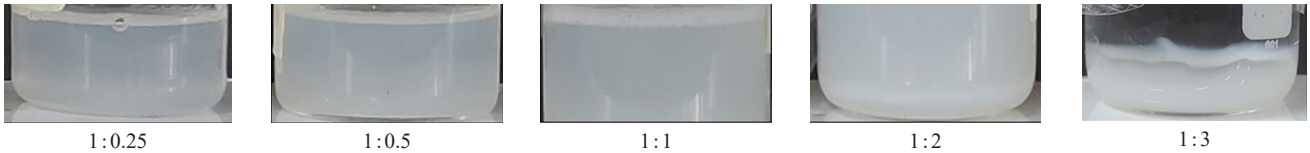

Fig. 1. Images of IBU-CSNPs fabricated from different CS/TPP ratios

to 1 : 3 (mg/mg). The highest EE and LC of the fabricated nanoparticles are respectively 77.70% and 46.62% at the CS/TPP ratio of 1 : 1 (mg/mg). Under this synthesis condition, the drug LC of the IBU-CSNPs in this work is almost 2 times higher than that fabricated by Balde *et al.* (EE and LC of 68.94% and 28%, respectively) [7].

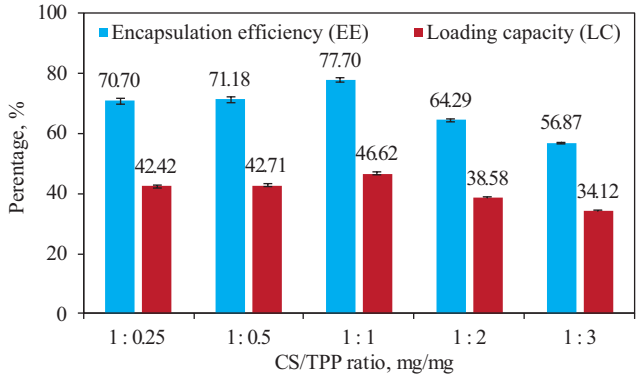

Fig. 2. Drug loading performance of the IBU-CSNPs with varying CS/TPP ratios

As can be seen from Fig. 2, an increase in the TPP concentration results in a higher cross-linking density of the IBU-CSNPs and a smaller nanoparticle size, permitting more IBU to be encapsulated within the nanoparticle core. The increased concentration of TPP also enhances the stability of the IBU-CSNPs colloids. Therefore, both EE and LC of the IBU-CSNPs achieve the highest values at the CS/TPP ratio of 1 : 1 (mg/mg). However, the stability of the nanoparticles diminishes as the CS/TPP ratio decreases to 1 : 2 and 1 : 3 (mg/mg) due to particle aggregation to significantly reduce the possibility for the ibuprofen-chitosan interactions and the entrapment of the drug within the cross-linked network of the nanoparticles. Consequently, there is a substantial decline in both EE and LC of the IBU-CSNPs down to 56.87% and 34.12% in the given order at the CS/TPP ratio of 1 : 3 (mg/mg).

3.2. Characteristics of the IBU-CSNPs

3.2.1. Chemical-crystalline profile and morphology of the IBU-CSNPs

In order to analyze the chemical structure of the fabricated nanoparticles, FTIR spectra of the chitosan nanoparticles both with and without encapsulating ibuprofen and components (chitosan, TPP, and ibuprofen) are illustrated in Fig. 3a. Characteristic absorption bands appearing in the range of 3000–3500 cm^{-1} are attributed to hydroxyl and amino groups of chitosan chains. The strong bands at 1642, 1555, and 1240 cm^{-1} are assigned to vibrations of C=O stretching, N–H bending and C–N stretching in the given order. The significant intensity in the peak at 1035 cm^{-1} indicates the presence of C–O–C linkages in the chitosan chains [14]. For TPP, the peaks at 1076 and 1208 cm^{-1} refer to the P=O linkages, whereas the band at 1126 cm^{-1} is attributed to P–O–R bonds in the phosphate groups [18]. Ibuprofen is characterized by the peaks at 1708 and 2955 cm^{-1}, which present functional groups of carboxylic acid and hydroxyl. There is a strong absorption bond found at 1230 cm^{-1} indicating the C–O–C bonds in the structure of ibuprofen. The aromatic ring in the ibuprofen structure is characterized by the two absorption bands at 1458 and 1506 cm^{-1}. Moreover, the rocking vibrations of CH_2 and CH_3 linkages are correspondingly identified at 776 and 933 cm^{-1} [7]. The lack of a characteristic peak at 1708 cm^{-1} in the spectrum of IBU-CSNPs corresponding with the carboxylic acid of ibuprofen indicates interactions between the drug and the polymeric matrix of the chitosan nanoparticles. Additionally, the absorption bands at the remaining peaks of ibuprofen are not intense in the IBU-CSNPs spectrum, further confirming the successful encapsulation of the ibuprofen in the network of the nanoparticles [7].

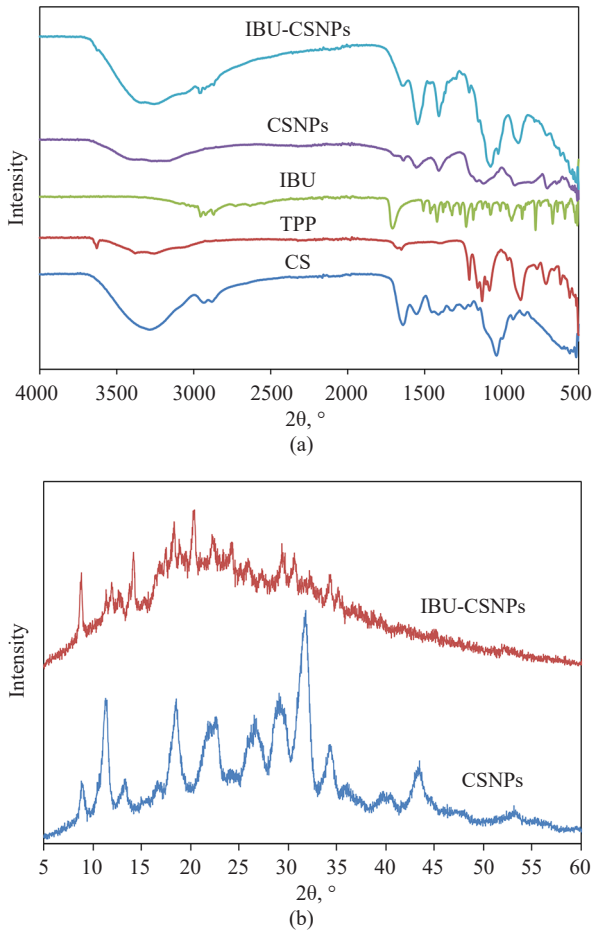

Fig. 3. FTIR (a) and XRD spectra (b) of CSNPs and IBU-CSNPs

The XRD analysis of the crystalline profile of the nanoparticles both with and without loaded ibuprofen is illustrated in Fig. 3b. According to the previous work, the neat chitosan exhibited diffraction peaks at 11.9° and 20°, whereas pure TPP showed various peaks at 19.05°, 19.77°, 33.60°, and 34.49° [19]. However, these characteristic peaks of chitosan and TPP are absent in the XRD pattern of CSNPs; instead, new multiple peaks appear at 11.5°, 13.4°, 18.6°, 22.7°, 26.6°, 29.2°, 31.8°, 34.4°, and 43.5°. This finding indicates that the interactions between the oppositely charged groups of chitosan and TPP cause the change in the packing structure of the chitosan chains. Moreover, there is a greater extent of chain bonding in the nanoparticles resulting from the cross-linking between chitosan and TPP. The previous work presented the XRD pattern of pure ibuprofen containing the diffraction peaks at 19.4°, 21.6°, 26.8°, 28.4°, and 33.2° [7]. In this study, the lack of signals at these peaks in the XRD spectrum of IBU-CSNPs demonstrates that the drug is encapsulated within the cross-linked network of the nanoparticles.

The morphology and particle size of the IBU-CSNPs are presented in Fig. 4. The uniform spherical shape of the IBU-CSNPs together with a smooth surface and nano size in the range of 50–60 nm confirms the success in the synthesis of the nanoparticles encapsulating hydrophobic ibuprofen. As already mentioned, the nano size of the chitosan-based delivery system increases its surface area, thus enhancing the efficiency of drug encapsulation within the polymer network and improving the solubility of hydrophobic drugs like ibuprofen.

3.2.2. Degradability of the IBU-CSNPs

Degradability is one of the crucial properties of drug delivery systems due to limiting the release behavior of the active compound and the toxicity potential of the material to the human body. In this work, the degradability of the synthesized nanoparticles is evaluated in the *in vitro* condition of simulated oral administration. Figure 5 depicts the degradability rate of CSNPs and IBU-CSNPs over time along with the images of the nanoparticles captured under microscopy as presented in Fig. 6. During the initial 3-h period in an acidic environment, the nanoparticles exhibit low degradation with the respective degradability of 3.93 and 6.40% for CSNPs and IBU-CSNPs. Figure 6b also shows that there is no significant change in the morphology of the IBU-CSNPs clusters after 3-h immersion in SGF. According to the previous study by Lin *et al*. [20], it was found that CS/TPP polyelectrolyte complex gel microspheres completely degraded within 2 h at pH 1.4. In contrast, both CSNPs and IBU-CSNPs in this work exhibit effective acid resistance. This can be attributed to the dense cross-linking within the polymeric matrix of the nanoparticles via the strong electrostatic interactions between the protonated amino groups of chitosan under an acidic environment and the negatively charged

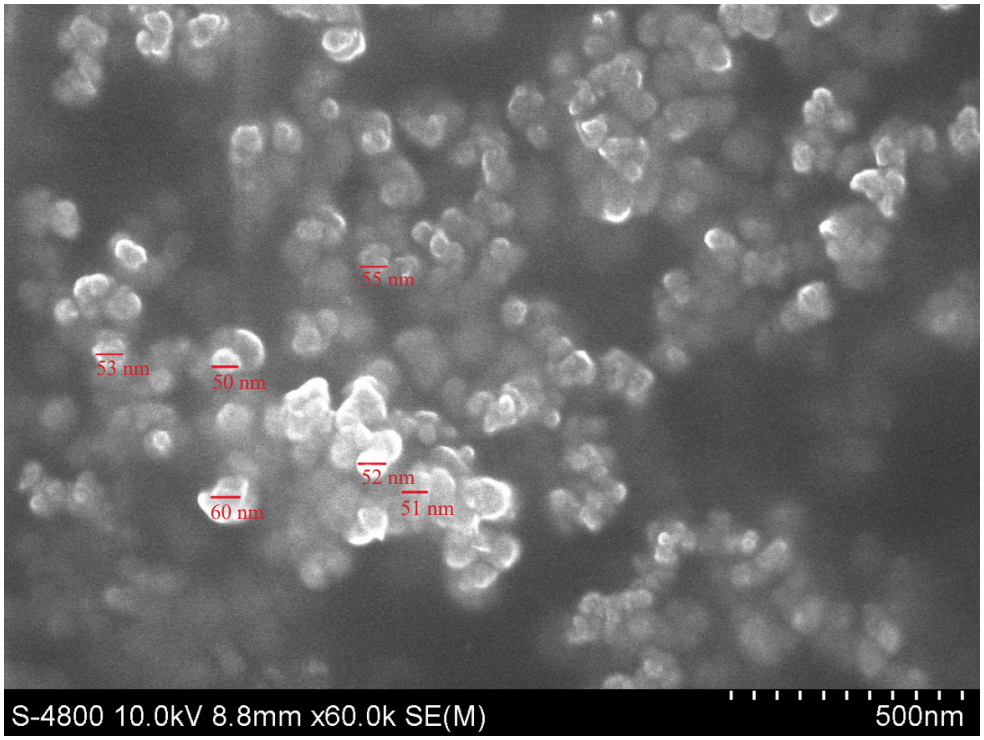

Fig. 4. Morphology of the IBU-CSNPs synthesized at a CS/TPP ratio of 1 : 1 (mg/mg)

phosphate groups of TPP. The high stability witnessed in SGF demonstrates the ability of the IBU-CSNPs to withstand the harsh conditions of the stomach and protect the drug from first-pass metabolism.

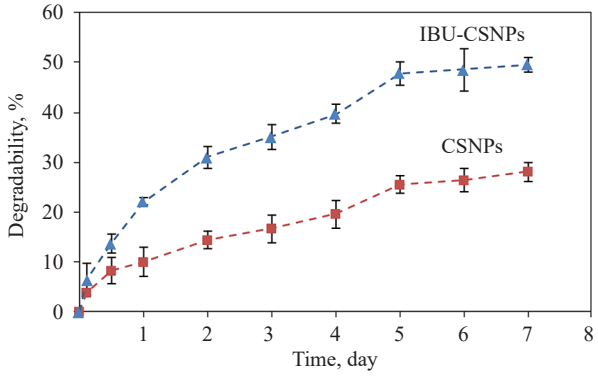

Fig. 5. Degradability of CSNPs with and without encapsulating ibuprofen under sequential pH change conditions (SGF at pH 1.2 for 3 h, followed by SIF at pH 6.8 for the remaining duration)

When the experimental environment changes to SIF, the degradation of the nanoparticles occurs more prominently with the corresponding degradability of 28.03% and 49.62% after 7 days for CSNPs and IBU-CSNPs. The looser structure of the polymeric matrix resulted from the partial deprotonation of chitosan chains, while the high solubility of ibuprofen in a neutral environment (pH 6.8) contributes to the weakening of the interactions between the drug and chitosan chains, promoting the diffusion of drug molecules from the nanoparticles. As a result, voids and porous channels are created within the structure of the nanoparticles, allowing the penetration of the environment fluid and causing more deprotonation of chitosan. Therefore, the degradation of IBU-CSNPs is considerably greater than that of CSNPs at the same time interval. Figure 6c demonstrates the evident degradation of IBU-CSNPs clusters in the SIF characterized by the presence of discrete fragments with various morphologies.

3.3. *In vitro* release kinetics of the IBU-CSNPs

The release kinetics of IBU-CSNPs under different simulated fluid conditions are depicted in Fig. 7. The equilibrium release state of IBU-CSNPs in all investigated environments is achieved after 5 days with approximately the entire ibuprofen-loaded content being released from the nanoparticles. In particular, at the same time point of 1 day after exposure to the environment, the CDR of the IBU-CSNPs in SGF and SIF is 23.13% and 67.58% in the given order. These values are all lower than the CDR reported in the study by Balde *et al*. (around 80%) [7]. Therefore, the as-fabricated IBU-CSNPs exhibit prolonged ibuprofen release demonstrated by their slow release rate in comparison with the previous work.

The distinct release behavior of the IBU-CSNPs among the environments indicates the pH-responsive release capability of the synthesized delivery system. In particular, the SIF condition strongly promotes the ibuprofen release from the nanoparticles, whereas the SGF environment inhibits the diffusion of drug molecules into the medium (Fig. 7a), similar to the findings in the degradation assessment. The maximum ibuprofen concentration is achieved after 4 days and 2 days in respective environmental pH values of 1.2 and 6.8. The specific maximum drug concentration is correspondingly 28.48 and 27.36 mg/L (Fig. 7b). In comparison with previous studies, the pattern of the ibuprofen concentration in the aqueous media over time is similar to the drug concentration-time profile of a sustained release delivery system [21, 22]. Moreover,

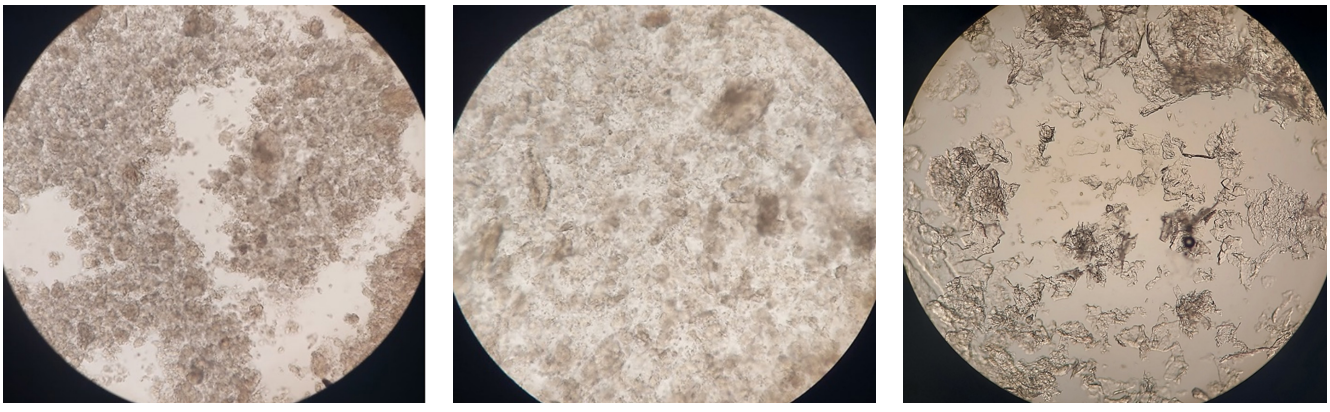

(a) (b) (c)

Fig. 6. Alteration in the morphology of IBU-CSNPs before the experiment (a), after 3h-immersion in SGF (b), and the next 5-day cultivation in SIF (c)

the therapeutic concentration range for ibuprofen analgesic and anti-inflammatory effects is approximately 10–50 mg/L [23]. According to the experimental data, the ibuprofen concentration in the SIF reaches 20.55 mg/L and remains within the therapeutic window of ibuprofen until the 12th day. While IBU-CSNPs in SGF also exhibit a similar trend in the drug release behavior, the therapeutic concentration is only achieved on the 2nd day from the beginning.

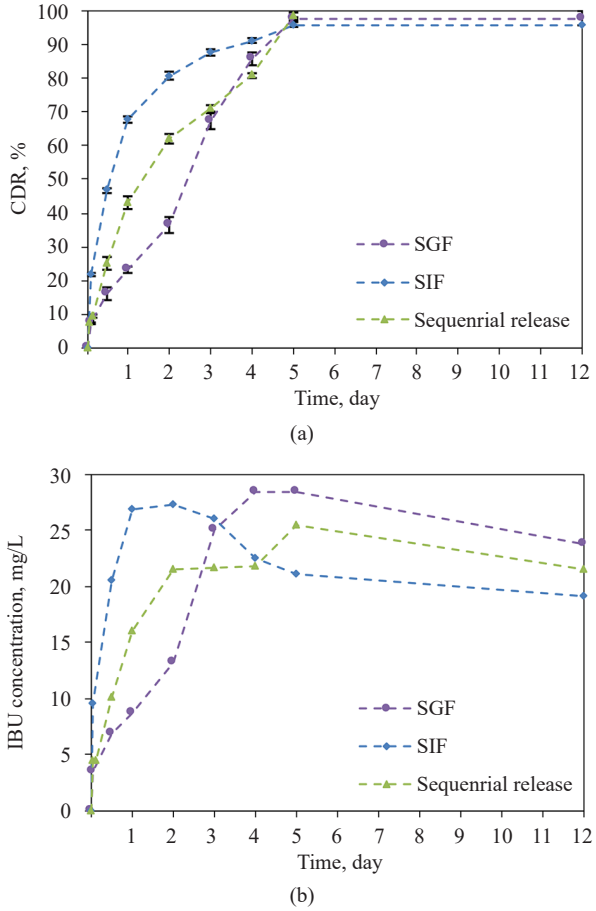

Fig. 7. *In vitro* release of IBU-CSNPs in terms of the CDR (a) and ibuprofen concentration (b) recorded under SGF, SIF, and sequential pH-changing conditions

In the sequential pH condition, the ibuprofen release profile of the IBU-CSNPs is a combination of the release patterns witnessed in SGF and SIF, but at different CDR and ibuprofen concentrations. The release kinetics of the drug-loaded nanoparticles under the sequentially changing pH condition exhibit distinctions starting from the transition of the environment with a slower ibuprofen release rate. In this case, the maximum ibuprofen concentration is reached after 5 days along with the therapeutic drug concentration achieved after 12 h and continuously maintained in the range of 10.05–21.57 mg/L until the 12th day. As depicted in Fig. 7, the findings of this biomimetic evaluation indicate that the higher CDR and ibuprofen concentration in SIF than in SGF enables effective drug delivery to the intestine as well as avoids drug leakage in the stomach.

The release kinetics of IBU-CSNPs in SGF, SIF, and biomimetic conditions are mathematically analyzed by the determined models including zero order, first order, Higuchi, Kormeyer–Peppas, and Kopcha. The results from the analysis are tabulated in Table 2.

Table 2. Analysis of IBU-CSNPs release kinetics by mathematical models

Model	Model coefficient	Experimental condition		
		SGF	SIF	Sequential release
Z-O	k_0	0.196	0.162	0.185
	R^2	0.987	0.750	0.939
F-O	k_1	0.491	0.230	0.456
	R^2	0.908	0.636	0.754
H	k_H	0.171	0.134	0.160
	R^2	0.897	0.563	0.789
K–P	k_{KP}	0.237	0.697	0.416
	n	0.917	0.470	0.622
	R^2	0.983	0.999	0.997
Kopcha	A	0.076	0.494	0.375
	B	0.167	0.000	0.025
	R^2	0.994	0.966	0.995

The release profile of IBU-CSNPs follows the Korsmeyer–Peppas model in SIF (R^2 of 0.999) and the Kopcha model in SGF (R^2 of 0.994). Both models show an extremely high correlation with the ibuprofen release kinetics under the sequentially pH-changing condition. The release exponent of 0.470 determines the anomalous or non-Fickian transport for the release kinetics of IBU-CSNPs governed by the drug diffusion, swelling, and degradation of the nanoparticles. On the contrary, the mechanism of the drug release into the acidic environment is predominantly controlled by the erosion of the nanoparticles according to the greater erosion constant (B) than the diffusion constant (A) in the Kopcha model. For the simulated oral drug delivery by changing pH, the release exponent below 0.85 (Korsmeyer–Peppas model) and A/B ratio above 1 (Kopcha model) confirm that the ibuprofen diffusion is the primary mechanism controlling the drug release from the IBU-CSNPs. This finding is reasonable due to the much longer exposure duration of the nanoparticles encapsulating ibuprofen in SIF than in SGF.

4. CONCLUSIONS

The IBU-CSNPs successfully synthesized following the synthesis procedure with the CS/TPP ratio from 1 : 0.25 to 1 : 1 (mg/mg) show a uniform spherical shape and a particle size of 50–60 nm. The CS/TPP ratio influences the drug entrapment efficiency of the developed nanoparticles. When the ratio decreases below 1 : 1 (mg/mg), there is a failure in the drug loading of the CSNPs as evidenced by a remarkable reduction in both EE and LC. Under the simulated condition of oral drug delivery, the IBU-CSNPs have a degradability of about 50% after 7 days and excellent acid resistance, as well as demonstrating a controlled pH-responsive release. In the first 3 h within the SGF environment, only 9.44% of ibuprofen is released, demonstrating the high efficiency of ibuprofen protection within the CSNPs system. The release gradually increases in the SIF environment to reach 25.07% at the 12-h mark having an ibuprofen concentration of 10.05 mg/mL. The ibuprofen concentration keeps increasing, reaching its peak at 25.50 mg/mL after 5 days of IBU-CSNP exposure to SIF. The erosion of nanochitosan contributes to the slow ibuprofen release in SGF, while the sustained release in SIF follows the non-Fickian process governed by diffusion, swelling, and degradation of the IBU-CSNPs.

Acknowledgments

Nga H.N. Do was funded by the Master, PhD Scholarship Program of Vingroup Innovation Foundation (VINIF), code VINIF.2023.TS.071. We acknowledge Ho Chi Minh City University of Technology (HCMUT), VNU-HCM for supporting this study.

Authors' contributions

All authors contributed equally to the research.

The authors declare no conflicts of interest.

REFERENCES

1. Irvine J., Afrose A., Islam N. Formulation and delivery strategies of ibuprofen: challenges and opportunities. *Drug. Dev. Ind. Pharm*. 2018;44(2):173–183. https://doi.org/10.1080/03639045.2017.1391838
2. Susilo S.P., Pertiwi S.H., Ainurofiq A. Development and validation of analytical methods for multicomponent crystals of ibuprofen with malic and tartaric acid using spectrophotometry. *J. Phys: Conf. Ser*. 2022;2190:012033. https://doi.org/10.1088/1742-6596/2190/1/012033
3. Volans G.. Human Toxicity of Ibuprofen. In: Rainsford K.D. (Ed). *Ibuprofen*. UK: John Wiley & Sons, Ltd,; 2015. P. 498–517. https://doi.org/10.1002/9781118743614.ch12
4. Janus E., Ossowicz P., Klebeko J., Nowak A., Duchnik W., Kucharski Ł., *et al.* Enhancement of ibuprofen solubility and skin permeation by conjugation with l-valine alkyl esters. *RSC Adv*. 2020;10:7570–7584. https://doi.org/10.1039/D0RA00100G
5. Bensouiki S., Belaib F., Sindt M., Magri P., Rup-Jacques S., Bensouici C., *et al.* Evaluation of anti-inflammatory activity and *in vitro* drug release of ibuprofen-loaded nanoparticles based on sodium alginate and chitosan. *Arab. J. Sci. Eng*. 2020;45:7599–7609. https://doi.org/10.1007/s13369-020-04720-2
6. Li C., Wang K., Xie D. Green fabrication and release mechanisms of pH-sensitive chitosan–ibuprofen aerogels for controlled transdermal delivery of ibuprofen. *Front. Chem*. 2021;9:767923. https://doi.org/10.3389/fchem.2021.767923
7. Balde A., Kim S.-K., Abdul N.R. Crab (*Charybdis natator*) exoskeleton derived chitosan nanoparticles for the *in vivo* delivery of poorly water-soluble drug: Ibuprofen. *Int. J. Biol. Macromol*. 2022;212:283–293. https://doi.org/10.1016/j.ijbiomac.2022.05.131
8. Olvera Rodríguez I., Mora-Muñoz J.M., Pérez V., Campos-Guillén J., Gallegos-Reyes M.A., García-Solís P., *et al*. Development and evaluation of ibuprofen-loaded chitosan nanoparticles for pulmonary therapy. *Front. Nanotechnol*. 2024;6:1429889. https://doi.org/10.3389/fnano.2024.1429889
9. Thirugnanasambandan T., Gopinath S.C.B. Laboratory to industrial scale synthesis of chitosan-based nanomaterials: A review. *Process Biochem*. 2023;130:147–155. https://doi.org/10.1016/j.procbio.2023.04.008
10. Najafabadi A.H., Abdouss M., Faghihi S. Synthesis and evaluation of PEG-O-chitosan nanoparticles for delivery of poor water soluble drugs: Ibuprofen. *Mater. Sci. Eng. C*. 2014;41:91–99. https://doi.org/10.1016/j.msec.2014.04.035
11. Pereira A.K. dos S., Reis D.T., Barbosa K.M., Scheidt G.N., da Costa L.S., Santos L.S.S. Antibacterial effects and ibuprofen release potential using chitosan microspheres loaded with silver nanoparticles. *Carbohydr. Res*. 2020;488:107891. https://doi.org/10.1016/j.carres.2019.107891
12. Zhang Y., Chen J., Zhang G., Lu J., Yan H., Liu K. Sustained release of ibuprofen from polymeric micelles with a high loading capacity of ibuprofen in media simulating gastrointestinal tract fluids. *React. Funct. Polym*. 2012;72(6):359–364. https://doi.org/10.1016/j.reactfunctpolym.2012.03.010
13. Sorasitthiyanukarn F.N., Muangnoi C., Rojsitthisak P., Rojsitthisak P. Stability and biological activity enhancement of fucoxanthin through encapsulation in alginate/chitosan nanoparticles. *Int. J. Biol. Macromol*. 2024;263(Part 1):130264. https://doi.org/10.1016/j.ijbiomac.2024.130264
14. Do N.H.N., Huynh T.N.A., Le T.X., Ha A.C., Le P.K. Encapsulation of *Triphasia trifolia* extracts by pH and thermal dual-sensitive chitosan hydrogels for controlled release. *Carbohydr. Polym*. 2023;320:121264. https://doi.org/10.1016/j.carbpol.2023.121264
15. Jonassen H., Kjøniksen A.-L., Hiorth M. Stability of chitosan nanoparticles cross-linked with tripolyphosphate. *Biomacromolecules*. 2012;13(11):3747–3756. https://doi.org/10.1021/bm301207a
16. Dhandapani R.K., Gurusamy D., Howell J.L., Palli S.R. Development of CS-TPP-dsRNA nanoparticles to enhance RNAi efficiency in the yellow fever mosquito, *Aedes aegypti*. *Sci. Rep*. 2019;9(1):8775. https://doi.org/10.1038/s41598-019-45019-z

17. Sawtarie N., Cai Y., Lapitsky Y. Preparation of chitosan/tripolyphosphate nanoparticles with highly tunable size and low polydispersity. *Colloids Surf. B: Biointerfaces*. 2017;157:110–117. https://doi.org/10.1016/j.colsurfb.2017.05.055
18. Tomaz A.F., de Carvalho S.M.S., Barbosa R.C., Silva S.M.L., Gutierrez M.A.S., de Lima A.G.B., *et al*. Ionically Crosslinked Chitosan Membranes Used as Drug Carriers for Cancer Therapy Application. *Materials*. 2018;11(10):2051. https://doi.org/10.3390/ma11102051
19. Alehosseini E., Shahiri Tabarestani H., Kharazmi M.S., Jafari S.M. Physicochemical, thermal, and morphological properties of chitosan nanoparticles produced by ionic gelation. *Foods*. 2022;11(23):3841. https://doi.org/10.3390/foods11233841
20. Lin W.-C., Yu D.-G., Yang M.-C. pH-sensitive polyelectrolyte complex gel microspheres composed of chitosan/sodium tripolyphosphate/dextran sulfate: swelling kinetics and drug delivery properties. *Colloids Surf. B: Biointerfaces*. 2005;44(2-3):143–151. https://doi.org/10.1016/j.colsurfb.2005.06.010
21. Anand O., Pepin X.J.H., Kolhatkar V., Seo P. The use of physiologically based pharmacokinetic analyses—in biopharmaceutics applications-regulatory and industry perspectives. *Pharm. Res*. 2022;39:1681–1700. https://doi.org/10.1007/s11095-022-03280-4
22. Muhammad Saeed J., Waqas A., Madeeha S. Fundamentals Applications of Controlled Release Drug Delivery. In: Abdur R. (Ed.). *Drug Development and Safety*. Rijeka: IntechOpen; 2023. P. 1–12. http://doi.org/10.5772/intechopen.113283
23. Mazaleuskaya L.L., Theken K.N., Gong L., Thorn C.F., FitzGerald G.A., Altman R.B., *et al.* PharmGKB summary: ibuprofen pathways. *Pharmacogenetics Genom*. 2015;25(2):96–106. https://doi.org/10.1097/FPC.0000000000000113

About the Authors

Nga H.N. Do, PhD, Faculty of Chemical Engineering, Ho Chi Minh City University of Technology (HCMUT) (268 Ly Thuong Kiet Street, Ho Chi Minh City, Viet Nam); Vietnam National University Ho Chi Minh City (Linh Trung Ward, Thu Duc District, Ho Chi Minh City, Viet Nam). E-mail: dnhnga.sdh21@hcmut.edu.vn. Scopus Author ID 57211145353, https://orcid.org/0000-0002-1606-4522

Phuong Khanh Thy Vo, Undergraduate Student, Faculty of Chemical Engineering, Ho Chi Minh City University of Technology (HCMUT) (268 Ly Thuong Kiet Street, Ho Chi Minh City, Viet Nam); Vietnam National University Ho Chi Minh City (Linh Trung Ward, Thu Duc District, Ho Chi Minh City, Viet Nam). E-mail: khanh.vokthh21@hcmut.edu.vn

Thanh V.N. Le, Bachelor of Chemical Engineering, Ho Chi Minh City University of Technology (HCMUT) (268 Ly Thuong Kiet Street, Ho Chi Minh City, Viet Nam); Vietnam National University Ho Chi Minh City (Linh Trung Ward, Thu Duc District, Ho Chi Minh City, Viet Nam). E-mail: thanh.le10102002@hcmut.edu.vn

Hung D. Vuong, Bachelor of Chemical Engineering, Ho Chi Minh City University of Technology (HCMUT) (268 Ly Thuong Kiet Street, Ho Chi Minh City, Viet Nam); Vietnam National University Ho Chi Minh City (Linh Trung Ward, Thu Duc District, Ho Chi Minh City, Viet Nam). E-mail: hung.vuongvdh272@hcmut.edu.vn

Trang P.T. Nguyen, Bachelor of Chemical Engineering, Ho Chi Minh City University of Technology (HCMUT) (268 Ly Thuong Kiet Street, Ho Chi Minh City, Viet Nam); Vietnam National University Ho Chi Minh City (Linh Trung Ward, Thu Duc District, Ho Chi Minh City, Viet Nam). E-mail: trang.nguyen200502@hcmut.edu.vn

Phung K. Le, Associate Professor, Dr. of Chemical Engineering, CIRTech Institute, HUTECH University (Ho Chi Minh City, Viet Nam). E-mail: ltk.phung@hutech.edu.vn

Anh C. Ha, Associate Professor, Dr. of Chemical Engineering, Ho Chi Minh City University of Technology (HCMUT) (268 Ly Thuong Kiet Street, Ho Chi Minh City, Viet Nam). E-mail: hcanh@hcmut.edu.vn. Scopus Author ID 56485522100, https://orcid.org/0000-0001-7919-4028

The text was submitted by the authors in English
and edited for English language and spelling by Thomas A. Beavitt

Tonkie Khimicheskie Tekhnologii = Fine Chemical Technologies.
2025;20(5):441–453 ISSN 2686-7575 (Online)

UDC 577.115.083:577.112.345
https://doi.org/10.32362/2410-6593-2025-20-5-441-453
EDN ARSHVH

RESEARCH ARTICLE

Symmetrical and asymmetric dimeric cationic amphiphiles based on lipopeptides of irregular structure as potential components of cationic liposomes

Timofey A. Volodin, Polina P. Polikashina, Ulyana A. Budanova✉, Yurii L. Sebyakin

MIREA – Russian Technological University (M.V. Lomonosov Institute of Fine Chemical Technologies), Moscow, 119454 Russia

✉ *Corresponding author, e-mail: c-221@yandex.ru*

Abstract

Objectives. Gene therapy techniques based on the introduction of therapeutic nucleic acids into body cells are currently being developed for the treatment of diseases with a genetic etiology. Among modern drug delivery systems, nonviral agents based on the use of a variety of lipids to produce liposomes and micelles occupy a special place. This work sets out to synthesize and study the properties of dimeric cationic amphiphiles of irregular structure with symmetric and asymmetric hydrophobic blocks in order to determine the influence of structure on physicochemical properties and evaluate the prospects of their application as transfection agents.

Methods. The formation of hydrophobic and hydrophilic blocks involves reactions of L-cystine derivatives and L-glutamic acid and diethanolamine diesters using the condensing agents: dicyclohexylcarbodiimide (DCC) + 4-(dimethylamino)pyridine (DMAP) or hexafluorophosphate benzotriazole tetramethyl uranium (HBTU) + diisopropylethylamine (DIPEA). In order to isolate the reaction products from the reaction mixture, column chromatography and/or preparative thin-layer chromatography on silica gel were used. The structure of the obtained compounds was confirmed by ^{1}H nuclear magnetic resonance spectroscopy and mass spectrometry. Synthesized lipopeptides in aqueous medium formed liposomal dispersions whose particle size was determined by photon correlation spectroscopy.

Results. Schemes for the preparation of novel dimeric cationic amphiphiles based on L-cystine derivatives were devised. The hydrophobic blocks of the obtained compounds include diesters of diethanolamine and L-glutamic acid (C10, C14, and C16). Targeted lipopeptides were used to obtain liposomal dispersed systems mixed with natural lipids. The hydrodynamic size of the particles formed in all dispersions was determined to be within the range of 50 to 200 nm.

Conclusions. The physicochemical properties of aqueous dispersions based on the synthesized compounds were investigated. Dimeric amphiphiles mixed with phosphatidylcholine and cholesterol form liposomal particles. The impact of amphiphile structure on aggregate size was demonstrated. The number of L-ornithine residues (0, 1, 2) in the target products was found to be the most significant parameter affecting the particle size.

Keywords

symmetric and asymmetric dimeric cationic amphiphiles, L-cystine derivatives, cationic liposomes, lipopeptides

Submitted: 11.12.2024
Revised: 07.04.2025
Accepted: 05.09.2025

For citation

Volodin T.A., Polikashina P.P., Budanova U.A., Sebyakin Yu.L. Symmetrical and asymmetric dimeric cationic amphiphiles based on lipopeptides of irregular structure as potential components of cationic liposomes. *Tonk. Khim. Tekhnol. = Fine Chem. Technol*. 2025;20(5): 441–453. https://doi.org/10.32362/2410-6593-2025-20-5-441-453

НАУЧНАЯ СТАТЬЯ

Симметричные и асимметричные димерные катионные амфифилы на основе липопептидов нерегулярного строения в качестве потенциальных компонентов катионных липосом

Т.А. Володин, П.П. Поликашина, У.А. Буданова✉, Ю.Л. Себякин

МИРЭА – Российский технологический университет (Институт тонких химических технологий им. М.В. Ломоносова), Москва, 119454 Россия

✉ *Автор для переписки, e-mail: c-221@yandex.ru*

Аннотация

Цели. В настоящее время для лечения заболеваний, имеющих генетическое происхождение, разрабатываются методы генной терапии, основанные на доставке в клетки организма терапевтических нуклеиновых кислот. Среди современных систем доставки лекарственных средств особое место занимают невирусные средства, основанные на использовании разнообразных липидов для получения липосом и мицелл. Целью данной работы является синтез и изучение свойств димерных катионных амфифилов нерегулярного строения с симметричным и ассиметричным гидрофобным блоком для определения влияния структуры на физико-химические свойства, что позволит оценить перспективы их применения в качестве трансфекционных агентов.

Методы. Формирование гидрофобных и гидрофильных блоков предполагает проведение реакций производных L-цистина и диэфиров L-глутаминовой кислоты и диэтаноламина с помощью конденсирующих агентов: *N*,*N*-дициклогексилкарбодиимида (DCC) + 4-диметиламинопиридина (DMAP) или гексафторфосфат бензотриазолтетраметилурония (HBTU) + диизопропилэтиламина (DIPEA). Для выделения продуктов реакции из реакционной смеси применялась колоночная хроматография и/или препаративная тонкослойная хроматография на силикагеле. Структура полученных соединений подтверждена данными спектроскопии ядерного магнитного резонанса ^{1}H и масс-спектрометрии. Синтезированные липопептиды в водной среде образовывали липосомальные дисперсии, размер частиц которых определяли методом фотонно-корреляционной спектроскопии.

Результаты. Разработаны схемы получения новых димерных катионных амфифилов на основе производных L-цистина. Гидрофобные блоки полученных соединений включают диэфиры диэтаноламина и L-глутаминовой кислоты (C10, C14 и C16). Целевые липопептиды были использованы для получения липосомальных дисперсных систем в смеси с природными липидами. Для всех дисперсий определен гидродинамический размер сформированных частиц, который находится в интервале от 50 до 200 нм.

Выводы. Изучены физико-химические свойства водных дисперсий на основе синтезированных соединений. Димерные амфифилы в смеси с фосфатидилхолином и холестерином образуют липосомальные частицы. Показано влияние структуры амфифилов на размер получаемых агрегатов. Установлено, что наиболее значимым параметром, влияющим на размер частиц, является число остатков L-орнитина (0, 1, 2) в составе целевых продуктов.

Ключевые слова

симметричные и асимметричные димерные катионные амфифилы, производные L-цистина, катионные липосомы, липопептиды

Поступила: 11.12.2024
Доработана: 07.04.2025
Принята в печать: 05.09.2025

Для цитирования

Володин Т.А., Поликашина П.П., Буданова У.А., Себякин Ю.Л. Симметричные и асимметричные димерные катионные амфифилы на основе липопептидов нерегулярного строения в качестве потенциальных компонентов катионных липосом. *Тонкие химические технологии*. 2025;20(5):441–453. https://doi.org/10.32362/2410-6593-2025-20-5-441-453

INTRODUCTION

Gene therapy has the potential to treat hematological and cardiovascular diseases, neurological disorders, cancers, and genetic disorders. Modern treatment methods are based on the use of nucleic acids, including small interfering RNAs, antisense oligonucleotides, and aptamers. More recently, mRNA-based vaccines against COVID-19 have been approved in this area [1].

Positive results from gene therapy can be observed in the treatment of many diseases, such as spinal muscular atrophy, hemophilia, ophthalmological diseases, some cancers [2], and viral diseases [3].

For the successful correction of genetic abnormalities, the efficiency of delivering nucleic acids and establishment of conditions for their long-term functioning are important factors. Various viral and nonviral vectors are being developed to deliver genetic materials into cells, each having its own advantages and disadvantages [4].

Liposomal systems belong to a broad class of nonviral nucleic acid delivery agents. Such delivery agents were among the first nonviral systems to demonstrate effective gene delivery and undergo preclinical and clinical trials [5].

It is known that the structure of amphiphiles influences the size and type of packing of the resulting aggregates. By varying different blocks and the nature of the spacer, the physicochemical properties of aggregates based on these molecules and their subsequent interaction with biological membranes can be studied. The high transfection efficiency of cationic dimeric derivatives with short spacer groups is likely due to the presence of two coexisting lamellar structures [6]. It has also been shown that a longer fragment in the hydrophobic block (C16, C18) promotes the release of the nucleic acids from the lipoplex [1, 6, 7].

The aim of the present work is to obtain and study the properties of irregular cationic amphiphiles having symmetric and asymmetric hydrophobic blocks to determine the influence of structure on the properties of the vesicles they form in an aqueous medium. This is then used as a basis for assessing the prospects for their application as transfection agents.

The use of natural amino acids in the structure of nucleic acid binding agents is a promising approach. It is known that natural amino acids are natural components of biological systems, and their catabolism does not produce toxic metabolites. It explains the low toxicity and high biocompatibility of delivery agents based on natural amino acids [8, 9]. Also, due to the ability of amphiphiles containing amino acid residues to protonate, positively charged cationic amphiphiles are formed, which can subsequently be used to create complexes with negatively charged nucleic acids. In the structure of the target amphiphiles, the natural amino acid L-cystine was used as a spacer unit to connect the hydrophobic and hydrophilic domains. The disulfide group is a potentially sensitive site to the action of intracellular reductants, such as glutathione. Disulfide bond disruption can reduce lipoplex stability and promote the release of nucleic acids, thereby increasing transfection efficiency [10, 11].

The introduction of polar blocks of synthesized dimers of one or two L-ornithine residues attached to the amino groups of L-cystine allows for the achievement of a multivalent effect, which improves the ability of cationic liposomes and genetic material to form a stable lipoplex [1].

The present authors have previously proposed various types of hydrophobic blocks, which are diesters of diethanolamine and L-glutamic acid (Glu) (C10, C14, and C16). The high hydrophobicity of such compounds potentially allows for increased transfection efficiency [1, 4].

EXPERIMENTAL

Materials and methods

The following commercially available reagents were used without further purification: di-*tert*-butyl dicarbonate, *N*,*N*′-dicyclohexylcarbodiimide (DCC), 4-dimethylaminopyridine (DMAP), hexafluorophosphate benzotriazole tetramethyl uranium (HBTU), diisopropylethylamine (DIPEA) (*Sigma-Aldrich*, Germany); sodium bicarbonate (*Khimmed*, Russia); trifluoroacetic acid (*Biochem*, France); soybean phosphatidylcholine (PC) brand Lipoid S100 (*Lipoid GmbH*, Germany); cholesterol (Chol) (*Sigma-Aldrich*, Germany); dichloromethane (DCM), chloroform (trichloromethane, TCM), toluene, ethyl acetate, petroleum ether, and methanol (MeOH) (*Komponent-reaktiv*, Russia).

Bis-*N*,*N*′-(*tert*-butoxycarbonyl)-L-cystine (**1**), *O*,*O*′-dipalmitoyl-diethanolamine (**2a**), and *O*,*O*′-dimyristoyl-diethanolamine (**2b**), dihexadecyl L-glutamate (**9**), didecyl L-glutamate (**11**), and bis-*N*,*N*′-(*tert*-butoxycarbonyl)-L-ornithine (Boc_2Orn) were obtained according to the methods described in [12, 13].

^1H nuclear magnetic resonance (NMR) spectra were recorded in deuterated chloroform ($CDCl_3$) (*Solvex-D*, Russia) on a Bruker WM-300 NMR spectrometer (*Bruker BioSpin*, Germany) operating at a frequency of 300 MHz. Mass spectra of the substances were recorded using a Bruker Ultraflex II high-resolution time-of-flight mass spectrometer (*Bruker Corporation*, Germany),

with MALDI ionization (matrix-assisted laser desorption/ionization) and 2,5-dihydroxybenzoic acid (*Sigma-Aldrich*, Germany) as the matrix.

Column chromatography was performed using 63–200 μm of Silica Gel 60 (*ISOLAB Gmbh*, Germany) and a chromatographic column (*Borosil*, Russia). Preparative thin-layer chromatography (TLC) was performed on Silica 60 gel (*Macherey-Nagel*, Germany) coated on a glass plate. Analytical TLC was performed on Sorbfil (*IMID*, Russia) and Silufol (*Avalier*, Czech Republic) plates using the following solvent systems: (A) toluene/ethyl acetate = 4 : 1; (B) toluene/ethyl acetate = 2 : 1; (C) TCM/MeOH = 10 : 1; (D) petroleum ether/ethyl acetate = 4 : 1; (E) toluene/ethyl acetate = 5 : 1.

To visualize the substance spots on the TLC chromatograms, they were immersed in a 3% ninhydrin solution (*Acros Organics*, Belgium) and then heated to 100°C.

Solvents were removed using a RV 3 vacuum rotary evaporator at 20–300 rpm (*IKA*, Germany).

Bis-*N,N′*-(*tert*-butoxycarbonyl)-L-cystine bis(*O,O′*-dipalmitoyl-diethanolamide) (3a)

To a solution of 0.250 g (0.56 mmol) of compound **1** in DCM cooled to 0°C, 0.253 g (1.23 mmol) of DCC and a catalytic amount of 0.007 g (0.056 mmol) of DMAP were added. After 30 min, 0.650 g (1.1 mmol) of **2a** was added. The mixture was kept at 0°C for 1 h and at 25°C for 24 h. The precipitate was filtered off. The solvent was removed using a rotary evaporator. The product was isolated by column chromatography in system (A). 0.414 g (59.8%) of compound **3a** was obtained, with a retention factor R_f (A) of 0.33.

^{1}H NMR spectrum of compound **3a**: 0.88 (12H, t, J = 6.7 Hz, C$\underline{H}_3$); 1.27 (96H, s, –C$\underline{H}_2$–); 1.43 (18H, s, CC$\underline{H}_3$); 1.60 (8H, s, β-C$\underline{H}_2$); 2.26–2.33 (8H, m, α-C$\underline{H}_2$); 3.01 (4H, br. s, C$\underline{H}_2$–S); 3.47–3.90 (8H, m, C$\underline{H}_2$–CH$_2$–O); 4.20–4.28 (8H, m, CH$_2$–C$\underline{H}_2$–O); 4.93 (2H br. s, C$\underline{H}$–CH$_2$–S); 5.32–5.38 (2H, m, CON$\underline{H}$CHCO).

Bis-*N,N′*-(*tert*-butoxycarbonyl)-L-cystine bis-(*O,O′*-dimyristoyl-diethanolamide) (3b)

The reaction was carried out similarly to the preparation of compound **3a**. From 0.183 g (0.416 mmol) of compound **1**, 0.189 g (0.915 mmol) of DCC and a catalytic amount of 0.005 g (0.042 mmol) of DMAP, as well as 0.460 g (0.874 mmol) of compound **2b**, 0.070 g (11.6%) of compound **3b** was obtained. The product was isolated by preparative chromatography on a silica gel plate in system (B). R_f (B) 0.22.

^{1}H NMR spectrum of compound **3b**: 0.88 (12H, t, J = 6.7 Hz, C$\underline{H}_3$); 1.28 (80H, s, –C$\underline{H}_2$–); 1.44 (18H, s, CC$\underline{H}_3$); 1.55–1.7 (8H, m, β-C$\underline{H}_2$); 2.25–2.40 (8H, m, α-C$\underline{H}_2$); 3.15 (4H, br. s, C$\underline{H}_2$–S); 3.48–3.70 (8H, m, C$\underline{H}_2$–CH$_2$–O); 4.20–4.38 (8H, m, CH$_2$–C$\underline{H}_2$–O); 5.78 (2H, br. s, CON$\underline{H}$CHCO).

L-Cystine bis(*O,O′*-dipalmitoyl-diethanolamide) (4a)

A solution of 1.1 mL (14.8 mmol) of trifluoroacetic acid in 3 mL of TCM was added to 0.116 g (0.074 mmol) of compound **3a**. After 2 h, the solvent was removed using a rotary evaporator, then the reaction mixture was dissolved in TCM and washed with a 5% solution of sodium bicarbonate. The organic residue was filtered on a pleated filter wetted with TCM, and the solvent was removed under vacuum. 0.101 g (99.8%) of compound **4a** was obtained, R_f (C) 0.55.

L-Cystine bis(*O,O′*-dimyristoyl diethanolamide) (4b)

The synthesis of compound **4b** was carried out similarly to compound **4a**. From 0.07 g (0.048 mmol) of **3b**, 0.044 g of product **4b** was obtained with a yield of 72%, R_f (B) 0.33. MALDI TOF (*m/z*): calculated for $[C_{70}H_{136}N_4O_{10}S_2]^{2+}$ 628.331, found 628.326 $[M+2H]^{2+}$.

^{1}H NMR spectrum of compound **4b**: 0.88 (12H, t, J = 6.7 Hz, C$\underline{H}_3$); 1.26 (80H, s, –C$\underline{H}_2$–); 1.57–1.66 (8H, m, β-C$\underline{H}_2$); 2.27–2.45 (8H, m, α-C$\underline{H}_2$); 3.30–3.72 (8H, m, C$\underline{H}_2$–CH$_2$–O); 4.10–4.30 (8H, m, CH$_2$–C$\underline{H}_2$–O); 4.5 (4H, br. s, CHN$\underline{H}_2$).

N-[N^{α},N^{δ}-bis(*tert*-butoxycarbonyl)-L-ornithyl]-L-cystine bis(*O,O′*-dipalmitoyl-diethanolamide) (5a)

To a solution of 0.068 g (0.205 mmol) of Boc$_2$Orn in DCM cooled to 0°C, 0.081 g (0.213 mmol) of HBTU and 0.028 g (0.213 mmol) of DIPEA were added with stirring, and the mixture was stirred for 30 min. Then 0.101 g (0.074 mmol) of compound **4a** was added. The process was then carried out similarly to the preparation of compound **3a**. The product was isolated by preparative chromatography on a silica gel plate in system (B). 0.030 g (24%) of compound **5a** was obtained, R_f (B) 0.6.

^{1}H NMR spectrum of compound **5a**: 0.88 (12H, t, J = 6.7 Hz, C$\underline{H}_3$); 1.25 (96H, s, –C$\underline{H}_2$–); 1.43 (18H, s, CC$\underline{H}_3$); 1.54–1.65 (8H, m, β-C$\underline{H}_2$); 2.26–2.34 (8H, m, α-C$\underline{H}_2$); 2.95–3.06 (4H, m, C$\underline{H}_2$–S); 3.4–3.9 (8H, m, C$\underline{H}_2$–CH$_2$–O); 4.15–4.29 (8H, m, CH$_2$–C$\underline{H}_2$–O); 4.88–4.98 (2H, m, C–CH$_2$–S); 5.30–5.38 (2H, m, CON$\underline{H}$CHCO).

Bis-*N,N′*-[(bis-N^{α},N^{δ}-*tert*-butoxycarbonyl)-L-ornithyl]-L-cystine bis-(*O,O′*-dimyristoyldiethanolamide) (6b)

Much like the preparation of compound **3a**, from 0.020 g (0.06 mmol) of Boc_2Orn and 0.0315 g (0.025 mmol) of compound **4b**, 0.013 g (28%) of compound **6b** was obtained. The product was isolated by preparative chromatography in system (D), R_f (D) 0.42.

^{1}H NMR spectrum of compound **6b**: 0.88 (12H, t, J = 6.7 Hz, C$\underline{H}_3$); 1.26 (80H, s, –C$\underline{H}_2$–); 1.42 (36H, s, CC$\underline{H}_3$); 1.55–1.66 (8H, m, β-C$\underline{H}_2$); 2.26–2.37 (8H, m, α-C$\underline{H}_2$); 3.05–3.14 (4H, m, C$\underline{H}_2$–S); 3.46–3.67 (8H, m, C$\underline{H}_2$–CH_2–O); 4.12–4.25 (8H, m, CH_2–C$\underline{H}_2$–O); 4.60 (2H, br. s, C$\underline{H}$-CH_2–S); 5.00–5.04 (2H, m, CON$\underline{H}$CHCO).

N-(L-Ornithyl)-L-cystine bis(*O,O′*-dipalmitoyl-diethanolamide) trifluoroacetate (7a)

To 0.013 g (0.0078 mmol) of compound **5a**, 0.230 mL (3.09 mmol) of trifluoroacetic acid in 3 mL of DCM was added. The reaction progress was monitored by TLC. They were stirred for 1 h. After that, the solvent was removed using a rotary evaporator. 0.010 g (75%) of compound **7a** was obtained, R_f (C) 0.1. MALDI TOF (*m/z*): calculated for $[C_{83}H_{160}N_6O_{11}S_2]^+$ 1481.159, found 1481.157 $[M]^+$.

^{1}H NMR spectrum of compound **7a**: 0.88 (12H, t, J = 6.7 Hz, C$\underline{H}_3$); 1.26 (96H, s, –C$\underline{H}_2$–); 1.56–1.64 (8H, m, β-C$\underline{H}_2$); 1.72–2.15 (4H, m, (Orn)–C$\underline{H}_2$–); 2.26–2.34 (8H, m, α-C$\underline{H}_2$); 2.95–3.06 (4H, m, C$\underline{H}_2$–S); 3.5–3.68 (8H, m, C$\underline{H}_2$–CH_2–O); 4.35–4.44 (8H, m, CH_2–C$\underline{H}_2$–O); 4.45–4.56 (2H, m, C$\underline{H}$–CH_2–S); 7.93 (3H, br. s, CH_2N$\underline{H}_3$); 8.97 (6H, br. s, C(O)CHN$\underline{H}_3$).

Trifluoroacetate of bis-*N,N′*-(L-ornithyl)-L-cystine bis-(*O,O′*-dimyristoyl-diethanolamide) (8b)

The reaction was carried out similarly to the preparation of compound **7a**. 0.126 mL (1.7 mmol) of trifluoroacetic acid was added to 0.008 g (0.0042 mmol) of compound **6b**. 0.005 g (71%) of compound **8b** was obtained, R_f (C) 0.1. MALDI TOF (*m/z*): calculated for $[C_{80}H_{158}N_8O_{12}S_2]^{4+}$ 371.786, found 371.785 $[M+4H]^{4+}$.

^{1}H NMR spectrum of compound **8b**: 0.88 (12H, t, J = 6.7 Hz, C$\underline{H}_3$); 1.26 (80H, s, –C$\underline{H}_2$–); 1.55–1.65 (8H, m, β-C$\underline{H}_2$); 1.70–2.11 (8H, m, (Orn)–C$\underline{H}_2$–); 2.26–2.37 (8H, m, α-C$\underline{H}_2$); 2.95–3.06 (4H, m, C$\underline{H}_2$–S); 3.52–3.68 (8H, m, C$\underline{H}_2$–CH_2–O); 4.35–4.44 (8H, m, CH_2–C$\underline{H}_2$–O); 7.94 (6H, br. s, CH_2N$\underline{H}_3$); 9.12 (6H, br. s, C(O)CHN$\underline{H}_3$).

[*N,N′*-bis(*tert*-butoxycarbonyl)-L-cystine] dihexadecyl-L-glutamate (10)

Much like the preparation of compound **3a**, from 0.330 g (0.75 mmol) of compound **1** and 0.350 g (0.60 mmol) of compound **9**, 0.043 g (22%) of compound **10** was obtained. The product was isolated by preparative TLC in system (A), R_f (B) 0.8.

^{1}H NMR spectrum of compound **10**: 0.87 (6H, t, J = 6.7 Hz, CH_3); 1.3 (58H, s, CH_2); 1.44–1.50 (18H, m, CCH_3); 1.6 (4H, s, β-CH_2); 1.86–1.92 (4H, m, α-C$\underline{H}_2$); 3.25 (2H, s, C$\underline{H}_2$–S); 3.67 (2H, t, J = 6.5 Hz, C$\underline{H}_2$–S); 3.8 (1H, t, J = 6.5 Hz, C(O)–NH–Glu); 4.8 (2H br. s, C$\underline{H}$–CH_2–S); 5.44–5.58 (2H, m, $\underline{H}_3$CCNH–CH(COOH)–CH_2).

[*N,N′*-bis(*tert*-butoxycarbonyl)-L-cystine] dihexadecyl-L-glutamate *O,O′*-dipalmitoyl-diethylamine (12a)

Much like the preparation of compound **3a**, from 0.032 g (0.032 mmol) of compound **10** and 0.019 g (0.032 mmol) of **2a**, 0.040 g (77%) of compound **12a** was obtained. The product was isolated by preparative TLC in system (E), R_f (B) 0.9.

^{1}H NMR spectrum of compound **12a**: 0.91 (12H, t, J = 6.7 Hz, C$\underline{H}_3$); 1.3 (106H, s, C$\underline{H}_2$); 1.41–1.47 (18H, m, CC$\underline{H}_3$); 1.53 (8H, s, β-C$\underline{H}_2$); 1.6–1.7 (8H, m, α-C$\underline{H}_2$); 3.35(4H, dd, C$\underline{H}_2$–S–); 3.65–3.76 (4H, m, C$\underline{H}_2$–CH_2–O); 4.10–4.20 (4H, m, CH_2–C$\underline{H}_2$–O); 4.8 (2H br. s, C$\underline{H}$–CH_2–S); 5.38–5.46 (2H, m, CON$\underline{H}$CHCO).

[*N,N′*-bis(*tert*-butoxycarbonyl)-L-cystinyl](dihexadecyl-L-glutamate)-(didecyl-L-glutamate) (12b)

Much like the preparation of compound **3a**, from 0.065 g (0.064 mmol) of **10** and 0.030 g (0.064 mmol) of **11**, 0.015 g (17%) of compound **12b** was obtained, R_f (B) 0.78.

^{1}H NMR spectrum of compound **12b**: 0.88 (12H, t, J = 6.7 Hz, C$\underline{H}_3$); 1.27 (90H, s, C$\underline{H}_2$); 1.44–1.47 (18H, m, CC$\underline{H}_3$); 1.82 (8H, dd, O–CH_2–C$\underline{H}_2$); 2.35–2.5 (8H, m, O–C$\underline{H}_2$–CH_2); 3.64 (4H, t, J = 6.5 Hz, C$\underline{H}_2$–S); 4.78 (2H br. s, C$\underline{H}$–CH_2–S); 5.56–5.6 (4H, m, CON$\underline{H}$CHCO).

L-Cystinyl-(dihexadecyl-L-glutamate)-(*O,O′*-dipalmitoyl-diethylamine) trifluoroacetate (13)

A solution of 1 mL (14.7 mmol) of trifluoroacetic acid in 3 mL of TCM was added to 0.040 g (0.025 mmol) of compound **12a**. After 2 h, the solvent was removed using a rotary evaporator. 0.029 g of product **13** with was

obtained an 82% yield, R_f (E) 0.9. MALDI TOF (*m/z*): calculated for $[C_{79}H_{152}N_4O_{10}S_2]^{2+}$ 690.751, found 690.748 $[M+2H]^{2+}$.

^{1}H NMR spectrum of compound **13**: 0.91 (12H, t, *J* = 6.7 Hz, C$\underline{H}_3$); 1.3 (106H, s, C$\underline{H}_2$); 1.53 (8H, s, β-C$\underline{H}_2$); 1.64–1.72 (8H, m, α-C$\underline{H}_2$); 3.35 (4H, dd, C$\underline{H}_2$–S–); 3.60–3.73 (4H, m, C$\underline{H}_2$–CH$_2$–O); 4.13–4.27 (4H, m, CH$_2$–C$\underline{H}_2$–O); 4.8 (2H br. s, C$\underline{H}$–CH$_2$–S); 6.91 (6H, br. s, CHN$\underline{H}_3$).

L-cystinyl-(dihexadecyl-L-glutamate)-(didecyl-L-glutamate) trifluoroacetate (14)

The synthesis of compound **14** was carried out similarly to compound **13**. From 0.015 g (0.011 mmol) of **12b**, 0.007 g of product **14** was obtained with a yield of 50%, R_f (B) 0.8. MALDI TOF (*m/z*): calculated for $[C_{68}H_{132}N_4O_{10}S_2]^{2+}$ 614.716, found 614.719 $[M+2H]^{2+}$.

^{1}H NMR spectrum of compound **14**: 0.92 (12H, t, *J* = 6.7 Hz, C$\underline{H}_3$); 1.27 (80H, m, C$\underline{H}_2$); 1.77 (8H, dd, O–CH$_2$–C$\underline{H}_2$); 2.04–2.08 (8H, m, O–C$\underline{H}_2$–CH$_2$); 2.3–2.35 (8H, m, (Glu)–C$\underline{H}_2$); 3.07–3.15 (2H, m, N$\underline{H}$); 4.05–4.12 (4H, m, CH–C$\underline{H}_2$–S); 4.48 (2H, m, CONHC$\underline{H}$CO); 4.6 (6H, br. s, CHN$\underline{H}_3$); 4.78 (2H br. s, C$\underline{H}$–CH$_2$–S).

Bis-[*N,N′*-di-(*tert*-butoxycarbonyl)-L-ornithyl]-L-cystinyl-(dihexadecyl-L-glutamate)-(didecyl-L-glutamate) (15)

0.007 mg (0.0053 mmol) of compound **14** was dissolved in TCM and washed with a 5% solution of sodium bicarbonate. The organic residue was filtered on a pleated filter wetted with TCM. Next, following a similar procedure to that used to obtain compound **3a**, 4.2 g (0.012 mol) of Boc$_2$Orn were added, yielding 0.002 g (70%) of compound **15**. The product was isolated by preparative chromatography in system (E), R_f (E) 0.38.

^{1}H NMR spectrum of compound **15**: 0.9 (12H, t, *J* = 6.7 Hz, C$\underline{H}_3$); 1.27 (84H, m, C$\underline{H}_2$); 1.3–1.5 (36H, m, CC$\underline{H}_3$); 1.65–1.75 (16H, m, C$\underline{H}_2$); 1.77 (8H, dd, O–CH$_2$–C$\underline{H}_2$); 2.04–2.08 (8H, m, O–C$\underline{H}_2$–CH$_2$); 3.07–3.15 (6H, m, N$\underline{H}$); 4.05–4.12 (4H, m, CH–C$\underline{H}_2$–S); 4.78 (2H br. s, C$\underline{H}$–CH$_2$–S).

Trifluoroacetate of bis-*N,N′*-(L-ornithyl)-L-cystine-dihexadecyl-L-glutamate-didecyl-L-glutamate (16)

The reaction was carried out similarly to the preparation of compound **7a**. 1.5 mL (0.026 mol) of trifluoroacetic acid was added to 0.002 g (0.0011 mmol) of compound **15**. 0.004 g (70%) of compound **16** was obtained, R_f (E) 0.1. MALDI TOF (*m/z*): calculated for $[C_{78}H_{153}N_8O_{12}S_2]^{3+}$ 487.317, found 487.313 $[M+3H]^{3+}$.

^{1}H NMR spectrum of compound **16**: 0.9 (12H, t, *J* = 6.7 Hz, C$\underline{H}_3$); 1.27 (84H, m, C$\underline{H}_2$); 1.51–1.60 (16H, m, C$\underline{H}_2$); 1.65–1.81 (8H, m, (Orn)–C$\underline{H}_2$–); 1.94 (8H, dd, O–CH$_2$–C$\underline{H}_2$); 2.14–2.21 (8H, m, O–C$\underline{H}_2$–CH$_2$); 4.04–4.13 (4H, m, CH–C$\underline{H}_2$–S); 4.78 (2H br. s, C$\underline{H}$–CH$_2$–S); 7.84 (6H, br. s, CH$_2$N$\underline{H}_3$); 8.36 (6H, br. s, C(O)CHN$\underline{H}_3$).

Preparation of liposomal dispersions

The synthesized substances (5 mg), PC (5 mg), and Chol (3 mg) were dissolved in a TCM/MeOH mixture (5 : 1). The solvents were slowly evaporated on a rotary evaporator at 30°C and 30 rpm until a thin film formed, and then dried under vacuum for 30 min. Following hydration with distilled water for 30 min with stirring, the films were treated in an ultrasonic bath for 30 min at 60°C. Liposomal dispersions were obtained with an amphiphile concentration of 2 mg/mL.

The size distribution of liposomal particles was assessed using photon correlation spectroscopy, which is based on the principles of dynamic light scattering (DLS). Measurements of the average particle diameter and ζ potential were performed using a Delsa Nano C instrument (*Beckman Coulter*, USA). Each measurement was taken three times. The obtained correlation functions were analyzed using the Delsa NanoUi Software version 2.73, which is included with the instrument (*Beckman Coulter*, USA, https://www.beckmancoulter.com).

RESULTS AND DISCUSSION

In this study, schemes were developed and a series of new dimeric cationic lipopeptides with an irregular structure based on L-cystine were synthesized (Schemes 1 and 2).

The hydrophobic block was attached to Boc-protected L-cystine using the carbodiimide method. Following the isolation of products **3a**–**b** by silica gel chromatography, their structures were confirmed by ^{1}H NMR spectroscopy data. In the ^{1}H NMR spectra of compounds **3a**–**b**, characteristic signals were observed for the methyl group protons (0.88 ppm), as well as the methylene units of the fatty acid hydrocarbon chains and the methyl group protons of the *tert*-butoxycarbonyl protecting group (1.4 ppm).

The low yield of compound **3b** (11.6%) is due to difficulties in its isolation from the reaction mixture by column chromatography as a result of its unexpectedly low chromatographic mobility compared to compound **3a**. Compound **3b** could only be isolated using preparative TLC.

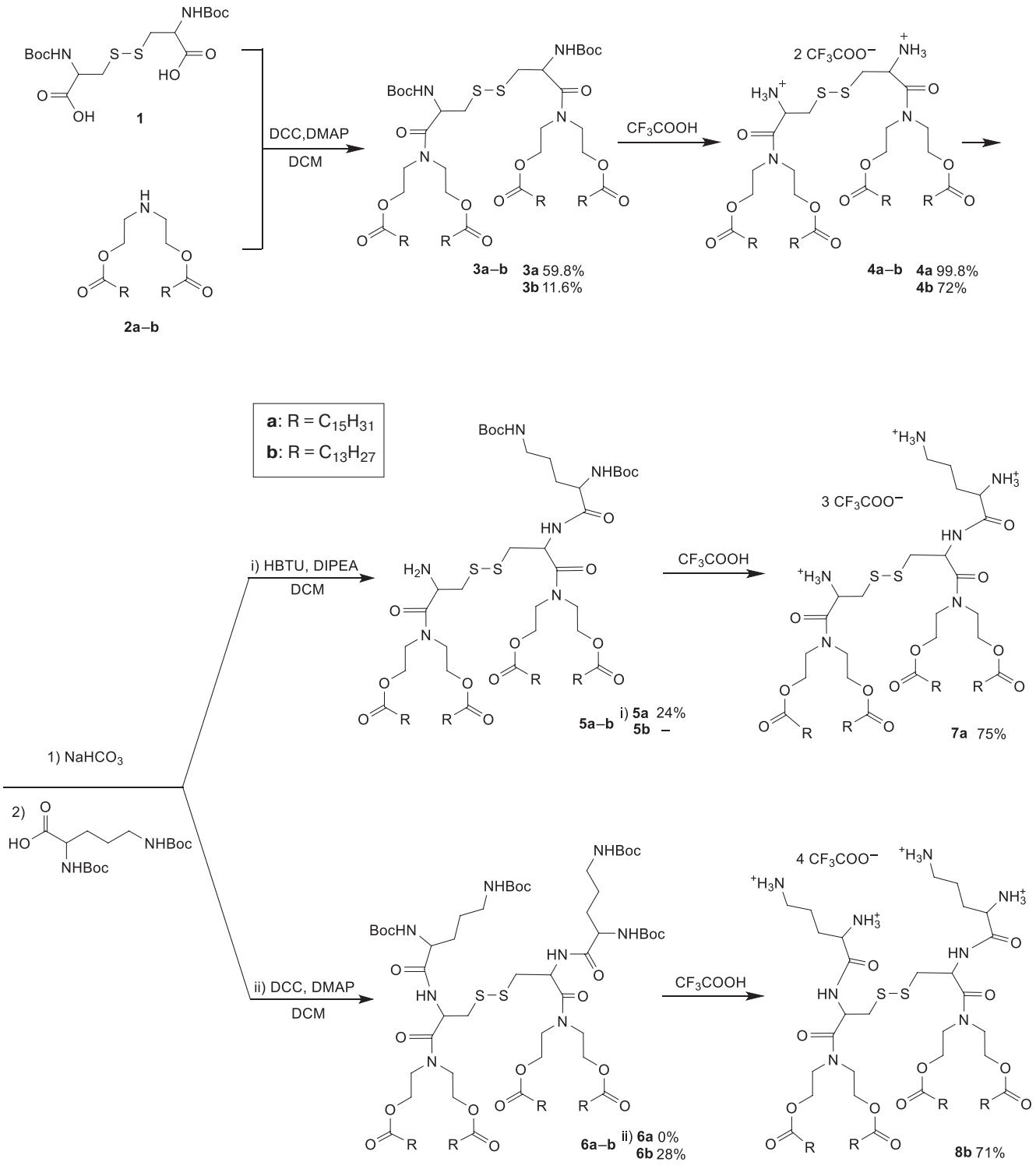

Scheme 1. Synthesis of dimeric amphiphiles with a symmetrical hydrophobic block

Compounds **4a**–**b**, **13**, and **14** were obtained by removing the protecting groups with trifluoroacetic acid in DCM, followed by treatment of the trifluoroacetates with a 5% solution of sodium bicarbonate. In the ^{1}H NMR spectra of the obtained compounds, the signal corresponding to the Boc protecting groups disappeared. Then Boc_2Orn was added to compounds **4a**–**b** and **14**.

When using DCC and DMAP reagents for compounds **4b** and **14**, the reaction mixture predominantly contained products **6b** and **15** with two molecules of L-ornithine attached to the amino groups of L-cystine. The reaction of Boc_2Orn in the presence of DCC and DMAP reagents on compound **4a** did not yield the target dimer **6a**. When HBTU and DIPEA were used

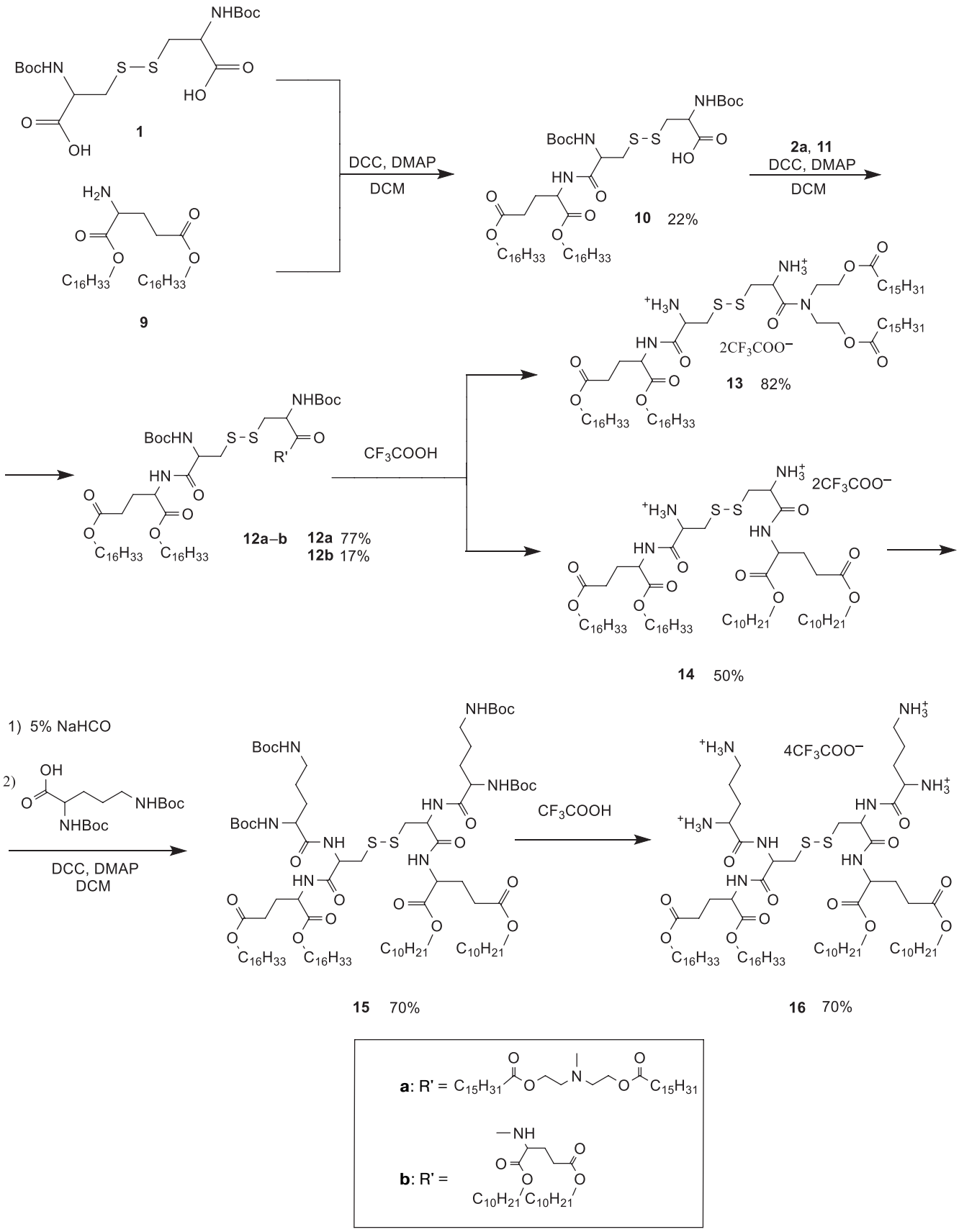

Scheme 2. Synthesis of dimeric amphiphiles with an asymmetric hydrophobic block

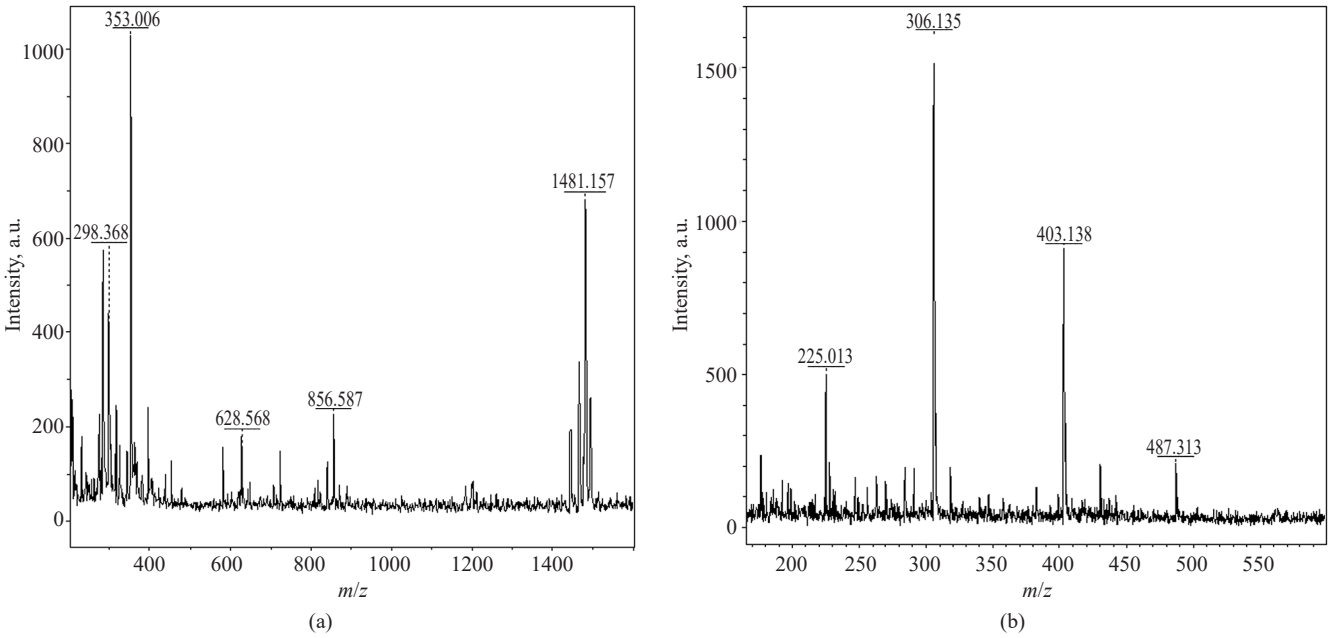

Fig. 1. MALDI TOF mass spectra of compounds **7a** (a) and **16** (b)

in the reaction involving **4a** at the same reagent ratios, product **5a** was formed, containing one molecule of L-ornithine in the hydrophilic block. In this connection, it is possible that the high hydrophobicity of the four 16-carbon chains creates a barrier to the interaction of the amino groups with the activated carboxyl component.

Products **5**–**6**, **10**, **12a**–**b**, and **15** were isolated by preparative TLC on silica gel and their structure confirmed by ^{1}H NMR spectroscopy data. The spectra showed the appearance of proton signals corresponding to Boc protecting groups, the ornithine hydrocarbon skeleton, and peptide bond protons (around 5 ppm).

Final products **7a**, **8b**, and **15** were obtained by removing the protecting groups with trifluoroacetic acid in DCM. The mass spectra of the obtained compounds showed molecular ion peaks (Fig. 1).

Liposomal dispersions were prepared by the thin film hydration method using compounds **7a**, **8b**, **14**, and **16**, trifluoroacetate salts of compounds **4b** and **13**, soybean PC, and Chol. A mass ratio of synthesized compound/PC/Chol = 5 : 5 : 3 was chosen for all films [14].

The average hydrodynamic size of the obtained particles was determined from the obtained DLS dispersions (Fig. 2). The results are presented in the table.

Table. Particle diameter and ζ potential measurement results

System of components	Diameter of the obtained particles, nm	Polydispersity index	ζ potential, mV
4b–PC–Chol	43 ± 8	0.313 ± 0.03	+51 ± 5
7a–PC–Chol	72 ± 13	0.297 ± 0.03	+82 ± 12
8b–PC–Chol	81 ± 17	0.241 ± 0.02	+62 ± 9
13–PC–Chol	80 ± 56	0.301 ± 0.03	+51 ± 8
14–PC–Chol	93 ± 66	0.245 ± 0.02	+46 ± 5
16–PC–Chol	157 ± 72	0.306 ± 0.03	+38 ± 6

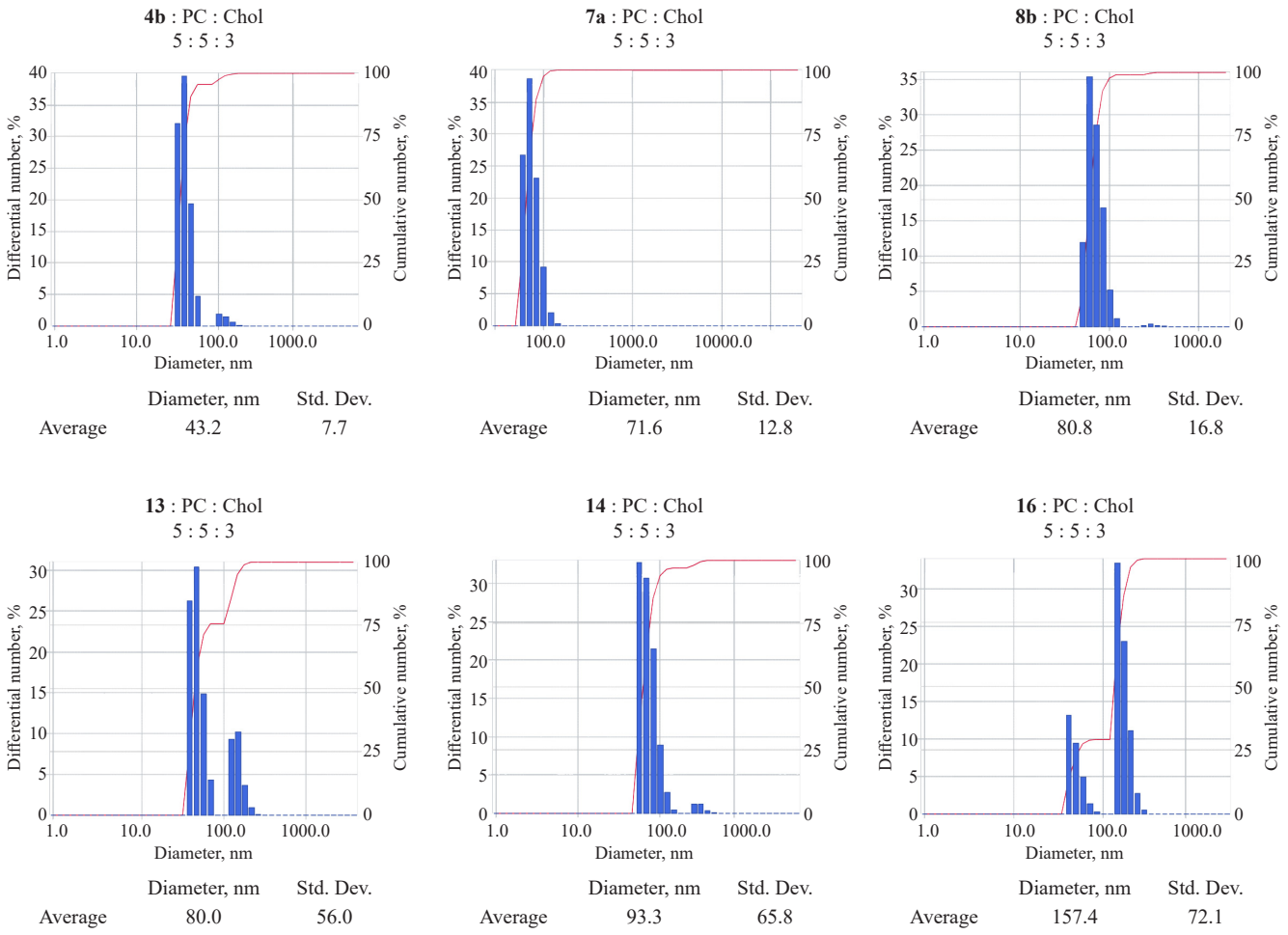

Fig. 2. Hydrodynamic diameters of liposomal particles based on compounds **4b**, **7a**, **8b**, **13**, **14**, and **16**

The resulting average particle diameter falls within the range of 50 to 200 nm, which is optimal for creating transport systems. Thanks to the enhanced permeability and retention effect due to increased vascular perforation, there is an increased accumulation of such liposomal delivery systems in the affected area compared to healthy tissues [15, 16]. The synthesized symmetric dimeric amphiphiles are observed to form liposomal dispersions with a smaller particle diameter than their asymmetric counterparts. Compounds **4b**, **7a**, and **8b**, having a symmetrical hydrophobic block, formed liposomal particles with a smaller diameter than similar asymmetrical compounds **13**, **14**, and **16** (43–80 nm *vs* 80–160 nm). Symmetrical amphiphiles form smaller liposomes than asymmetrical ones. This is probably because the aliphatic chains of the former are packed more tightly in a bilayer due to hydrophobic interactions, leading to the formation of more compact aggregates.

The ζ potential values for the formed dispersions were determined to be in the range of +38 to +82 mV. Such high values are due to the presence of several positively charged groups in the amphiphile molecules, which can provide stability and efficient complex formation of liposomal particles with nucleic acid through electrostatic interactions.

Compared to similar compounds, the resulting amphiphiles form smaller aggregates with a higher surface charge density, which may provide better compaction of nucleic acids in the lipoplex [10].

CONCLUSIONS

As a result of the study, a scheme for obtaining irregular dimeric lipopeptides was developed and the corresponding synthesis was carried out. The physicochemical properties of aqueous dispersions based on the synthesized compounds were studied. The amphiphiles mixed with PC and Chol formed liposomal particles with an average diameter ranging from 50 to 200 nm. The influence of amphiphile structure on the size of the resulting aggregates is demonstrated.

It is established that the most significant parameter influencing particle size is the number of L-ornithine residues (0, 1, 2) in the composition of the target products.

Acknowledgments

This work was performed using the equipment of the Center for Collective Use at the RTU MIREA and supported by the Ministry of Science and Higher Education of the Russian Federation (agreement No. 075-15-2021-689 dated September 01, 2021).

Authors' contributions

T.A. Volodin—conducting research, collecting and providing material, and writing the text of the article.

P.P. Polikashina—conducting research, collecting and providing material, writing the text of the article.

U.A. Budanova—advising on the individual stages of research, scientific editing the article.

Y.L. Sebyakin—research idea, literature analysis, and scientific editing the article.

The authors declare no conflicts of interest.

REFERENCES

1. Yadav M.R., Kumar M., Murumkar P.R. Further studies on cationic gemini amphiphiles as carriers for gene delivery-the effect of linkers in the structure and other factors affecting the transfection efficacy of these amphiphiles. *ACS Omega*. 2021;6(49): 33370–33388. https://doi.org/10.1021/acsomega.1c03667
2. Schambach A., Buchholz C.J., Torres-Ruiz R., Cichutek K., Morgan M., Trapani I., Büning H. A new age of precision gene therapy. *The Lancet*. 2024;403(10426):568–582. https://doi.org/10.1016/s0140-6736(23)01952-9
3. Pashkov E.A., Korotysheva M.O., Pak A.V., Faizuloev E.B., Sidorov A.V., Poddubikov A.V., Bystritskaya E.P., Dronina Yu.E., Solntseva V.K., Zaiceva T.A., Pashkov E.P., Bykov A.S., Svitich O.A., Zverev V.V. Investigation of the anti-influenza activity of siRNA complexes against the cellular genes *FLT4*, *Nup98*, and *Nup205 in vitro*. *Tonk. Khim. Tekhnol. = Fine Chem. Technol*. 2022;17(2):140–151. https://doi.org/10.32362/2410-6593-2022-17-2-140-151
4. Sharma D., Arora S., Singh J., Layek B. A review of the tortuous path of nonviral gene delivery and recent progress. *Int. J. Biol. Macromol*. 2021;183:2055–2073. https://doi.org/10.1016/j.ijbiomac.2021.05.192
5. John R., Monpara J., Swaminathan S., Kalhapure R. Chemistry and Art of Developing Lipid Nanoparticles for Biologics Delivery: Focus on Development and Scale-Up. *Pharmaceutics*. 2024;16(1):131. https://doi.org/10.3390/pharmaceutics16010131
6. Muñoz-Úbeda M, Misra S.K., Barrán-Berdón A.L., Datta S., Aicart-Ramos C., Castro-Hartmann P., Kondaiah P., Junquera E., Bhattacharya S., Aicart E. How does the spacer length of cationic gemini lipids influence the lipoplex formation with plasmid DNA? Physicochemical and biochemical characterizations and their relevance in gene therapy. *Biomacromolecules*. 2012;13(12):3926–3937. https://doi.org/10.1021/bm301066w
7. Yang H.W., Yi J.W., Bang E.K., Jeon E.M., Kim B.H. Cationic nucleolipids as efficient siRNA carriers. *Org. Biomol. Chem*. 2011;9(1):291–296. https://doi.org/10.1039/C0OB00580K
8. Chang D.C., Zhang Y.M., Zhang J., Liu Y.H., Yu X.Q. Cationic gemini lipids with cyclen headgroups: interaction with DNA and gene delivery abilities. *RSC Adv.* 2014;4(83): 44261–44268. https://doi.org/10.1039/C4RA05974C
9. Koloskova O.O., Nikonova A.A., Budanova U.A., Shilovskiy I.P., Kofiadi I.A., Ivanov A.V., Smirnova O.A., Zverev V.V., Sebaykin Y.L., Andreev S.M., Khaitov M.R. Synthesis and evaluation of novel lipopeptide as a vehicle for efficient gene delivery and gene silencing. *Eur. J. Pharm. Biopharm*. 2016;102:159–167. https://doi.org/10.1016/j.ejpb.2016.03.014

СПИСОК ЛИТЕРАТУРЫ

1. Yadav M.R., Kumar M., Murumkar P.R. Further studies on cationic gemini amphiphiles as carriers for gene delivery-the effect of linkers in the structure and other factors affecting the transfection efficacy of these amphiphiles. *ACS Omega*. 2021;6(49): 33370–33388. https://doi.org/10.1021/acsomega.1c03667
2. Schambach A., Buchholz C.J., Torres-Ruiz R., Cichutek K., Morgan M., Trapani I., Büning H. A new age of precision gene therapy. *The Lancet*. 2024;403(10426):568–582. https://doi.org/10.1016/s0140-6736(23)01952-9
3. Пашков Е.А., Коротышева М.О., Пак А.В., Файзулоев Е.Б., Сидоров А.В., Поддубиков А.В., Быстрицкая Е.П., Дронина Ю.Е., Солнцева В.К., Зайцева Т.А., Пашков Е.П., Быков А.С., Свитич О.А., Зверев В.В. Исследование противогриппозной активности комплексов миРНК против клеточных генов *FLT4*, *Nup98* и *Nup205* на модели *in vitro*. *Тонкие химические технологии*. 2022;17(2):140–151. https://doi.org/10.32362/2410-6593-2022-17-2-140-151
4. Sharma D., Arora S., Singh J., Layek B. A review of the tortuous path of nonviral gene delivery and recent progress. *Int. J. Biol. Macromol*. 2021;183:2055–2073. https://doi.org/10.1016/j.ijbiomac.2021.05.192
5. John R., Monpara J., Swaminathan S., Kalhapure R. Chemistry and Art of Developing Lipid Nanoparticles for Biologics Delivery: Focus on Development and Scale-Up. *Pharmaceutics*. 2024;16(1):131. https://doi.org/10.3390/pharmaceutics16010131
6. Muñoz-Úbeda M., Misra S.K., Barrán-Berdón A.L., Datta S., Aicart-Ramos C., Castro-Hartmann P., Kondaiah P., Junquera E., Bhattacharya S., Aicart E. How does the spacer length of cationic gemini lipids influence the lipoplex formation with plasmid DNA? Physicochemical and biochemical characterizations and their relevance in gene therapy. *Biomacromolecules*. 2012;13(12):3926–3937. https://doi.org/10.1021/bm301066w
7. Yang H.W., Yi J.W., Bang E.K., Jeon E.M., Kim B.H. Cationic nucleolipids as efficient siRNA carriers. *Org. Biomol. Chem*. 2011;9(1):291–296. https://doi.org/10.1039/C0OB00580K
8. Chang D.C., Zhang Y.M., Zhang J., Liu Y.H., Yu X.Q. Cationic gemini lipids with cyclen headgroups: interaction with DNA and gene delivery abilities. *RSC Adv.* 2014;4(83): 44261–44268. https://doi.org/10.1039/C4RA05974C
9. Koloskova O.O., Nikonova A.A., Budanova U.A., Shilovskiy I.P., Kofiadi I.A., Ivanov A.V., Smirnova O.A., Zverev V.V., Sebaykin Y.L., Andreev S.M., Khaitov M.R. Synthesis and evaluation of novel lipopeptide as a vehicle for efficient gene delivery and gene silencing. *Eur. J. Pharm. Biopharm*. 2016;102:159–167. https://doi.org/10.1016/j.ejpb.2016.03.014

10. Kedika B., Patri S.V. Synthesis and Gene Transfer Activities of Novel Serum Compatible Reducible Tocopherol-Based Cationic Lipids. *Mol. Pharm*. 2012;9(5):1146–1162. https://doi.org/10.1021/mp200435y
11. Li D., Zhang R., Liu G., Kang Y., Wu J. Redox-Responsive Self-Assembled Nanoparticles for Cancer Therapy. *Adv. Healthc. Mater*. 2020;9(20):2000605. https://doi.org/10.1002/adhm.202000605
12. Korotkin M.D., Filatova S.M., Denieva Z.G., Budanova U.A., Sebyakin Y.L. Synthesis of diethanolamine-based amino acid derivatives with symmetric and asymmetric radicals in their hydrophobic domain and potential antimicrobial activity. *Tonk. Khim. Tekhnol. = Fine Chem. Technol*. 2022;17(1):50–64. https://doi.org/10.32362/2410-6593-2022-17-1-50-64
13. Denieva Z.G., Budanova U.A., Sebyakin Y.L. Synthesis of Cationic and Ionizable Amphiphiles Based on Heminal Aminodiol as Potential siRNA Delivery Systems. *Tonk. Khim. Tekhnol. = Fine Chem. Technol*. 2019;14(3):42–49 (in Russ.). https://doi.org/10.32362/2410-6593-2019-14-3-42-49
14. Bukharin G.A., Budanova U.A., Denieva Z.G., *et al*. Cationic and ionizable amphiphiles based on di-hexadecyl ester of *L*-glutamic acid for liposomal transport of RNA. *Biochem. Moscow Suppl. Ser. A*. 2024;18(4):313–323. https://doi.org/10.1134/S1990747824700314
[Original Russian Text: Bukharin G.A., Budanova U.A., Denieva Z.G., Dubrovin E.V., Sebyakin Y.L. Cationic and ionizable amphiphiles based on di-hexadecyl ester of *L*-glutamic acid for liposomal transport of RNA. *Biologicheskie membrany*. 2024;41(4):309–321 (in Russ.). https://doi.org/10.31857/S0233475524040035]
15. Maritim S., Boulas P., Lin Y. Comprehensive analysis of liposome formulation parameters and their influence on encapsulation, stability and drug release in glibenclamide liposomes. *Int. J. Pharm.* 2021;592:120051. https://doi.org/10.1016/j.ijpharm.2020.120051
16. Liu Y., Castro Bravo K.M., Liu J. Targeted liposomal drug delivery: a nanoscience and biophysical perspective. *Nanoscale Horiz*. 2021;6(2):78–94. https://doi.org/10.1039/D0NH00605J

10. Kedika B., Patri S.V. Synthesis and Gene Transfer Activities of Novel Serum Compatible Reducible Tocopherol-Based Cationic Lipids. *Mol. Pharm*. 2012;9(5):1146–1162. https://doi.org/10.1021/mp200435y
11. Li D., Zhang R., Liu G., Kang Y., Wu J. Redox-Responsive Self-Assembled Nanoparticles for Cancer Therapy. *Adv. Healthc. Mater*. 2020;9(20):2000605. https://doi.org/10.1002/adhm.202000605
12. Короткин М.Д., Филатова С.М., Дениева З.Г., Буданова У.А., Себякин Ю.Л. Синтез производных аминокислот на основе диэтаноламина с симметричными и асимметричными радикалами в гидрофобном домене с потенциальной антимикробной активностью. *Тонкие химические технологии*. 2022;17(1):50–64. https://doi.org/10.32362/2410-6593-2022-17-1-50-64
13. Дениева З.Г., Буданова У.А., Себякин Ю.Л. Синтез катионных и ионизируемых амфифилов на основе геминального аминодиола как потенциальных транспортных систем миРНК. *Тонкие химические технологии*. 2019;14(3):42–49. https://doi.org/10.32362/2410-6593-2019-14-3-42-49
14. Бухарин Г.А., Буданова У.А., Дениева З.Г., Дубровин Е.В., Себякин Ю.Л. Катионные и ионизируемые амфифилы на основе дигексадецилового эфира *L*-глутаминовой кислоты для липосомального транспорта РНК. *Биологические мембраны*. 2024;41(4):309–321. https://doi.org/10.31857/S0233475524040035
15. Maritim S., Boulas P., Lin Y. Comprehensive analysis of liposome formulation parameters and their influence on encapsulation, stability and drug release in glibenclamide liposomes. *Int. J. Pharm.* 2021;592:120051. https://doi.org/10.1016/j.ijpharm.2020.120051
16. Liu Y., Castro Bravo K.M., Liu J. Targeted liposomal drug delivery: a nanoscience and biophysical perspective. *Nanoscale Horiz*. 2021;6(2):78–94. https://doi.org/10.1039/D0NH00605J

About the Authors

Timofey A. Volodin, Master Student, N.A. Preobrazhensky Department of Chemistry and Technology of Biologically Active Compounds, Medicinal and Organic Chemistry, M.V. Lomonosov Institute of Fine Chemical Technologies, MIREA – Russian Technological University (78, Vernadskogo pr., Moscow, 119454, Russia). E-mail: c-221@yandex.ru. https://orcid.org/0009-0009-5974-4809

Polina P. Polikashina, Master Student, N.A. Preobrazhensky Department of Chemistry and Technology of Biologically Active Compounds, Medicinal and Organic Chemistry, M.V. Lomonosov Institute of Fine Chemical Technologies, MIREA – Russian Technological University (78, Vernadskogo pr., Moscow, 119454, Russia). E-mail: c-221@yandex.ru. https://orcid.org/0009-0006-2510-617X

Ulyana A. Budanova, Cand. Sci. (Chem.), Associate Professor, N.A. Preobrazhensky Department of Chemistry and Technology of Biologically Active Compounds, Medical and Organic Chemistry, M.V. Lomonosov Institute of Fine Chemical Technologies, MIREA – Russian Technological University (78, Vernadskogo pr., Moscow, 119454, Russia). E-mail: c-221@yandex.ru. Scopus Author ID 14622352500, ResearcherID E-1659-2014, https://orcid.org/0000-0003-1702-9435

Yurii L. Sebyakin, Dr. Sci. (Chem.), Professor, N.A. Preobrazhensky Department of Chemistry and Technology of Biologically Active Compounds, Medical and Organic Chemistry, M.V. Lomonosov Institute of Fine Chemical Technologies, MIREA – Russian Technological University (78, Vernadskogo pr., Moscow, 119454, Russia). E-mail: c-221@yandex.ru. Scopus Author ID 6701455145, ResearcherID T-2835-2019, https://orcid.org/0000-0002-7027-378X

Об авторах

Володин Тимофей Алексеевич, магистрант, кафедра химии и технологии биологически активных соединений, медицинской и органической химии им. Н.А. Преображенского, Институт тонких химических технологий им. М.В. Ломоносова, ФГБОУ ВО «МИРЭА – Российский технологический университет» (119454, Россия, Москва, пр-т Вернадского, д. 78). E-mail: c-221@yandex.ru. https://orcid.org/0009-0009-5974-4809

Поликашина Полина Павловна, магистрант, кафедра химии и технологии биологически активных соединений, медицинской и органической химии им. Н.А. Преображенского, Институт тонких химических технологий им. М.В. Ломоносова, ФГБОУ ВО «МИРЭА – Российский технологический университет» (119454, Россия, Москва, пр-т Вернадского, д. 78). E-mail: c-221@yandex.ru. https://orcid.org/0009-0006-2510-617X

Буданова Ульяна Александровна, к.х.н., доцент, кафедра химии и технологии биологически активных соединений, медицинской и органической химии им. Н.А. Преображенского, Институт тонких химических технологий им. М.В. Ломоносова, ФГБОУ ВО «МИРЭА – Российский технологический университет» (119454, Россия, Москва, пр-т Вернадского, д. 78). E-mail: c-221@yandex.ru. Scopus Author ID 14622352500, ResearcherID E-1659-2014, SPIN-код РИНЦ 3901-8710, https://orcid.org/0000-0003-1702-9435

Себякин Юрий Львович, д.х.н., профессор, профессор кафедры химии и технологии биологически активных соединений, медицинской и органической химии им. Н.А. Преображенского, Институт тонких химических технологий им. М.В. Ломоносова, ФГБОУ ВО «МИРЭА – Российский технологический университет» (119454, Россия, Москва, пр-т Вернадского, д. 78). E-mail: c-221@yandex.ru. Scopus Author ID 6701455145, ResearcherID T-2835-2019, SPIN-код РИНЦ 3491-3514, https://orcid.org/0000-0002-7027-378X

Translated from Russian into English by H. Moshkov
Edited for English language and spelling by Thomas A. Beavitt

Tonkie Khimicheskie Tekhnologii = Fine Chemical Technologies.
2025;20(5):454–473 ISSN 2686-7575 (Online)

UDC 661.727.83
https://doi.org/10.32362/2410-6593-2025-20-5-454-473
EDN NYBHED

RESEARCH ARTICLE

Dichloromethane solvent for furfural recovery from potato peels: Thermodynamic and kinetic investigations

Abdulhalim Musa Abubakar[1,✉], Iyisikwe Tanimu Umar[1], Abass-Giwa Muhammed Akintunde[2], Muhammad Jimada Aliyu[3], Marwea Al-Hedrewy[4,5], Uday Raheja[6]

[1] *Department of Chemical Engineering, Faculty of Engineering, Modibbo Adama University, P.M.B. 2076, Yola, Adamawa State, Nigeria*

[2] *Department of Chemical Engineering, Faculty of Engineering, University of Maiduguri, P.M.B. 1069, Bama Road, Maiduguri, Borno State, Nigeria*

[3] *Chemical Engineering Department, School of Infrastructure, Process Engineering and Technology, Federal University of Technology, Minna, Niger State, Nigeria*

[4] *College of Technical Engineering, the Islamic University, Najaf, Iraq*

[5] *College of Technical Engineering, the Islamic University of Al Diwaniyah, Al Diwaniyah, Iraq*

[6] *Center for Research Impact & Outcome, Chitkara University Institute of Engineering and Technology (CUIET), Chitkara University, Rajpura, 140401, Punjab, India*

✉ *Corresponding author, e-mail: abdulhalim@mau.edu.ng*

Abstract

Objectives. This study aims to investigate the kinetics and thermodynamics of furfural extraction from sweet potato peels using dichloromethane (CH_2Cl_2) as a solvent and sulfuric acid as a catalyst. To that end, we set out to determine the kinetic parameters for furfural production using first- and second-order models, optimize the extraction temperature, and evaluate the thermodynamic properties of the reaction.

Methods. Potato peels, selected for their high hemicellulose content, cost-effectiveness, and sustainability, were processed with dichloromethane, selected for its safety, low energy requirements, and compatibility with green extraction processes. Experimental conditions involved varying temperatures (60, 70, and 80°C) and peel powder particle sizes (<5 mm), with the reaction being monitored to fit kinetic models and calculate thermodynamic properties.

Results. Experimental findings revealed that the first-order kinetic model provided the best fit, with an activation energy (E_a) of 85.99 kJ/mol. Thermodynamic analysis showed an enthalpy change (ΔH) of 83.14 kJ/mol, entropy change (ΔS) of −86.08 J/(mol·K), and Gibbs free energy (ΔG) values ranging from 111.80 to 112.66 kJ/mol across the studied temperatures. Optimal extraction conditions were achieved at 80°C, yielding the highest furfural concentration through acid-catalyzed hydrolysis. The energy-intensive yet controlled nature of the reaction highlights the need for further optimization.

Conclusions. This study demonstrates the effectiveness of dichloromethane as a solvent for furfural extraction from sweet potato peels under optimized conditions. The kinetic and thermodynamic findings elucidate the reaction mechanism and its industrial applicability. Future studies should focus on simulating furfural separation from ternary solvent systems using Aspen Plus to enhance sustainability and scalability.

Keywords
furfural extraction, dichloromethane, potato peels, extraction kinetics, Eyring–Polanyi model

Submitted: 13.01.2025
Revised: 17.03.2025
Accepted: 03.09.2025

For citation
Abubakar A.M., Umar I.T., Akintunde A.-G.M., Aliyu M.J., Al-Hedrewy M., Raheja U. Dichloromethane solvent for furfural recovery from potato peels: Thermodynamic and kinetic investigations. *Tonk. Khim. Tekhnol. = Fine Chem. Technol.* 2025;20(5):454–473. https://doi.org/10.32362/2410-6593-2025-20-5-454-473

НАУЧНАЯ СТАТЬЯ

Экстракция фурфурола из картофельной шелухи с помощью дихлорметана: термодинамика и кинетика

Abdulhalim Musa Abubakar[1]✉, Iyisikwe Tanimu Umar[1], Abass-Giwa Muhammed Akintunde[2], Muhammad Jimada Aliyu[3], Marwea Al-Hedrewy[4,5], Uday Raheja[6]

[1] *Department of Chemical Engineering, Faculty of Engineering, Modibbo Adama University, P.M.B. 2076, Yola, Adamawa State, Nigeria*

[2] *Department of Chemical Engineering, Faculty of Engineering, University of Maiduguri, P.M.B. 1069, Bama Road, Maiduguri, Borno State, Nigeria*

[3] *Chemical Engineering Department, School of Infrastructure, Process Engineering and Technology, Federal University of Technology, Minna, Niger State, Nigeria*

[4] *College of Technical Engineering, the Islamic University, Najaf, Iraq*

[5] *College of Technical Engineering, the Islamic University of Al Diwaniyah, Al Diwaniyah, Iraq*

[6] *Center for Research Impact & Outcome, Chitkara University Institute of Engineering and Technology (CUIET), Chitkara University, Rajpura, 140401, Punjab, India*

✉ *Автор для переписки, e-mail: abdulhalim@mau.edu.ng*

Аннотация

Цели. Целью данного исследования является изучение кинетики и термодинамики экстракции фурфурола из кожуры сладкого картофеля с использованием дихлорметана (CH_2Cl_2) в качестве растворителя и серной кислоты в качестве катализатора. Для этого было решено определить кинетические параметры производства фурфурола, используя модели первого и второго порядка, оптимизировать температуру экстракции и оценить термодинамические свойства реакции.

Методы. Картофельная кожура была выбрана для экстракции фурфурола из-за высокого содержания в ней гемицеллюлозы, экономичности и экологичности. В качестве растворителя был выбран дихлорметан благодаря его безопасности, низкой энергоемкости и совместимости с экологически чистыми процессами экстракции. Условия эксперимента включали варьирование температур (60, 70 и 80°C) и размеров частиц порошка (<5 мм). В процессе эксперимента осуществлялся контроль на соответствие реакции кинетическим моделям и расчет термодинамических характеристик.

Результаты. Экспериментальные результаты показали, что кинетическая модель первого порядка лучше описывает реакцию, энергия активации (E_a) равна 85.99 кДж/моль. Термодинамический анализ показал изменение энтальпии (ΔH) на 83.14 кДж/моль, изменение энтропии (ΔS) на −86.08 Дж/(моль·К), а свободная энергия Гиббса (ΔG) варьировалась от 111.80 до 112.66 кДж/моль в зависимости от выбранных температур. При температуре 80°C были достигнуты оптимальные условия экстракции, и получена наиболее высокая концентрацию фурфурола методом гидролиза с использованием серной кислоты в качестве катализатора. Реакция имеет энергоемкий, но контролируемый характер, что говорит о необходимости дальнейшей оптимизации процесса.

Выводы. Исследование продемонстрировало эффективность дихлорметана в качестве растворителя для экстракции фурфурола из кожуры сладкого картофеля при оптимальных условиях. Кинетические и термодинамические результаты проясняют механизм реакции и обосновывают ее промышленное применение. Будущие исследования должны быть сосредоточены на моделировании выделения фурфурола из тройных систем растворителей с использованием Aspen Plus для повышения устойчивости и масштабируемости.

Ключевые слова
экстракция фурфурола, дихлорметан, картофельная шелуха, кинетика экстракции, модель Эйринга–Полани

Поступила: 13.01.2025
Доработана: 17.03.2025
Принята в печать: 03.09.2025

Для цитирования
Abubakar A.M., Umar I.T., Akintunde A.-G.M., Aliyu M.J., Al-Hedrewy M., Raheja U. Dichloromethane solvent for furfural recovery from potato peels: Thermodynamic and kinetic investigations. *Tonk. Khim. Tekhnol. = Fine Chem. Technol*. 2025;20(5):454–473. https://doi.org/10.32362/2410-6593-2025-20-5-454-473

INTRODUCTION

Furfural (or furan-2-carbaldehyde, $C_5H_4O_2$) is a colorless or yellowish aromatic aldehyde with a furan ring (a 5-membered aromatic ring containing 1 oxygen atom) and an aldehyde group (–CHO) attached to the 2-position of the furan ring [1, 2]. It finds application in diverse areas, including oil and gas (such as, jet fuel blend stocks), petroleum refining (as a solvent), medicine (e.g., for creation of tuberculosis remedies, as well as antimicrobial, antibiotic, or antifungal agents), agriculture (as a fertilizer, insecticide, nematicide, fungicide or herbicide), food science technology (e.g., flavoring agent), pharmaceuticals, plastic (synthetic fibers and phenolic resins), milling (grinding and abrasive wheels), detergents, cosmetics, rubber, nylon, polymer (as a polyurethane-polyurea copolymer), construction, metal coatings, biofuel and chemical production (pyrrole, pyrrolidine, lysine, lubricants, adhesives, dihydropyran, furan, furfuryl alcohol, tetrahydrofuran, furoic acid, and methyltetrahydrofuran) [3–7]. The precursors of furfural are the arabinan, xylan, and pentosan components derived from agricultural waste rich in hemicellulose and other lignocellulosic materials [8, 9], such as sawdust, rice straw, cotton seed hull bran, flax shives, hazelnut shells, spruce wood, beech wood, pine wood, Douglas-fir wood, poplar, corn stover, oat hulls, sunflower hull, cotton husk, almond shells, corncob, barley hull, sorghum straw, and sugarcane bagasse [10–12]. In [13], Clauser *et al*. used the technology of steam explosion pretreatment of pine sawdust and evaluated the economic, mass, and energy balances involved in furfural recovery from a jacketed batch reactor. Ideally, hemicellulose hydrolysis releases pentoses (e.g., xylose), which are capable of dehydrating under acidic conditions to form furfural [14, 15]. The examples include the stripping of furfural from pentosan-rich corncob by Agirrezabal–Telleria *et al*. [16] and rice husk by Nunez *et al.* [17]. The list of catalysts includes superheated water [18], ionic liquids [19, 20], metallic oxides [11], chlorides (e.g., $AlCl_3$, $FeCl_3$, NaCl, $CaCl_2$, $MgCl_2$, $SnCl_4$, and $CuCl_2$) [21, 22], enzyme [23], silicoaluminophosphate (e.g., SAPO-44) [24], *p*-TsOH [25], γ-alumina (γ-Al_2O_3) [15], HZSM-5 zeolite [26], H-β-zeolite [27], betaine [28], formic acid [29], acetic acid [30], maleic acid [31], hydrochloric acid [32], sulfuric acid [33, 34], phosphoric acid [35], hectorites, fluorohectorites [36], Lewis and Brønsted acid [37, 38]. These are employed via hydrothermal [39] or other processes, as shown in Table 1. Ji *et al.* [25] and Weidener *et al.* [35] proposed a novel recycling scheme as a sustainable and economically feasible way of utilizing mineral acid catalyst to reduce costs and environmental intoxication, as possible solutions to the challenges highlighted in Zhang *et al.* [40], Yong *et al.* [41], and Muryanto *et al.* [42]. The scheme of the aforementioned authors can be extended to extraction projects employing acid solvents as reported by Lee and Wu [43] (see Table 1), despite the need to exercise caution when applying deep eutectic solvents (DES) as mentioned in [44].

Table 1. Biomass employed previously for the extraction of furfural

Method	Solvent	Raw material	Reaction/Extraction parameters	Author
Thermochemical process (supercritical conditions)	Supercritical ethanol	Oil palm	Temp. = 240–280°C; reaction time = 1–30 min; biomass solid loading = 0.4–0.8 g; alcohol/acid ratios = 1 : 1 and 1 : 2	[7]
Subcritical thermochemical process	Subcritical ethanol	Oil palm frond	Temp. = 230°C; reaction time = 20 min; solid loading = 1 g	[45]
Hydrolysate dehydration	Sulfuric acid	Dried oil palm empty fruit bunch	Temp. = 198°C and reaction time = 11 min	[46]

Table 1. Continued

Method	Solvent	Raw material	Reaction/Extraction parameters	Author
Liquid–liquid extraction	Methyl isobutyl ketone (MIBK)	Oil palm empty fruit bunch	Temp. = 105°C and reaction time = 30 min	[47]
Acid hydrolysis followed by dehydration	Sulfuric acid	Oil palm empty fruit bunch	Reaction time = 90 min and 15% acid	[48]
Steam explosion	Sulfuric acid	Oil palm trunk	Temp. = 110, 130, and 170°C; reaction time = 2 and 3 h	[49]
Non-isothermal autohydrolysis	–	Wheat straw and *Eucalyptus globulus*	Temp. = 220°C	[6]
Microwave-assisted process	Hydrochloric acid	Wheat straw	pH 0.22 or 1.77; temp. = 146 or 195°C; L : S ratios = 84 or 90 mL/g; residence times = 31 or 34 min	[32]
Microwave irradiations	MIBK	Wheat straw	Reaction time = 1–2 h and temp. = 120–150°C	[28]
Isothermal autohydrolysis	–	Eucalyptus globulus	Temp. = 220°C and reaction time = 60 min	[50]
Acid hydrolysis	–	Eucalyptus globulus	Medium operation time = 15 min; low temperature = 170°C; pH 2	[51]
Microwave-assisted process	Sulfuric acid	Olive stone	Temp. = 200°C and the addition of 0.1 M $FeCl_3$	[52]
Dilute-acid hydrolysis	Sulfuric acid	Olive stone	Temp. < 40°C and reaction time < 120 s	[34]
Distillation and transesterification reaction	Butanol	Algae and switchgrass	Temp. = 30°C, pressure = 4 bar, time = 8 h, and water amount = 0 g	[23]
Non-isothermal autohydrolysis	MIBK	Birch (*Betula alba*) wood	Temp. = 170°C and reaction time = 60 min	[53]
Acid hydrolysis	Sulfuric acid	Birch wood	Biomass pretreatment time = 90 min	[9]
Acid hydrolysis	Sulfuric acid	Birch wood	Temp. = 147°C and reaction time = 90 min	[54], [55]
In vitro spectrophotometric assays	Fungi metabolism	Cellulose garbage	pH 5.5 and incubation time = 14 days	[5]
Autohydrolysis and separation	Chloroform	Southern cattail (*Typha domingensis*)	Temp. = 177–189°C and reaction time = 30–45 min	[56]
Acid hydrolysis	Sulfuric acid	Pistachio green hulls	Reaction temp. = 152–272°C; acid concentration = 0.5–4.0 mol/L; reaction time = 30–600 s	[57]
Enzymatic hydrolysis	MIBK–water biphasic system	Corn bran	10% KOH solution and aqueous ethanol solution = 40–90%	[58]
N_2- and steam-stripping	Toluene	Corncob	Experimental and Aspen Plus simulation data	[16]
Steam distillation	–	Corncob	Temp. = 180°C and reaction time = 30 min	[21]
Steam distillation at hydrolysis conditions	Concentrated seawater	Corncob	Temp. = 190°C	[59]
Hydrodistillation and autohydrolysis Kraft process	Sulfuric, hydrochloric, and phosphoric acids	Corncobs, sugarcane bagasse, and eucalypt wood	Acid concentration = 1.5–5.2 mol/L	[60]
Acid hydrolysis	Sulfuric acid	Sugarcane bagasse, *Eucalyptus globulus*, and *Acacia longifolia*	Temp. = 150–170°C and reaction time = 30–90 min	[61]

Table 1. Continued

Method	Solvent	Raw material	Reaction/Extraction parameters	Author
Acid hydrolysis	Sulfuric acid	Rice husk	Temp. = 200°C; acid concentration = 0.1% (*w*/*w*); reaction time = 40 min	[62]
Distillation and separation	Sulfuric acid	Rice straw and bagasse	Evaporator temp. = 40°C and acid volume = 4.17 L	[63]
Distillation process	Chloroform	Rice straw	Evaporator temp. = 4°C	[64]
Acid hydrolysis	Sulfuric acid	Rice husk and bagasse	S : L ratio = 1 : 15; temp. = 180°C; 0.4% acid	[65]
Distillation process	Water	Bagasse	Temp. = 170–200°C and reaction time = 40 min	[10]
Distillation process	Hexane	Sugarcane bagasse	S : L ratio = 1 : 15 and temp. = 110°C	[66]
Distillation process	Dichloromethane	Sugarcane bagasse	S : L ratio = 1 : 15; temp. = 110°C; steam pressure = 1.05 kg/cm^2	[67]
Hydrolysis	Phosphoric acid	Sugarcane bagasse	Acetone/water ratio = 7 : 3 *v*/*v* and temp. = 150°C	[68]
Acid hydrolysis	Glycine-based ionic liquid	Sugarcane bagasse	Temp. = 180°C; reaction time = 10 min; 10 eq. of ionic liquid	[69]
One-pot processing	Toluene–water	Bagasse, rice husk, and wheat straw	Temp. = 170°C and reaction time = 10 h	[24]
One-pot system and BRD	*p*-TsOH	Corncob	Effect of temperature and time	[70]
Acid hydrolysis	Sulfuric acid	Corncob	Temp. = 60–160°C; reaction time = 30–90 min; acid concentration = 5–20 wt %	[25]
Acid hydrolysis	Sulfuric acid	Corncob	Temp. = 140–200°C and pressure = 350–1550 kPa	[18]
Microwave irradiation	γ-Valerolactone	Corncob	Temp. = 190°C and S : L ratio = 1 : 20	[71]
Hydrolysis	Sulfuric acid–toluene biphasic system	Corncob	Water/solid ratio ≤ 1 and reaction time = 10 min	[72]
Enzymatic hydrolysis	Ethanol	Milled wood lignin and corncob	Involves Soxhlet extraction	[73]
Microwave-assisted	Butyl acetate–NaCl biphasic system	Corncob and xylose	Temp. = 160°C and reaction time = 60 min	[74]
Microwave-assisted	Toluene	Almond shells	Reaction time = 1 h	[36]
Steam explosion	–	SELRS	Catalyst = 60 g/kg; reaction temp. = 160°C; extraction steam flow rate = 2.5 cm^3/min; sugar concentration = 61.4 kg/m^3	[26]
Fractionation and enzymatic hydrolysis	Aqueous choline chloride (ChCl)	Switchgrass	Pretreatment temp. = 120°C; extraction temp. = 130–160°C; $AlCl_3$ added = 2% *w*/*v*; reaction time = 15–50 min	[75]
Ultrasonic pretreatment followed by DES reaction	Aqueous ChCl–oxalic acid	Oil palm fronds	Temp. = 120°C and reaction time = 60 min	[76]
Acid-catalyzed hydrolysis	Sulfuric acid	Tea leaves and rice hull	S : L ratio = 25 mL/g and acid concentration = 20% (*w*/*w*)	[11]
Microwave-assisted dehydration	CPME	Xylose, xylan, and rice husk	Temp. = 170°C and pH 1.9–2.3	[29]
Multiphase dehydration	Water	Xylose	Substrate concentration = 1.2 mol L^{-1}; catalyst = 10 mol %; reaction temp. = 120–160°C	[77]

Table 1. Continued

Method	Solvent	Raw material	Reaction/Extraction parameters	Author
Acid hydrolysis	Sulfuric acid	Rice husk and soybean peel	Temp. = 120°C; reaction time = 3 and 4 h	[78]
Acid hydrolysis	Hydrochloric acid, ethanol, and MIPK	Rice straw	Initial xylose concentration = 60 g/L; reaction temp. = 150°C; Pt/Al_2O_3 weight = 0.75 g; acid concentration = 5 wt %	[79]
Acid hydrolysis	Sulfuric acid	Miscanthus	Biomass loading = 9 wt %; acid concentration = 0.5 M; temp. = 185°C	[80]
Soxhlet and distillation	*n*-Hexane	Date palm seed	Humidity = 7.71%; pH 5.5; water activity = 0.365	[81]
Simple distillation	Hexane	Date seed	Distillation temp. = 60°C	[82]
Monophasic system	γ-Valerolactone	Corn fiber, xylose, arabinose, and ribose	10 mL thick-walled glass reactors	[27]
Hydrolysis	Dilute sulfuric acid–MIBK biphasic system	Bamboo	Particle size analysis	[83]
Microwave-assisted	Biphasic medium	Xylose and bamboo	Reaction temp. = 80–160°C; residence time = 0–60 min; water amount = 0–1.2 mL; biphasic medium/substrate ratio = (2 : 1)–(18 : 1)	[84]
LLE and HS-SPME	No need for solvent	Wood hydrolysates	Temp. = 180–200°C and reaction time = 5–15 min	[85]
Hydrolysis	Sulfuric acid	Hardwood	Temp. = 190°C; ZSM-5 = 1 g; NaCl = 1.05 g; solvent-to-aqueous phase ratio = 30 : 15 *v*/*v*; reaction time = 3 h	[86]
Hydrolysis	MIBK	Hardwood PHL	Temp. = 170°C and reaction time = 100 min	[87]
Hydrolysis	Sulfuric acid and acetic acid	Hardwood PHL	Temp. = 150–190°C	[30]
Enzymatic hydrolysis	MTHF	Sugarcane bagasse	0.45 g bagasse; 9 mL MTHF; 9 mL water; 0.1 M $AlCl_3$; temp. = 150°C; reaction time = 45 min; 10 wt % NaCl	[22]
Hydrolysis	Sulfuric acid	Sugarcane bagasse	Temp. = 170°C and acid concentration = 0.25 wt %	[88]
Acid hydrolysis	Sulfuric acid	Orange peel pectin	0.01 M acid; reaction time = 90 min; temp. = 160°C	[89]
Acid hydrolysis	Ethanol	Decorative plants (*Mimusops elengi, Madhuca indica, Hiptage benghalensis*, and *Polyalthia longifolia*)	50 mL ethanol and 50 mL distilled water	[90]
Hydrolysis	Chloroform	Mikania micrantha	50 mL chloroform and distillation temp. = 70°C	[91]
Acid hydrolysis	Hydrochloric acid	Theobrama cacao	Extraction time = 35 min; HCl concentration = 5 M and; amount of NaCl = 7 g	[92]
Microwave and oil bathing heating	MIBK, benzene, cyclohexane, and 1,4-dioxane	*Camellia oleifera* fruit shell	$[Bmim]HSO_4$ catalyst	[93]
Autohydrolysis	Water	Biomass hydrolysate	Temp. = 200°C and reaction time = 3 h	[94]

Table 1. Continued

Method	Solvent	Raw material	Reaction/Extraction parameters	Author
Solvent extraction	Ethyl acetate	Mustard (*Brassica carinata*)	Time = 4–5 h	[95]
Hydrolysis	Butanone–water biphasic system	C5 carbohydrate	Experimental and molecular dynamic simulation	[20]
Hydrolysis	DES	Sunflower stalk	Temp. = 180°C and reaction time = 15 min	[96]
Microwave-assisted	MIBK	Chestnut shell	Temp. = 180°C and reaction time = 15 min	[97]
One-pot processing	ChCl–DES–MIBK biphasic system	Eucalyptus urophylla	Temp. = 140°C and reaction time = 90 min	[98]
Sodium hydroxide hydrogenation	Sulfuric acid	Maize cob, elephant grass, sunflower, and baobab pulp	Temp. = 160°C and reaction time = 160 min	[99]

Note: L : S = liquid–solid; S : L = solid–liquid; MIBK = methyl isobutyl ketone; BRD = batch reaction incorporating distillation; *p*-TsOH = *p*-toluenesulfonic acid; SELRS = steam explosion liquor of rice straw; CPME = cyclopentylmethyl ether; MTHF = 2-methyltetrahydrofuran; MIPK = methyl isopropyl ketone; PHL = pre-hydrolysis liquor; LLE = liquid–liquid extraction; HS-SPME = headspace solid phase microextraction.

According to García *et al.* [56] and Dutta *et al.* [100], from all sources, ≤200–700 kilotons of furfural is produced per annum. The first industrial manufacture occurred between 1921–1923 at Quaker Oats Plant, Iowa, USA [12, 40, 101]. Potato peels as a feedstock for furfural production offer several advantages, including reduced waste generation in the food industry, lower production costs compared to conventional feedstocks, and a potential for higher furfural yields due to the high pentosan content therein. Given its toxicity, efficient extraction of furfural from foods, beverages, or lignocellulosic materials should consider the safety aspect. Exposure to furfural could lead to skin and eye irritation, and trigger liver cancer [64, 102]. It can inhibit growth in plants [103]. The works published during 1991–2024, reviewed as part of this study, revealed zero utilization of potato peels for furfural synthesis. At the same time, Gebre *et al.* [10] mentioned its presence in nectarines and sweet potatoes. Presumably, this gap can be attributed to the complex composition of potato peels and the difficulty of obtaining sufficient/appreciable yield, compared to its conversion to other products such as biobutanol [104] and bioethanol, as well as its application as a adsorbent. The concentration or purity of furfural and its identification is usually carried out using gas chromatography–mass spectrometry (GC–MS), high-performance liquid chromatography (HPLC), nuclear magnetic resonance (NMR) spectroscopy, aniline acetate color reaction, infrared spectrophotometry, ultraviolet–visible spectrophotometry, colorimetric spectrophotometry, and refractive index technologies [56, 81, 105, 106].

Australia and the USA are markets for furfural. The kinetics of furfural production have been studied using plug flow reactors in either single- or two-stage systems and other processes [38, 77, 80], a vapor-releasing reactor system [94], or continuous flow reactors as reported by Nsubuga *et al.* [107], along with its optimization by the Response Surface Methodology (RSM) [47, 61, 69, 88, 92, 108] and Aspen Plus [109], [110]. Thus, Li *et al.* [111] studied the kinetics of furfural yield from corncob using a sulfuric acid catalyst; Xia *et al.* [84] kinetically analyzed the recovery of furfural from xylose and bamboo. Acetic and sulfuric acid catalysts were employed by Liu *et al.* [30] to manufacture furfural PHL hardwood.

To the best of our knowledge, it was only Uppal and Kaur [67] who used dichloromethane (CH_2Cl_2) as a solvent to separate the organic layer in a distillation flask, which Xiang and Runge [112] conflictingly described as an energy-intensive process. Thus, the choice of CH_2Cl_2 as a solvent in our study is governed by the selection criteria discussed by Ye *et al.* [113], in particular, its low energy requirements to balance against its high cost. In addition, we aim to analyze the kinetics and thermodynamics of furfural production when using a sulfuric acid catalyst frequently employed in the literature, to extract furfural from potato peels in view of the significant xylose content therein, earlier pointed out by Gebre *et al.* [10]. The kinetic study includes both first- and second-order furfural production rate analysis, of which only first-order models have thus far been considered. An acid hydrolysis technique is used to determine the energy parameters of the extraction process. Since the physical and chemical properties of potato peels have been comprehensively reported in the literature, we rely on those studies and, instead, concentrate on the gaps identified in Table 1.

Fundamentally, the novelty of this study lies in the use of CH_2Cl_2 solvent and potato peels. According to reports, CH_2Cl_2 is safer than conventional acid types, thereby enabling a greener approach discussed by Cousin *et al.* [114] and lower energy requirements compared to distillation [104].

METHODOLOGY

2.1. Materials and equipment

Furfural extraction from ground potato peels was carried out using CH_2Cl_2 solvent (density = 1.325 g/mL at 20°C; ≥99.9% purity) used by Uppal and Kaur [67], sulfuric acid (5.4% H_2SO_4, approx. 1 M solution) catalyst reported by Iroha *et al.* [115], and water. Further purification of the chemical reagents employed herein was not required [116]. The equipment comprised an R-1001-VN distillation apparatus by *Zhengzhou Wollen Instrument Equipment Co.* (China), a separation funnel by *Shiv Dial Sud & Sons* (India) https://www.shivsons.com/product/separatory-funnel/, a round bottom flask by RB Flask manufacturers, a heating mantle by *Shiv Dial Sud & Sons*, and beakers produced by *HIRSCHMANN* (Germany).

2.2. Potato peel preparation

Fresh sweet potato peels were obtained from the Girei Local Government Area market situated in the Adamawa State, Northeastern Nigeria. It is located based on the GPS coordinate; between latitude 9°22'11.83"N and longitude 12°33'0.74"E, in a close proximity to Yola, the state capital. The collected samples were then washed with tap water before manual size reduction using a steel knife. As shown in Fig. 1, the peel was sun-dried for 4 days before its grinding into powder (size <5 mm) as described by Riera *et al.* [18]. This approach is similar to that used by Mao *et al.* [21], who ensured a particle size of 5–10 mm for the corncob used. It should be noted that no further increase in furfural yield could be achieved when the particle size is reduced to 495 μm, as confirmed by Singh *et al.* [65]. It is typical of 35 mesh sieves[1] in the U.S. Standard Sieve Series (ASTM E11). The use of finely ground potato peel (with a particle size of 500 μm) will significantly reduce internal diffusion resistance by increasing the surface area and enhancing the reactant accessibility.

(a) (b) (c)

Fig. 1. Preparation stages of sweet potato peel: (a) fresh sweet potato peels; (b) dried sweet potato peels; (c) grounded potato peels

Prior to the experiment, personal protective equipment was worn. This included Viton™-made gloves, lab coats, and closed-toe shoes. A ventilated environment was ensured, since the end product (furfural) has a pungent odor smelling like almonds, with a toxicity ranging from highly toxic to relatively non-toxic as based on the records of EPA[2] and Sashikala and Ong [63].

2.3. Extraction of furfural

About 100 g of ground sweet potato peel was weighed and placed into a 500 mL round bottom flask. The hydrolysis process was initiated by adding 200 mL of 1 M H_2SO_4 solution to the flask. Subsequently, the mixture was heated at a temperature of 60°C to reflux for 1 h using a heating mantle [107], adopting a similar duration reported by Sanchez *et al.* [36] who employed a microwave-enhanced process. The mixture (as shown in Fig. 2a) was allowed to cool to room temperature (25°C) then filtered using filter paper to separate the liquid from the solid residues, as mentioned by LaForge [117] and Lee *et al.* [76]. The filtrate (Fig. 2b) was collected in a clean container. The filtrate was transferred into a separatory funnel followed by addition of 50 mL equal volume of nonpolar solvent (in this case, CH_2Cl_2 shown in Fig. 2c) to the separatory funnel. The mixture was then shaken gently for 20 min. Observable layers were allowed to separate naturally, as conducted by Li *et al.* [118]. It should be noted that furfural was expected to be in the organic (lower) layer [87]. The organic layer was later separated and collected in a clean beaker. Next, the organic layer was transferred to a round bottom flask. The procedure was similar to that described by Iriany *et al.* [91] who separated furfural from water using chloroform, resulting in the formation of two layers.

The distillation apparatus was set up as shown in Fig. 2d, and the flask was gently heated to distill off the solvent at 39.6°C. The distillate was collected in a clean

[1] 35 mesh is a medium size of the U.S. Standard mesh size with a 0.0197" (500 μm) nominal sieve opening with a typical wire diameter of 0.315 mm.

[2] EPA, "Pesticide Fact Sheet," 2006, *United States Environmental Protection Agency, Office of Prevention, Pesticide and Toxic Substance* (*7501P*). Available: https://www3.epa.gov/pesticides/chem_search/reg_actions/registration/fs_PC-043301_01-Sep-06.pdf

(a) (b) (c) (d)

Fig. 2. (a) Solution obtained by acid hydrolysis, (b) filtrate after cooling, (c) extraction solvent, and (d) a simple fractional distillation setup

container and heated until the temperature reached 162°C (the boiling point of furfural) in order to isolate the furfural content. The concentration of the oily furfural recovered was then measured at this particular temperature after 1, 1.25, 1.5, and 2 h. It was observed that, when exposed to air, furfural was changing its color from its original colorless/yellowish to a brown-black color, as discussed by Al-Rahbi and Dwivedi [82] and observed by Sashikala and Ong [63] and Gebre *et al.* [10]. At the specified time interval, the experiment was repeated at 70 and 80°C. At least three independent experiments were conducted for each temperature condition to ensure reliability and to minimize experimental error. At the end, only the average values were used to carry out kinetic and thermodynamics analyses.

2.4. Rate law for product formation

In this study, we used no kinetic rate models developed previously [119]. For the first-order rate expression for product formation in Eq. 1, the concentration of furfural is expected to increase over time. Mazar *et al.* [120] emphasized the importance of residence time or reaction time in furfural production.

$$[\mathrm{FF}]_t = [\mathrm{FF}]_{\max}\left(1 - \mathrm{e}^{-kt}\right), \quad (1)$$

wherein $[\mathrm{FF}]_t$ is the concentration of furfural at time t (g/mL), $[\mathrm{FF}]_{\max}$ is the maximum concentration of furfural at equilibrium (g/mL), k is the first-order rate constant, and t is time (h). In order to determine k from Eq. 1, it was linearized such that to plot a graph of $\ln\left(1 - \frac{[\mathrm{FF}]_t}{[\mathrm{FF}]_{\max}}\right)$ against t.

$$\ln\left(1 - \frac{[\mathrm{FF}]_t}{[\mathrm{FF}]_{\max}}\right) = -k_1 t\,. \quad (2)$$

In Eq. 2, $[\mathrm{FF}]_{\max}$ is the highest recorded constant concentration obtained at the maximum time specified for the reaction to take place. Hence, the slope of the straight linear plot is expected to give the value of k. For convenience, the rate constant for the specific reaction order is differentiated using a subscripted number. Herein, k_1 was made to represent the first-order case. In the second-order case, the rate of product formation depends on the square of the reactant concentration or a bimolecular interaction. Thus, the linearized version of the second-order rate (Eq. 3), i.e., Eq. 4, was employed to analyze the experimental data at all the temperatures studied. Lastly, the second-order rate, k_2, was determined by plotting $\frac{1}{[\mathrm{FF}]_t}$ against $\frac{1}{t}$.

$$[\mathrm{FF}]_t = \frac{[\mathrm{FF}]_{\max}^2 kt}{1 + [\mathrm{FF}]_{\max} kt}, \quad (3)$$

$$\frac{1}{[\mathrm{FF}]_t} = \frac{1}{k_2 t} + [\mathrm{FF}]_{\max}\,. \quad (4)$$

Ideally, Eqs. 1 and 3 for first- and second-order reaction rates were based on the conversion of pentosan into furfural, according to Reaction 5 [57], [105].

$$\mathrm{C_5H_{10}O_5} \xrightarrow{\mathrm{H_2SO_4,\ Heat}} \mathrm{C_5H_4O_2} + 3\mathrm{H_2O} \quad (5)$$

Indeed, furfural formation from potato peels is a chemical process, primarily involving acid hydrolysis of hemicelluloses (mainly pentosans, viz., 3.2–6.0% xylose) present in the peels [121], followed by their dehydration to form furfural, in accordance with Reaction 5 [122]. In this study, the possibility of side reactions, as noted by Mazar *et al.* [120], was ignored.

2.5. Thermodynamic computations

Changes in activation energy E_a, enthalpy ΔH, entropy ΔS, and Gibbs-Free energy ΔG occurring during the extraction, were determined using the Arrhenius expression (Eq. 6) [53], Eyring model (Eq. 7), as well as Eqs. 8 and 9, respectively.

$$\ln k_n = \ln k_0 - \frac{E_a}{R}\left(\frac{1}{T}\right), \quad (6)$$

$$k_n = k^* \frac{k_B T}{h} e^{\frac{\Delta G}{RT}}, \quad (7)$$

$$\ln \frac{k_n}{T} = \frac{-\Delta H}{R}\left(\frac{1}{T}\right) + \left(\ln k^* + \ln \frac{k_B}{h} + \frac{\Delta S}{R}\right), \quad (8)$$

$$\Delta G = \Delta H - T\Delta S, \quad (9)$$

wherein, E_a is the activation energy (kJ/mol); k_0 is the frequency factor; R = 8.314 J/(mol·K) is the universal gas constant; k^* is the transmission coefficient usually taken as 1; k_B is the Boltzmann constant = $1.38 \cdot 10^{-23}$ J/K; ΔH is the enthalpy change (kJ/mol); ΔS is the entropy change in kJ/(mol·K), n is the order of reaction (i.e., 1 or 2), and the Planck's constant $h = 6.63 \cdot 10^{-34}$ J·s = $1.842 \cdot 10^{-37}$ J·h. From a plot of ln k_n against $\frac{1}{T}$, k_0 was also determined, similar to the study undertaken by Eifert and Liauw [77]. Conversely, ΔH was computed from the slope of a plot of $\ln \frac{k_n}{T}$ against $\frac{1}{T}$ following the method adopted by Kim *et al.* [31]. For convenience, thermodynamic calculations were conducted for the order of reaction that best fit the furfural extraction data.

RESULTS AND DISCUSSION

3.1. Product concentration

At all temperatures, furfural concentration increases with time, indicating the progress of the acid-catalyzed dehydration reaction converting pentosans (from potato peels) to furfural. In this case, the temperature-dependent kinetic trends were consistent with reaction-controlled mechanisms rather than with diffusion-controlled ones, eliminating the need for the Thiele modulus or Weisz–Prater criterion confirmation. After reaching a certain point, the rate of increase slows down and stabilizes, which could indicate the equilibrium stage or the depletion of reactants. In Fig. 3, the concentration of furfural increases more rapidly, in accord with the findings of Uppal and Kaur [67], Kim *et al.* [31], and Liu *et al.* [94].

Higher temperatures accelerate the reaction rate due to increased molecular motion and collision frequency, as evident from the kinetics parameters where the rate constant k is higher at 80°C compared to 60 and 70°C. Specific behavior of the curve is observed at 60°C, where the reaction progresses slowly, reaching a lower maximum concentration over the same duration of 1–2 h compared to that at higher temperatures. However, at 70°C, the reaction is faster than at 60°C, with a steeper initial increase in furfural concentration and a higher maximum value, in line with the findings of Montanã *et al.* [34]. Eventually, the reaction achieves the highest maximum concentration at 80°C, over the shortest period of time, indicating an optimal conversion efficiency at this temperature, as shown in Fig. 3. As a clear deviation from the trend observed in Fig. 3, Xu *et al.* [124] showed that, along with an increase in time, furfural production declines rapidly at higher temperatures between 150–180°C. Based on the curve behavior in Fig. 3 and the data in Table 1, 80°C is recommended for furfural production. It offers the highest furfural yield in the shortest time frame (i.e., 0.56 g/cm^3), making it the most efficient temperature among those studied. However, such practical considerations as energy consumption and the potential for thermal degradation of furfural should be assessed before finalizing the process parameters. Previously, a significant furfural degradation under an increase in time was observed, when corncob was employed by Ji *et al.* [70].

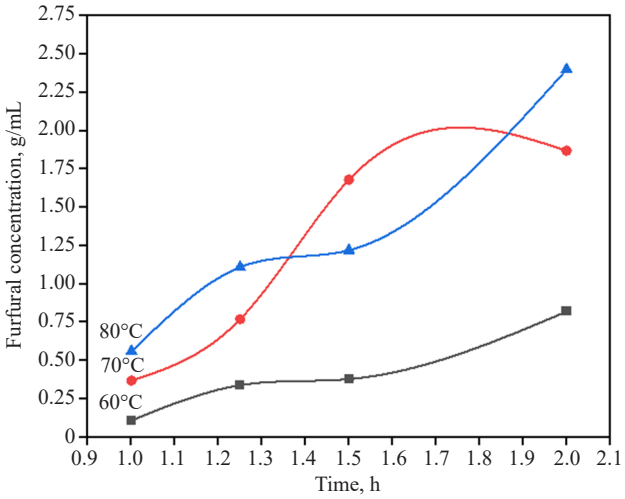

Fig. 3. Furfural concentration–time relationship at various temperatures

3.2. Kinetic study

Table 2 presents the furfural concentration at 60, 70, and 80°C over time, along with the data relevant to first-order and second-order reaction kinetics. As mentioned earlier, at higher temperatures (70 and 80°C), furfural concentrations increase more rapidly and achieve higher values, reflecting faster reaction rates and greater product yields as compared to those at 60°C.

Table 2. Concentration of furfural and representative kinetic plot data

t, h	$[FF]_t$, g/mL	$\frac{[FF]_t}{[FF]_{max}}$	$1-\frac{[FF]_t}{[FF]_{max}}$	$\ln\left(1-\frac{[FF]_t}{[FF]_{max}}\right)$	$\frac{1}{[FF]_t}$, mL/g
60°C					
1.00	0.11	0.134146341	0.865853659	−0.144039370	9.090909
1.25	0.34	0.414634146	0.585365854	−0.535518236	2.941176
1.50	0.38	0.463414634	0.536585366	−0.622529613	2.631579
2.00	0.82	1	0	–	1.219512
70°C					
1.00	0.37	0.451219512	0.548780488	−0.600056757	2.702703
1.25	0.77	0.939024390	0.060975610	−2.797281335	1.298701
1.50	1.68	2.048780488	−1.048780488	–	0.595238
2.00	1.87	2.280487805	−1.280487805	–	0.534759
80°C					
1.00	0.56	0.682926829	0.317073171	−1.148622709	1.785714
1.25	1.11	1.353658537	−0.353658537	–	0.900901
1.50	1.22	1.487804878	−0.487804878	–	0.819672
2.00	2.40	2.926829268	−1.926829268	–	0.416667

The term inside the logarithm, $1-\frac{[FF]_t}{[FF]_{max}}$, depends on the ratio of the furfural concentration at time, t, $[FF]_t$, to the maximum concentration, $[FF]_{max}$. As the reaction progresses and $[FF]_t$ approaches $[FF]_{max}$, the expression $1-\frac{[FF]_t}{[FF]_{max}}$ approaches zero. The logarithm of zero is undefined; therefore, this term cannot be calculated and is marked with a dash ('–') in Table 2. The increasing number of dashes with temperature progression ('1' at 60°C, '2' at 70°C, '3' at 80°C) highlights the influence of higher temperatures on reaction kinetics, bringing the system closer to equilibrium faster, which subsequently impacts the logarithmic calculations in the data table. This pattern of dashes confirms the temperature-dependent kinetics of furfural production, with 80°C being the most efficient temperature for achieving the maximum concentration rapidly. Xia *et al.* [84] reported a low furfural generation at this temperature during furfural synthesis from bamboo and xylose.

3.2.1. First-order reaction

A straight-line trend in Figs. 4a and 4b agrees well with the theoretical prediction of Eq. 2 (first-order furfural product formulation); however, the reaction may involve secondary processes which affect the data slightly. The coefficient of determination (R^2) = 0.8811 at 60°C in Fig. 4a indicates a reasonably good fit to the first-order model and suggests that the reaction at this temperature moderately follows first-order kinetics. At the same time, some deviations from linearity might exist (Fig. 4b). The near-perfect linear relationship between $\ln\left(1-\frac{[FF]_t}{[FF]_{max}}\right)$ and time (i.e., R^2 = 1) implied that the reaction at 70°C is predominantly governed by the first-order rate law, above other temperatures examined. In Fig. 4c, the plot shows only one data point, which is insufficient to establish a linear trend or calculate an R^2 value reliably.

The single data point at 80°C (−1.149 when t = 1 h) highlights the challenge of collecting sufficient data for kinetic modeling when reactions proceed rapidly to equilibrium. Nonetheless, the overall trend supports the applicability of the first-order model to describe the reaction, in particular, at intermediate temperatures of about 70°C.

3.2.2. Second-order reaction

Rate plots in Fig. 5 were constructed to test the relationship between $\frac{1}{[FF]_t}$ and $\frac{1}{t}$ as well as to evaluate the correspondence of the experimental data with the second-order model. The R^2 values progress

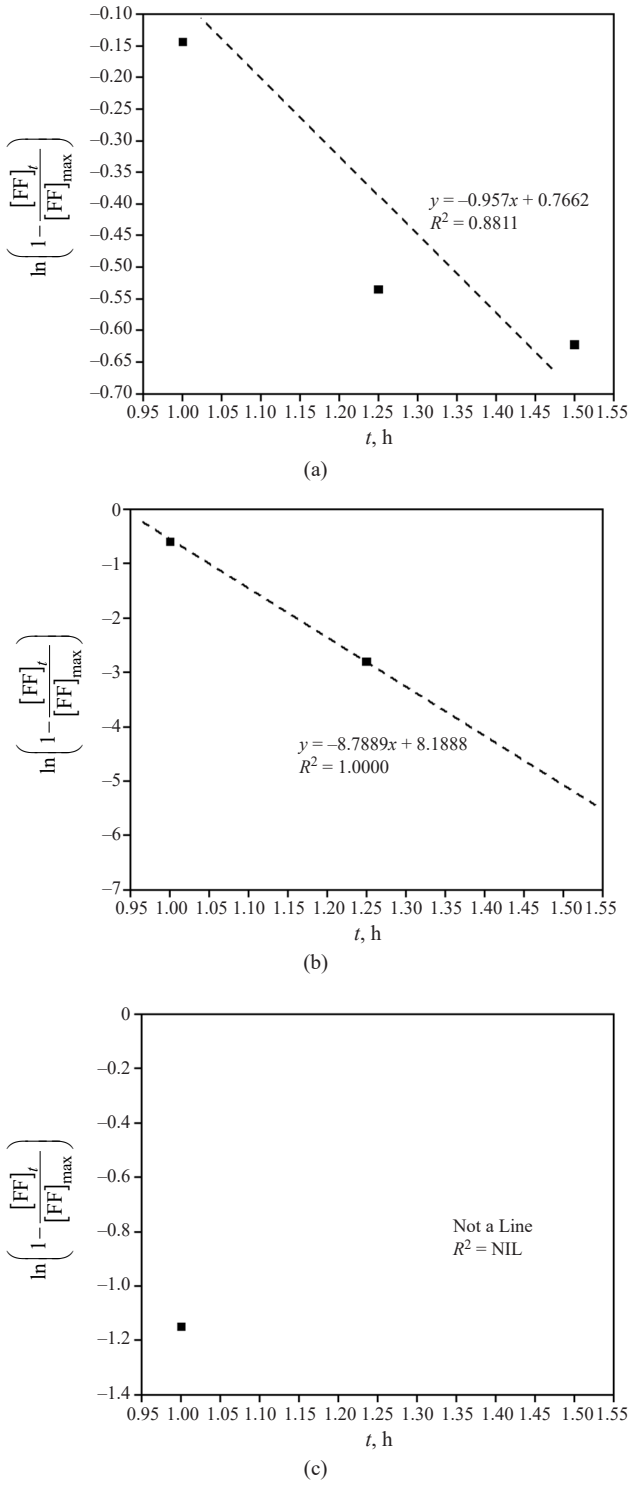

Fig. 4. Rate plots for the first-order furfural formation at (a) 60, (b) 70, and (c) 80°C

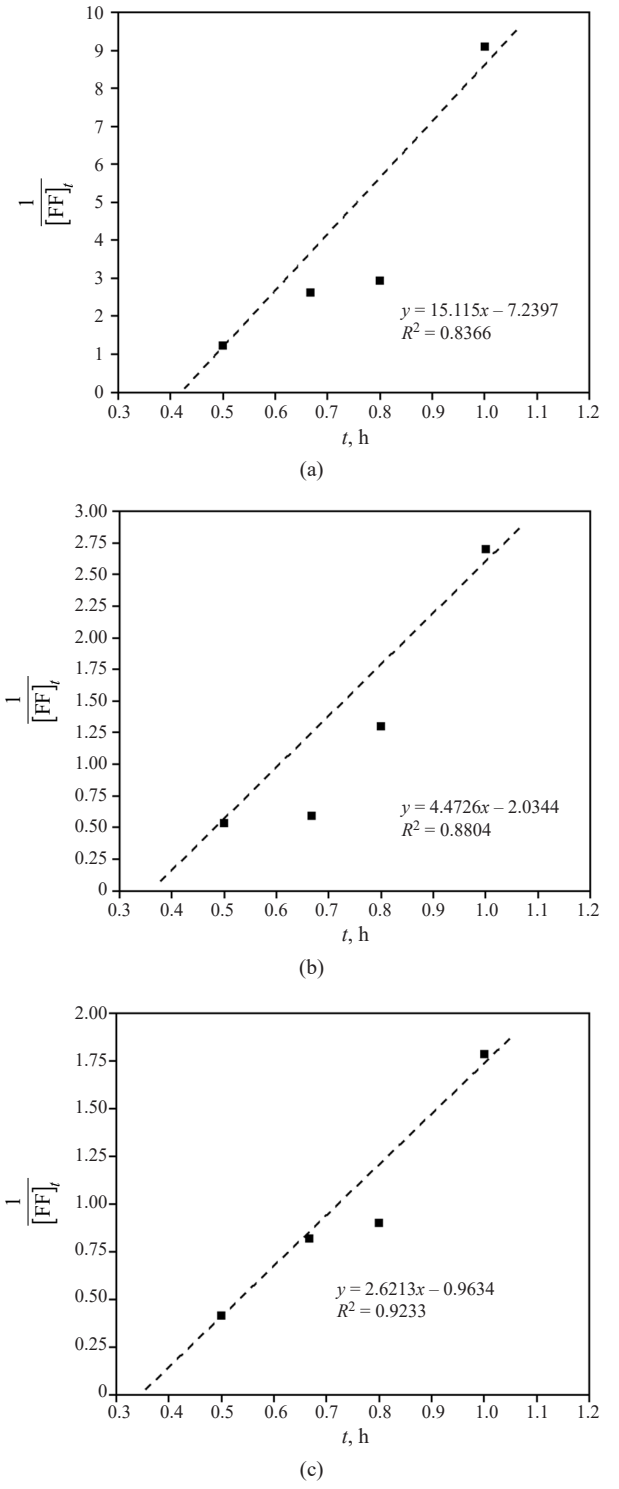

Fig. 5. Rate plots for the second-order furfural formation at (a) 60, (b) 70, and (c) 80°C

from 0.8366 at 60°C to 0.9233 at 80°C, reflecting that the reaction kinetics adhere more strongly to the second-order model at higher temperatures. This trend suggests that temperature plays a critical role in enhancing the applicability of the second-order kinetics in describing furfural formation.

The extraction data align more closely with the first-order assumptions at lower and intermediate temperatures (60 and 70°C), since the straight-line trends in Fig. 4 have better fits (R^2 values) to the first-order rate law. At 80°C, the second-order model shows a stronger fit, possibly due to temperature-induced changes in reaction

dynamics. However, the first-order model remains the overall better descriptor of the reaction kinetics across the temperature range studied.

3.2.3. Estimated kinetic parameters

It is well known that k unit depends on the order of reaction. As such, the terminology 'units' would be use for appropriateness. The increase in k with temperature for both the first-order and second-order reactions, as shown in Table 3, can be explained by the fundamental principles of chemical kinetics, particularly the Arrhenius equation and the temperature dependence of reaction rates. Reasons for this increase of k with temperature are due to enhanced molecular energy, exponential relationship and increased reaction rates.

Table 3. Calculated first- and second-order kinetic constants

Reaction order	Temperature, °C	Slope	k, units	R^2
1	60	−0.9570	0.9570	0.8811
	70	−8.7889	8.7889	1.0000
	80	–	–	
2	60	15.1150	0.066159	0.8366
	70	4.4726	0.223584	0.8804
	80	2.6213	0.381490	0.9233

As temperature increases, molecules gain kinetic energy, leading to more frequent and energetic collisions between the reactants. It results in a higher proportion of molecules having sufficient energy to overcome the activation energy barrier (E_a). The Arrhenius equation shows an exponential dependence of k on T. Even an insignificant increase in temperature can significantly enhance the rate constant due to the exponential term. And at higher temperatures, the reaction progresses more rapidly, reflected in the larger values of k for both first-order (8.7889) and second-order reactions (0.3815). In the first-order model, k increases from 0.957 at 60°C to 8.7889 at 70°C, indicating a dramatic rise in the reaction rate with a modest temperature increase. In the second-order model, the rise in k is less steep compared to the first-order reaction, reflecting differences in the response of the reaction mechanism to temperature changes. Generally, at n = 1, the reaction rate depends linearly on the concentration of one reactant; hence, k increases more sharply with temperature due to its direct effect on the formation rate of furfural. However, at n = 2, the rate depends on the square of the reactant concentration or a bimolecular interaction, leading to a more moderate increase in k with temperature.

3.3. Thermodynamic study

Equations 6 and 8 were key to finding the thermodynamic energy parameters of the solvent extraction process, through the calculated data in Table 4. The rate constant, k_1, reflects the reaction speed. At 70°C, the reaction rate is significantly higher compared to 60°C, resulting in a higher value of k_1.

Table 4. Axis data for straight-line plots for energy parameter determination

T, °C	T, K	k_1, h^{-1}	$\frac{1}{T}$, $\frac{1}{\text{K}}$	ln k_1	$\ln\frac{k_1}{T}$
		n = 1			
60	333.15	0.9570	0.003002	−0.04395	−5.85254
70	343.15	8.7889	0.002914	2.17349	−3.66468
80	353.15	–	–	–	–
T, °C	T, K	k_2, units	$\frac{1}{T}$, $\frac{1}{\text{K}}$	ln k_2	$\ln\frac{k_2}{T}$
		n = 2			
60	333.15	0.066159	0.003002	−2.71569	−8.52429
70	343.15	0.223584	0.002914	−1.49797	−7.33614
80	353.15	0.381490	0.002832	−0.96367	−6.83056

Ln k_1 is the natural logarithm of the rate constant k_1. For k_1 values greater than 1 (as observed at 70°C for the first-order reaction), ln k_1 becomes positive. The 70°C temperature likely represents an optimal point where the reaction proceeds efficiently without the limitations observed at lower (a slower reaction) or higher temperatures (equilibrium reached too rapidly). This results in a k_1 value sufficiently large to make ln k_1 positive (at 2.1735). Figures 6 and 7 displays the Arrhenius plot as well as the Eyring model plot described earlier for the two reaction rates. To determine which thermodynamic plot provides the best fit and supports a particular order of reaction, the fit quality (e.g., linearity and R^2 values) and trends in Figs. 6 and 7 should be analyzed. The fit quality or linearity as well as R^2 values of unity aligned best with the furfural experimental data for first-order Arrhenius and Eyring-Polanyi models, as observed in Fig. 6. However, it appears less linear in the second-order case shown in Fig. 7 with a lower average R^2 value of 0.9573.

While both the first- and second-order models show reasonable fits, the first-order thermodynamic plots (Figs. 6a and 6b) provide the best overall fit, making the first-order reaction the most plausible mechanism for the extraction process under the conditions studied. Through simplification of Eq. 8, ΔS was calculated using Eq. 10,

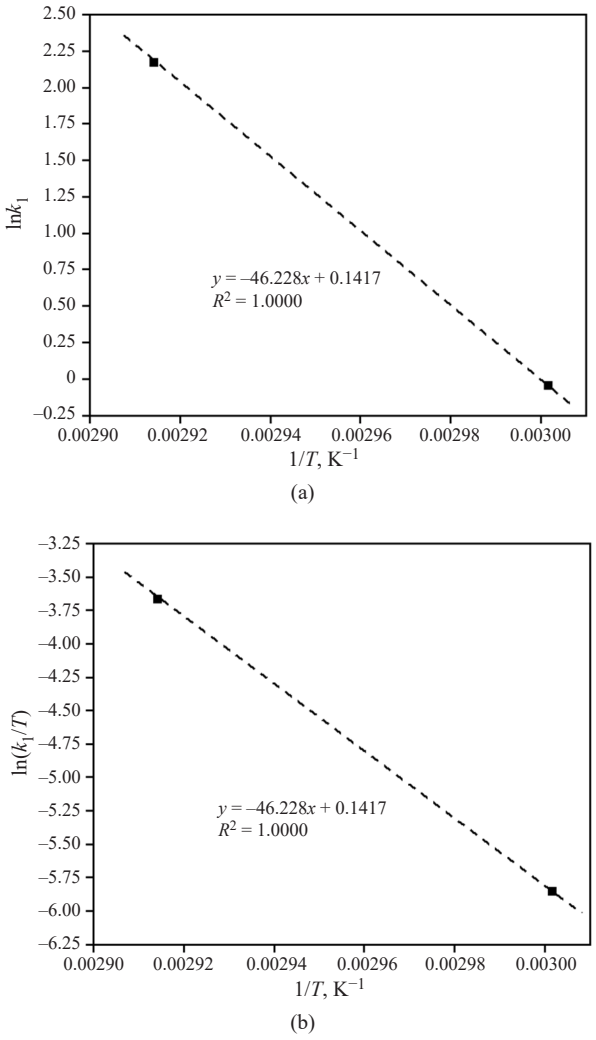

Fig. 6. First-order thermodynamic plots: (a) Arrhenius and (b) Eyring models

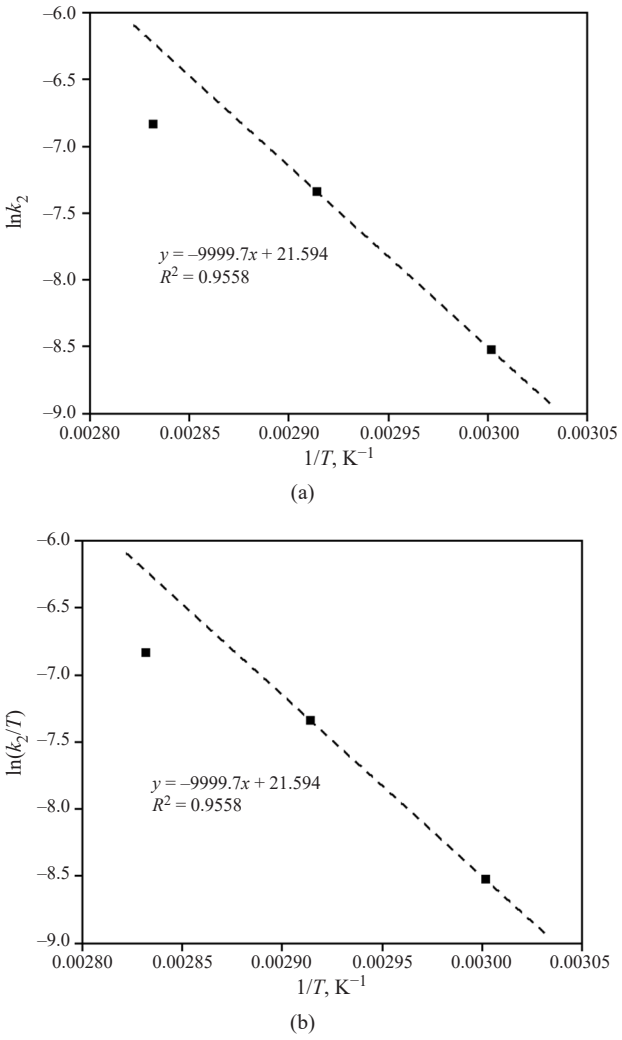

Fig. 7. Second-order thermodynamic plots: (a) Arrhenius and (b) Eyring models

by substituting the known constant values and the intercept in Fig. 6b.

$$31.9476 + \frac{\Delta S}{R} = \text{Intercept.} \quad (10)$$

The higher E_a = 85.992 kJ/mol for the first-order reaction indicates a higher energy barrier for the reaction to occur. By implication, the first-order reaction requires a greater energy input to initiate compared to the second-order reaction, potentially making it slower at lower temperatures. Both E_a are by far < 115 kJ/mol obtained by Liu *et al.* [30] who utilized hardwood PHL for furfural manufacture, although being > 28.69 and 34.72 kJ/mol realized by Xu *et al.* [123]. Provided that this high energy requirement is approved, potato peel has the potential to add to the existing global furfural tonnage, whose expected compound annual growth rate equals 6.5% [124]. Likewise, the higher ΔH = 83.138 kJ/mol in the first-order reaction compared to the second-order version implies its more endothermic character, thus requiring a greater energy input to proceed. Thus, it aligns with its higher observed E_a in Table 5. In contrast, the higher first-order k_0 > 4.77 units in the second-order reaction signifies a greater likelihood of successful collisions leading to furfural product formation. It indicates that while the energy barrier is higher, the reaction has a stronger dependence on the frequency of molecular collisions.

Table 5. Energy parameters computed for both reaction orders

Parameter	First-order	Second-order
E_a, J/mol	85991.702	4822.951
k_0, units	$2.22549 \cdot 10^{12}$	4.773119
ΔH, J/mol	83137.5058	1972.081
ΔS, J/mol·K	−86.0798304	−309.467
ΔG at 333 K, J/mol	111802.0893	105024.6
ΔG at 343 K, J/mol	112662.8876	108119.3
ΔG at 353 K, J/mol	–	111213.9

A less negative ΔS for the first-order reaction suggests a smaller decrease in the system disorder during the reaction, which could indicate a more favorable pathway compared to the second-order reaction. However, the higher ΔG values for the first-order reaction at all temperatures suggest its being less thermodynamically favorable than the second-order reaction. Lower ΔG values for the second-order reaction, as illustrated in Fig. 8, implied its more spontaneous character. In a nutshell, for $n = 1$, the high E_a, ΔH, and ΔG indicate that while it is less spontaneous and more energy-intensive, it may offer greater control and predictability under optimized conditions. On the other hand, for $n = 2$, the lower E_a, ΔH, and ΔG specify that it is less energy-demanding and more thermodynamically favorable, making it potentially more efficient under practical conditions.

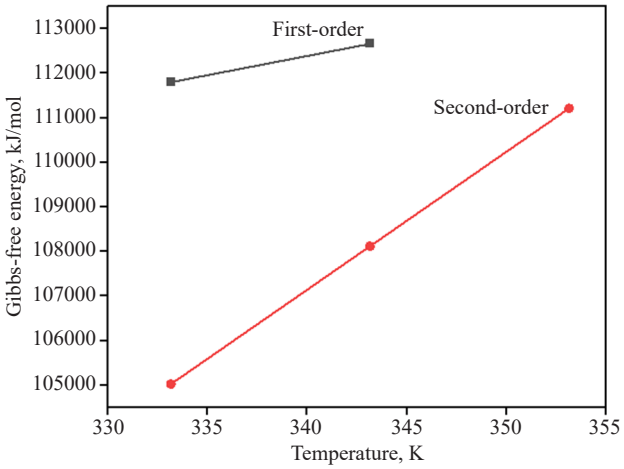

Fig. 8. Effect of temperature change on Gibbs energy

Hence, the second-order reaction can be recommended for the extraction of furfural from potato peels due to its lower energy and thermodynamic barriers, indicating its greater efficiency and practicality for large-scale applications. However, the first-order reaction might be selected in cases where precise reaction control and selectivity are critical.

CONCLUSIONS

Furfural, regarded as "the sleeping beauty of bio-renewable chemicals," was successfully produced via the acid-catalyzed hydrolysis technique over the time interval of 1–2 h, separately at 60, 70, and 80°C. Optimal extraction was achieved at 80°C, ensuring the highest furfural yield within the shortest duration of 2 h. The first-order reaction kinetic mechanism was shown to be the primary pathway under most conditions given its perfect fit ($R^2 = 1$) at 70°C and $k_1 = 8.7889$ min^{-1}. Thermodynamic analyses indicated that while the second-order reaction displayed lower energy and entropic barriers, the first-order reaction offered greater precision in modeling the process. Thus, utilization of sweet potato peels as feedstock not only provides a cost-effective alternative but also promotes the valorization of agricultural waste, aligning with global efforts toward circular economy practices. The use of dichloromethane and the effectiveness of sulfuric acid as a catalyst attest to the potential of sweet potato peels for appreciable extraction of furfural. Future work should explore the integration of greener solvents and advanced separation techniques to further improve furfural purity and energy efficiency. Scaling this process to industrial applications could significantly contribute to meeting the growing demand for bio-renewable chemicals, thus fostering a sustainable chemical industry. The utilization of Aspen Plus to simulate the efficiency of solvent recovery and to assess large-scale applicability is recommended. Purification of the extracted furfural by fractional distillation appears beneficial, although only when necessary.

Authors' contributions

Abdulhalim Musa Abubakar conceived and supervised the study,

Iyisikwe Tanimu Umar contributed to experimental design and data collection,

Abass-Giwa Muhammed Akintunde handled data analysis and interpretation,

Muhammad Jimada Aliyu provided technical validation and review,

Marwea Al-Hedrewy offered international collaboration and critical insights, and

Uday Raheja assisted in manuscript writing and editing.

REFERENCES

1. Rachamontree P., Douzou T., Cheenkachorn K., Sriariyanun M., Rattanaporn K. Furfural: A sustainable platform chemical and fuel. *Appl. Sci. Eng. Prog.* 2020;13(1):3–10. https://doi.org/10.14416/j.asep.2020.01.003
2. Win D.T. Furfural–Gold from garbage. *Assumpt. Univ. J. Technol.* (*AU J.T.*). 2005;8(4):185–190. Available: https://www.thaiscience.info/Journals/Article/AUJT/10290551.pdf. Accessed January 5, 2025.
3. Nagaraju T V., Rao M V., Sunil B. M., Chaudhary B. Furfural-extracted corncob ash: A new geomaterial for sustainable construction. In: Hazarika H., Haigh S.K., Chaudhary B., Murai M., Manandhar S. (Eds.). *Sustainable Construction Resources in Geotechnical Engineering* (*IC-CREST 2023*). *Lecture Notes in Civil Engineering*. Singapore: Springer, 2024. V. 448. P. 155–162. https://doi.org/10.1007/978-981-99-9227-0_15

4. Kabbour M., Luque R. Furfural as a platform chemical: from production to applications. In: *Recent Advances in Development of Platform Chemicals*. Elsevier B.V.; 2020. Ch. 10. P. 283–297. https://doi.org/10.1016/B978-0-444-64307-0.00010-X
5. Madloom A.A., Jabbar S.M., Kadhim N.J. Furfural production based cellulosic garbage. *Plant Arch.* 2019;19(2):345–350. Available: https://www.plantarchives.org/SPL%20ISSUE%20SUPP%202,2019/63%20(345-350).pdf. Accessed January 5, 2025.
6. Garcıa-Domınguez M.T., Garcıa-Domınguez J.C., Lopez F., De Diego C.M., Diaz M.J. Maximizing furfural concentration from wheat straw and Eucalyptus globulus by nonisothermal autohydrolysis. *Environ. Prog. Sustain. Energy*. 2015;34(K):1236–1242. https://doi.org/10.1002/ep.12099
7. Yong T.L.-K., Mohamad N., Yusof N.N.M. Furfural production from oil palm biomass using a biomass-derived supercritical ethanol solvent and formic acid catalyst. *Procedia Eng.* 2016;148:392–400. https://doi.org/10.1016/j.proeng.2016.06.495
8. Eseyin A.E., Steele P.H. An overview of the applications of furfural and its derivatives. *Int. J. Adv. Chem.* 2015;3(2):42–47. https://doi.org/10.14419/ijac.v3i2.5048
9. Brazdausks P., Puke M., Vedernikovs N., Kruma I. Influence of biomass pretreatment process time on furfural extraction from birch wood. *Environ. Clim. Technol.* 2013;11:5–11. https://doi.org/10.2478/rtuect-2013-0001
10. Gebre H., Fisha K., Kindeya T., Gebremicha T. Synthesis of furfural from bagasse. *Int. Lett. Chem. Phys. Astron.* 2015;57:72–84. https://doi.org/10.56431/p-5301hc, https://doi.org/10.18052/www.scipress.com/ILCPA.57.72
11. Yahyazadeh A. Extraction and investigation of furfural in tea leaves and comparing with furfural in rice hull. *J. Pharm. Res.* 2011;4(12):4338–4339. Available: https://www.jpronline.info. Accessed January 5, 2025.
12. Croker J.R. *The Production of Furfural from Agricultural Waste in Australia*: Masters Thesis. Degree of Master of Science in Food Technology. School of Food Technology, University of New South Wales. 1983. 139 p. https://doi.org/10.26190/unsworks/5665
13. Clauser N.M., Area M.C., Felissia F.E., Vallejos M.E. Techno-economic assessment of carbonyxlic acids, furfural, and pellet production in a pine sawdust biorefinery. *Biofuels Bioprod. Biorefining*. 2018;12(6):997–1012. https://doi.org/10.1002/bbb.1915
14. Luo A.Y., Li Z., Li X., *et al.* The production of furfural directly from hemicellulose in lignocellulosic biomass: A review. *Catal. Today*. 2018;319:14–24. https://doi.org/10.1016/j.cattod.2018.06.042
15. Gürbüz E.I., Gallo J.M.R., Alonso D.M., Wettstein S.G., Lim W.Y., Dumesic J.A. Conversion of hemicellulose into furfural using solid acid catalysts in γ -Valerolactone. *Angew. Chem. Int. Ed. Zuschriften*. 2013;52(4):1270–1274. https://doi.org/10.1002/anie.201207334
16. Agirrezabal-Telleria I., Gandarias I., Arias P.L. Production of furfural from pentosan-rich biomass: Analysis of process parameters during simultaneous furfural stripping. *Bioresour. Technol.* 2013;143:258–264. https://doi.org/10.1016/j.biortech.2013.05.082
17. Nunez F., Sumoza D., Garcia F., Rosales C., Jhonny J.M.B. Recovery and characterization of furfural obtained from rice husk. *Ciencia en Revoluc.* 2021;7(22):121–127. https://doi.org/10.5281/zenodo.6429799
18. Riera F.A., Alvarez R., Coca J. Production of furfural by acid hydrolysis of corncobs. *J. Chem. Technol. Biotechnol.* 1991;50(2):149–155. https://doi.org/10.1002/jctb.280500202
19. Peleteiro S., Rivas S., Alonso J.L., Santos V., Parajó J.C. Furfural production using ionic liquids: A review. *Bioresour. Technol.* 2016;202:181–191. https://doi.org/10.1016/j.biortech.2015.12.017
20. Zhao Y., Xu H., Wang K., *et al.* Enhanced furfural production from biomass and its derived carbohydrates in renewable butanone–water solvent system. *Sustain. Energy Fuels*. 2019;3(11):3208–3218. https://doi.org/10.1039/C9SE00459A
21. Mao L., Zhang L., Gao N., Li A. $FeCl_3$ and acetic acid co-catalyzed hydrolysis of corncob for improving furfural production and lignin removal from residue. *Bioresour. Technol.* 2012;123:324–331. https://doi.org/10.1016/j.biortech.2012.07.058
22. Li X.-K., Fang Z., Luo J., Su T.-C. Co-production of furfural and easily hydrolysable residue from sugarcane bagasse in MTHF/aqueous biphasic system: influence of acid species, NaCl addition and MTHF. *ACS Sustain. Chem. Eng.* 2016;4(10):5804–5813. https://doi.org/10.1021/acssuschemeng.6b01847
23. Martín M., Grossmann I.E. Optimal production of furfural and DMF from algae and switchgrass. *Ind. Eng. Chem. Res.* 2016;55(12):3192–3202. https://doi.org/10.1021/acs.iecr.5b03038
24. Bhaumik P., Dhepe P.L. Exceptionally high yields of furfural from assorted raw biomass over solid acids. *RSC Adv.* 2014;4(50):26215–26221. https://doi.org/10.1039/c4ra04119d
25. Ji H., Chen L., Zhu J., Gleisner R., Zhang X. Reaction kinetics based optimization of furfural production from corncob using a fully recyclable solid acid. *Ind. Eng. Chem. Res.* 2016;55(43):11253–11259. https://doi.org/10.1021/acs.iecr.6b03243
26. Chen H., Qin L., Yu B. Furfural production from steam explosion liquor of rice straw by solid acid catalysts (HZSM-5). *Biomass and Bioenergy*. 2014;73:77–83. https://doi.org/10.1016/j.biombioe.2014.12.013
27. Gallo J.M.R., Alonso D.M., Mellmer M.A., Yeap J.H., Wong H.C., Dumesic J.A. Production of furfural from lignocellulosic biomass using beta zeolite and biomass-derived solvent. *Top Catal*. 2013;56(18–20):1774–1781. https://doi.org/10.1007/s11244-013-0113-3
28. Liu F., Boissou F., Vignault A., *et al.* Conversion of wheat straw to furfural and levulinic acid in a concentrated aqueous solution of betaıne hydrochloride. *RSC Adv.* 2014;4(55):28836–28841. https://doi.org/10.1039/C4RA03878A
29. Delbecq F., Wang Y., Len C. Conversion of xylose, xylan and rice husk into furfural via betaine and formic acid mixture as novel homogeneous catalyst in biphasic system by microwave-assisted dehydration. *J. Mol. Catal. A Chem.* 2016;423:520–525. https://doi.org/10.1016/j.molcata.2016.07.003
30. Liu H., Hu H., Baktash M.M., Jahan M.S., Ahsan L., Ni Y. Kinetics of furfural production from pre-hydrolysis liquor (PHL) of a kraft-based hardwood dissolving pulp production process. *Biomass and Bioenergy*. 2014;66:320–327. https://doi.org/10.1016/j.biombioe.2014.02.003
31. Kim E.S., Liu S., Abu-Omar M.M., Mosier N.S. Selective conversion of biomass hemicellulose to furfural using maleic acid with microwave heating. *Energy Fuels*. 2012;26(2):1298−1304. https://doi.org/10.1021/ef2014106
32. Yemis O., Mazza G. Optimization of furfural and 5-hydroxymethylfurfural production from wheat straw by a microwave-assisted process. *Bioresour. Technol.* 2012;109:215–223. https://doi.org/10.1016/j.biortech.2012.01.031
33. Mandalika A.S., Runge T.M. Improved method of producing furfural from biomass. In: *Conf. Dallas, Texas, July 29 – August 1, 2012*. 2012. 121337810. http://doi.org/10.13031/2013.41836

34. Montanã D., Salvadã J., Torras C., Farriol X. High-temperature dilute-acid hydrolysis of olive stones for furfural production. *Biomass and Bioenergy*. 2002;22(4): 295–304. https://doi.org/10.1016/S0961-9534(02)00007-7
35. Weidener D., Leitner W., De Maria P.D., Klose H., Grande P.M. Lignocellulose fractionation using recyclable phosphoric acid: Lignin, cellulose and furfural production. *ChemSusChem.* 2020;14(3):909–916. https://doi.org/10.1002/cssc.202002383
36. Sanchez V., Dafinov A., Salagre P., Llorca J., Cesteros Y. Microwave-assisted furfural production using hectorites and fluorohectorites as catalysts. *Catalysts*. 2019;9(9):706. https://doi.org/10.3390/catal9090706
37. Fan B., Kong L., He Y. Highly efficient production of furfural from corncob by barley hull biochar-based solid acid in cyclopentyl methyl ether–water system. *Catalysts*. 2024;14(9):583. https://doi.org/10.3390/catal14090583
38. Bao Y., Du Z., Liu X., *et al.* Furfural production from lignocellulosic biomass: one-step and two-step strategies and techno-economic evaluation. *Green Chem.* 2024;26(11): 6318–6338. https://doi.org/10.1039/D4GC00883A
39. Zhao Y., Lu K., Xu H., Zhu L., Wang S. A critical review of recent advances in the production of furfural and 5-hydroxymethylfurfural from lignocellulosic biomass through homogeneous catalytic hydrothermal conversion. *Renew. Sustain. Energy Rev.* 2021;139:110706. https://doi.org/10.1016/j.rser.2021.110706
40. Zhang T., Li W., Xiao H., Jin Y., Wu S. Recent progress in direct production of furfural from lignocellulosic residues and hemicellulose. *Bioresour. Technol.* 2022;354:127126. https://doi.org/10.1016/j.biortech.2022.127126
41. Yong K.J., Wu T.Y., Lee C.B.T.L., *et al.* Furfural production from biomass residues: Current technologies, challenges and future prospects. *Biomass and Bioenergy*. 2022;161:106458. https://doi.org/10.1016/j.biombioe.2022.106458
42. Muryanto M., Sudiyani Y., Harahap A.F.P., Gozan M. Furfural and derivatives from bagasse and corncob. In: Abd-Aziz S., Gozan M., Ibrahim M.F., Phang L.-Y. (Eds.). *Chemical Substitutes from Agricultural and Industrial By-Products: Bioconversion, Bioprocessing, and Biorefining*. 2023. Ch. 14. P. 279–300. https://doi.org/10.1002/9783527841141.ch14
43. Lee C.B.T.L. and Wu T.Y. A review on solvent systems for furfural production from lignocellulosic biomass. *Renew. Sustain. Energy Rev.* 2020;137:110172. https://doi.org/10.1016/j.rser.2020.110172
44. Zhang X., Zhu P., Li Q., Xia H. Recent advances in the catalytic conversion of biomass to furfural in deep eutectic solvents. *Front. Chem.* 2022;10:911674. https://doi.org/10.3389/fchem.2022.911674
45. Mohamad N., Abd-Talib N., Yong T.-L.K. Furfural production from oil palm frond (OPF) under subcritical ethanol conditions. *Mater. Today Proc.* 2020;31(Part 1):116–121. https://doi.org/10.1016/j.matpr.2020.01.256
46. Raman J.K. and Gnansounou E. Furfural production from empty fruit bunch–A biorefinery approach. *Ind. Crops Prod.* 2015;69:371–377. https://doi.org/10.1016/j.indcrop.2015.02.063
47. Qatrunnada A., Muryanto M., Darmawan M.A., Gozan M. Optimization of furfural liquid-liquid extraction from oil palm empty fruit bunch hydrolysate solution with solvent variations. *AIP Conf. Proc*. 2024;3080(1):050002. (*The 15th Asian Congress on Biotechnology in conjunction with the 7th International Symposium on Biomedical Engineering* (*ACB-ISBE 2022*)). https://doi.org/10.1063/5.0198973
48. Othman N.E.A., Abd Aziz A., Wan Hassan W.H., Jailani N.F., Abd Hamid F., Abdul Wahab N. Production of furfural from oil palm fibres. *J. Oil Palm Res.* 2020;33(3): 473–481. Available: http://jopr.mpob.gov.my/. Accessed January 5, 2025.
49. Tareen A.K., Punsuvon V., Parakulsuksatid P. Conversion of steam exploded hydrolyzate of oil palm trunk to furfural by using sulfuric acid , solid acid, and base catalysts in one pot. *Energy Sources, Part A: Recover. Util. Environ. Eff.* 2020;46(1): 6126-6137. https://doi.org/10.1080/15567036.2020.1741733
50. García-Domínguez M.T., García-Domínguez J.C., Feria M.J., Gómez-Lozano D.M., López F., Díaz M.J. Furfural production from Eucalyptus *globulus*: Optimizing by using neural fuzzy models. *Chem. Eng. J.* 2013;221:185–192. https://doi.org/10.1016/j.cej.2013.01.099
51. López F., *et al.* Optimization of furfural production by acid hydrolysis of Eucalyptus *globulus* in two stages. *Chem. Eng. J.* 2014;240:195–201. https://doi.org/10.1016/j.cej.2013.11.073
52. Padilla-Rascón C., Romero-García J.M., Ruiz E., Romero I., Castro E. Microwave-assisted production of furfural from the hemicellulosic fraction of olive stones. *Process Saf. Environ. Prot.* 2021;152:630–640. https://doi.org/10.1016/j.psep.2021.06.035
53. Rivas S., Vila C., Santos V., Parajó J.C. Furfural production from birch hemicelluloses by two-step processing: a potential technology for biorefineries. *Holzforschung*. 2016;70(10): 901–910. https://doi.org/10.1515/hf-2015-0255
54. Brazdausks P., Puke M., Vedernikovs N., Irçna K. The effect of catalyst amount on the production of furfural and acetic acid from birch wood in a biomass pretreatment process. *Baltic Forestry.* 2014;20(1):106–114. Available: https://ortus.rtu.lv/science/en/publications/18956. Accessed January 5, 2025.
55. Brazdausks P., Vedernikovs N., Puke M., Kruma I. Effect of the acid hydrolysis temperature on the conversion of birch wood hemicelluloses into furfural. *Key Eng. Mater.* 2014;604: 245–248. https://doi.org/10.4028/www.scientific.net/KEM.604.245
56. García M.T., Zamudio M.A.M., Loaiza J.M., *et al.* Characterization and use of southern cattail for biorefining-based production of furfural. *Biomass Convers. Bioref.* 2019;9:333–339. https://doi.org/10.1007/s13399-018-0355-1
57. Kazemi M., Zand-Monfared M.R. Furfural production from pisthachio green hulls as agricultural residues. *J. Appl. Chem. Res.* 2010;3(12):19–24. Available: http://www.sid.ir/. URL: https://citeseerx.ist.psu.edu/document?repid=rep1&type=pdf&doi=a614365d06f93de64cb2c2345fe3855f7824b198. Accessed January 5, 2025.
58. Yue Z., Sun L.-L., Sun S.-N., Cao X.-F., Wen J.-L., Zhu M.-Q. Structure of corn bran hemicelluloses isolated with aqueous ethanol solutions and their potential to produce furfural. *Carbohydr. Polym.* 2022;288:119420. https://doi.org/10.1016/j.carbpol.2022.119420
59. Mao L., Zhang L., Gao N., Li A. Seawater based furfural production via corncob hydrolysis catalyzed by $FeCl_3$ in acetic acid steam. *Green Chem.* 2013;15(3):727–737. https://doi.org/10.1039/C2GC36346A
60. Barbosa B.M., Colodette J.L., Junior D.L., Gomes F.J.B., Martino D.C. Preliminary studies on furfural production from lignocellulosics. *J. Wood Chem. Technol.* 2014;34(3):37–41. https://doi.org/10.1080/02773813.2013.844167
61. Soludongwe S.M. Co-production of furfural and wood composite products from bio-based processing residues: Thesis for Degree of Master of Agricultural Sciences. Faculty of AgriSciences, Stellenbosch University. 2020. Available: https://scholar.sun.ac.za. Accessed January 5, 2025.

62. Bariani M., Boix E., Cassella F., Cabrera M.N. Furfural production from rice husks within a biorefinery framework. *Biomass Convers. Bioref.* 2021;11:781–794. https://doi.org/10.1007/s13399-020-00810-1
63. Sashikala M., Ong H.K. Synthesis and identification of furfural from rice straw. *J. Trop. Agric. Food Sci.* 2007;35(1):165–172. Available: https://jtafs.mardi.gov.my/jtafs/35-1/Furfural.pdf. Accessed January 5, 2025.
64. Sashikala M., Ong H.K. Synthesis, identification and evaluation of furfural from rice straw. *J. Trop. Agric. Food Sci.* 2009;37(1):95–101. Available: https://www.cabidigitallibrary.org/doi/pdf/10.5555/20113329392. Accessed January 5, 2025.
65. Singh A., Das K., Sharmab D.K. Production of xylose, furfural, fermentable sugars and ethanol from agricultural residues. *J. Chem. Technol. Biotechnol.* 1984;34(2):51–61. https://doi.org/10.1002/jctb.5040340203
66. Uppal S.K., Gupta R., Dhillon R.S., Bhatia S. Potential of sugarcane bagasse for production of furfural and its derivatives. *Sugar Tech*. 2009;10(4):298–301. http://doi.org/10.1007/s12355-008-0053-6
67. Uppal S.K., Kaur R. Hemicellulosic furfural production from sugarcane bagasse using different acids. *Sugar Tech*. 2011;13(2):166–169. https://doi.org/10.1007/s12355-011-0081-5
68. Wang Q., Zhuang X., Wang W., Tan X., Yu Q., Qi W. Rapid and simultaneous production of furfural and cellulose-rich residue from sugarcane bagasse using a pressurized phosphoric acid-acetone-water system. *Chem. Eng. J.* 2017;334:698–706. https://doi.org/10.1016/j.cej.2017.10.089
69. Gomes G.R., Scopel E., Breitkreitz M.C., Rezende C.A., Pastre J.C. Valorization of sugarcane bagasse C5-fraction by furfural production mediated by renewable glycine-based ionic liquid. *Ind. Crops Prod.* 2022;191(Part A):115940. https://doi.org/10.1016/j.indcrop.2022.115940
70. Ji H., Zhu J.Y., Gleisner R. Integrated production of furfural and levulinic acid from corncob in a one-pot batch reaction incorporating distillation using step temperature profiling. *RSC Adv.* 2017:7(73):46208–46214. https://doi.org/10.1039/c7ra08818c
71. Ren J., Wang W., Yan Y., Deng A., Chen Q., Zhao L. Microwave-assisted hydrothermal treatment of corncob using tin(IV) chloride as catalyst for furfural production. *Cellulose*. 2016;23(3):1649–1661. https://doi.org/10.1007/s10570-016-0898-x
72. Wang Q., *et al.* Production of furfural with high yields from corncob under extremely low water/solid ratios. *Renew. Energy*. 2019;144:139–146. https://doi.org/10.1016/j.renene.2018.07.095
73. Bu L., Tang Y., Gao Y., Jian H., Jiang J. Comparative characterization of milled wood lignin from furfural residues and corncob. *Chem. Eng. J.* 2011;175:176–184. https://doi.org/10.1016/j.cej.2011.09.091
74. Castro G.A.D., Batista R.C., De Sousa R. de C.S., Carneiro A. de C.O., Fernandes S.A. Green synthesis of furfural from xylose and corn cob biomas. *React. Chem. Eng.* 2023;(8):1969–1980. https://doi.org/10.1039/D3RE00017F
75. Chen Z., Reznicek W.D., Wan C. Aqueous choline chloride: A novel solvent for switchgrass fractionation and subsequent hemicellulose conversion into furfural. *ACS Sustain. Chem. Eng.* 2018;6(8):6910–6919. https://doi.org/10.1021/acssuschemeng.8b00728
76. Lee C.B.T.L., Wu T.Y., Cheng C.K., Siow L.F., Chew I.M.L. Nonsevere furfural production using ultrasonicated oil palm fronds and aqueous choline chloride-oxalic acid. *Ind. Crops Prod.* 2021;166:113397. https://doi.org/10.1016/j.indcrop.2021.113397
77. Eifert T., Liauw M.A. Process analytical technology (PAT) applied to biomass valorisation: a kinetic study on the multiphase dehydration of xylose to furfural. *React. Chem. Eng.* 2016;1(5):521–532. https://doi.org/10.1039/C6RE00082G
78. Scapin E., Rambo M.K.D., Viana G.C.C., *et al.* Sustainable production of furfural and 5-hidroximetilfurfural from rice husks and soybean peel by using ionic liquid. *Food Sci. Technol.* 2020;40(Suppl. 1):83–87. https://doi.org/10.1590/fst.04419
79. Lin K.-H., Huang M.-H., Chang A.C.-C. Liquid phase reforming of rice straw for furfural production. *Int. J. Hydrogen Energy*. 2013;38(35):15794–15800. https://doi.org/10.1016/j.ijhydene.2013.06.088
80. Dussan K., Girisuta B., Haverty D., Leahy J.J., Hayes M.H.B. Kinetics of levulinic acid and furfural production from *Miscanthus x giganteus*. *Bioresour. Technol.* 2013;149:216–224. https://doi.org/10.1016/j.biortech.2013.09.006
81. Al Rashdi S., Al Balushi A., Patil G. Optimized extraction of furfural from omani date palm seeds: A comparative study of soxhlet and distillation techniques. *Multidiscip. Sci. J.* 2025;7:e2025005. https://doi.org/10.31893/multiscience.2025005
82. Al-Rahbi B.S.N., Dwivedi P.B. Extraction and characterization of furfural from waste Omani date seeds. *Green Chem. Technol. Lett.* 2016;2(4):219–223. https://doi.org/10.18510/gctl.2016.249
83. Sweygers N., Depuydt D.E.C., Vuure A.W.V., *et al.* Simultaneous production of 5-hydroxymethylfurfural and furfural from bamboo (*Phyllostachys nigra* 'Boryana') in a biphasic reaction system. *Chem. Eng. J.* 2020;386:123957. https://doi.org/10.1016/j.cej.2019.123957
84. Xia Q., Peng H., Zhang Y., *et al.* Microwave-assisted furfural production from xylose and bamboo hemicellulose in a biphasic medium. *Biomass Convers. Bioref.* 2021;13(9):7895–7907. https://doi.org/10.1007/s13399-021-01870-7
85. Senila L., Miclean M., Senila M., Roman M., Roman C. New analysis method of furfural obtained from wood applying an autohydrolysis pretreatment. *Rom. Biotechnol. Lett.* 2013;18(1):7947–7955. Available: https://www.biotehgen.eu/RBL/8 Senila.pdf. Accessed January 5, 2025.
86. Gao H., Liu H., Pang B., *et al.* Production of furfural from waste aqueous hemicellulose solution of hardwood over ZSM-5 zeolite. *Bioresour. Technol.* 2014;172:453–456. https://doi.org/10.1016/j.biortech.2014.09.026
87. Liu H., Hu H., Jahan M.S., Ni Y. Furfural formation from the pre-hydrolysis liquor of a hardwood kraft-based dissolving pulp production process. *Bioresour. Technol.* 2013;131:315–320. https://doi.org/10.1016/j.biortech.2012.12.158
88. Ntimbani R.N., Farzad S., Görgens J.F. Furfural production from sugarcane bagasse along with co-production of ethanol from furfural residues. *Biomass Convers. Bioref.* 2021;12:5257–5267. https://doi.org/10.1007/s13399-021-01313-3
89. Rivera-Cedillo E.E., González-Chávez M.M., Handy B.E., Quintana-Olivera M.F., López-Mercado J., Cárdenas-Galindo M. Acid-catalyzed transformation of orange waste into furfural: the effect of pectin degree of esterification. *Bioresour. Bioprocess.* 2024;11:52. https://doi.org/10.1186/s40643-024-00768-2
90. Sattar M.A., Chakraborty A.K., Al-Reza S.M., Islam S. Extraction and estimation of furfural from decorative plants grown in Bangladesh. *Bangladesh J. Sci. Ind. Res.* 2007;42(4):495–498. https://doi.org/10.3329/bjsir.v42i4.759
91. Iriany I., Taslim T., Bani O., Pratama A.J. Potential of lime as a green catalyst in the manufacture of furfural from *Mikania micrantha*. *IOP Conf. Ser.: Earth Environ.* 2021;713(1):012038. http://doi.org/10.1088/1755-1315/713/1/012038

92. Uy J.R., Careo N.D., Llarena D., Barajas J.R. Optimization of furfural extraction from *Theobrama* cacao wastes using response surface methodology. *MATEC Web Conf.* (*RSCE 2018*). 2019;268(4):06010. https://doi.org/10.1051/MATECCONF/201926806010
93. Huang L., Peng H., Xiao Z., *et al.* Production of furfural and 5-hydroxymethyl furfural from *Camellia oleifera* fruit shell in [Bmim]HSO_4/H_2O/1,4-dioxane biphasic medium. *Ind. Crops Prod.* 2022;184(18):15006. https://doi.org/10.1016/j.indcrop.2022.115006
94. Liu L., Chang H.-M., Jameel H., Park S. Furfural production from biomass pretreatment hydrolysate using vapor-releasing reactor system. *Bioresour. Technol.* 2018;252: 165–171. https://doi.org/10.1016/j.biortech.2018.01.006
95. Stamigna C., Chiaretti D., Chiaretti E., Prosini P.P. Oil and furfural recovery from *Brassica carinata. Biomass and Bioenergy*. 2012;39:478–483. https://doi.org/10.1016/j.biombioe.2011.12.024
96. Gong L., Zha J., Pan L., Ma C., He Y.-C. Highly efficient conversion of sunflower stalk-hydrolysate to furfural by sunflower stalk residue-derived carbonaceous solid acid in deep eutectic solvent/organic solvent system. *Bioresour. Technol.* 2022;351:126945. https://doi.org/10.1016/j.biortech.2022.126945
97. Zha J., Fan B., He J., He Y.-C., Ma C. Valorization of biomass to furfural by chestnut shell-based solid acid in methyl isobutyl ketone–water–sodium chloride system. *Appl. Biochem. Biotechnol.* 2022;194:2021–2035. https://doi.org/10.1007/s12010-021-03733-3
98. Yue Z., Sun L.-L., Wen J.-L., Yao S.-Q., Sun S.-N., Cao X.-F. Simultaneous production of furfural, lignin and cellulose-rich residue from by ChCl/1,2-propanediol/MIBK biphasic system pretreatment. *Int. J. Biol. Macromol.* 2024;271(Part 1):133522. https://doi.org/10.1016/j.ijbiomac.2024.133522
99. Adebayo A.J., Ogunjobi J.K., Oluwasina O.O., Lajide L. Comparative production and optimisation of furfural and furfuryl alcohol from agricultural wastes. *Chem. Africa*. 2023;6:2401–2417. https://doi.org/10.1007/s42250-023-00594-7
100. Dutta S., De S., Saha B., Alam I. Advances in conversion of hemicellulosic biomass to furfural and upgrading to biofuels. *Catal. Sci. Technol.* 2012;2(10):2025–2036. https://doi.org/10.1039/c2cy20235b
101. Cai C.M., Zhang T., Kumar R., Wyman C.E. Integrated furfural production as a renewable fuel and chemical platform from lignocellulosic biomass. *J. Chem. Technol. Biotechnol.* 2014;89(1):2–10. https://doi.org/10.1002/jctb.4168
102. Piñeiro-García A., González-Alatorre G., Vega-Díaz S.M., Pérez-Pérez M.C.I., Tristan F., Patiño-Herrera R. Reduced graphene oxide coating with high performance for the solid phase micro-extraction of furfural in espresso coffee. *J. Food Meas. Charact.* 2019;14(4):314–321. https://doi.org/10.1007/s11694-019-00293-3
103. Jung K., You S.K., Moon S., Lee U. Furfural from pine needle extract inhibits the growth of a plant pathogenic fungus, *Alternaria mali*. *Mycobiology*. 2018;35(1):39–43. https://doi.org/10.4489/MYCO.2007.35.1.039
104. Zhuang Y., Si Z., Pang S., Wu H., Zhang X., Qin P. Recent progress in pervaporation membranes for furfural recovery: A mini review. *J. Clean. Prod.* 2023;396:136481. https://doi.org/10.1016/j.jclepro.2023.136481
105. Ambalkar V.U., Talib M.I. Synthesis of furfural from lignocellulosic biomass as agricultural residues: A review. *Int. J. Eng. Sci.* 2012;1(1):30–36. Available: http://www.theijes.com/papers/v1-i1/G011030036.pdf. Accessed January 5, 2025.
106. Hidajati N. The treatment of the corn-knob as a raw material for making furfural. *J. Ilmu Dasar*. 2007;8(1):45–53. Available: https://jurnal.unej.ac.id/index.php/JID/article/view/129. Accessed January 5, 2025.
107. Nsubuga H., Basheer C., Al-Muallem H.A.S., Kalanthoden A.N. Isolation, characterization and evaluation of photochemical potential of rice husk-based furfural via continuous fl ow reactor. *J. Environ. Chem. Eng.* 2016;4(1): 857–863. https://doi.org/10.1016/j.jece.2015.12.026
108. Li Q., Ma C.-L., Zhang P.-Q., Li Y.-Y., Zhu X., He Y.-C. Effective conversion of sugarcane bagasse to furfural by coconut shell activated carbon-based solid acid for enhancing whole-cell biosynthesis of furfurylamine. *Ind. Crop. Prod.* 2020;160:113169. https://doi.org/10.1016/j.indcrop.2020.113169
109. Sherif N., Gadalla M., Kamel D. Acid–hydrolysed furfural production from rice straw bio-waste: Process synthesis, simulation, and optimisation. *South African J. Chem. Eng.* 2021;38:34–40. https://doi.org/10.1016/j.sajce.2021.08.002
110. Contreras-Zarazúa G., Martin-Martin M., Sanchez-Ramirez E., Segovia-Hernandez J.G. Furfural production from agricultural residues using different intensified separation and pretreatment alternatives . Economic and environmental assessment. *Chem. Eng. Process. Intensif.* 2021;171:108569. https://doi.org/10.1016/j.cep.2021.108569
111. Li X., Liu Q., Luo C., Gu X., Lu L., Lu X. Kinetics of furfural production from corn cob in γ-Valerolactone using dilute sulfuric acid as catalyst. *ACS Sustain. Chem. Eng.* 2017;5(10): 8587–8593. https://doi.org/10.1021/acssuschemeng.7b00950
112. Xiang Z., Runge T. Co-production of feed and furfural from dried distillers' grains to improve corn ethanol profitability. *Ind. Crop. Prod.* 2014;55:207–216. https://doi.org/10.1016/j.indcrop.2014.02.025
113. Ye L., Han Y., Wang X., Lu X., Qi X., Yu H. Recent progress in furfural production from hemicellulose and its derivatives: Conversion mechanism, catalytic system, solvent selection. *Mol. Catal.* 2021;515:111899. https://doi.org/10.1016/j.mcat.2021.111899
114. Cousin E., Namhaed K., Pérès Y., *et al.* Towards efficient and greener processes for furfural production from biomass: A review of the recent trends. *Sci. Total Environ.* 2022;847: 157599. https://doi.org/10.1016/j.scitotenv.2022.157599
115. Iroha N.B., Akaranta O., James A.O. Red onion skin extract-furfural resin as corrosion inhibitor for aluminium in acid medium. *Der Chem. Sin.* 2012;3(4):995–1001. Available: http://www.pelagiaresearchlibrary.com/der-chemica-sinica/vol3-iss4/DCS-2012-3-4-995-1001.pdf. Accessed January 5, 2025.
116. Nie Y., Hou Q., Li W., Bai C., Bai X., Ju M. Efficient synthesis of furfural from biomass using $SnCl_4$ as catalyst in ionic liquid. *Molecules*. 2019;24(3):594. https://doi.org/10.3390/molecules24030594
117. LaForge F.B. The production of furfural by the action of superheated water on aqueous corncob extract. *J. Ind. Eng. Chem.* 2000;13(11):1024–1025. https://doi.org/10.1021/ie50143a029
118. Li H., Dai Q., Ren J., *et al.* Effect of structural characteristics of corncob hemicelluloses fractionated by graded ethanol precipitation on furfural production. *Carbohydr. Polym.* 2016;136:203–209. https://doi.org/10.1016/j.carbpol.2015.09.045
119. Edumujeze D., Fournier-Salaün M.-C., Leveneur S. Production of furfural: From kinetics to process assessment. *Fuel*. 2025;381(Part B):133423. https://doi.org/10.1016/j.fuel.2024.133423

120. Mazar A., Jemaa N., Al Dajani W.W., Marinova M., Perrier M. Furfural production from a pre-hydrolysate generated using aspen and maple chips. *Biomass and Bioenergy*. 2017;104: 8–16. https://doi.org/10.1016/j.biombioe.2017.05.016
121. Noda T., Takahata Y., Sato T. Sugar composition of cell wall material from sweet potatoes differing in stages of development, tissue zone and variety. *Oyo Toshitsu Kagaku*. 1994;41(3):311–316. Available: https://www.jstage.jst.go.jp/article/jag1994/41/3/41_3_311/_pdf. Accessed January 5, 2025.
122. Dias A.S., Lima S., Pillinger M., Valente A.A. Furfural and furfural-based industrial chemicals. In: Pignataro B. (Ed.). *Ideas in Chemistry and Molecular Sciences: Advances in Synthetic Chemistry. Part III. Chemical Reactions, Sustainable Processes, and Environment.* Weinheim: WILEY-VCH Verlag GmbH & Co. KGaA; 2010. Ch. 8. P. 165–185. https://doi.org/10.1002/9783527630554.ch8
123. Xu W., Zhang S., Lu J., Cai Q. Furfural production from corncobs using Thiourea as additive. *Environ. Prog. Sustain. Energy*. 2017;36(3):690–695. https://doi.org/10.1002/ep.12489
124. Jorqueira D.S.S., de Lima L.F., Maya S.F., *et al.* Critical review of furfural and furfuryl alcohol production: Past, present, and future on heterogeneous catalysis. *Appl. Catal. A: Gen.* 2023;665:119360. https://doi.org/10.1016/j.apcata.2023.119360

About the Authors

Abdulhalim Musa Abubakar, Master (Eng.), Lecturer, Department of Chemical Engineering, Faculty of Engineering, Modibbo Adama University, P.M.B. 2076, Yola, Adamawa State, Nigeria). E-mail: abdulhalim@mau.edu.ng. Scopus Author ID 58150539400, https://orcid.org/0000-0002-1304-3515

Iyisikwe Tanimu Umar, Bachelor (Eng.), Undergraduate Student, Department of Chemical Engineering, Faculty of Engineering, Modibbo Adama Federal University of Technology (P.M.B. 2076, Yola, Adamawa State, Nigeria). E-mail: iyisikwetanimu@gmail.com.

Abass-Giwa Muhammed Akintunde, Bachelor (Eng.), Undergraduate Student, Department of Chemical Engineering, Faculty of Engineering, University of Maiduguri (P.M.B. 1069, Bama Road, Maiduguri, Borno State, Nigeria). E-mail: akintundemuhammedabass-giwa@unimaid.edu.ng. https://orcid.org/0009-0003-3047-3116

Muhammad Jimada Aliyu, Bachelor (Eng.), Graduate Trainee Engineer, Chemical Engineering Department, School of Infrastructure, Process Engineering and Technology, Federal University of Technology (P.M.B. 65, Minna, Niger State, Nigeria). E-mail: ajimada.m1600354@st.futminna.edu.ng. https://orcid.org/0009-0006-0592-8985

Marwea Al-Hedrewy, PhD., Associate Professor, College of Technical Engineering, the Islamic University, Najaf, Iraq; College of Technical Engineering, the Islamic University of Al Diwaniyah, Al Diwaniyah, Iraq. E-mail: mereng@iunajaf.edu.iq. Scopus Author ID 59331742300, https://orcid.org/0009-0008-7371-6364

Uday Raheja, Bachelor (Eng.), Student, Center for Research Impact & Outcome, Chitkara University Institute of Engineering and Technology (CUIET), Chitkara University (140401, Rajpura, Punjab, India). E-mail: uday_raheja@outlook.com. https://orcid.org/0009-0000-6546-279X

The text was submitted by the authors in English
and edited for English language and spelling by Thomas A. Beavitt

Tonkie Khimicheskie Tekhnologii = Fine Chemical Technologies.
2025;20(5):474–482 ISSN 2686-7575 (Online)

Chemistry and technology of organic substances
Химия и технология органических веществ

UDC 547.841+547.836.1
https://doi.org/10.32362/2410-6593-2025-20-5-474-482
EDN PIYYFN

RESEARCH ARTICLE

Synthesis and properties of cyclic acetals of Wallach ketone

Bogdan V. Vazhenin, Alexander A. Golovanov, Yulianna G. Borisova✉, Gul'nara Z. Raskil'dina, Simon S. Zlotskii

Ufa State Petroleum Technological University, Ufa, 450064 Russia

✉ *Corresponding author, e-mail: yulianna_borisova@mail.ru*

Abstract

Objectives. The work set out to obtain the corresponding cyclohexenyl derivatives of 1,4-dioxaspiro[4.5]decane, 1,5-dioxaspiro[5.5]-undecane, and 1,4-dithiaspiro[4.5]decane by condensation of 2-(cyclohexen-1-yl)cyclohexanone (Wallach ketone) with 1,2-, 1,3-diols, and 1,2-ethanedithiol; to determine reaction duration and process temperature at which the maximum possible yield of the target cyclic derivatives of 2-(cyclohexen-1-yl)cyclohexanone is achieved; to evaluate the anticorrosive properties of the obtained acetals in an acidic medium; to carry out dichlorocarbenation using 1,4-dioxaspiro[4.5]decane as an example, and to establish the structure of the obtained isomers.

Methods. Target compounds including cyclic acetals were obtained by a classical organic synthesis method involving condensation of 2-(cyclohexen-1-yl)cyclohexanone (Wallach ketone) with 1,2-, 1,3-diols, and 1,2-ethanedithiol. The following analysis methods were used to determine the qualitative and quantitative composition of the reaction masses: gas–liquid chromatography (Crystallux-4000M chromatograph with a flame ionization detector, a 25 m × 0.33 mm capillary column containing 100% polydimethylsiloxane as a stationary phase 0.5 μm), nuclear magnetic resonance spectroscopy (BrukerAM-500 device with operating frequencies of 500 and 125 MHz), and elemental microanalysis (rapid gravimetry method). Chlorine and sulfur were determined by the Schöniger method.

Results. Under conditions of thermal heating of Wallach ketone with 1,2-, 1,3-diols, and 1,2-ethanedithiol, 1,4-dioxaspiro[4.5]decane, 1,5-dioxaspiro[5.5]undecane, and 1,4-dithiaspiro[4.5]decane were obtained with a yield of 95%. 5,5-Dimethyldioxane derivative was found to have a moderate inhibitory effect on acid corrosion of carbon steel St20 at a temperature of 60°C. Dichlorocarbenation of 1,4-dioxaspiro[4.5]decane was shown to occur with the formation of a mixture of two diastereomers (ratio is 1 : 2) as evidenced by doubled signals of carbon atoms in the carbon spectrum.

Conclusions. 2-(Cyclohexen-1-yl)cyclohexanone **1** condenses with 1,2-, 1,3-diols, and ethanedithiol to form the corresponding spirocyclic derivatives in high yields. It is shown that 1,4-dioxaspiro[4.5]decane undergoes dichlorocarbenation under Mąkosza reaction conditions to form polycyclic *gem*-dichlorocyclopropane as a mixture of two diastereomers. 7-(Cyclohex-1-en-1-yl)-3,3-dimethyl-1,5-dioxaspiro[5.5]undecane is confirmed to inhibit steel corrosion in acidic media.

Keywords

Wallach ketone, cyclic acetals, diols, cyclocondensation, acid catalysis, dichlorocarbenation, anti-corrosion activity

Submitted: 16.11.2024
Revised: 10.04.2025
Accepted: 05.09.2025

For citation

Vazhenin B.V., Golovanov A.A., Borisova Yu.G., Raskil'dina G.Z., Zlotskii S.S. Synthesis and properties of cyclic acetals of Wallach ketone. *Tonk. Khim. Tekhnol. = Fine Chem. Technol*. 2025;20(5):474–482. https://doi.org/10.32362/2410-6593-2025-20-5-474-482

НАУЧНАЯ СТАТЬЯ

Синтез и свойства циклических ацеталей кетона Валлаха

Б.В. Важенин, А.А. Голованов, Ю.Г. Борисова✉, Г.З. Раскильдина, С.С. Злотский

Уфимский государственный нефтяной технический университет, Уфа, 450064 Россия

✉ *Автор для переписки, e-mail: yulianna_borisova@mail.ru*

Аннотация

Цели. Конденсацией 2-(циклогексен-1-ил)циклогексанона (кетона Валлаха) с 1,2-, 1,3-диолами и 1,2-этандитиолом получить соответствующие циклогексенильные производные 1,4-диоксаспиро[4.5]декана, 1,5-диоксаспиро[5.5]ундекана и 1,4-дитиаспиро[4.5]декана; определить длительность реакции и температуру проведения процесса, при которых достигается максимально возможный выход целевых циклических производных 2-(циклогексен-1-ил)циклогексанона и оценить антикоррозионные свойства полученных ацеталей в кислой среде; на примере 1,4-диоксаспиро[4.5]декана осуществить дихлоркарбенирование и установить строение полученных изомеров.

Методы. Целевые соединения, такие как циклические ацетали, были получены классическим способом органического синтеза — конденсацией 2-(циклогексен-1-ил)циклогексанона (кетона Валлаха) с 1,2-, 1,3-диолами и 1,2-этандитиолом. Для определения качественного и количественного состава реакционных масс были использованы следующие методы анализа: газожидкостная хроматография (хроматограф Кристаллюкс-4000М с пламенно-ионизационным детектором, капиллярной колонкой 25 м × 0.33 мм, содержащей 100%-й полидиметилсилоксан в качестве неподвижной фазы 0.5 μm), спектроскопия ядерного магнитного резонанса (прибор «BrukerAM-500» с рабочими частотами 500 и 125 МГц) и элементный микроанализ (метод экспресс-гравиметрии; хлор и серу определяли методом Шёнигера).

Результаты. В условиях термического нагрева кетона Валлаха с 1,2-, 1,3-диолами и 1,2-этандитиолом получены 1,4-диоксаспиро[4.5]декан, 1,5-диоксаспиро[5.5]ундекан и 1,4-дитиаспиро[4.5]декан с выходом 95%. Установлено, что 5,5-диметилдиоксановое производное обладает умеренным ингибирующим эффектом по отношению к кислотной коррозии углеродистой стали Ст20 при температуре 60°С. Определено, что дихлоркарбенирование 1,4-диоксаспиро[4.5]декана протекает с образованием смеси двух диастереомеров (соотношение 1 : 2), о чем свидетельствуют удвоенные сигналы атомов углерода в углеродном спектре.

Выводы. 2-(Циклогексен-1-ил)циклогексанон **1** конденсируется с 1,2-, 1,3-диолами и этандитиолом с образованием соответствующих спироциклических производных с высокими выходами. Показано, что 1,4-диоксаспиро[4.5]декан вступает в реакцию дихлоркарбенирования в условиях реакции Макоши с образованием полициклического *гем*-дихлорциклопропана в виде смеси двух диастереомеров. Найдено, что 7-(циклогекс-1-ен-1-ил)-3,3-диметил-1,5-диоксаспиро[5.5]ундекан способен тормозить коррозию стали в кислых средах.

Ключевые слова

кетон Валлаха, циклические ацетали, диолы, циклоконденсация, кислотный катализ, дихлоркарбенирование, антикоррозионная активность

Поступила: 16.11.2024
Доработана: 10.04.2025
Принята в печать: 05.09.2025

Для цитирования

Важенин Б.В., Голованов А.А., Борисова Ю.Г., Раскильдина Г.З., Злотский С.С. Синтез и свойства циклических ацеталей кетона Валлаха. *Тонкие химические технологии*. 2025;20(5):474–482. https://doi.org/10.32362/2410-6593-2025-20-5-474-482

INTRODUCTION

Linear and cyclic ketals are widely used in organic and medicinal chemistry [1, 2]. Glycerol ketals are effective repellent additives [3], while diacetals of diglycerol and dipentaerythritol have been proposed as components for polymer materials [4, 5]. In recent years, cyclic ketone ketals have attracted increased attention from researchers due to their ability to inhibit acid corrosion, reduce corrected wear spot diameter, and act as additives to fuels and oils [6, 7]. Cyclohexanone is used as an industrial ketone in large-scale synthesis of caprolactam, polyamides, and adipic acid [8]. During these reactions, dimers and oligomers of cyclohexanone are formed as byproducts in an amount of 5–15% [9, 10], among which the main compound is 2-(cyclohexen-1-yl) cyclohexanone referred to as Wallach ketone (**1**) [11]. The literature describes the synthesis of antimalarial [12] and antirheumatic [9] compounds, as well as high-density jet fuel components based on ketone **1** [10]. The combination of the bicyclic fragment of ketone **1** and the cycloacetal group allows for the creation of compounds with cytotoxicity against tumor cell lines [13], herbicides [14], and fuel additives [15, 16]. In this regard, the aim of this study was to develop a method for obtaining polycyclic spiroacetals and spirothioacetals based on 2-(cyclohexen-1-yl)cyclohexanone **1.**

MATERIALS AND METHODS

^{1}H and ^{13}C nuclear magnetic resonance (NMR) spectra were recorded in $CDCl_3$ (25°C) using an Avance-III HD spectrometer (*Bruker*, USA) at operating frequencies of 500 and 125 MHz for ^{1}H and ^{13}C nuclei, respectively. The residual solvent signals served as the internal standard: δ_H 7.66, δ_C 77.0 ppm for the ^{1}H and ^{13}C spectra, respectively. Gas chromatographic analysis of reaction mixtures and isolated compounds was performed on a Crystallux-4000M chromatograph (*Meta-Chrom*, Russia) equipped with a flame ionization detector and a capillary column (25 m × 0.33 mm) containing 100% polydimethylsiloxane as the stationary phase (0.5 μm). Elemental microanalysis was performed using the express gravimetric method; chlorine and sulfur were determined using the Schöniger method.

Ketone **1** was obtained according to a known method [17]. Commercially available diols (*Sigma-Aldrich*, USA), solvents, and other reagents were used without further purification.

The physical constants, elemental analysis data, and spectral characteristics of the obtained compounds are presented in Tables 1 and 2, while the yields are given in Table 3.

General method for obtaining 1,4-dioxaspiro[4.5]decanes 3a,c and dithiaspiro[4.5]decane 3b

A mixture of 35.7 g (0.20 mol) of ketone **1**, 0.3 mol of the corresponding diol or ethanedithiol, 0.3 g (1.6 mmol, 0.8 mol %) of TsOH H_2O, and 100 mL of benzene was heated with a Dean–Stark apparatus for the time indicated in Table 3, monitoring the composition of the reaction mixture by gas–liquid chromatography (GLC). The reaction mixture was then cooled and stirred vigorously for 5 min with 50 mL of a saturated $NaHCO_3$ solution. The aqueous part was extracted three times with ether, the combined organic phase was dried over Na_2SO_4, the solvents were evaporated on a rotary evaporator, and the residue was distilled under vacuum.

General method for obtaining 1,4-dithiaspiro[4.5]decanes 3d,e

A mixture of 35.7 g (0.20 mol) of ketone **1**, 0.1 mol of the corresponding diol, 0.3 g of TsOH H_2O, and 100 mL of benzene was heated with a Dean–Stark apparatus for 1 h, then an additional 0.15 mol of the diol was added with continued heating for the total period indicated in Table 3. The composition of the reaction mixture was monitored by GLC. After cooling, the reaction mixture was treated as described above.

Method for obtaining 6-(7,7-dichlorobicyclo[4.1.0]heptan-1-yl)-1,4-dioxaspiro[4.5]decane (mixture of diastereomers 4a,b) [16]

To a solution of 11.1 g (50.0 mmol) of ethylene ketal **3a**, 331 mg (1.47 mmol) of Et_3BnNCl, and 0.5 mL of 96% EtOH in 150 mL (1.85 mol) of $CHCl_3$, cooled in an ice bath and stirred vigorously (overhead stirrer, 1000 rpm), a cooled solution of 50 g (1.25 mol) of NaOH in 50 mL of water was added dropwise. After adding the NaOH solution, the reaction mixture was stirred for another hour, after which point GLC showed complete conversion of the starting compound **3a**. After adding 500 mL of water to the reaction mixture, the organic layer was separated, washed with 5% AcONa, water, and dried over Na_2SO_4. Following evaporation of the solvent, the residue was distilled under vacuum. We thus obtained 28.1 g (92%) of a colorless liquid that gradually darkens during storage.

Table 1. Physical constants, elemental analysis data and ^{1}H NMR spectra of compounds **3a**–**d** and **4a**,**b**

No.	T_{boil}, °C (mm Hg)	Found, %		Gross formula	Calculated, %		^{1}H NMR spectrum (500.00 MHz; δ, ppm; *J*, Hz)
		C	H		C	H	
3a	138–140 (2.0)	75.63	10.18	$C_{14}H_{22}O_2$	75.63	9.97	5.47 (s, 1H), 3.87–3.69 (m, 4H), 2.06–1.88 (m, 5H), 1.67–1.59 (m, 4H), 1.56–1.34 (m, 7H), 1.22–1.12 (m, 1H)
3b[1]	151–152 (0.5)	66.01	9.09	$C_{14}H_{22}S_2$	66.09	8.72	5.72 (s, 1H), 3.24–3.13 (m, 4H), 2.24–2.16 (m, 4H), 2.06–1.93 (m, 3H), 1.77–1.33 (m, 4H), 1.62–1.48 (m, 5H), 1.31–1.20 (m, 1H)
3c	110–122 (0.4)	76.53	10.56	$C_{15}H_{24}O_2$	76.23	10.24	5.44 (s, 1H), 4.04–3.98 (m, 1H), 3.88–3.71 (m, 3H), 2.76–2.70 (m, 1H), 2.25–2.16 (m, 1H), 2.06–1.87 (m, 6H), 1.79–1.50 (m, 6H), 1.43–1.20 (m, 4H), 1.06–0.98 (m, 1H)
3d	153–155 (0.6)	77.30	10.62	$C_{17}H_{28}O_2$	77.22	10.67	5.40 (s, 1H), 3.71–3.66 (m, 2H), 3.57–3.50 (m, 2H), 2.80–2.76 (m, 2H), 2.00–1.91 (m, 4H), 1.68–1.44 (m, 11H), 1.04 (s, 3H), 0.67 (s, 3H)
4[2]	160–161 (0.5)	59.29	7.49	$C_{15}H_{22}Cl_2O_2$	59.02	7.27	4.04–3.91 (m), 2.58–2.49 (m), 1.86–1.01 (m)

[1]Found 25.34% S; calculated 25.20% S.

[2]Found 23.07% Cl; calculated 23.23% Cl.

Table 2. ^{13}C NMR spectra of compounds **3a**–**d** and **4a**,**b**

No.	^{13}C NMR spectrum (125 MHz; δ, ppm)							
	C^1	C^2	C^3	C^4	C^5	C^6	CH_2	R*
3a	64.88, 64.82		110.94	52.89	137.54	124.15	36.94, 29.41, 29.00, 25.71, 25.65, 24.11, 23.62, 22.61	–
3b	45.79, 39.47		73.34	56.44	139.13	125.27	38.12, 32.03, 29.82, 26.49, 25.83, 25.65, 23.59, 22.57	–
3c	58.93, 58.72		99.40	55.36	138.68	123.58	28.61, 28.49, 28.11, 25.99, 25.64, 25.60, 23.50, 22.73, 22.58	–
3d[1]	69.36, 69.09		99.09	54.10	137.93	123.51	29.29, 28.31, 27.75, 26.10, 25.59, 23.54, 22.76, 22.66	23.07, 22.18
4a,**b**[2]	64.77, 63.63, 63.54, 63.49		111.85, 110.90	51.40, 50.33	31.65, 29.89	32.74, 31.65	36.79, 35.23, 28.48, 27.14, 25.98, 25.44, 24.11, 23.82, 21.67, 21.10, 20.30, 20.25, 19.71, 19.65, 19.17, 19.07	–

Note: *R = H (**3a**–**3c**, **3e**, **4a**,**b**); Me (**3d**).

[1]δ ($\underline{C}Me_2$): 30.15 ppm.

[2]δ ($\underline{C}Cl_2$): 74.40, 73.90 ppm.

Table 3. Synthesis of cyclic acetals **3a**,**c**,**d** and thioacetal **3b**

Diol (dithiol)				Reaction time, h	Acetal (thioacetal)	
No.	R	X	*n*		No.	Yield, %
2a	H	O	0	2	**3a**	85
2b	H	S	0	2	**3b**	83
2c	H	O	1	6	**3c**	69
2d	Me	O	1	4	**3d**	74
2e	H	O	2	48	**3e**	0

Method for determining the anticorrosion activity of substances in an acidic environment

The inhibitory activity tests of the synthesized compounds were conducted on St20 steel samples (composition, wt %: Ni + Cu < 0.3%, As < 0.08%, Mn 0.35%, Cr < 0.25%, Si 0.17–0.37%, S 0.040%, P < 0.035%) measuring 60 × 20 × 1 mm. Prior to testing, the samples were sequentially treated with PS-11 and PS-12 sandpaper and their surface area was measured using calipers. Next, they were washed with water, ethanol and acetone, then dried in a desiccator. The corrosive environment was a 1 M hydrochloric acid solution. Corrosion rate was measured gravimetrically by the decrease in the mass of the metal sample. The effectiveness of the protective action of inhibitor **3d** was determined as the ratio of the corrosion rates of steel samples in inhibited and uninhibited 1 M HCl solution at a concentration of the compound under study of 4 g/L^{-1}. The inhibitor was evaluated based on the braking coefficient $\gamma = k_0/k_{inh}$, where k_0 and k_{inh} are the corrosion rates in the background solution and in the solution with the studied **3d** inhibitor additive, as well as based on the protection efficiency $Z = (1 - 1/\gamma)\cdot 100$ (%).

RESULTS AND DISCUSSION

The condensation of ketone **1** with ethylene glycol **2a** was carried out under standard conditions (acid catalyst, water removal by Dean–Stark method). The target 1,4-dioxaspiro[4.5]decane **3a** was formed with an 85% yield [18] (Scheme 1, Table 3). The reaction of 1,2-ethanedithiol **2b** with ketone **1** was carried out under the same conditions to yield 1,4-dithiaspiro[4.5]-decane **3b** at 83%.

When transitioning from 1,2-diols **2a**,**b** to 1,3-diols **2c**,**d**, it was necessary to increase the reaction time by 2–3 times to achieve acceptable yields (64–70%) of acetals **3c**,**d**. When 1,4-butanediol was used, the formation of the corresponding seven-membered ring **3e** was not observed.

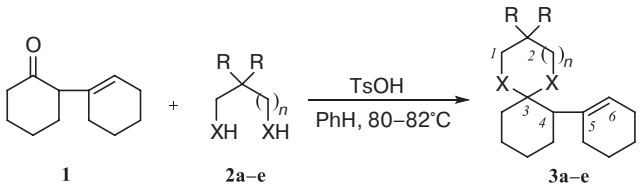

Scheme 1. Interaction of Wallach ketone **1** with reagents **2a**–**e** (the details of substituents, heteroatoms and ring size are given in Table 3)

To confirm the structure of the obtained heterocycles, ^{13}C NMR spectra obtained using the dept-135 technique are the most informative. The spectra of acetals **3a**,**c**,**b** show characteristic signals at δ_C 58–82 ppm that correspond to the α-carbon atoms of the 1,3-dioxocycloalkane fragments ($C^{1,2}$), signals for the nodal atom (C^3) at δ_C 99–113 ppm and the CH group (C^4) at δ_C 51–56 ppm, as well as the carbon atoms of the double bond at δ_C 137–139 (C^5) and δ_C 122–125 (C^5) ppm. In the ^{13}C NMR spectrum of thioacetal **3b**, the signals for the C^1, C^2, and C^3 carbon atoms of the heterocycle are shifted to a higher field as compared to acetals **3a**,**c**,**b** (Table 2). In the ^{1}H NMR spectra of compounds **3a**–**d**, the characteristic proton signal at the double bond (H^6) in the region of δ_H 5.4–5.7 ppm is reliably interpreted. The signals from the remaining protons are in a strong field and represent poorly resolved groups of multiplets (see Materials and Methods section, Table 1).

It was previously shown that the carbon-carbon double bond in ketone **1** [19, 20] and acetal **3a** [21] is sufficiently reactive to form three-membered rings. In this regard, we performed dichlorocarbenation

of acetal **3a** under Makosha reaction conditions to form *gem*-dichlorocyclopropane **4**. As evidenced by the doubled signals of carbon atoms $C^{1,2}$ (δ_C 64.77, 63.63, 63.54, 63.49 ppm), C^3 (δ_C 111.85, 110.90 ppm), C^4 (δ_C 51.40, 50.33 ppm), C^5 (δ_C 51.40, 50.33 ppm), C^6 (δ_C 32.74, 31.65 ppm) in the ^{13}C NMR spectra, dichlorocarbenation occurs with the formation of a mixture of two diastereomers **4a**,**b** (Scheme 2, Table 2). According to the ^1H NMR spectra (based on the intensity of characteristic signals) and the results of gas chromatography, the diastereomer ratio is 1 : 2.

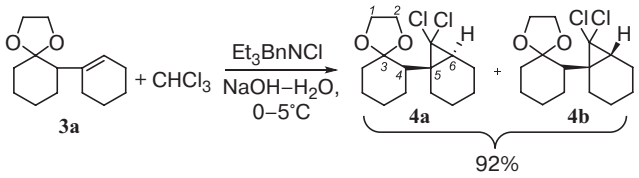

Scheme 2. Carbenation of acetal **3a** under Makosza reaction conditions

Ketone **1** is known to inhibit acid corrosion [22]. We found that ketal **3d** has a slightly lower inhibiting effect (67%) than ketone **1** (85%) under acidic corrosion conditions (1 M HCl) of St20 carbon steel at 60°C. The remaining acetals showed even less protective ability. Thus, the introduction of a cycloacetal fragment into the structure of the Wallach ketone reduces its ability to inhibit the acid corrosion of steel, which is likely due to the decreased polarity of acetals **3** compared to ketone **1**.

CONCLUSIONS

It is established that 2-(cyclohexen-1-yl)cyclohexanone (Wallach ketone) condenses with 1,2-, 1,3-diols, and ethanedithiol to form the corresponding spirocyclic derivatives in high yields. It is shown that the double bond of the cyclohexene fragment of the heterocycle readily adds dichlorocarbene under Mąkosza reaction conditions to form a polycyclic *gem*-dichlorocyclopropane as a mixture of two diastereomers. 7-(Cyclohex-1-en-1-yl)-3,3-dimethyl-1,5-dioxaspiro[5.5]undecane is confirmed to inhibit steel corrosion in acidic environments.

Acknowledgments

The work was carried out within the state assignment of the Ministry of Science and Education of the Russian Federation in the field of scientific activity, FEUR – 2022-0007 “Petrochemical Reagents, Oils, and Materials for Thermal Power Engineering.”

Authors’ contributions

B.V. Vazhenin—conducting research, literature review.

A.A. Golovanov—collecting and processing the material, statistical processing.

Yu.G. Borisova—collecting and processing the material, writing the text of the article.

G.Z. Raskil’dina—advising on planning, methodology, and implementation of the research.

S.S. Zlotskii—conceptualization of the research paper, critical revision with the introduction of valuable intellectual content.

The authors declare no conflicts of interest.

REFERENCES

1. Raskil’dina G.Z., Sultanova R.M., Zlotskii S.S. *gem*-Dichlorocyclopropanes and 1,3-dioxacyclanes: synthesis based on petroleum products and use in low-tonnage chemistry. *Rev. and Adv. in Chem.* 2023;13(1):15–27. https://doi.org/10.1134/S2634827623700150
2. Sultanova R.M. Borisova Yu.G., Khusnutdinova N.S., *et al.* 1,3-Dioxacyclanes: synthesis based on petrochemicals, chemical transformations and applications. *Russ. Chem. Bull.* 2023;72(10):2297–2318. https://doi.org/10.1007/s11172-023-4027-3 [Original Russian Text: Sultanova R.M. Borisova Yu.G., Khusnutdinova N.S., Raskil’dina G.Z., Zlotskii S.S. 1,3-Dioxacyclanes: synthesis based on petrochemicals, chemical transformations and applications. *Izvestiya Akademii nauk. Seriya khimicheskaya.* 2023;72(10):2297–2318 (in Russ.). https://elibrary.ru/sudxha]
3. Romero A., Santos A., Escrig D., Simon E. Comparative dehydrogenation of cyclohexanol to cyclohexanone with commercial copper catalysts: activity and impurities formed. *Appl. Catal. A: Gen.* 2011;392(1–2):19–27. https://doi.org/10.1016/j.apcata.2010.10.036

СПИСОК ЛИТЕРАТУРЫ

1. Raskil’dina G.Z., Sultanova R.M., Zlotskii S.S. *gem*-Dichlorocyclopropanes and 1,3-dioxacyclanes: synthesis based on petroleum products and use in low-tonnage chemistry. *Rev. and Adv. in Chem.* 2023;13(1):15–27. https://doi.org/10.1134/S2634827623700150
2. Султанова Р.М., Борисова Ю.Г., Хуснутдинова Н.С., Раскильдина Г.З., Злотский С.С. 1,3-Диоксацикланы: синтез на основе продуктов нефтехимии, химические превращения и применение. *Известия Академии наук. Серия химическая.* 2023;72(10):2297–2318. https://elibrary.ru/sudxha
3. Romero A., Santos A., Escrig D., Simon E. Comparative dehydrogenation of cyclohexanol to cyclohexanone with commercial copper catalysts: activity and impurities formed. *Appl. Catal A: Gen.* 2011;392(1–2):19–27. https://doi.org/10.1016/j.apcata.2010.10.036
4. Раскильдина Г.З., Султанова Р.М., Злотский С.С. Карбо- и гетероциклические соединения из нефтехимического сырья и их использование в малотоннажной химии. *Известия Уфимского Научного центра РАН.* 2019;3:5–18. https://doi.org/10.31040/2222-8349-2019-0-3-5-18

4. Raskil'dina G.Z., Sultanova R.M., Zlotsky S.S. Carbo- and heterocyclic platform compounds from petrochemical raw materials and their use in low-tonnage chemistry (review). *Izvestiya Ufimskogo Nauchnogo tsentra RAN = Proceedings of the RAS Ufa Scientific Center.* 2019;3:5–18 (in Russ.). https://doi.org/10.31040/2222-8349-2019-0-3-5-18
5. Sedrik R., Bonjour O., Laanesoo S., Liblikas I., Pehk T., Jannasch P., Vares L. Chemically Recyclable poly(β-thioether ester)s based on rigid spirocyclic ketal diols derived from citric acid. *Biomacromolecules.* 2022;23(6):2685–2696. https://doi.org/10.1021/acs.biomac.2c00452
6. Lorenzo D., Simón E., Santos A. Kinetic Model of Catalytic Self-Condensation of Cyclohexanone over Amberlyst 15. *Ind. Eng. Chem. Res.* 2014;53(49):19117–19127. https://doi.org/10.1021/ie5032265
7. Mahajan Y.S., Kamath R.S., Kumbhar P.S., Mahajani S.M. Self-condensation of cyclohexanone over ion exchange resin catalysts: kinetics and selectivity aspects. *Ind. Eng. Chem. Res.* 2008;47(1):25–33. https://doi.org/10.1021/ie061275b
8. Fisher W.B., VanPeppen J.F. Cyclohexanol and Cyclohexanone. In: Kirk-Othmer (Ed). *Kirk-Othmer Encyclopedia of Chemical Technology*: 4th ed. John Wiley & Sons, Inc.; 2004. P. 425–428. https://doi.org/10.1002/0471238961.0325031206091908.a01
9. Zhou S., Zou H., Huang G., Chen G., Zhou X., Huang S. Design, synthesis and anti-rheumatoid arthritis evaluation of double-ring conjugated enones. *Bioorg. Chem.* 2021;109(4):104701. https://doi.org/10.1016/j.bioorg.2021.104701
10. Deng Q., Nie G., Pan L., Zou J.-J., Zhang X., Wang L. Highly selective self-condensation of cyclic ketones using mof-encapsulating phosphotungstic acid for renewable high-density fuel. *Green Chem.* 2015;17(8):4473–4481. https://doi.org/10.1039/C5GC01287B
11. Svetozarskii S.V., Zil'berman E.N. Autocondensation of Cyclic Ketones. *Russ. Chem. Reviews.* 1970;39(7):553–561. https://doi.org/10.1070/RC1970v039n07ABEH002006
[Original Russian Text: Svetozarskii S.V., Zil'berman E.N. Autocondensation of Cyclic Ketones. *Uspekhi khimii*. 1970;39(7):1173–1189 (in Russ.). https://doi.org/10.1070/RC1970v039n07ABEH002006]
12. Brindisi M., Gemma S., Kunjir S., Di Cerbo L., Brogi S., Parapini S., D'Alessandro S., Taramelli D., Habluetzel A., Tapanelli S., Lamponi S., Novellino E., Campiani G., Butini S. Synthetic spirocyclic endoperoxides: new antimalarial scaffolds. *Med. Chem. Commun.* 2015;6(2):357–362. https://doi.org/10.1039/C4MD00454J
13. Kuz'mina U.S., Raskil'dina G.Z., Ishmetova D.V., *et al*. Cytotoxic Activity Against SH-SY_5Y Neuroblastoma Cells of Heterocyclic Compounds Containing *gem*-Dichlorocyclopropane and/or 1,3-Dioxacycloalkane Fragments. *Pharm. Chem. J.* 2022;55(12):1293–2022. https://doi.org/10.1007/s11094-022-02574-6
[Original Russian Text: Kuz'mina U.Sh., Raskil'dina G.Z., Ishmetova D.V., Sakhabutdinova G.N., Dzhumaev Sh. Sh., Borisova Yu.G., Vakhitova Yu.V., Zlotskii S.S. Cytotoxic activity of hererocyclic compounds containing *gem*-dichlorocyclopropane and/or 1,3-dioxacycloalkane fragments against SH-SY_5Y neuroblastoma cells. *Khimiko-Farmatsevticheskii Zhurnal*. 2021;55(12):27–32 (in Russ.). https://doi.org/10.30906/0023-1134-2021-55-12-27-32]
14. Borisova Y.G., Dzhumaev S.S., Khusnutdinova N.S. *et al.* Synthesis and Herbicidal Activity of Some Substituted 1,3-Dioxacycloalkanes and *gem*-Dichlorocyclopropanes. *Russ. J. Gen. Chem.* 2022;92(1):1–5. https://doi.org/10.1134/S1070363222010017
5. Sedrik R., Bonjour O., Laanesoo S., Liblikas I., Pehk T., Jannasch P., Vares L. Chemically Recyclable poly(β-thioether ester)s based on rigid spirocyclic ketal diols derived from citric acid. *Biomacromolecules.* 2022;23(6):2685–2696. https://doi.org/10.1021/acs.biomac.2c00452
6. Lorenzo D., Simón E., Santos A. Kinetic Model of Catalytic Self-Condensation of Cyclohexanone over Amberlyst 15. *Ind. Eng. Chem. Res.* 2014;53(49):19117–19127. https://doi.org/10.1021/ie5032265
7. Mahajan Y.S., Kamath R.S., Kumbhar P.S., Mahajani S.M. Self-condensation of cyclohexanone over ion exchange resin catalysts: kinetics and selectivity aspects. *Ind. Eng. Chem. Res.* 2008;47(1):25–33. https://doi.org/10.1021/ie061275b
8. Fisher W.B., VanPeppen J.F. Cyclohexanol and Cyclohexanone. In: Kirk-Othmer (Ed). *Kirk-Othmer Encyclopedia of Chemical Technology*: 4th ed. John Wiley & Sons, Inc.; 2004. P. 425–428. https://doi.org/10.1002/0471238961.0325031206091908.a01
9. Zhou S., Zou H., Huang G., Chen G., Zhou X., Huang S. Design, synthesis and anti-rheumatoid arthritis evaluation of double-ring conjugated enones. *Bioorg. Chem.* 2021;109(4):104701. https://doi.org/10.1016/j.bioorg.2021.104701
10. Deng Q., Nie G., Pan L., Zou J.-J., Zhang X., Wang L. Highly selective self-condensation of cyclic ketones using mof-encapsulating phosphotungstic acid for renewable high-density fuel. *Green Chem.* 2015;17(8):4473–4481. https://doi.org/10.1039/C5GC01287B
11. Светозарский С.В., Зильберман Е.Н. Автоконденсация циклических кетонов. *Успехи химии.* 1970;39(7):1173–1189. https://doi.org/10.1070/RC1970v039n07ABEH002006
12. Brindisi M., Gemma S., Kunjir S., Di Cerbo L., Brogi S., Parapini S., D'Alessandro S., Taramelli D., Habluetzel A., Tapanelli S., Lamponi S., Novellino E., Campiani G., Butini S. Synthetic spirocyclic endoperoxides: new antimalarial scaffolds. *Med. Chem. Commun.* 2015;6(2):357–362. https://doi.org/10.1039/C4MD00454J
13. Кузьмина У.Ш., Раскильдина Г.З., Ишметова Д.В., Сахабутдинова Г.Н., Джумаев Ш.Ш., Борисова Ю.Г., Вахитова Ю.В., Злотский С.С. Цитотоксическая активность гетероциклических соединений, содержащих *гем*-дихлорциклопропановый и/или 1,3- диоксациклоалкановый фрагменты, в отношении клеток линии SH-SY_5Y. *Хим.-фарм. журн.* 2021;55(12):27–32. https://doi.org/10.30906/0023-1134-2021-55-12-27-32
14. Борисова Ю.Г., Джумаев Ш.Ш., Хуснутдинова Н.С., Мрясова Л.М., Раскильдина Г.З., Злотский С.С. Синтез и гербицидная активность ряда замещенных 1,3-диоксациклоалканов и *гем*-дихлорциклопропанов. *Журн. общей химии.* 2022;92(1):3–8. https://doi.org/10.31857/S0044460X22010012
15. Sudarsanam P., Mallesham B., Prasad A.N., Reddy P.S., Reddy B.M. Synthesis of bio-additive fuels from acetalization of glycerol with benzaldehyde over molybdenum promoted green solid acid catalysts. *Fuel Process. Technol.* 2013;106:539–545. https://doi.org/10.1016/j.fuproc.2012.09.025
16. Kumar K., Pathak S., Upadhyayula S. Acetalization of 5-hydroxymethyl furfural into biofuel additive cyclic acetal using protic ionic liquid catalyst – A thermodynamic and kinetic analysis. *Renew. Energy.* 2021;167:282–293. https://doi.org/10.1016/j.renene.2020.11.084
17. Bell T.W., Vargas J.R., Crispino G.A. Interannular diastereoselectivity in the hydroboration of functionalized 1-cyclohexylcyclohexenes. *J. Org. Chem.* 1989;54(8):1978–1987. https://doi.org/10.1021/jo00269a042
18. Jennings P.W., Gingerich S.B. A Synthetic Scheme for the Preparation of Oxygen Labelled Furan Compounds. *J. Label. Compd. Radiopharm.* 1982;20:591–603.

[Original Russian Text: Borisova Y.G., Dzhumaev S.S., Raskil'dina G.Z., Zlotskii S.S., Khusnutdinova N.S., Mryasova L.M. Synthesis and herbicidal activity of some substituted 1,3-dioxacycloalkanes and *gem*-dichlorocyclopropanes. *Zhurnal Obshchei Khimii.* 2022;92(1): 3–8 (in Russ.). https://doi.org/10.31857/S0044460X22010012]

15. Sudarsanam P., Mallesham B., Prasad A.N., Reddy P.S., Reddy B.M. Synthesis of bio-additive fuels from acetalization of glycerol with benzaldehyde over molybdenum promoted green solid acid catalysts. *Fuel Process. Technol.* 2013;106: 539–545. https://doi.org/10.1016/j.fuproc.2012.09.025
16. Kumar K., Pathak S., Upadhyayula S. Acetalization of 5-hydroxymethyl furfural into biofuel additive cyclic acetal using protic ionic liquid catalyst – A thermodynamic and kinetic analysis. *Renew. Energy.* 2021;167:282–293. https://doi.org/10.1016/j.renene.2020.11.084
17. Bell T.W., Vargas J.R., Crispino G.A. Interannular diastereoselectivity in the hydroboration of functionalized 1-cyclohexylcyclohexenes. *J. Org. Chem.* 1989;54(8): 1978–1987. https://doi.org/10.1021/jo00269a042
18. Jennings P.W., Gingerich S.B. A Synthetic Scheme for the Preparation of Oxygen Labelled Furan Compounds. *J. Label. Compd. Radiopharm.* 1982;20:591–603.
19. Reese J. Über 2-Cyclohexyliden-cyclohexanon, ein Isomeres des 2-Δ^1-Cyclohexenyl-cyclohexanons. *Chem. Ber.* 1942;75(4): 384–394. https://doi.org/10.1002/cber.19420750414
20. Bao J., Tian H., Yang P., Deng J., Gui J. Modular synthesis of functionalized butenolides by oxidative furan fragmentation. *Eur. J. Org. Chem.* 2020;2020(3):339–347. https://doi.org/10.1002/ejoc.201901613
21. Creese M.W., Smissman E.E. Reaction of 2-(1,2-epoxycyclohex-1-yl)cyclohexanone ketal with boron trifluoride etherate. *J. Org. Chem.* 1976;41(1):169–170. https://doi.org/10.1021/jo00863a047
22. Ostapenko G.I., Gloukhov P.A., Bunev A.S. Investigation of 2-Cyclohexenylcyclohexanone as Steel Corrosion Inhibitor and Surfactant in Hydrochloric Acid. *Corros. Sci.* 2014;82(5): 265–270. https://doi.org/10.1016/j.corsci.2014.01.029

19. Reese J. Über 2-Cyclohexyliden-cyclohexanon, ein Isomeres des 2-Δ^1-Cyclohexenyl-cyclohexanons. *Chem. Ber.* 1942;75(4): 384–394. https://doi.org/10.1002/cber.19420750414
20. Bao J., Tian H., Yang P., Deng J., Gui J. Modular synthesis of functionalized butenolides by oxidative furan fragmentation. *Eur. J. Org. Chem.* 2020;2020(3):339–347. https://doi.org/10.1002/ejoc.201901613
21. Creese M.W., Smissman E.E. Reaction of 2-(1,2-epoxycyclohex-1-yl)cyclohexanone ketal with boron trifluoride etherate. *J. Org. Chem.* 1976;41(1):169–170. https://doi.org/10.1021/jo00863a047
22. Ostapenko G.I., Gloukhov P.A., Bunev A.S. Investigation of 2-Cyclohexenylcyclohexanone as Steel Corrosion Inhibitor and Surfactant in Hydrochloric Acid. *Corros. Sci.* 2014;82(5): 265–270. https://doi.org/10.1016/j.corsci.2014.01.029

About the Authors

Bogdan V. Vazhenin, Laboratory Assistant, Youth Scientific Laboratory "Petrochemical Reagents, Oils and Materials for Thermal Power Engineering," Ufa State Petroleum Technological University (1, Kosmonavtov ul., Ufa, 450064, Russia). E-mail: pan.bogdan2017@yandex.ru. ResearcherID LKO-1960-2024, RSCI SPIN-code 8372-0494, https://orcid.org/0009-0003-6021-2769

Alexander A. Golovanov, Dr. Sci. (Chem.), Senior Researcher, Ufa State Petroleum Technological University (1, Kosmonavtov ul., Ufa, 450064, Russia). E-mail: aleksandgolovanov@yandex.ru. Scopus Author ID 55651599300, ResearcherID I-4040-2017, RSCI SPIN-code 9460-7742, https://orcid.org/0000-0001-7133-3070

Yulianna G. Borisova, Cand. Sci. (Chem.), Associate Professor, Department of General, Analytical and Applied Chemistry, Ufa State Petroleum Technological University (1, Kosmonavtov ul., Ufa, 450064, Russia). E-mail: yulianna_borisova@mail.ru. Scopus Author ID 56526865000, ResearcherID P-9744-2017, RSCI SPIN-code 3777-0375, https://orcid.org/0000-0001-6452-9454

Gul'nara Z. Raskil'dina, Dr. Sci. (Chem.), Professor, Department of General, Analytical and Applied Chemistry, Ufa State Petroleum Technological University (1, Kosmonavtov ul., Ufa, 450064, Russia). E-mail: graskildina444@mail.ru. Scopus Author ID 56069888400, ResearcherID F-1619-2017, RSCI SPIN-code 2183-3333, https://orcid.org/0000-0001-9770-5434

Simon S. Zlotskii, Dr. Sci. (Chem.), Professor, Head of the Department of General, Analytical and Applied Chemistry, Ufa State Petroleum Technological University (1, Kosmonavtov ul., Ufa, 450064, Russia). E-mail: nocturne@mail.ru. Scopus Author ID 6701508202, ResearcherID W-6564-2018, RSCI SPIN-code 6529-3323, https://orcid.org/0000-0001-6365-5010

Об авторах

Важенин Богдан Валентинович, лаборант, молодежная научная лаборатория «Нефтехимические реагенты, масла и материалы для теплоэнергетики», ФГБОУ ВО «Уфимский государственный нефтяной технический университет» (450064, Россия, г. Уфа, ул. Космонавтов, д. 1). E-mail: pan.bogdan2017@yandex.ru. ResearcherID LKO-1960-2024, SPIN-код РИНЦ 8372-0494, https://orcid.org/0009-0003-6021-2769

Голованов Александр Александрович, д.х.н., старший научный сотрудник, ФГБОУ ВО «Уфимский государственный нефтяной технический университет» (450064, Россия, г. Уфа, ул. Космонавтов, д. 1). E-mail: aleksandgolovanov@yandex.ru. Scopus Author ID 55651599300, ResearcherID I-4040-2017, SPIN-код РИНЦ 9460-7742, https://orcid.org/0000-0001-7133-3070

Борисова Юлианна Геннадьевна, к.х.н., доцент кафедры общей, аналитической и прикладной химии, ФГБОУ ВО «Уфимский государственный нефтяной технический университет» (450064, Россия, г. Уфа, ул. Космонавтов, д. 1). E-mail: yulianna_borisova@mail.ru. Scopus Author ID 56526865000, ResearcherID P-9744-2017, SPIN-код РИНЦ 3777-0375, https://orcid.org/0000-0001-6452-9454

Раскильдина Гульнара Зинуровна, д.х.н., профессор кафедры общей, аналитической и прикладной химии, ФГБОУ ВО «Уфимский государственный нефтяной технический университет» (450064, Россия, г. Уфа, ул. Космонавтов, д. 1). E-mail: graskildina444@mail.ru. Scopus Author ID 56069888400, ResearcherID F-1619-2017, SPIN-код РИНЦ 2183-3333, https://orcid.org/0000-0001-9770-5434

Злотский Семен Соломонович, д.х.н., заведующий кафедрой общей, аналитической и прикладной химии ФГБОУ ВО «Уфимский государственный нефтяной технический университет» (450064, Россия, г. Уфа, ул. Космонавтов, д. 1). E-mail: nocturne@mail.ru. Scopus Author ID 6701508202, ResearcherID W-6564-2018, SPIN-код РИНЦ 6529-3323, https://orcid.org/0000-0001-6365-5010

Translated from Russian into English by H. Moshkov
Edited for English language and spelling by Thomas A. Beavitt

Tonkie Khimicheskie Tekhnologii = Fine Chemical Technologies.
2025;20(5):483–496 ISSN 2686-7575 (Online)

UDC 665.6
https://doi.org/10.32362/2410-6593-2025-20-5-483-496
EDN MLHKXX

RESEARCH ARTICLE

Effect of cavitation on the structural characteristics of oil asphaltenes

Denis V. Nikishin✉, Boris V. Peshnev, Alexander I. Nikolaev

MIREA – Russian Technological University (M.V. Lomonosov Institute of Fine Chemical Technologies), Moscow, 119454 Russia

✉ *Corresponding author, e-mail: nikishin@mirea.ru*

Abstract

Objectives. To investigate the influence of hydrodynamic cavitation on the group hydrocarbon composition of straight-run fuel oil and the structural characteristics of its asphaltenes.

Methods. The cavitation treatment of fuel oil was carried out in hydrodynamic mode using a Donor-2 device. The pressure drop in the working part was 50 MPa, while the number of treatment cycles varied from 1 to 10. In some cases, to intensify the process, the fuel oil was compounded with low-boiling hydrocarbons (propane-butane fraction, decalin). The determination of the group hydrocarbon composition of the sample was based on the different solubility of hydrocarbons in polar and nonpolar solvents; asphaltenes were studied by diffractometry and Raman spectroscopy.

Results. It is shown that the group hydrocarbon composition of the sample changes as a result of the cavitation effect: the content of resins and asphaltenes decreases, the amount of the oil fraction increases, and its group hydrocarbon composition is altered. It was found that cavitation exposure also changes the structural characteristics of asphaltenes: they decrease the L_a and L_c crystallite parameters that characterize their dimensions in plane and height, as well as increase the distance between alkyl substituents and the degree of plasticity of asphaltenes. The processing of Raman spectra by various methods demonstrated consistent results: in all cases, an increase in the intensity of exposure led to an increase in the structural disorder of asphaltenes. In the case of preliminary compounding of the sample with low-boiling hydrocarbons, the effect of cavitation was enhanced.

Conclusions. The results obtained may indicate the localization of cavitation bubbles at the boundaries of complex structural units of the dispersed petroleum system formed by asphalt-resinous substances and a dispersion medium. For this reason, it is resins and asphaltenes that are most exposed to the thermal effects that occur when cavitation bubbles collapse. The destruction of resins and asphaltenes leads to a decrease in the size of complex structural units and consequent decrease in the viscosity of the petroleum dispersed system, while the oil fraction is enriched with saturated hydrocarbons.

Keywords

hydrodynamic cavitation, petroleum and petroleum products, straight-run fuel oil, asphaltenes, a complex structural unit, group composition, viscosity

Submitted: 09.12.2024
Revised: 27.01.2025
Accepted: 05.09.2025

For citation

Nikishin D.V., Peshnev B.V., Nikolaev A.I. Effect of cavitation on the structural characteristics of oil asphaltenes. *Tonk. Khim. Tekhnol.* = *Fine Chem. Technol.* 2025;20(5):483–496. https://doi.org/10.32362/2410-6593-2025-20-5-483-496

НАУЧНАЯ СТАТЬЯ

Влияние кавитационного воздействия на структурные характеристики асфальтенов нефти

Д.В. Никишин✉, Б.В. Пешнев, А.И. Николаев

МИРЭА – Российский технологический университет (Институт тонких химических технологий им. М.В. Ломоносова), Москва, 119454 Россия

✉ *Автор для переписки, e-mail: nikishin@mirea.ru*

Аннотация

Цели. Рассмотреть влияние гидродинамической кавитации на групповой углеводородный состав прямогонного мазута и структурные характеристики его асфальтенов.

Методы. Кавитационную обработку мазута проводили в гидродинамическом режиме с использованием аппарата «Донор-2». Перепад давления в рабочей части составлял 50 МПа, число циклов обработки варьировали от 1 до 10. В ряде случаев, для интенсификации процесса, мазут компаундировали с низкокипящими углеводородами (пропан-бутановой фракцией, декалином). Определение группового углеводородного состава образца основывалось на различной растворимости углеводородов в полярных и неполярных растворителях, асфальтены исследовались методами дифрактометрии и спектроскопии комбинационного рассеяния (рамановской спектроскопии).

Результаты. Показано, что в результате кавитационного воздействия изменяется групповой углеводородный состав образца, в нем снижается содержание смол и асфальтенов, возрастает доля масляной фракции и при этом изменяется ее групповой углеводородный состав. Кроме этого установлено, что при кавитационном воздействии изменяются структурные характеристики асфальтенов: у них снижаются параметры кристаллитов L_a и L_c, характеризующие их размеры в плоскости и по высоте, увеличиваются расстояние между алкильными заместителями и степень ароматичности асфальтенов. Обработка спектров комбинационного рассеяния различными методами показала принципиальную схожесть результатов: увеличение интенсивности воздействия приводило к увеличению структурной разупорядоченности асфальтенов. В случае предварительного компаундирования образца с низкокипящими углеводородами эффект от кавитационной обработки усиливался.

Выводы. Полученные результаты могут свидетельствовать о локализации пузырьков кавитации на границах сложных структурных единиц нефтяной дисперсной системы, сформированных асфальто-смолистыми веществами и дисперсионной средой. В связи с этим, именно смолы и асфальтены подвергаются наибольшему термическому воздействию, возникающему при схлопывании кавитационных пузырьков. Деструкция смол и асфальтенов приводит к уменьшению размеров сложных структурных единиц и, соответственно, снижению вязкости нефтяной дисперсной системы, а масляная фракция при этом обогащается насыщенными углеводородами.

Ключевые слова

гидродинамическая кавитация, нефть и нефтепродукты, прямогонный мазут, асфальтены, сложная структурная единица, групповой состав, вязкость

Поступила: 09.12.2024
Доработана: 27.01.2025
Принята в печать: 05.09.2025

Для цитирования

Никишин Д.В., Пешнев Б.В., Николаев А.И. Влияние кавитационного воздействия на структурные характеристики асфальтенов нефти. *Тонкие химические технологии*. 2025;20(5):483–496. https://doi.org/10.32362/2410-6593-2025-20-5-483-496

INTRODUCTION

One of the current priorities of the oil refining industry is to increase the depth of oil processing, which is achieved by improving the efficiency and technological sophistication of the processing of raw materials arriving at oil refineries. However, the search for solutions to such problems is complicated by the trend towards the extraction of heavier crude oil fractions. Therefore, the development of methods and technologies aimed at increasing the yield of light petroleum products becomes a significant and relevant task.

The scientific literature discusses several options for increasing the depth of oil processing through physical methods: using ultrasonic, hydrodynamic, magnetic, electrohydraulic and other treatment methods [1–5]. With each passing year, interest in the application of such pre-treatment methods in oil refining continues to grow. One of the most effective processing approaches is based on the use of cavitation phenomena [2].

Cavitation treatment involves creating conditions under which cavitation bubble nuclei form, grow, and subsequently collapse [6]. The result of the collapse of an individual bubble is the emergence of extreme pressures up to 1000 MPa and temperatures up to 5000 K in a localized area to release energy of about $2.5 \cdot 10^{-5}$ J [7, 8]. As confirmed by experimental studies, cavitation treatment of oil dispersion systems (ODS) can lead to changes in their properties and hydrocarbon composition [9–11]. However, the observed changes described in the literature [10, 12–15] are not always unambiguous: for example, in the study [13], it is indicated that cavitation treatment led to a decrease in the density of the raw material, while in the study [12], it led to an increase. The viscosity of the oil system after such treatment decreases [3, 5, 9, 16, 17], but then, over time, it returns to values close to the initial ones, although not reaching them [16, 17]. Such a change in viscosity may indicate the destruction of the ODS structure due to the disruption of intermolecular interactions (2–10 kJ/mol), Van der Waals forces (10–20 kJ/mol), and hydrogen bonds (20–160 kJ/mol) of asphaltenes and resins, representing the least stable and most high-molecular-weight components of the oil system, to form supramolecular complex structural units (CSU) [18, 19].

The CSU core consists of asphaltenes and resins surrounded by a solvate shell of compounds whose molecular weight decreases from the center to the periphery to form a dispersed phase of the system that has an interface with the dispersion medium. The presence of resins and asphaltenes in oil and petroleum products is an important factor that must be taken into account in the processes of extraction, transportation, and refining. At the extraction stage, they form asphaltene-resin-paraffin deposits in collectors and pipelines resulting in reduced throughput. Increased viscosity of the oil as a result of resin and asphaltene content increases transportation costs, while their presence in high-temperature processes leads to increased coking.

In studies [20, 21], the formation of cavitation bubble nuclei is shown to be promoted by the presence of a phase boundary. In the case of ODS, such a boundary is formed between the dispersed phase, which is composed of resins and asphaltenes, and the dispersion medium. It can be assumed that the cavitation bubbles are localized precisely at this boundary. Therefore, as a result of bubble collapse, the hydrocarbons forming the phase boundary—including resins with asphaltenes—should be subjected to the most intense thermal processing.

In this study, the structural changes of fuel oil asphaltenes under the influence of hydrodynamic cavitation are examined. The samples were studied using methods of Raman spectroscopy and powder X-ray diffraction.

EXPERIMENTAL

The object of the study is a sample of straight-run vacuum residue obtained at the ELOU-AVT-6 unit of the *Gazpromneft-MNPZ* plant (Moscow, Russia). Cavitation treatment of the fuel oil was conducted in hydrodynamic mode on the Donor-2 apparatus (*Experimental Plant of Scientific Instrumentation of the Russian Academy of Sciences*, Russia) [16] at a temperature of 50°C. The pressure drop in the working part of the device was 50 MPa; the number of processing cycles varied from 1 to 10. In several publications, the addition of gaseous or liquid components into the treated system is proposed as a means to enhance the efficiency of cavitation processing [18, 22–25]. In the current study, propane-butane fraction (PBF) was used as such intensifying components with the following composition (in vol %): C_2H_6 ~ 15, C_3H_8 ~ 65, C_4H_{10} ~ 20, and a decalin-containing additive (hereinafter referred to as decalin) with the following composition (in wt %): decahydronaphthalene ($C_{10}H_{18}$) ~ 83.0, bicyclopentyl ($C_{10}H_{18}$) ~ 5.5, bicyclo[5.3.0]decane ($C_{10}H_{18}$) ~ 5.2. Identification was carried out using gas chromatography-mass spectrometry analysis. PBF was added by gas bubbling through the sample layer with a gas flow rate of 75 and 225 cm³/min for 30 min immediately before treatment.

Viscosity was determined using viscometers for opaque liquids (*EKROSKHIM*, Russia) according to

GOST 33-2016[1]. The group composition of the samples was determined using the method described in study [26]. When precipitating asphaltenes, the mass ratio of the sample to the solvent was taken to be 1 : 40. Asphaltenes were precipitated for 24 h. The resulting solution was filtered using a decolorized paper filter of the Blue Ribbon brand (*Melior XXI*, Russia). The isolated asphaltenes were washed from co-precipitated paraffins and resins in a Soxhlet apparatus for 2 h with petroleum ether 40–70°C (pure, *EKOS-1*, Russia) and dried in a laboratory vacuum oven for 1 h. As an adsorbent in the column, silica gel of the ASCG grade[2] (*ChromLab*, Russia) with a fraction of 0.25–0.50 mm was used. Petroleum ether, toluene (chemically pure, *Base No. 1 for Chemical Reagents*, Russia), and isopropyl alcohol (chemically pure, *Base No. 1 for Chemical Reagents*, Russia) were used as solvents. For the precipitation and washing of asphaltenes, as well as for the isolation of saturated hydrocarbons, petroleum ether was used; for the isolation of aromatic hydrocarbons—toluene; for the isolation of resins—a mixture of toluene and isopropyl alcohol in a 30 to 70 ratio. The volumetric ratio of silica gel to sample was 100 : 1.

The asphaltenes extracted from the samples of fuel oil were studied using powder diffractometry and Raman spectroscopy. The following sample numbering is used in the study: (1) asphaltenes extracted from the original fuel oil; (2) asphaltenes extracted from the fuel oil after cavitation treatment; (3) asphaltenes extracted from the fuel oil after treatment (the fuel oil was purged with PBF immediately before the treatment at a flow rate of 225 cm³/min); (4) asphaltenes extracted from a fuel oil compound with decalin (at a concentration of 2 wt %) after its treatment. In all cases, five cycles of treatment were carried out.

The diffraction patterns of the isolated asphaltenes were recorded at room temperature using an X-ray diffractometer XRD 6000 (CuK_α radiation, wavelength $\lambda = 0.1542$ nm, *Shimadzu Corporation*, Japan) at angles $2\theta = 10°–80°$. The speed of the goniometer rotation was 0.02°/s. The obtained diffractograms were processed in the Origin software. For separating the obtained peaks, Gaussian functions were used.

The Raman spectra of asphaltenes were obtained at room temperature (20°C) using a Confotec Uno confocal Raman microscope (*SOL Instruments*®, Belarus) in the shift range from 400 to 4000 cm^{-1}. At a radiation power 10% of the maximum possible value (50 mW), the wavelength of the radiation was 532 nm; the test duration was 50 s. The obtained spectra were processed in the Origin software. To separate the obtained spectra into peaks D1–D4 and G, Gaussian, Lorentzian, and Voigt functions were applied (method 1) [27]. The separation of the obtained spectra into their constituent peaks was carried out using the method described in study [28], in which the G peak (approximately at the maximum position ~1580 cm^{-1}) corresponds to the presence of an ideal graphite structure (the response is formed by the vibrations of carbon atoms with sp^2 hybridization, forming the planes of condensed aromatic layers), while the D peak (~1350–1370 cm^{-1}) corresponds to defects in the lattice of the ideal graphite structure and its edges (method 2). While the assignment of peaks SL (~1230 cm^{-1}), VR (~1380 cm^{-1}), VL (~1460 cm^{-1}), GR (~1540 cm^{-1}), G2 (~1600 cm^{-1}) to various structural fragments is revealed in studies [28–30], it was only possible to reliably interpret the ratio of the integral intensities of the D and G peaks.

The structural parameters of asphaltenes were determined based on the results of X-ray structural analysis using formulas (1)–(8) [31, 32].

The distance between aromatic layers d_m was calculated using the Bragg–Wulf formula (1):

$$d_m = \frac{\lambda}{2\sin\theta_{002}}, \quad (1)$$

where λ is the wavelength of X-ray radiation, Å; θ_{002} is the angle corresponding to the maximum of the 002 peak, degrees.

The distances between aliphatic chains or cycles d_γ were calculated using formula (2):

$$d_\gamma = \frac{\lambda}{2\sin\theta_\gamma}. \quad (2)$$

The average diameter of the aromatic layers L_a was calculated using formula (3):

$$L_a = \frac{0.92}{FWHM_{10}}, \quad (3)$$

where $FWHM_{10}$ (full width at half maximum) is the full width of the halo at half its maximum height, measured in units of $(\sin\theta)/\lambda$, degrees.

The average height of the stack of aromatic layers L_c (crystallite size) was calculated using formula (4):

$$L_c = \frac{0.45}{FWHM_{002}}, \quad (4)$$

where $FWHM_{002}$ is the full width at half maximum of halo 002, measured in units of $(\sin\theta)/\lambda$, degrees.

[1] GOST 33-2016. Interstate Standard. Petroleum and petroleum products. Transparent and opaque liquids. Determination of kinematic and dynamic viscosity. Moscow: Standartinform; 2017.

[2] Activated silica gel, coarse-pored, granulated.

The average number of carbon atoms in the aromatic layer C_{au} (au stands for atomic units) was estimated using formula (5):

$$C_{au} = \frac{L_a + 1.23}{0.65}. \quad (5)$$

The average number of aromatic rings NO_a in the layer was estimated using formula (6):

$$NO_a = \frac{L_a}{2.667}. \quad (6)$$

The average number of aromatic layers in the pack M was estimated using formula (7):

$$M = \frac{L_c}{d_m} + 1. \quad (7)$$

The degree of aromaticity of asphaltenes f_a was determined using formula (8):

$$f_a = \frac{A_{002}}{A_{002} + A_\gamma}, \quad (8)$$

where A_{002} and A_γ are the areas of the 002 and γ-band peaks.

Based on the results of processing the Raman spectra of asphaltenes, the parameters R_1 and R_2 were calculated using formulas (9) and (10) [33] to assess the disorder of their structure:

$$R_1 = \frac{I_{D1}}{I_G}, \quad (9)$$

$$R_2 = \frac{I_{D1}}{I_G + I_{D1}}, \quad (10)$$

where I_{D1} and I_G are the areas (integral intensities) of the D1 and G peaks.

The evaluation of the aromatic layer diameter based on the results of Raman spectroscopy (RS) L_a^{RS} (nm) was conducted using formula (11) [27, 34]:

$$L_a^{RS} = 4.4 \frac{A_G}{A_{D1}}. \quad (11)$$

The average number of aromatic rings in the layer NO_a based on the results of Raman spectroscopy was estimated using formula (12) [27]:

$$NO_a = \frac{L_a^{RS} \cdot 10}{2.667}. \quad (12)$$

RESULTS AND DISCUSSION

Figure 1 shows the results confirming the information about the reduction in the viscosity of the ODS due to cavitation effects. The results demonstrate that the number of processing cycles has a significant influence on the rheological characteristics of the system. The subsequent increase in viscosity aligns with previously obtained results. As previously mentioned, the reduction in the viscosity of petroleum products as a result of cavitation treatment is associated with the destruction of weak intermolecular CSU bonds. Over time, these bonds are restored to increase CSU sizes, resulting in an increase in viscosity. More importantly, the viscosity does not return to its original values, which can be seen as evidence of deeper changes in the CSU as a result of cavitation, including intramolecular transformations of resins and asphaltenes.

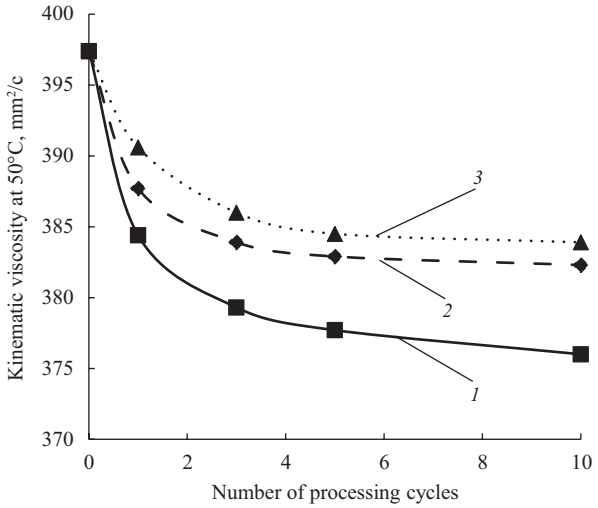

Fig. 1. Effect of hydrodynamic treatment conditions on the viscosity of straight–run fuel oil: (*1*) immediately after treatment; (*2*) after 5 days; (*3*) after 20 days

The data given in Table 1 confirm the change in the group composition of the fuel oil. It is evident that after cavitation treatment, the content of asphaltenes and resins in the sample decreased, while the amount of oil fractions increased. This effect, which can be increased by intensifying the cavitation process by saturating the feedstock before treatment with PBF or adding decalin, also increases the more PBF is introduced into the system. A change in the composition of the oil fractions, i.e., the ratio of saturated to aromatic hydrocarbons, was noted. Following cavitation treatment in the presence of an initiating agent (PBF or decalin), the content of saturated structures in the oil fraction increased, while the concentration of arenes decreased. This cannot be explained by the introduction of saturated hydrocarbons (decalin) into the sample, since the share of arenes in the oil fraction decreased to 34.7–35.0 wt % following the preliminary saturation of the fuel oil with PBF. Such a change in the hydrocarbon composition of the object under study can be explained by the destruction of resins and asphaltenes during processing. For example, the cleavage of alkyl substituents from the polycyclic

core. One of the possible transformation mechanisms in the asphaltene–resin–oil chain is considered in the studies [35]. It is possible that the incomplete relaxation of the viscosity of the fuel oil to its initial values following treatment is related to the destruction of the molecules constituting the CSU.

To confirm the hypothesis about the destruction of resins and asphaltenes in oil under cavitation impact, the asphaltenes extracted from the samples were studied using powder diffraction and Raman spectroscopy methods. Table 2 provides information on the structural characteristics of asphaltenes.

When comparing the characteristics of asphaltenes extracted from the original sample of fuel oil (sample 1) with those of asphaltenes extracted from the fuel oil after cavitation treatment (samples 2–4), several changes can be noted. As a result of the treatment, the average height of the aromatic layer stack L_c decreased, i.e., the size of the asphaltenes (CSU cores) became smaller, and the degree of aromaticity f_a of the asphaltenes increased, thus confirming the assumption of the detachment of alkyl substituents from them. This also aligns with the data on the increase in the parameter d_γ, which characterizes the distance between alkyl substituents.

During cavitation treatment of fuel oil in the presence of additives (PBF, decalin), the aromaticity of asphaltenes (samples 3 and 4) increased even more, while the average diameter of the aromatic layer L_a decreased. It should be noted that for asphaltenes, it is more accurate to speak not of the size of the aromatic layer, but rather of the size of the polycyclic layer formed by condensed aromatic and naphthenic rings. It is likely that in the case of samples 3 and 4, not only did the cleavage of alkyl chains occur, but also the opening of boundary saturated cycles with the subsequent detachment of the formed alkyl substituents, i.e., a more profound destruction of the compounds. This is consistent with the observed changes in group composition (see Table 1). When processing fuel oil compounded with PBF or decalin, a more significant increase in oil content was observed compared to processing without additives.

The described changes in the structural characteristics of asphaltenes are confirmed by the results of Raman spectrometry (Fig. 2, Table 3, Table 4).

Regardless of the method of processing Raman spectra and the functions used, a general trend is observed for asphaltene samples: an increase in the intensity of processing the initial oil leads to a more

Table 1. Change in the group composition of the straight-run fuel oil sample after its cavitation treatment under various conditions

Fraction, wt %	Initial sample	Cavitation treatment conditions*			
		Without additives	With propane-butane fraction, mL/min		With decalin
			75	225	
Asphaltenes	4.4	3.7	2.1	0.5	1.5
Resins	13.3	12.0	9.6	7.6	12.0
Oils	82.3	84.3	88.3	91.9	86.5

* Five cycles of exposure.

Table 2. Changes in the structural characteristics of fuel oil asphaltenes after treatment under various conditions

Sample	d_m, Å	d_γ, Å	L_a, Å	L_c, Å	C_{au}	NO_a	M	f_a
1	3.63	4.87	19.97	14.66	32.61	7.49	5.03	0.38
2	3.64	4.93	21.44	12.92	34.88	8.04	4.55	0.40
3	3.65	4.91	18.91	13.72	30.98	7.09	4.76	0.42
4	3.63	4.88	18.73	13.49	30.71	7.02	4.71	0.44

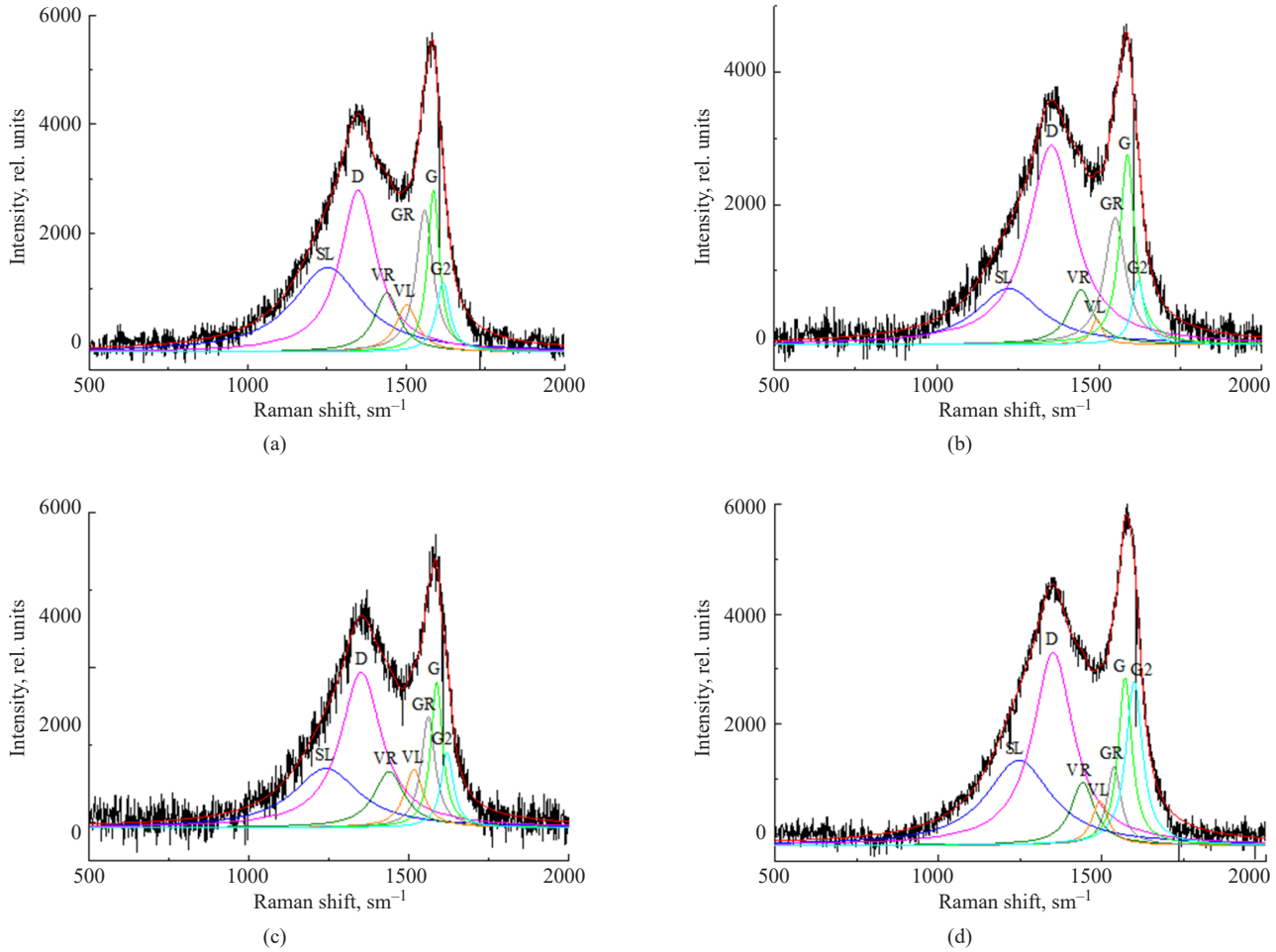

Fig. 2. Raman spectra of asphaltenes processed according to the method [28]:
(a) sample 1, (b) sample 2, (c) sample 3, (d) sample 4. The black line is the spectrum obtained experimentally; the red line is the curve describing the spectrum; the lines of the remaining colors are curves obtained by spectrum decomposition

pronounced increase in the disorder of the asphaltene structure, which is characterized by parameters R_1 and R_2. The increase in the values of parameters R_1 and R_2, as well as the intensity of peak D1 (see Table 4) relative to other peaks, indicates the emergence of additional defects in the structure of asphaltenes, which confirms the assumption of their destruction during cavitation processing.

It is significant that no significant changes in the parameters R_1 and R_2 were observed during the processing of fuel oil in the presence of decalin (sample 4, table 3). This may be due to the fact that decalin, having a higher boiling point compared to PBF (by 190–220°C), is less prone to the active formation of cavitation nuclei and the intensification of the process under cavitation treatment conditions.

Table 3. Results of processing Raman spectra (RS) by various methods and functions

Sample	R_1	R_2	L_a^{RS}, nm	NO_a
Method 1 [27]				
Gaussian function				
1	1.52	0.58	2.90	10.86
2	1.83	0.64	2.41	9.03
3	2.75	0.73	1.60	6.00
4	1.75	0.62	2.51	9.42

Table 3. Continued

Sample	R_1	R_2	L_a^{RS}, nm	NO_a
Lorentzian function				
1	1.13	0.53	3.89	14.58
2	1.22	0.55	3.62	13.58
3	1.65	0.62	2.66	9.98
4	1.22	0.55	3.60	13.50
Voigt function				
1	1.91	0.63	2.30	8.64
2	2.34	0.70	1.88	7.02
3	3.16	0.76	1.39	5.22
4	1.83	0.65	2.40	9.01
Method 2 [28]				
Lorentzian function				
1	3.11	0.76	1.42	5.31
2	3.29	0.77	1.34	5.01
3	3.79	0.79	1.16	4.35
4	3.39	0.77	1.30	4.87

Table 4. Analysis of the peaks of the first order of the Raman spectra of asphaltenes using various techniques and functions

Sample	Peak	Position, cm^{-1}	Intensity, rel. units	Width, cm^{-1}	Area, rel. units	Part, %
Method 1 [27]						
Gaussian function						
1	D4	1211	1242	271	357816	21.2
	D1	1362	3394	188	679850	40.5
	D3	1494	1471	99	155556	9.3
	G	1581	4953	85	447654	26.6
	D2	1665	665	57	40016	2.4
2	D4	1152	737	224	175558	12.7
	D1	1363	3225	216	740574	53.8
	D3	1478	492	68	35503	2.6
	G	1576	3761	101	405487	29.5
	D2	1674	372	47	18754	1.4
3	D4	1019	230	37	9116	0.9
	D1	1357	2337	290	722131	72.0
	D3	–	–	–	–	–
	G	1578	2529	98	262872	26.2
	D2	1674	204	42	9047	0.9

Table 4. Continued

Sample	Peak	Position, cm^{-1}	Intensity, rel. units	Width, cm^{-1}	Area, rel. units	Part, %
4	D4	1188	1117	257	305144	17.1
	D1	1360	3914	200	832291	46.7
	D3	1497	1420	94	142759	8.0
	G	1580	5199	86	475110	26.6
	D2	1664	585	44	27671	1.6
Lorentzian function						
1	D4	1236	1291	183	342872	18.9
	D1	1348	3213	135	643801	35.4
	D3	1471	1420	125	262639	14.4
	G	1579	4963	76	568910	31.3
	D2	–	–	–	–	–
2	D4	1229	914	200	262821	17.3
	D1	1351	2693	143	568004	37.4
	D3	1461	1107	136	221718	14.6
	G	1579	3951	79	467266	30.7
	D2	–	–	–	–	–
3	D4	1255	757	184	201775	18.0
	D1	1364	2122	161	498641	44.6
	D3	1510	757	103	116392	10.4
	G	1581	2824	71	301695	27.0
	D2	–	–	–	–	–
4	D4	1245	1472	178	379750	19.8
	D1	1353	3485	137	706699	36.8
	D3	1471	1427	121	255871	13.3
	G	1577	5210	74	578393	30.1
	D2	–	–	–	–	–
Voigt function						
1	D4	1180	1111	227	339072	19.5
	D1	1355	3663	192	758723	43.6
	D3	1505	1653	111	195718	11.3
	G	1583	4720	79	397212	22.9
	D2	1662	681	66	47894	2.8
2	D4	1153	518	246	138946	9.5
	D1	1363	3241	224	885906	60.6
	D3	1491	611	76	49185	3.4
	G	1581	3805	93	378077	25.9
	D2	1680	220	40	9378	0.6

Table 4. Continued

Sample	Peak	Position, cm^{-1}	Intensity, rel. units	Width, cm^{-1}	Area, rel. units	Part, %
3	D4	–	–	–	–	–
	D1	1361	2381	293	813860	76.0
	D3	–	–	–	–	–
	G	1580	2555	95	257397	24.0
	D2	–	–	–	–	–
4	D4	1115	597	183	116732	6.3
	D1	1353	4199	248	1109710	59.5
	D3	1496	497	61	32397	1.7
	G	1579	5268	93	605744	32.5
	D2	–	–	–	–	–
Method 2 [28]						
Lorentzian function						
1	SL	1252	1545	268	649719	28.6
	D	1350	2958	141	653498	30.5
	VR	1439	1089	94	161356	7.7
	VL	1502	864	83	112850	5.4
	GR	1559	2596	64	262344	12.6
	G	1587	2953	45	210196	10.2
	G2	1617	1274	52	104211	5.0
2	SL	1221	843	246	325267	17.0
	D	1352	3007	172	812491	44.0
	VR	1443	824	90	116626	6.5
	VL	1492	381	40	24135	1.4
	GR	1549	1916	78	233752	13.1
	G	1586	2864	55	246851	14.0
	G2	1619	958	47	69986	4.0
3	SL	1240	765	251	301243	21.6
	D	1350	2005	156	491390	36.8
	VR	1437	723	115	131168	10.0
	VL	1515	751	71	84750	6.5
	GR	1559	1433	53	119445	9.3
	G	1586	1872	44	129677	10.2
	G2	1619	970	47	71379	5.6
4	SL	1246	1546	242	588545	24.5
	D	1351	3508	151	830365	36.0
	VR	1441	1143	88	157084	7.0
	VL	1494	804	60	75508	3.4
	GR	1537	1431	53	118196	5.3
	G	1571	3048	51	245220	11.1
	G2	1599	2983	60	283111	12.7

CONCLUSIONS

The obtained results indirectly confirm the assumption about the formation of cavitation bubbles at the phase boundaries represented by CSU in oil and fuel oil products. In this regard, the destructive impact of the treatment is primarily directed at the components forming the CSU. As a result of the destruction of resins and asphaltenes, the group composition of the fuel oil changes (the share of resins and asphaltenes decreases, asphaltenes become more aromatic, and the oil fractions are enriched with saturated hydrocarbons) along with its rheological characteristics, which is reflected in the reduction of viscosity. The reduction in the size of the core forming the CSU means that the viscosity characteristics of the system do not return to their initial values even after the relaxation of intermolecular interactions between the core and the solvation layers. It is shown that the processes of CSU destruction under cavitation impact are intensified by the preliminary compounding of fuel oil with low-boiling hydrocarbons.

Acknowledgments

The work was carried out using the equipment of the Center for Collective Use at the RTU MIREA with the support of the Ministry of Science and Higher Education of the Russian Federation under agreement No. 075-15-2021-689 dated September 1, 2021. The authors thank the staff of the Department of Physics and Technical Mechanics of the Institute of Advanced Technologies and Industrial Programming at the RTU MIREA, A.D. Maksimov and N.A. Sanzharovskiy, for recording the Raman spectra of the provided samples.

Authors' contributions

D.V. Nikishin—identification of research objects, conducting experiments, analysis and processing of experimental data obtained and analysis of literary sources, writing and editing the text of the article.

B.V. Peshnev—formulation of the purpose and objectives of the research, analysis of literary sources, writing and editing the text of the article, development of methodology and analysis of the results obtained.

A.I. Nikolaev—consulting on the instrument base, methodology issues, editing the text of the article.

The authors declare no conflicts of interest.

REFERENCES

1. Pivovarova N.A. Use of wave effect in processing of the hydrocarbonic raw material (Review). *Pet. Chem*. 2019;59(6): 559–569 (in Russ.). https://doi.org/10.1134/S0965544119060148 [Original Russian Text: Pivovarova N.A. Use of wave effect in processing of the hydrocarbonic raw material (Review). *Neftekhimiya*. 2019;59(7):727–738 (in Russ.). https://doi.org/10.1134/S002824211907013X]
2. Geller S.V. Technical and economic assessment of the possibility of using innovative wave technology in oil refining and oil production. *Neft. Gaz. Novacii = Oil. Gas. Innovations*. 2010;9:20–26 (in Russ.).
3. Gafarova E.B., Sviridov S.V. Technologies for reducing viscosity of oil and petroleum products. *Oborudovanie i tekhnologii dlya neftegazovogo kompleksa = Equipment and Technologies for Oil and Gas Complex*. 2020;116(2):71–78 (in Russ.). https://doi.org/10.33285/1999-6934-2020-2(116)-71-78
4. Nurullaev V.H. Conditions formation of cavitation zones and its action on the physical and chemical characteristics crude oils. *Transport i khranenie nefteproduktov i uglevodorodnogo syr'ya = Transportation and Storage of Oil Products and Hydrocarbons*. 2017;1:38–42 (in Russ.).
5. Sunagatullin R.Z., Kutukov S.E., Golyanov A.I., Chetverikova O.V., Zverev F.S. Control of rheological properties by exposure to physical methods. *Neftyanoe khozyaistvo = Oil Industry J*. 2021;1:92–97 (in Russ.). https://doi.org/10.24887/0028-2448-2021-1-92-97
6. Avvaru B., Venkateswaran N., Uppara P., Iyengar S.B., Katti S.S. Current knowledge and potential applications of cavitation technologies for the petroleum industry. *Ultrason. Sonochem*. 2018;42:493–507. https://doi.org/10.1016/j.ultsonch.2017.12.010
7. Ivanitskiy G.K. Numerical simulation of bubble cloud behavior in hydrodynamic cavitation. *Sovremennaya nauka: issledovaniya, idei, rezul'taty, tekhnologii = Modern Science: Research, Ideas, Results, Technologies*. 2011;7:52–58 (in Russ.).

СПИСОК ЛИТЕРАТУРЫ

1. Пивоварова Н.А. Использование волновых воздействий в переработке углеводородного сырья (обзор). *Нефтехимия*. 2019;59(7):727–738. https://doi.org/10.1134/S002824211907013X
2. Геллер С.В. Технико-экономическая оценка возможности применения инновационной волновой технологии в нефтепереработке и нефтедобыче. *Нефть. Газ. Новации*. 2010;9:20–26.
3. Гафарова Э.Б., Свиридов С.В. Технологии снижения вязкости нефти и нефтепродуктов. *Оборудование и технологии для нефтегазового комплекса*. 2020;116(2):71–78. https://doi.org/10.33285/1999-6934-2020-2(116)-71-78
4. Нуруллаев В.Х. Условия образования кавитационных зон и их действия на физико-химические характеристики нефтей. *Транспорт и хранение нефтепродуктов и углеводородного сырья*. 2017;1:38–42.
5. Сунагатуллин Р.З., Кутуков С.Е., Гольянов А.И., Четверткова О.В., Зверев Ф.С. Управление реологическими характеристиками нефтей физическими методами воздействия. *Нефтяное хозяйство*. 2021;1:92–97. https://doi.org/10.24887/0028-2448-2021-1-92-97
6. Avvaru B., Venkateswaran N., Uppara P., Iyengar S.B., Katti S.S. Current knowledge and potential applications of cavitation technologies for the petroleum industry. *Ultrason. Sonochem*. 2018;42:493–507. https://doi.org/10.1016/j.ultsonch.2017.12.010
7. Иваницкий Г.К. Численное моделирование динамики пузырькового кластера в процессах гидродинамической кавитации. *Современная наука: исследования, идеи, результаты, технологии*. 2011;7:52–58.
8. Аганин А.А., Ганиев О.Р., Давлетшин А.И., Украинский Л.Е. Нагрев жидкости при схлопывании одиночного кавитационного пузырька. *Проблемы машиностроения и надежности машин*. 2020;1:31–38. https://doi.org/10.31857/S0235711920010022

8. Aganin A.A., Ganiev O.R., Davletshin A.I., *et al*. Liquid heating during the collapse of a single cavitation bubble. *J. Mach. Manuf. Reliab*. 2020;49(1):24–30. https://doi.org/10.3103/S1052618820010021 [Original Russian Text: Aganin A.A., Ganiev O.R., Davletshin A.I., Ukrainskyi L.E. Liquid heating during the collapse of a single cavitation bubble. *Problemy mashinostroeniya i nadezhnosti mashin*. 2020;49(1):24–30 (in Russ.). https://doi.org/10.31857/S0235711920010022]
9. Promtov M.A., Sunagatullin R.Z., Kutukov S.E., Koliukh A.N., Sheina O.A., Zverev F.S., Sukhovei M.V. Change of rheological parameters of high-paraffin oil under multifactorial impact in a rotor-stator device. *Problemy sbora, podgotovki i transporta nefti i nefteproduktov = Problems of Gathering, Treatment and Transportation of Oil and Oil Products*. 2020;127(5):76–88 (in Russ.). https://doi.org/10.17122/ntj-oil-2020-5-76-88
10. Torkhovsky V.N., Antonyuk S.N., Golovanov A.B., Vorobyov S.I., Nikolaeva M.V., Dvoretkov P.A. Processing of Compounded Oil Feedstock with Pre-Activation of Initial Raw Material Flows. *Tekhnologii nefti i gaza = Oil and Gas Technologies*. 2021;133(2):3–7 (in Russ.). https://doi.org/10.32935/1815-2600-2021-133-2-3-7
11. Khamidullin R.F., Kharlampidi K.E., Nikulin R.M., *et al.* Increasing the Yield of Light Distillates by Activation of Oil Stock. *Chem. Technol. Fuels Oils*. 2017;52(6):670–678. https://doi.org/10.1007/s10553-017-0759-9 [Original Russian Text: Khamidullin R.F., Kharlampidi K.E., Sitalo A.V., Sharaf F.A., Nikulin R.M. Increasing the Yield of Light Distillates by Activation of Oil Stock. *Khimiya i tekhnologiya topliv i masel.* 2016;598:29–34 (in Russ.).]
12. Promtov M.A. Hydro-Pulse Cavitation Treatment of Crude Oil in the Rotor-Stator Device. *Vestnik Tambovskogo gosudarstvennogo tekhnicheskogo universiteta = Transactions of TSTU*. 2018;24(3):455–460 (in Russ.). https://doi.org/10.17277/vestnik.2018.03.pp.455-460
13. Nurullaev V.H., Ismayilov G.G. Of quality indicators cargo crude oils with cavitation technologies and gravity determination taking into account the water cut. *Transport i khranenie nefteproduktov i uglevodorodnogo syr'ya = Transportation and Storage of Oil Products and Hydrocarbons*. 2015;1:7–13 (in Russ.).
14. Vikarchuk A.A., Rastegaeva I.I., Chernyaeva E.Y. Technology and equipment for oil treatment and processing of solid oil sludge and liquid oil waste. *Vektor nauki Tolyattinskogo gosudarstvennogo universiteta*. 2012;21: 70–75 (in Russ.).
15. Torkhovsky V.N., Antonyuk S.N., Chizhevskaya E.V., Vorobyev S.I., Nikolaeva M.V., Arnatsky V.A. Activation of compounded oil feed. *Tekhnologii nefti i gaza = Oil and Gas Technologies*. 2019;123:3–11 (in Russ.).
16. Peshnev B.V., Nikolaev A.I., Nikishin D.V., Alhamedi M.Kh.I. Prospects of using the cavitation phenomenon in oil refining. *Izvestiya vysshikh uchebnykh zavedenii. Khimiya i khim. tekhnologiya = ChemChemTech*. 2023;66(4): 110–116. https://doi.org/10.6060/ivkkt.20236604.6760
17. Yakimenko K.Yu., Vengerov A.A., Brand A.E. Technology application of hydrodynamic cavitation treatment of high-viscosity oil processing in order of improving the efficiency of transportation. *Fundamental'nye issledovaniya = Fundamental Research*. 2016;5-3:531–536 (in Russ.).
18. Cui J., Zhang Z., Liu X., Liu L., Peng J. Analysis of the viscosity reduction of crude oil with nano-Ni catalyst by acoustic cavitation. *Fuel*. 2020;275:117976. https://doi.org/10.1016/j.fuel.2020.117976
9. Промтов М.А., Сунагатуллин Р.З., Кутуков С.Е., Колиух А.Н., Шеина О.А., Зверев Ф.С., Суховей М.В. Изменение реологических параметров высокопарафинистой нефти при многофакторном воздействии в роторном импульсном аппарате. *Проблемы сбора, подготовки и транспорта нефти и нефтепродуктов*. 2020;127(5): 76–88. https://doi.org/10.17122/ntj-oil-2020-5-76-88
10. Торховский В.Н., Антонюк С.Н., Голованов А.Б., Воробьев С.И., Николаева М.В., Дворецков П.А. Переработка компаундированного нефтяного сырья с предварительной активацией исходных сырьевых потоков. *Технологии нефти и газа*. 2021;133(2):3–7. https://doi.org/10.32935/1815-2600-2021-133-2-3-7
11. Хамидуллин Р.Ф., Харлампиди Э., Никулин Р.М., Ситало А.В., Шараф Ф.А. Увеличение выхода светлых дистиллятов при помощи активации нефтяного сырья. *Химия и технология топлив и масел*. 2016;598:29–34.
12. Промтов М.А. Гидроимпульсная кавитационная обработка нефти в роторном импульсном аппарате. *Вестник Тамбовского государственного технического университета*. 2018;24(3): 455–460. https://doi.org/10.17277/vestnik.2018.03.pp.455-460
13. Нуруллаев В.Х., Исмайылов Г.Г. Транспорт нефтей с применением кавитационных технологий и определение плотности с учетом обводненности. *Транспорт и хранение нефтепродуктов и углеводородного сырья*. 2015;1:7–13.
14. Викарчук А.А., Растегаева И.И., Чернохаева Е.Ю. Технология и оборудование для обработки нефти и переработки твердых нефтешламов и жидких нефтеотходов. *Вектор науки Тольяттинского государственного университета*. 2012;21:70–75.
15. Торховский В.Н., Антонюк С.Н., Чижевская Е.В., Воробьев С.И., Николаева М.В., Арнацкий В.А. Активация компаундированного нефтяного сырья. *Технологии нефти и газа*. 2019;123:3–11.
16. Пешнев Б.В., Николаев А.И., Никишин Д.В., Алхамеди М.Х.И. Перспективы использования явления кавитации при переработке нефти. *Известия высших учебных заведений. Химия и хим. технология*. 2023;66(4): 110–116. https://doi.org/10.6060/ivkkt.20236604.6760
17. Якименко К.Ю., Венгеров А.А., Бранд А.Э. Применение технологии гидродинамической кавитационной обработки высоковязких нефтей с целью повышения эффективности транспортировки. *Фундаментальные исследования*. 2016;5-3:531–536.
18. Cui J., Zhang Z., Liu X., Liu L., Peng J. Analysis of the viscosity reduction of crude oil with nano-Ni catalyst by acoustic cavitation. *Fuel*. 2020;275:117976. https://doi.org/10.1016/j.fuel.2020.117976
19. Padula L., Balestrin Lia B.S., Rocha N., Carvalho C., Westfahl H., Cardoso M.B., Sabadini E., Loh W. Role of asphaltenes and additives on the viscosity and microscopic structure of heavy crude oils. *Energy Fuels*. 2016;30(5): 3644–3651. https://doi.org/10.1021/acs.energyfuels.5b02103
20. Витенько Т.Н., Гумницкий Я.М. Механизм активирующего действия гидродинамической кавитации на воду. *Химия и технология воды*. 2007;29(5):422–432.
21. Капранова А.Б., Лебедев А.Е., Мельцер А.М., Неклюдов С.В., Серов Е.М. О методах моделирования основных стадий развития гидродинамической кавитации. *Фундаментальные исследования*. 2016;3-2: 268–273.
22. Lomakin V., Bibik O. Numerical prediction of the gas content effect on the cavitation characteristics of the pump using the simplified Rayleigh–Plesset equation. *IOP Conf. Ser.: Mater. Sci. Eng*. 2019;492:012037. https://doi.org/10.1088/1757-899X/492/1/012037

19. Padula L., Balestrin Lia B.S., Rocha N., Carvalho C., Westfahl H., Cardoso M.B., Sabadini E., Loh W. Role of asphaltenes and additives on the viscosity and microscopic structure of heavy crude oils. *Energy Fuels*. 2016;30(5): 3644–3651. https://doi.org/10.1021/acs.energyfuels.5b02103
20. Vitenko T.N., Gumnitskii Ya.M. The mechanism of activating action of hydrodynamic cavitation on water. *Khimiya i tekhnologiya vody*. 2007;29(5):422–432 (in Russ.).
21. Kapranova A.B., Lebedev A.E., Mel'tser A.M., Neklyudov S.V., Serov E.M. Methods of modeling the developmental stages of hydrodynamic cavitation. *Fundamental'nye issledovaniya = Fundamental Research*. 2016;3-2:268–273 (in Russ.).
22. Lomakin V., Bibik O. Numerical prediction of the gas content effect on the cavitation characteristics of the pump using the simplified Rayleigh–Plesset equation. *IOP Conf. Ser.: Mater. Sci. Eng.* 2019;492: 012037. https://doi.org/10.1088/1757-899X/492/1/012037
23. Gonzalez-Estrada O.A., Rojas-Nova M.A., Gonzalez-Silva G. Effect of temperature on a vortex reactor for hydrodynamic cavitation. *Ingeniería e Investigación*. 2022;43(2):e93419. https://doi.org/10.15446/ing.investig.93419
24. Wan C., Wang R., Zhou W., Li L. Experimental study on viscosity reduction of heavy oil by hydrogen donors using a cavitating jet. *RSC Adv*. 2019;9(5):2509–2515. https://doi.org/10.1039/c8ra08087a
25. Nikishin D.V., Peshnev B.V., Nikolaev A.I., Shebarshinova P.M. Intensification process of cavitation treatment of the heavy oil feedstock. *Izvestiya vysshikh uchebnykh zavedenii. Khimiya i khim. tekhnologiya = ChemChemTech*. 2024;67(9):111–117. https://doi.org/10.6060/ivkkt.20246709.7012
26. Safina I.R., Ibragimova D.A., Yaushev E.A., Khisamiev R.R. Application of the SARA analysis method to characterize oil dispersed systems. *Vestnik Kazanskogo tekhnologicheskogo universiteta = Herald of the Kazan Technological University*. 2014;17(24):212–213 (in Russ.).
27. AlHumaidan F.S., Rana M.S. Determination of asphaltene structural parameters by Raman spectroscopy. *J. Raman Spectrosc*. 2021;52(11):1878–1891. https://doi.org/10.1002/jrs.6233
28. Kossovich E., Epshtein S., Krasilova V., Hao J., Minin M. Effects of coals microscale structural features on their mechanical properties, propensity to crushing and fine dust formation. *Int. J. Coal Sci. Technol*. 2023;10(20). https://doi.org/10.1007/s40789-023-00578-5
29. Manoj B. A comprehensive analysis of various structural parameters of Indian coals with the aid of advanced analytical tools. *Int. J. Coal Sci. Technol*. 2016;3(2):123–132. https://doi.org/10.1007/s40789-016-0134-1
30. Xu J., Tang H., Su S., Liu J., Xu K., Qian K., Wang Y., Zhou Y., Hu S., Zhang A., Xiang J. A study of the relationships between coal structures and combustion characteristics: The insights from micro-Raman spectroscopy based on 32 kinds of Chinese coals. *Appl. Energy*. 2018;212:46–56. https://doi.org/10.1016/j.apenergy.2017.11.094
31. Antipenko V.R., Fedyaeva O.N., Vostrikov A.A. Macrostructural parameters of asphaltene nanoaggregates in natural asphaltite and in its supercritical water conversion products. *Pet. Chem*. 2021;61(7):787–793. https://doi.org/10.1134/S0965544121070069
[Original Russian Text: Antipenko V.R., Fedyaeva O.N., Vostrikov A.A. Macrostructural parameters of asphaltene nanoaggregates in natural asphaltite and in its supercritical water conversion products. *Neftekhimiya*. 2021;61(4):547–554 (in Russ.). https://doi.org/10.31857/S0028242121040109]

23. Gonzalez-Estrada O.A., Rojas-Nova M.A., Gonzalez-Silva G. Effect of temperature on a vortex reactor for hydrodynamic cavitation. *Ingeniería e Investigación*. 2022;43(2):e93419. https://doi.org/10.15446/ing.investig.93419
24. Wan C., Wang R., Zhou W., Li L. Experimental study on viscosity reduction of heavy oil by hydrogen donors using a cavitating jet. *RSC Adv*. 2019;9(5):2509–2515. https://doi.org/10.1039/c8ra08087a

25. Никишин Д.В., Пешнев Б.В., Николаев А.И., Шебаршинова П.М. Интенсификация процесса кавитационной обработки тяжелого нефтяного сырья. *Известия высших учебных заведений. Химия и хим. технология*. 2024;67(9): 111–117. https://doi.org/10.6060/ivkkt.20246709.7012
26. Сафина И.Р., Ибрагимова Д.А., Яушев Э.А., Хисмиев Р.Р. Применение метода SARA-анализа для характеристики нефтяных дисперсных систем. *Вестник Казанского технологического университета*. 2014;17(24):212–213.
27. AlHumaidan F.S., Rana M.S. Determination of asphaltene structural parameters by Raman spectroscopy. *J. Raman Spectrosc*. 2021;52(11):1878–1891. https://doi.org/10.1002/jrs.6233
28. Kossovich E., Epshtein S., Krasilova V., Hao J., Minin M. Effects of coals microscale structural features on their mechanical properties, propensity to crushing and fine dust formation. *Int. J. Coal Sci. Technol*. 2023;10(20). https://doi.org/10.1007/s40789-023-00578-5
29. Manoj B. A comprehensive analysis of various structural parameters of Indian coals with the aid of advanced analytical tools. *Int. J. Coal Sci. Technol*. 2016;3(2):123–132. https://doi.org/10.1007/s40789-016-0134-1
30. Xu J., Tang H., Su S., Liu J., Xu K., Qian K., Wang Y., Zhou Y., Hu S., Zhang A., Xiang J. A study of the relationships between coal structures and combustion characteristics: The insights from micro-Raman spectroscopy based on 32 kinds of Chinese coals. *Appl. Energy*. 2018;212:46–56. https://doi.org/10.1016/j.apenergy.2017.11.094
31. Антипенко В.Р., Федяева О.Н., Востриков А.А. Параметры макроструктуры наноагрегатов асфальтенов природного асфальтита и продуктов его конверсии в сверхкритической воде. *Нефтехимия*. 2021;61(4):547–554. https://doi.org/10.31857/S0028242121040109
32. Антипенко В.Р., Гринько А.А. Параметры макроструктуры нерастворимых продуктов термолиза смол и асфальтенов усинской нефти. *Известия Томского политехнического университета* (*Известия ТПУ*). 2021;332(4): 123–131.
33. Филиппов М.М. Рамановская спектроскопия как метод изучения глубоко углефицированного органического вещества. Часть 1. Основные направления использования. *Труды Карельского научного центра РАН*. 2014;1:115–134.
34. Ok S., Rajasekaran N., Sabti M.A., Joseph G.A. Спектроскопический анализ асфальтенов нефти на молекулярном уровне. *Нефтехимия*. 2020;60(4):520–528. https://doi.org/10.31857/S0028242120040115
35. Sawarkar A., Pandit A., Samant S., Joshi J. Use of ultrasound in petroleum residue upgradation. *Can. J. Chem. Eng*. 2009;87(3):329–342. http://doi.org/10.1002/cjce.20169

32. Antipenko V.R., Grinko A.A. Parameters of macrostructure of insoluble products obtaned by thermolysis of resins and asphaltenes of the Usinskaya oil. *Izvestiya Tomskogo politekhnicheskogo universiteta* (*Izvestiya TPU*) = *Bulletin of the Tomsk Polytechnic University*. 2021;332(4):123–131 (in Russ.).
33. Filippov M.M. Raman spectroscopy as a method for investigation of highly carbonized organic matter. Part 1. Major applications. *Trudy Karel'skogo nauchnogo tsentra RAN = Transactions of KarRC RAS*. 2014;1:115–134 (in Russ.).
34. Ok S., Rajasekaran N., Sabti M.A., Joseph G.A. Spectroscopic analysis of crude oil asphaltenes at molecular level. *Pet. Chem.* 2020;60(7):802–809. https://doi.org/10.1134/S0965544120070117 [Original Russian Text: Ok S., Rajasekaran N., Sabti M.A., Joseph G.A. Spectroscopic analysis of crude oil asphaltenes at molecular level. *Neftekhimiya*. 2020;60(4):520–528 (in Russ.). https://doi.org/10.31857/S0028242120040115]
35. Sawarkar A., Pandit A., Samant S., Joshi J. Use of ultrasound in petroleum residue upgradation. *Can. J. Chem. Eng*. 2009;87(3):329–342. http://doi.org/10.1002/cjce.20169

About the Authors

Denis V. Nikishin, Assistant, Department of Chemistry and Technology of Basic Organic Synthesis, M.V Lomonosov Institute of Fine Chemical Technologies, MIREA – Russian Technological University (78, Vernadskogo pr., Moscow, 119454, Russia). E-mail: nikishin@mirea.ru. RSCI SPIN-code 4089-6391, https://orcid.org/0000-0002-4466-4402

Boris V. Peshnev, Dr. Sci. (Eng.), Professor, Department of Chemistry and Technology of Basic Organic Synthesis, M.V Lomonosov Institute of Fine Chemical Technologies, MIREA – Russian Technological University (78, Vernadskogo pr., Moscow, 119454, Russia). E-mail: peshnev@mirea.ru. Scopus Author ID 6507362823, https://orcid.org/0000-0002-0507-2754

Alexander I. Nikolaev, Dr. Sci. (Eng.), Professor, Department of Chemistry and Technology of Basic Organic Synthesis, M.V Lomonosov Institute of Fine Chemical Technologies, MIREA – Russian Technological University (78, Vernadskogo pr., Moscow, 119454, Russia). E-mail: nikolaev_a@mirea.ru. Scopus Author ID 57197582338, https://orcid.org/0000-0001-8594-2985

Об авторах

Никишин Денис Васильевич, ассистент, кафедра химии и технологии основного органического синтеза, Институт тонких химических технологий им. М.В. Ломоносова, ФГБОУ ВО «МИРЭА – Российский технологический университет» (119454, Россия, Москва, пр-т Вернадского, д. 78). E-mail: nikishin@mirea.ru. SPIN-код РИНЦ 4089-6391, https://orcid.org/0000-0002-4466-4402

Пешнев Борис Владимирович, д.т.н., профессор кафедры химии и технологии основного органического синтеза, Институт тонких химических технологий им. М.В. Ломоносова, ФГБОУ ВО «МИРЭА – Российский технологический университет» (119454, Россия, Москва, пр-т Вернадского, д. 78). E-mail: peshnev@mirea.ru. Scopus Author ID 6507362823, https://orcid.org/0000-0002-0507-2754

Николаев Александр Игоревич, д.т.н., профессор кафедры химии и технологии основного органического синтеза, Институт тонких химических технологий им. М.В. Ломоносова, ФГБОУ ВО «МИРЭА – Российский технологический университет» (119454, Россия, Москва, пр-т Вернадского, д. 78). E-mail: nikolaev_a@mirea.ru. Scopus Author ID 57197582338, https://orcid.org/0000-0001-8594-2985

Translated from Russian into English by H. Moshkov
Edited for English language and spelling by Thomas A. Beavitt

Tonkie Khimicheskie Tekhnologii = Fine Chemical Technologies.
2025;20(5):497–515 ISSN 2686-7575 (Online)

UDC 547.53:661.7
https://doi.org/10.32362/2410-6593-2025-20-5-497-515
EDN WUQZIC

REVIEW ARTICLE

Review of contemporary ethylbenzene production technologies

Leonid A. Khakhin, Svetlana N. Potapova✉, Evgeniy V. Korolev, Salekh M. Masoud, Dmitry V. Svetikov
United Research and Development Center, Moscow, 119333 Russia
✉ *Corresponding author, e-mail: PotapovaSN@rdc.rosneft.ru*

Abstract

Objectives. Ethylbenzene is an important intermediate for styrene production. Most of the ethylbenzene synthesized worldwide is used to produce styrene, with smaller amounts used as a solvent or for the production of other chemicals. This article reviews contemporary technologies for the production of ethylbenzene.

Results. The liquid-phase method of ethylbenzene production using zeolite-containing catalysts for alkylation and transalkylation exhibits the highest efficiency and simplicity. In comparison with liquid-phase alkylation catalysts, e.g., aluminum chloride, zeolite-containing catalysts demonstrate high activity, selectivity, stability, and resistance to impurities. In addition, they are non-corrosive, environmentally friendly, regenerable, and have a prolonged cycle length between regenerations. More than half of the ethylbenzene synthesized globally is produced by the *Badger* EBMax process using a catalyst based on zeolite of the MWW family (MCM-22). This technology enables a low benzene to ethylene ratio (from 2.5 to 4), which reduces the benzene circulation rate, increases efficiency, and reduces the column throughput for benzene extraction. The main part of contemporary research in the field of benzene alkylation with ethylene into ethylbenzene is associated with the creation and use of zeolite-containing catalysts, which are solid porous systems containing an active component and a binder. The active component is USY, beta, mordenite, ZSM-5, ZSM-11, ZSM-12, ZSM-23, ZSM-35, ZSM-48, MCM-22, and MCM-49 zeolites. Among the preferred alkylation catalysts are Beta zeolite or zeolite of the MCM-22 family. The binder is Al_2O_3, SiO_2, or amorphous aluminosilicate. Current research also focuses on methods for creating zeolite materials with an increased mesoporous surface area by treating the initial zeolite precursor using various technologies, including combinations of acid treatment and surfactant treatment followed by alkaline solution treatment. Contemporary developments in the field of domestic alkylation and transalkylation catalysts for ethylbenzene production are presented.

Conclusions. The production of ethylbenzene and the further development of technologies for obtaining catalysts for its synthesis are highly promising and important directions in Russia. The technology of liquid-phase alkylation in the presence of contemporary highly active zeolite-containing catalysts offers significant advantages.

Keywords

ethylbenzene, styrene, alkylation, transalkylation, zeolites, zeolite catalysts

Submitted: 13.11.2024
Revised: 17.01.2025
Accepted: 03.09.2025

For citation

Khakhin L.A., Potapova S.N., Korolev E.V., Masoud S.M., Svetikov D.V. Review of contemporary ethylbenzene production technologies. *Tonk. Khim. Tekhnol. = Fine Chem. Technol.* 2025;20(5):497–515. https://doi.org/10.32362/2410-6593-2025-20-5-497-515

ОБЗОРНАЯ СТАТЬЯ

Обзор современных технологий производства этилбензола

Л.А. Хахин, С.Н. Потапова✉, Е.В. Королев, С.М. Масоуд, Д.В. Светиков

ООО «Объединенный центр исследований и разработок», Москва, 119333 Россия

✉ *Автор для переписки, e-mail: PotapovaSN@rdc.rosneft.ru*

Аннотация

Цели. Этилбензол (ЭБ) — важный промежуточный продукт для получения стирола. Для производства стирола используется бóльшая часть производимого в мире ЭБ. Меньшее его количество употребляется в качестве растворителя или для производства других химических веществ. Цель данной работы — провести обзор современных технологий производства ЭБ.

Результаты. Показано, что жидкофазный процесс получения ЭБ с использованием цеолитсодержащих катализаторов для алкилирования и трансалкилирования является наиболее перспективным подходом к производству ЭБ вследствие максимальной простоты и эффективности. Используемые цеолитсодержащие катализаторы по сравнению с жидкофазными катализаторами алкилирования, например, хлористым алюминием, отличаются высокой активностью, селективностью, стабильностью, устойчивостью к примесям; кроме того, они некоррозионноактивны, экологичны, регенерируемы, характеризуются высоким межрегенерационным пробегом. Более половины производимого ЭБ в мире получают по технологии EBMax с использованием катализатора на основе цеолита семейства MWW (MCM-22). Технология позволяет использовать низкое соотношение бензола к этилену (от 2.5 до 4), что снижает скорость циркуляции бензола, повышает эффективность и снижает пропускную способность колонны для извлечения бензола. Основная часть современных исследований в области технологии алкилирования бензола этиленом в ЭБ связана с созданием и использованием цеолитсодержащих катализаторов, представляющих собой твердые пористые системы, содержащие активный компонент и связующее вещество. Активным компонентом служат цеолиты USY, Beta, морденит, ZSM-5, ZSM-11, ZSM-12, ZSM-23, ZSM-35, ZSM-48, MCM-22, MCM-49. Предпочтительные катализаторы алкилирования включают цеолит Beta или цеолит семейства MCM-22. Связующими веществами являются оксид алюминия Al_2O_3, диоксид кремния SiO_2 или аморфный алюмосиликат. Современные исследования также посвящены способам создания цеолитных материалов, имеющих увеличенную площадь мезопористой поверхности, путем различных обработок исходного цеолитного предшественника, включающих комбинации кислотной обработки, обработки поверхностно-активными веществами с последующей обработкой щелочным раствором. Приведены современные разработки в области создания новых российских катализаторов алкилирования и трансалкилирования для получения ЭБ.

Выводы. Производство ЭБ и дальнейшее развитие технологии получения катализаторов для его производства имеют важное значение в России и большой потенциал. Преимуществом обладает технология жидкофазного алкилирования в присутствии современных высокоактивных цеолитсодержащих катализаторов.

Ключевые слова

этилбензол, стирол, алкилирование, трансалкилирование, цеолиты, цеолитные катализаторы

Поступила: 13.11.2024
Доработана: 17.01.2025
Принята в печать: 03.09.2025

Для цитирования

Хахин Л.А., Потапова С.Н., Королев Е.В., Масоуд С.М., Светиков Д.В. Обзор современных технологий производства этилбензола. *Тонкие химические технологии*. 2025;20(5):497–515. https://doi.org/10.32362/2410-6593-2025-20-5-497-515

INTRODUCTION

Among numerous petrochemical processes, the synthesis of ethylbenzene (EB) occupies one of the leading places, since EB is an important intermediate for the production of styrene. In 2023, the total global production capacity of this chemical product amounted to 48 mln t/year[1], continuing to grow rapidly at the level of 4–5% per year[2].

The list of companies engaged in the production of polystyrene through EB includes *Chevron Phillips Chemical* (USA), *LyondellBasell* (Netherlands), *Honeywell* (USA), *Ineos* (United Kingdom), *Dow Chemical* (USA), *DuPont* (USA), *Shell* (United Kingdom), *TotalEnergies* (France), *Versalis* (Italy), and others. In Russia, EB production is carried out by *Sibur-Khimprom, Gazprom Neftekhim Salavat, Nizhnekamskneftekhim*, and *Angarsk Polymer Plant*; however, the total capacity of EB production in Russia reaches only about 860000 t/year (1.7% of the global level) [1].

Altogether, there are 70 EB production plants in the world, of which 17 operate on aluminum chloride, a homogeneous catalyst, 28 use the gas-phase technology with heterogeneous zeolite-containing catalysts, and 25 apply a more contemporary liquid-phase technology [2]. In Russia, some enterprises continue to apply the alkylation of benzene with ethylene according to the Monsanto–Lummus method using homogeneous Friedel–Crafts catalysts based on aluminum chloride, including the *Angarsk Polymer Plant* (entered into operation in 1977 with the plant capacity of 55000 t/year) and *Nizhnekamskneftekhim* (entered into operation in 1977 with a capacity of 345000 t/year, designed by Voronezh Branch of the Scientific Research Institute for Synthetic Rubber (*NIISK*))[3].

In addition to the main alkylation reaction, a number of side reactions occur on aluminum chloride to produce polyalkylbenzenes (di-, tri-, and tetraethylbenzenes). They are used to obtain the target product by combining the alkylation reaction with the transalkylation reaction. The transalkylation reaction is reversible. Thus, after isolation from the alkylate product, polyalkylbenzenes are recycled to yield EB. However, the use of aluminum chloride presents numerous technological, environmental, and economic problems associated with the high corrosive activity of aluminum chloride and its toxicity, difficulties associated with its storage, use, and disposal. Additional challenges are an insufficiently high selectivity of the process (as a rule, the selectivity of the alkylation stage is up to 70%) [3, 4] and a large amount of wastewater, including acidic wastewater, resulting in high costs for its purification.

A solution to the above technological problems of the aluminum chloride-based liquid-phase alkylation technology is the transfer of alkylation and transalkylation stages to heterogeneous zeolite-containing catalysts. Their use simplifies the EB synthesis and reduces the costs involved in raw material preparation, washing the reaction mass, and neutralizing acidic wastewater. Moreover, it significantly reduces equipment corrosion. At the moment, the use of zeolite-containing catalysts for alkylation and transalkylation is the most promising approach to the production of EB[4,5]. Zeolite-containing catalysts are stable, resistant to impurities, highly active, selective, environmentally friendly, regenerable materials with an extended cycle length. Their advantages also involve the absence of waste and the possibility of using carbon structural steel.

The installations based on a homogeneous catalyst employ the liquid-phase alkylation technology, which facilitates their transfer to a liquid-phase technology based on zeolite-containing catalysts. With such a transfer, part of the rectification equipment can be released, which can be used in another similar process for the rectification of flows [5].

The transition to zeolite technologies for the synthesis of EB has already been implemented both at Russian (*Gazprom Neftekhim Salavat* in 2003 and *Sibur-Khimprom* in 2010 [5]) and foreign enterprises. Over 20 years, significant experience in working with zeolite-containing catalysts has been accumulated.

Several years ago, a process for obtaining EB by gas-phase alkylation of benzene with ethylene over an EBEMAX-1 zeolite-containing catalyst (*Clariant*, Switzerland) was introduced at the *Gazprom Neftekhim Salavat* enterprise in Russia [6]. The process ensures the selectivity of EB formation in the 87.4–91.0% range. However, the technology requires elevated process temperatures (370–420°C), which results in an increased energy consumption, an increased yield of propyl and butylbenzenes (impurities), a lower

1 https://www.statista.com/statistics/1063696/global-ethylbenzene-production-capacity/. Accessed June 28, 2023.

2 ICB Americans Chemical Profile. 2007. URL: www.icis.com. Accessed May 16, 2024.

3 Russian Petrochemical Forum. Gas. Oil. Technologies. The 26th International Exhibition. May 22–25, 2018. Ufa.

4 Ethylbenzene. Suppliers handbook. Aboutcompanies.ru. URL: http://b2bpoisk.ru/продукция/этилбензол. Accessed May 05, 2024. (In Russ.).

5 Zamalieva R.R. Friedel-Crafts reaction. Great Russian Encyclopedia. URL: https://bigenc.ru/c/reaktsiia-fridelia-kraftsa-b039a3. Accessed May 05, 2024. (In Russ.).

yield of EB, and a shorter service life of the catalyst as compared to that in the liquid-phase process.

In January 2022, the first industrial batch of the Russian KT-GA-1 catalyst based on a zeolite of the Mobil-type Five (MFI) family (Zeolite Socony Mobil-5, ZSM-5[6]) was released for the process of gas-phase alkylation of benzene with ethylene into EB. On July 19, 2022, pilot tests of the catalyst were launched, continuing up to the present day. During the first year of operation, it became obvious that the Russian catalyst was not inferior to its imported counterpart in terms of all aspects. Thus, when using two catalysts—foreign-made EBEMAX-1 and Russian KT-GA-1—the concentration of EB in the EB rectified product comprised 99.76% and 99.85%, respectively. The selectivity of EB formation on the KT-GA-1 catalyst was 86.9–90.4% [6].

A highly selective liquid-phase process for producing EB using the EBMax technology (more than 99%)[7] under a license from *Badger Licensing* (USA) has been implemented in Russia by *Sibur-Khimprom* (capacity 230000 t/year). The technology employs ExxonMobil zeolite catalysts containing zeolites of the MWW (Mobil twenty-two)[8] family (MCM-22, Mobil Composition of Matter No. 22). *ExxonMobil* (USA) maintains its position as one of the leading suppliers of catalysts for EB production in the world. Since 2001, almost two-thirds of all new and revamped EB capacities have been licensed by *Badger Licensing* and use *ExxonMobil* catalysts. *ExxonMobil* catalysts used in the *Badger* EBMax and *Badger* Vapor Phase[9] processes account for more than 56% of the global EB production, exceeding 20 mln metric t/year.

Since 2023, *Nizhnekamskneftekhim* has been upgrading its benzene alkylation unit with a transition to a zeolite-containing catalyst and increasing the EB capacity to 350000 t/year using the *Lummus/UOP* EBOne technology. In 2021, *Nizhnekamskneftekhim* signed an agreement with *Lummus* (USA) to license technologies for the production of EB (EBOne) and styrene monomer (CLASSIC SM). Efforts were implemented to reduce byproduct formation by altering reaction conditions. However, only the advent of liquid-phase and mixed technologies operating at temperatures below 270°C made it possible to synthesize high-purity EB through zeolite-catalyzed processes. EB-350/SM-400 units will be launched simultaneously with a new EP-600-1 unit (scheduled for early 2026).[10,11,12]

In this article, we set out to review and compare contemporary technologies for the production of EB, mainly liquid-phase technologies using zeolite-containing catalysts.

1. EB PRODUCTION TECHNOLOGIES

The details of applying zeolite-containing catalysts for EB synthesis involve the implementation of alkylation and transalkylation reactions in separate reactors. Zeolite-containing catalysts have been used in EB production processes since the 1980s in the gas-phase process and, since the 1990s, in the liquid-phase process. Zeolite-containing catalysts were developed by *UOP* (USA) and *ExxonMobil* (USA). *Mobil-Badger* (USA) introduced the first gas-phase process for benzene alkylation with ethylene using a catalyst based on a medium-porosity zeolite of the ZSM-5 type. However, due to the specific structure of this zeolite and the need to overcome diffusion limitations, the alkylation temperature exceeded 400°C.

The structure of this catalyst is characterized by perpendicularly intersecting channels with five-membered rings at the base. Zeolite ZSM-5 demonstrated pronounced activity and resistance to deactivation with coke in gas-phase processes. However, along with the development of liquid-phase technologies, its use in alkylation decreased due to insufficient activity and a tendency to rapid deactivation. However, this catalyst continues to be applied in gas-phase units, in particular, at the transalkylation stage.

At present, EBEMAX-11 and EBUF-1 catalysts manufacturing by *Clariant* are used in gas-phase alkylation, while EBEMAX-2 and EBUF-2 catalysts are used for transalkylation. The patent [7] proposed a method for producing a zeolite-containing catalyst for

6 ZSM-5 is a zeolite type according to the atlas of zeolites: Ch. Baerlocher *et al*. Atlas of Zeolite Framework Types. Elsevier; 2007. It is a synthetic zeolite belonging to the pentasil family.

7 Presentation of EQUATE Petrochemical Company. https://www.slideserve.com/laith-nunez/eb-plant-equate-petrochemical-company. Accessed January 10, 2025.

8 MWW is a thin-layered (or lamellar) zeolite with a honeycomb-like structure.

9 https://www.exxonmobilchemical.com/en/catalysts-and-technology-licensing/benzene-alkylation/ethylbenzene-alkylation. Accessed January 09, 2025.

10 https://smart-lab.ru/blog/859787.php. Accessed May 17, 2023. (In Russ.).

11 https://www.sibur.com/ru/press-center/news-and-press/sibur-postroit-dva-novykh-proizvodstva-v-nizhnekamske-/. Accessed July 02, 2025. (In Russ.).

12 https://www.ogj.com/refining-processing/refining/article/14202241/nknk-lets-contract-to-expand-existing-tatarstan-olefins-complex. Accessed May 17, 2023.

the alkylation of benzene with ethylene in a gas-phase process based on zeolite ZSM-5 without a binder.

It should be noted that the high temperature of gas-phase alkylation promotes oligomerization, cracking, isomerization, and hydrogen transfer reactions, thus affecting the purity of the final EB. In addition, narrow- and medium-porosity zeolites in the gas-phase process for producing EB are characterized by accelerated deactivation due to coke formation as a result of deposition of large molecules on the active sites of the zeolite. These molecules slowly diffuse from the porous structure of the zeolite.

Other disadvantages of the gas-phase process are related to low selectivity and low EB yield. Despite the efforts made to reduce the formation of byproducts in the gas-phase process by optimizing the reaction conditions, it was only the development of liquid-phase processes operating at temperatures below 270°C that made it possible to efficiently produce high-purity EB (99.9 wt %, with a toluene content of 450 ppmw, cumene of 100 ppmw, diethylbenzene (DEB) of 5 ppmw, xylenes of 10 ppmw). Having been developed in the 1990s, these processes are offered today by leading licensors of EB technologies (*Badger* EBMax, *Lummus* EBOne, and *Versalis*). In order to overcome diffusion limitations in the liquid-phase process, zeolite catalysts containing wide-pore zeolites of the common Faujasite (FAU) and BEA [4] structural types, or the more expensive MWW are used.

Such zeolites possess 3D structures with a branched system of cavities and channels, which improves catalytic activity and reaction selectivity. Lewis and Brønsted acid sites are present on the surface and in the pores of zeolites. These sites play a key role in alkylation catalysis and determine the efficiency of catalysis in the target reactions. Therefore, particular attention is paid to the number, accessibility, and strength of acid sites.

The MCM-22 zeolite of the MWW structural type is characterized by a large pore volume, high acidity, good hydrothermal stability, and molecular sieve properties that ensure high selectivity in alkylation and transalkylation processes [8]. It exhibits a higher selectivity than Beta zeolite, thus reducing the formation of polyalkylbenzenes and heavy products.

In comparison with the gas-phase process, the advantages of the liquid-phase process of benzene alkylation with ethylene involve:

- reduced energy costs due to lower process temperatures;
- increased EB yield and selectivity of its formation;
- reduced byproduct yield;
- increased catalyst service life and long cycle length between regenerations.

In the liquid-phase alkylation of benzene with ethylene using zeolite-containing catalysts, along with EB, the following byproducts are formed: polyethylbenzenes (PEB), in particular DEB and triethylbenzene (TEB), xylenes, and cumene. At the transalkylation stage, DEB and TEB are almost completely converted into EB, with only trace amounts of DEB remaining in the product, which are regulated. The content of xylenes and cumene inseparable during rectification in the product is also regulated.

The selectivity for EB in the liquid-phase process in the presence of zeolite-containing catalysts (in particular, Beta zeolite in the H-form) is at least 80% [4]. Moreover, the additional stage of liquid-phase transalkylation makes it possible to convert the remaining 20% of PEB into EB.

In Russia, zeolite-containing catalysts and technologies for the processes of benzene alkylation with ethylene and benzene transalkylation with DEB were initially developed by specialists of the Grozny Oil Research Institute. Today, active work is underway at the Institute of Petrochemical Synthesis of the Russian Academy of Sciences and the Scientific and Technical center of *Gazprom Neftekhim Salavat* [9]. In addition, *Zeolitika* (Moscow) is creating new technologies for the production of synthetic zeolites. The Boreskov Institute of Catalysis of the Siberian Branch of the Russian Academy of Sciences (Novosibirsk) actively conducts research in the field of chemical catalysis and catalytic processes.

The main part of contemporary research in the field of benzene alkylation technology with ethylene into EB is associated with the creation and use of zeolite-containing catalysts, which are solid porous systems containing an active component and a binder. The active components are Ultrastable Y (USY) zeolites, Beta, mordenite, ZSM-5, ZSM-11, ZSM-12, ZSM-23, ZSM-35, ZSM-48, MCM-22, and MCM-49. The preferred alkylation catalysts include Beta zeolite or a zeolite of the MCM-22 family. The binder is Al_2O_3, SiO_2, or amorphous aluminosilicate. After mixing the active component and the binder, granules are formed from the resulting mass, which are then dried and calcined. In some cases, the catalyst is then modified. Typically, the zeolite content in the catalysts ranges from 60 to 80 wt % [10, 11].

The works [12, 13] considered methods for creating zeolite materials with an increased mesoporous surface area compared to the precursor composition. The catalyst precursor composition has a high degree of crystallinity. The technology may involve treating this composition with a surfactant under conditions effective for creating or increasing mesoporosity

in the catalyst precursor composition. Large pore molecular sieves such as Beta zeolite, Zeolite Y, USY, ultrahydrophobic Y (UHP-Y), dealuminated Y (Deal Y), mordenite, ZSM-3, ZSM-4, ZSM-14, ZSM-18, ZSM-20, and mixtures thereof can be used as catalyst precursors.

Another class of molecular sieve materials that may be present in the catalyst precursor composition as an auxiliary component is the group of mesoporous crystalline materials, e.g., MCM-41 and MCM-48 materials. The study [12] reported methods for treating a zeolite material to increase its mesoporous surface area using a combination of acid treatment and surfactant treatment followed by treatment with an alkaline solution.

The surfactant used may be of a cationic nature, e.g., comprising one or more alkyl trimethyl ammonium salts and/or one or more dialkyl dimethyl ammonium salts, or of a non-ionic nature. The examples of suitable commercially available non-ionic surfactants include, e.g., Pluronic™ surfactants (e.g., Pluronic™ P123) manufactured by *BASF Societas Europaea* (Germany).

The acids used to treat the starting zeolite may be any organic or inorganic (mineral) acids. The amount of acid used in the treatment mixture may range from ~3 to ~6 mEq/g of the starting zeolite material, selected such that the pH of the treatment mixture ranged within 3–4. The mixture is then stirred for about 2 h. In addition, the treatment mixture may be heated to a temperature of from ~40 to ~80°C.

After treating the zeolite with the acid and surfactant, a portion of the resulting surfactant-treated zeolite material is recovered from the treatment mixture and washed with deionized water one or several times. Following recovery, the zeolite material is contacted with a base. Suitable bases include NaOH, NH_4OH, KOH, Na_2CO_3, TMAOH, and mixtures thereof. In some implementation variations, the base used may be in the form of an aqueous solution having a concentration in the range of 0.2–15 wt %. The amount of the base used in relation to the initial amount of the starting zeolite material ranges from 0.1 to 20 mmol per gram of the starting zeolite material. The treatment of the surfactant-treated zeolite material with a base can be carried out under elevated temperature conditions, including temperatures from ~50 to ~150°C for 16–18 h.

After treatment with a base, the resulting mesoporous zeolite material is isolated by filtration, washed, and dried. The treated zeolite is then molded with a commercially available alumina binder with a zeolite/binder weight ratio of 65/35. The mixture is extruded into 1/20-inch quadrilobes. The extrudates are dried in a stream of nitrogen at a temperature of 482°C followed by calcination at a temperature of 538°C in air.

It has been found that the treatment of zeolites leads to the creation of catalytic compositions with an increased mesoporous surface area, which allows the transalkylation process temperatures to be decreases and the catalytic activity of the catalysts to be increased.

A number of contemporary developments, including those in Russia, in the field of improving the process of liquid-phase transalkylation of benzene with DEB are devoted to the creation and use of zeolite [14, 15] and zeolite-containing [16, 17] catalysts based on Zeolite Y. Thus, starting from 2013 and up to the present time, the KT-BS-1 catalyst, a joint development of *NTC Salavatnefteorgsintez* and the Institute of Petrochemical Synthesis of the Russian Academy of Sciences (Moscow), has been successfully operated at the *Monomer* plant of the *Gazprom Neftekhim Salavat* enterprise. The KT-BS-1 catalyst is a deeply decationized Zeolite Y, containing no binders. The KT-BS-1 catalyst is produced in Russia (based on the set of necessary technological equipment) only by the *Ishimbay Catalyst Plant* (Ishimbay). The task of providing the necessary conditions for the production of a catalyst for benzene transalkylation with DEB to EB, comparable in quality to the KT-BS-1 brand catalyst, but using a fundamentally different technology, was set and successfully solved at the Scientific and Technical Center of *Gazprom Neftekhim Salavat* (hereinafter referred to as the STC).

As an alternative to the catalyst for benzene transalkylation with DEB of the KT-BS-1 brand, the STC developed a catalyst granulated with a binder [18] (hereinafter referred to as KT-SS). The catalyst contains 80 wt % of Zeolite Y in the acidic H^+ form and 20 wt % of alumina as a binder. In comparison with the zeolite KT-BS-1, the KT-SS catalyst is obtained using the conventional technology for producing zeolite-containing catalysts with a binder. As a result, the catalyst has a developed secondary porous structure which plays a transport role in the supply of reactants to the active centers of the catalyst and the removal of reaction products. In addition, this catalyst can be produced in the required tonnage at any catalyst factory in Russia. The developed catalyst for the benzene transalkylation with DEB provides DEB conversion at the level of 82–83% with an EB yield of 21–22 wt % based on the passed feedstock. These indicators are comparable with the process indicators when using the KT-BS-1 catalyst. In 2023, a batch of the catalyst was produced and loaded into the transalkylation unit of workshop No. 46 of the *Monomer* plant.

The main contemporary technologies for producing EB are presented below.

1.1. Technip Energies/Badger Ethylbenzene EBMax technology

In parallel with the development of the gas-phase process for producing EB (since 1976) on the EM-3000 (ZSM-5) catalyst, *Mobil-Badger* (*ExxonMobil-Badger*) developed a liquid-phase alkylation process under the EBMax trademark. A significant advantage of this technology consists in the use of a new MCM-22 type zeolite developed by *ExxonMobil*, as a catalyst, which surpasses zeolite Beta and zeolite Y in terms of selectivity [19]. Today, the technologies developed by *Mobil-Badger* account for about 55% of all EB produced, with more than its half being produced using the EBMax technology [20]. Since 1995, the EBMax technology has been licensed 40 times, both for new plants and for the expansion and reconstruction of plants based on earlier technologies.[13]

ExxonMobil is one of the leading suppliers of EB catalysts in the world. Since 2001, nearly two-thirds of all new and revamped EB capacity licensed by *Badger* has used *ExxonMobil* catalysts. As of 2017, *ExxonMobil* catalysts have been installed at approximately 35 EBMax customers. This enabled the construction of new plants, as well as the upgrading and expansion of EB production capacity at the world's largest plants. *ExxonMobil* catalysts account for more than 56% of the global EB production, exceeding 20 mln metric t/year, in the *Badger* EBMax (highly selective liquid phase) and *Badger* Vapor Phase (gas phase) processes.

The first commercial application of the process commenced in 1995 in Japan. Initially, the transalkylation process was carried out in the gas phase, using the ZSM-5 zeolite catalysis, in a manner similar to existing gas phase alkylation units.[14] Later, following the emergence of catalysts based on MCM-22 zeolite, the process also became a liquid-phase one. Table 1 presents the main parameters of the EBMax process and the catalysts used.

Table 1. Key parameters of the EBMax process and the catalysts used

Key parameters	Alkylation	Transalkylation	Catalysts	
			Alkylation	Transalkylation
Phase	Liquid	Liquid	EM-3300 (1995); EM-3210/EM-3310 (MSM-22 Zeolite)	EM-3700[15] (MSM-22 Zeolite)
Reaction temperature, °C	195–257	–		
Temperature of the feed mixture at the inlet to the transalkylation reactor, °C	–	200		
Reaction pressure, MPa	3.4	3.1		
Benzene/ethylene ratio (mol)	2.5–4	–		
Benzene/PEB ratio (wt)	–	2.0		
Ethylene conversion, %	100	–		
DEB conversion, %	–	62		
EB yield, wt %	99.5			
EB purity, vol %	min 99.8			
Cycle length between catalyst regenerations, years	More than 3			

[13] https://www.badgerlicensing.com/sites/badger/files/2024-06/flysheet_ethylbenzene.pdf. Accessed January 10, 2025.

[14] Koshkin S.A. Analysis and optimization of industrial technology for producing ethylbenzene on zeolite-containing catalysts. Cand. Sci. Thesis (Eng.). Tomsk. 2017.

[15] Previously, a gas-phase process on ZSM-5 zeolite was used.

In the EBMax process, benzene is fed to the bottom of a liquid-filled multi-bed reactor. Ethylene is fed together with benzene at the reactor inlet and between the catalyst beds. The PEBs, which consist mainly of DEB, are transalkylated with benzene in a second reactor to form additional EB (Fig. 1). A special feature of the EBMax technology is the use of a catalytic reactive guard bed necessitated the need to employ expensive *ExxonMobil* zeolite-containing alkylation and transalkylation catalysts based on MWW zeolite. These catalysts are sensitive to impurities of catalyst poisons in the feedstock. The presence of a highly selective catalyst based on MCM-22 in the technology allows the benzene to ethylene ratio to be decreased (from 2.5 to 4). This reduces the benzene circulation rate, increases efficiency, and reduces the throughput of the benzene extraction column. More than half of the EB produced in the world is obtained using the EBMax technology.

The cost of the steam produced in the process usually covers energy consumption and additional material costs. About 95% of the cost of EB production includes the cost of raw materials, with the remaining 5% being associated with energy and other costs [21]. Benzene accounts for the largest share of the cost of raw materials. In this context, the cost of EB production mainly depends on the price of benzene.

1.2. *Lummus/UOP* EBOne technology

The *Lummus/UOP* EBOne technology was first commercialized in 1990 by *Nippon Steel Chemical Company*, Japan. The liquid-phase EBOne process uses a *UOP* zeolite-containing fixed-bed catalyst with a cycle length between regenerations of three to five years. This eliminates the need for regeneration equipment. The process requires low capital investments, provides high yields, and is energy-efficient. The formation of xylene impurities is virtually eliminated, which results in EB of excellent quality. The regenerated catalyst shows an efficiency equal to fresh catalyst, which is commercially proven. There are more than 45 projects worldwide with a capacity of 100000 to 1250000 t/year calculated for EB.

The catalysts have undergone multiple regenerations without losing their mechanical strength or process characteristics. Q-Max catalysts are described in patents [22–24]. Initially, a Y-type zeolite was used at the alkylation stage. An USY-type zeolite was used at the transalkylation stage [11]. The technology development resulted in the use of new catalysts for alkylation and transalkylation catalysis under the trade names of *UOP* EBZ-500 (based on Beta zeolite) and EBZ-800 (based on USY zeolite) in 1996. Later, in the 2000s, *UOP* introduced a more contemporary alkylation catalyst, EBZ-800TL based on UZM-8 zeolite of the MWW structural type [25].

Table 2 presents the currently existing EB production plants operated based on the EBOne technology.

The process flow diagram of the EBOne process is shown in Fig. 2.

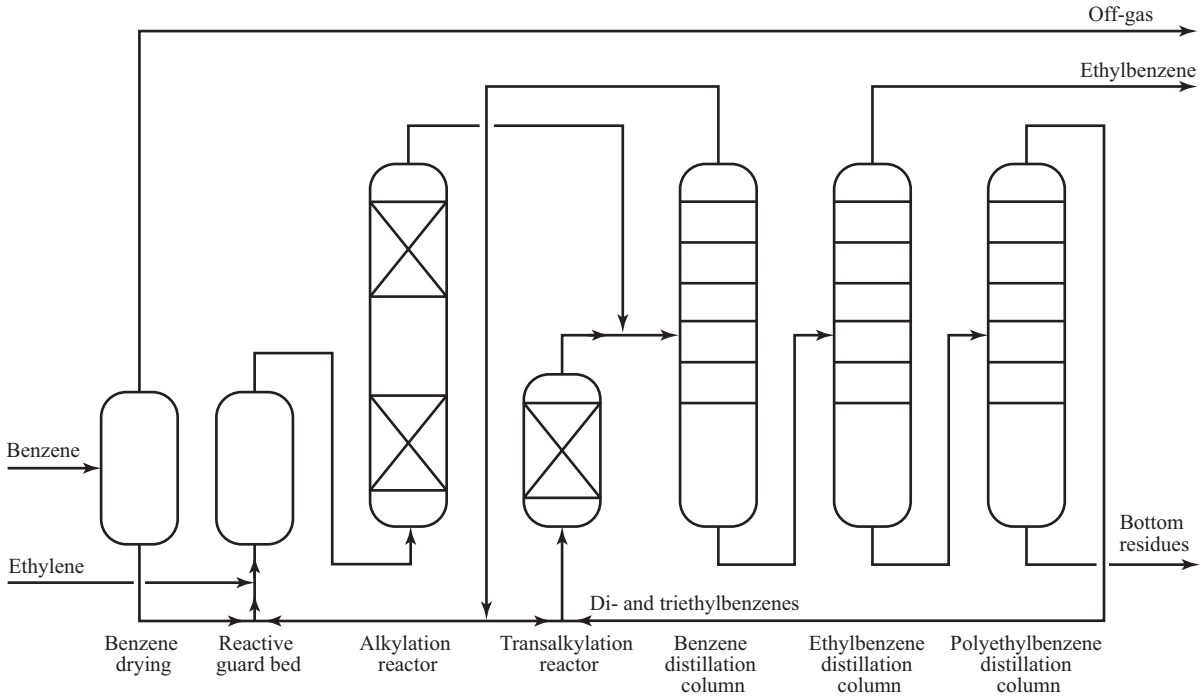

Fig. 1. Process flow diagram of the *Badger* EBMax process [19]

Table 2. Existing EB production plants using EBOne technology [26]

Company	Location	Capacity, t/year	Start
Carbon Holdings	Ain Sokhna, Egypt	424000	2020
Tianjin Bohua Chemical Development Co.	Tianjin, China	530000	2019
PetroChina Jilin (No. 2)	Jilin, China	342000	2012
CNOOC/Shell Nanhai B.V.	Huizhou, China	640000	2006
PetroChina Daqing	Daqing, China	95400	2005
Asahi Kasei Corporation	Mizushima, Japan	360000	2005
SECCO (*BP-SPC*)	Shanghai, China	719000 (695500) (535000)	2011 2009 2005
Synthos Litvinov (*Kaucuk*)	Litvinov, Czech Republic	300000	2004
LG Chem I and II	Yeosu, Republic of Korea	536472	2003
Asahi Kasei Corporation	Mizushima, Japan	355000	2003
LyondellBasell (*ARCO Chemical*)	Maasvlakte, The Netherlands	726000	2003
Repsol	Tarragona, Spain	505000 (380000)	2006 2000
SADAF (Styrene II Project)	Al Jubail, Saudi Arabia	530000	2000
Trinseo (Styron, Dow/BSL)	Böhlen, Germany	355000	1999
PT Styrindo Mono Indonesia (SM No. 2)	Merak, Indonesia	212000	1999
IRPC (*TPI*)	Rayong, Thailand	280000 (212000)	2013 1999
PetroChina Jilin (*JCI*) (No. 1)	Jilin, China	160000 (106000)	2002 1998
Tabriz Petrochemical Co.	Tabriz, Iran	106000	1998
BASF-Sinopec YPC Company	Nanjing, China	130000	1998
Sinopec Maoming	Maoming, China	106000	1996
Shell Chemicals Seraya I	Singapore	360000	1996
Denka (*Chiba Styrene Monomer*)	Chiba, Japan	265000	1994
Taiyo Oil Company (*Mitsui Toatsu Chemicals*)	Ube, Japan	288000	1993
NS Styrene Monomer (*Nippon Steel Chemical Co.*) (SM No. 3)	Oita, Japan	212000	1990

The EBOne process is essentially identical in design to the EBMax technology. It uses two reactors: one for benzene alkylation and one for DEB transalkylation. The reactors operate near the critical temperatures of the reaction mixtures to maximize EB yield.

The liquid-phase alkylation reactor comprises several zeolite catalyst beds operating adiabatically. The process conditions are selected such that to maintain the alkylation reaction mass in the liquid phase. Benzene is used in excess, and ethylene is introduced before each bed, which improves selectivity and increases the service life of the catalyst. Ethylene reacts completely in the alkylation reactor, thus leaving only inert components (ethane, etc.). These inert components pass through the reactor and are removed from the unit. The transalkylation reactor, similar in design to the alkylation reactor, also consists of several beds of zeolite catalyst. The conditions are also selected to conduct a liquid-phase process. The alkylation and transalkylation effluents are fed to a benzene column, where benzene is collected to the reactors as the top product for recirculation. The bottom part of the benzene column is fed to an EB column, where the product EB is obtained at the top. The distillation residue is withdrawn to a PAB (polyalkylbenzenes) column, from which DEB and TEB are withdrawn from the top as transalkylation feedstock. PAB resin is obtained from the bottom and is further used for fuel needs. The reboilers of the distillation columns can use hot oil, high-pressure steam, or direct heating. The overhead vapors are condensed in waste heat boilers to form industrial steam.

A typical range of operating parameters for the EBOne process and the catalysts used are given in Table 3.

The EBOne technology is highly flexible. An increase in the efficiency of the process to about 70% can be achieved without economic losses. After reaching the 70% range, some losses in energy efficiency may be appeared in the distillation section. However, the reaction system efficiency can be at least 50% without any adverse technological or economic consequences.

1.3. CDTech EB technology

CDTech EB is an advanced technology developed by Catalytic Distillation Technologies Inc (CDTech) that produces high-purity EB from ethylene and benzene using a patented catalytic distillation process. The CDTech EB process flow diagram differs from EBOne technology only in the alkylation reactor system (Fig. 3).

The CDTech EB process is based on a patented catalytic distillation concept that combines the catalytic reaction and distillation in a single operation. Gaseous ethylene is introduced into the bottom of each reaction zone (either directly or via the overhead of the benzene column). The reaction takes place in the catalytic zones of the reactor, while distillation occurs throughout the column, which results in a counter-current of vapor and liquid throughout the reactor.

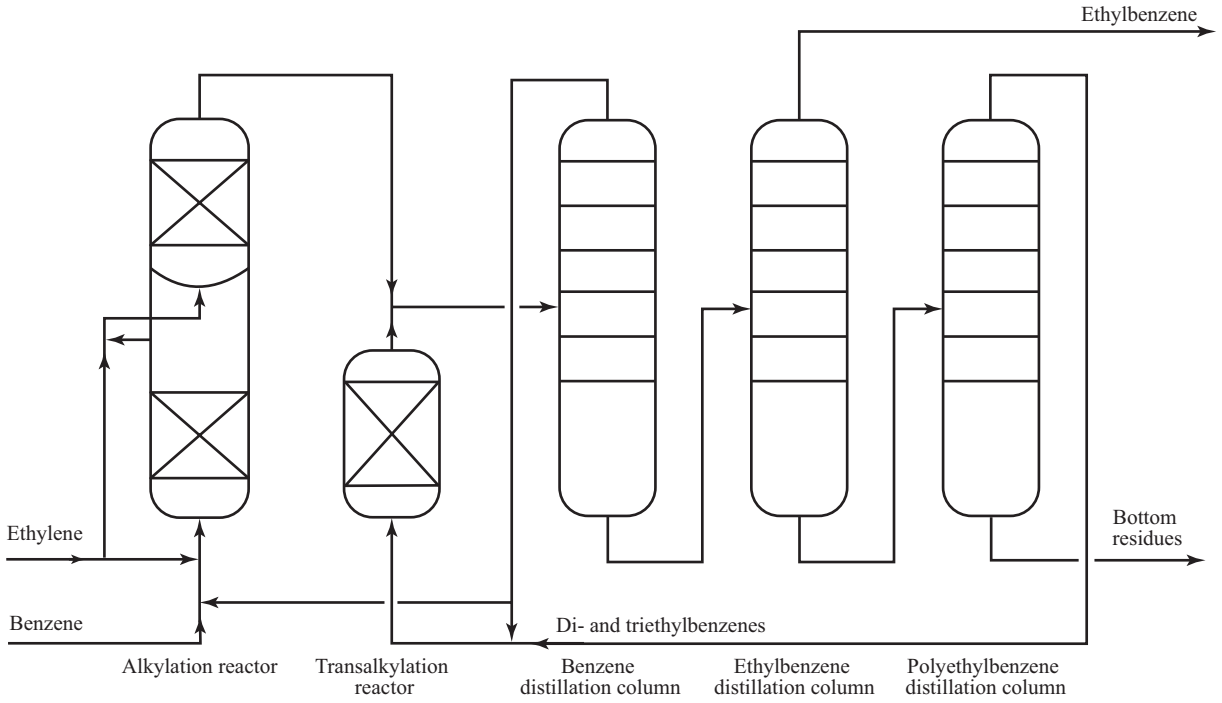

Fig. 2. Process flow diagram of the *UOP* EBOne process [25]

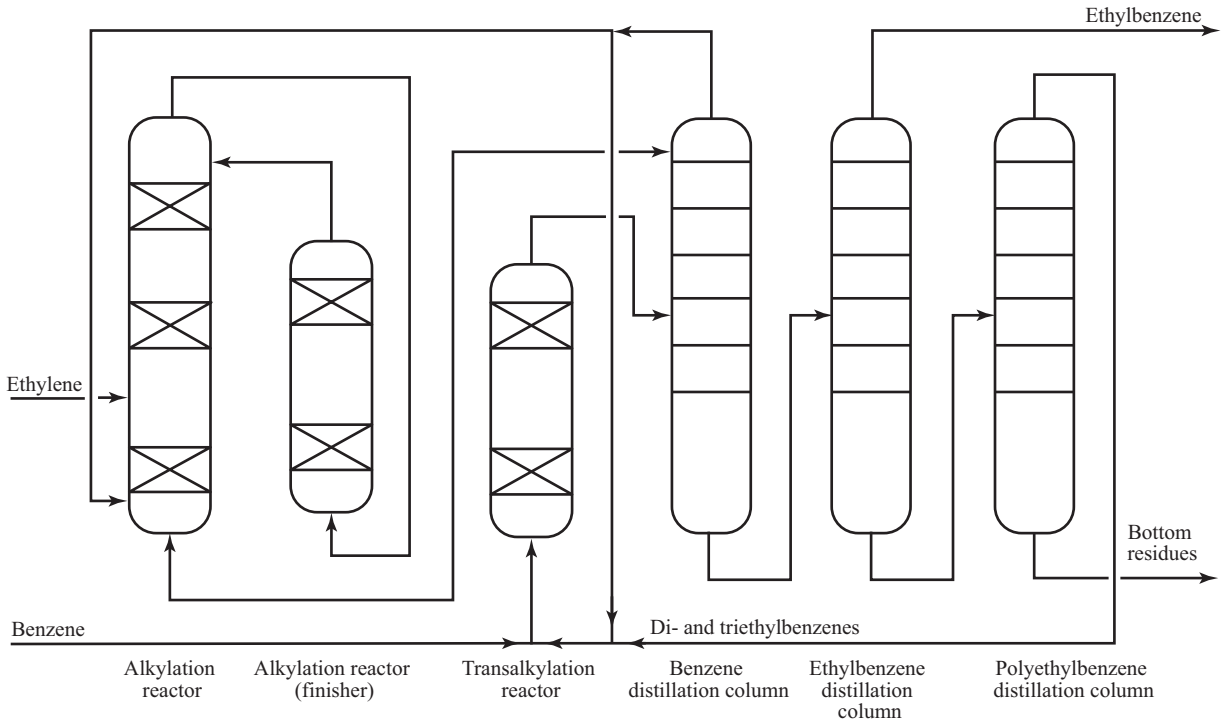

Fig. 3. Process flow diagram of the CDTech EB process [26]

Table 3. Key indicators of the EBOne process and the catalysts used

Key indicators of the process		Catalysts	
Phase	Liquid	Alkylation	Transalkylation
Reaction temperature, °C	~270	EBZ-800TL based on UZM-8 zeolite[16]	EBZ-100 based on Zeolite Y
Alkylation temperature difference at the input and output, °C	200–270		
Reaction pressure, MPa (excess)	3.0–4.0		
Alkylation, benzene/ethylene ratio (mol)	2.0–4.0		
Transalkylation , benzene/PAB ratio (mol)	2.0–4.0		
EB yield, wt %	99.8		
EB purity, vol %	min 99.8%		
Cycle length between catalyst regenerations, years	More than 3		

[16] UZM is a *UOP* zeolite material.

The reaction products are continuously removed from the catalytic zone by distillation, while any unreacted materials and other light components are removed from the top. The heat of the reaction is immediately removed due to evaporation of benzene, which allows the column to operate isothermally at the optimum reaction temperature. Ethylene vapor is introduced into the reactor at several points, coming into contact with liquid benzene entering from above. After that, the vapor is absorbed into the liquid phase. At equilibrium, most of the ethylene remains in the vapor phase. When a small amount of ethylene in the liquid comes into contact with the catalyst, it immediately reacts to form EB. This moves the ethylene concentration in the liquid phase away from equilibrium. The need for the vapor–liquid equilibrium results in "injection" of ethylene from the vapor phase into the liquid phase, thus restoring equilibrium. The alkylator can be designed to convert virtually all of the ethylene feedstock or only its part. In the latter case, an additional alkylator is provided to complete the ethylene conversion. Unreacted ethylene and benzene in the alkylator overhead are condensed and forwarded to an additional alkylator to ensure complete ethylene conversion.

The catalytic distillation column combines the alkylation and rectification processes in one stage. Alkylation occurs isothermally at reduced temperatures and pressures. In the catalytic distillation column, the products are removed from the reaction zone. These factors limit the formation of byproducts and increase the yield of the target product and its purity. Low reaction temperatures and pressures also reduce capital costs, increase plant safety, and minimize fugitive emissions. The multiphase environment of the catalytic distillation column maintains an extremely low ethylene concentration in the liquid phase (<0.1 wt %) due to its high volatility compared to benzene.

Configuring the EB synthesis unit as a catalytic distillation unit (instead of a separate alkylator and transalkylator) does not automatically result in a greater process efficiency. In order to achieve the desired efficiency, careful design of the reaction and separation conditions is required.

Since 1990, the CDTech EB technology has been selected for six projects worldwide. As shown in Table 4, three plants are currently in operation. The largest CDTech EB unit developed to date has been using a highly dilute ethylene feedstock containing less than 40 mol % of ethylene (the remainder consists primarily of hydrogen, methane, and ethane). Such a stream can be the products of the catalytic cracking process, which, according to the process thermodynamics, are characterized by a low yield of ethylene.

The CDTech EB process uses a specially developed zeolitic alkylation catalyst based on Y zeolite loaded into a catalytic distillation column. The catalyst is packed in specifically designed bags made of steel mesh and glass fiber fabric. The unique structure of the bags provides them with the necessary void fraction to allow steam to flow upward through the reactor. The glass fiber packing acts as a barrier preventing direct contact of the steam with the catalyst. The bags are approximately 30 cm in diameter and height, being easy to handle during loading operations. The CDTech proprietary bags containing the alkylation catalyst are stacked inside the alkylator similarly to the mode of structured packing (Fig. 4). This allows the alkylation reaction and distillation of the reactants and products to occur simultaneously. Multiple beds of stacked bags are used. The catalyst lifecycle is estimated to be over two years based on pilot tests (6000 h of continuous operation). At the same time, the high yield (99.7 wt %) and quality of the obtained EB (99.5 wt %) are maintained throughout the entire run [27].

The typical operating range for the CDTech EB process is shown in Table 5.

Thus, the low benzene/ethylene ratio makes the described process suitable for the reconstruction of obsolete plants. Among other things, it increases the capacity for EB production. The ratio of low process temperatures, pressures, as well as the simplicity and possibility of using carbon steel equipment makes this technology attractive in terms of minimal capital costs for construction as compared to competitors.

1.4. *Versalis* technology

Versalis offers contemporary technologies for producing EB on the basis of zeolite-containing PBE-1 (Polimeri Europa Beta zeolite[17]) catalysts for alkylation and PBE-2 for transalkylation based on Beta zeolite in the H-form. The technology has proven reliable following testing on an industrial scale at an EB plant with a capacity of 650000 t/year successfully launched in 2009. *Versalis* catalysts are described in the patent [28].

Specific features of the *Versalis* technology include the presence of primary benzene purification units to remove catalytic poisons, as well as preliminary mixing of benzene and ethylene (before the alkylation reactor). This increases the yield of target products. The catalyst used reduces the formation of ethylene oligomers and coke at high activity. This allows the process to be carried out under mild conditions, i.e., a temperature of 170–230°C and a relatively low pressure of 1–2 MPa. The benzene to ethylene ratio is at least 2 mol [11].

[17] The *Eni's* chemical division, formerly *Polimeri Europa*, rebranded as *Versalis*.

Table 4. Existing installations for producing EB using CDTech EB technology

Company	Location	Capacity, t/year	Start
S-Chem (*JCP Company*)	Al Jubail, Saudi Arabia	>770000	2008
INEOS Styrolution (*Nova Chemicals Corp.*)	Sarnia, Canada	477000	1998
Petroquimica Argentina SA. (*PASA*)	Puerto San Martin, Argentina	140000	1997

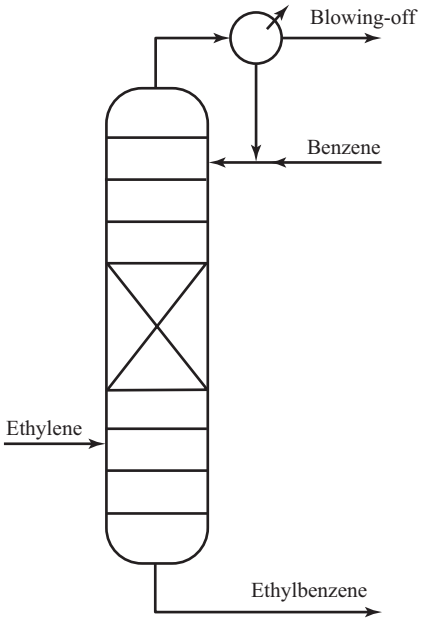

Fig. 4. Catalytic distillation column for EB synthesis [27]

Table 5. Operating range of the CDTech EB unit

Parameter	Value
Alkylation, benzene/ethylene ratio (mol)	2.0–4.0
Transalkylation, benzene/PAB ratio (mol)	2.0–4.0
Alkylation temperature range, °C	200 top, 240 bottom
Alkylator pressure, MPa	2.0–2.5
Ethylene consumption, kg/kg EB	0.264
Benzene consumption, kg/kg EB	0.738

The advantages of the *Versalis* technology are:

- high selectivity (at least 80%) and catalyst stability;
- high purity of EB (99.98%);
- 100% ethylene conversion and a total EB yield of 99.7% with an insignificant content of xylene byproducts (less than 10 ppmw);
- ease of operation;
- use of carbon steel;
- low capital investments and plant maintenance costs;
- easy handling of fresh catalyst and spent catalyst;
- catalyst regeneration intervals from 2 to 7 years;
- extended catalyst service life (up to five regenerations without performance degradation);
- efficient and reliable fresh benzene treatment to protect the catalyst from nitrogen contamination;
- low environmental impact;
- no acid waste stream and minimal gas emissions.

The PBE catalyst preparation procedures allow for optimum non-zeolitic porosity values, which increases the catalyst stability and reduces its deactivation rate.

The *Versalis* process does not generate liquid waste or gas emissions, with the exception of oil-containing water and vacuum pump vent emissions. The spent catalyst can be recycled after several regenerations.

The *Versalis* process flow diagram is shown in Fig. 5.

The *Versalis* technology includes adiabatic alkylation and transalkylation reactors with fixed catalyst beds, where the alkylation reactor contains several catalyst beds with fractional ethylene feed and is equipped with external intra-bed refrigerators to remove the exothermic reaction heat. The system for separating commercial EB and byproducts is virtually identical to that in the EBOne technology.

CONCLUSIONS

Ethylbenzene is a high-tonnage and high-margin product of petrochemical synthesis with a stable demand in the external and internal markets. More than 99% of EB is used in the production of styrene, a raw material for the production of polystyrene, ABS plastics[18], and synthetic rubbers.

The presented review of contemporary technologies for the production of EB (*Badger* EBMax, *UOP* EBOne, *Versalis*, CDTech EB) shows the liquid-phase technology using contemporary zeolite-containing catalysts to be the most promising option at the present stage.

In comparison with the gas-phase process, the advantages of the liquid-phase process of benzene alkylation with ethylene include reduced energy costs due to relatively low process temperatures (below

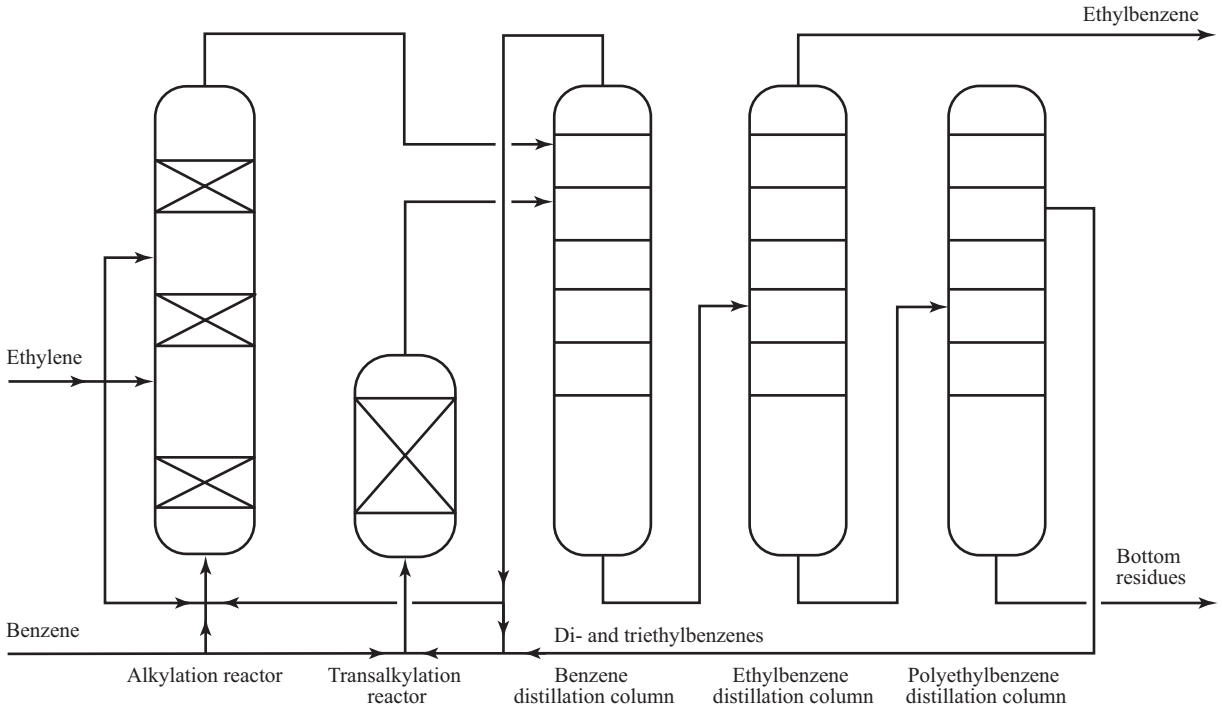

Fig. 5. Process flow diagram of the *Versalis* process [28]

[18] ABS is an acrylonitrile butadiene styrene plastic.

270°C), reduced byproduct yield, increased EB yield, increased service life and inter-regeneration cycle of the catalyst. More than half of the EB produced in the world is obtained according to the EBMax technology using a catalyst based on an MWW family zeolite (MCM-22). This technology enables a low benzene to ethylene ratio (from 2.5 to 4), which reduces the benzene circulation rate, increases efficiency, and reduces the throughput of the benzene extraction column.

Zeolite-containing catalysts are highly active, stable, environmentally friendly, and regenerable as compared to liquid-phase alkylation catalysts (aluminum chloride). The use of such catalysts simplifies the process of preparing raw materials and designing the equipment.

The conventional technology for producing EB based on $AlCl_3$ does not provide adequate efficiency in converting benzene into EB. This is reflected in low raw material utilization rates, the formation of a large amount of highly polluted wastewater, and high corrosion.

Contemporary research in the field of benzene alkylation technology with ethylene into EB is associated with the creation and use of zeolite-containing catalysts as solid porous systems containing an active component and a binder. The active component is USY, Beta, mordenite, ZSM-5, ZSM-11, ZSM-12, ZSM-23, ZSM-35, ZSM-48, MCM-22, and MCM-49 zeolites. The preferred alkylation catalysts include Beta zeolite or a zeolite of the MCM-22 family. The binder is Al_2O_3, SiO_2, or amorphous aluminosilicate. After mixing the active component and the binder, the resulting mass is used to form granules followed by their drying and calcination. In individual cases, the catalyst can then be modified. Typically, the zeolite content in the catalysts ranges from 60 to 80 wt %.

A number of works have described various approaches to treating the original zeolites with the purpose of increasing their mesoporous surface area. This allows the transalkylation process temperature to be reduced and the catalytic activity of the resulting catalysts to be increased.

In 2022, the first industrial batch of the KT-GA-1 catalyst based on a zeolite of the MFI family (ZSM-5) for the process of gas-phase alkylation of benzene with ethylene in EB was released in Russia. Pilot industrial tests of the catalyst commenced on July 19, 2022, continuing up to the present time. The first year of operation showed the Russian catalyst to be equivalent to its imported counterpart in all respects.

Contemporary developments in the field of catalysts for the process of transalkylation of benzene with DEB, including Russian ones, are devoted to the creation and use of zeolitic and zeolite-containing catalysts based on a FAU type zeolite (Zeolite Y).

The KT-BS-1 catalyst has been successfully operated in Russia at the *Monomer* plant of *Gazprom Neftekhim Salavat* starting from 2013 and up to the present time. This catalyst was developed jointly by *STC Salavatnefteorgsintez* and the Institute of Petrochemical Synthesis of the Russian Academy of Sciences (Moscow) on the basis of a deeply decationized Zeolite Y without binders. In addition, as an alternative to the catalyst for benzene transalkylation with DEB, KT-BS-1, the STC developed the KT-SS catalyst granulated with a binder: 80 wt % of Zeolite Y in the acidic H^+ form and 20 wt % of an alumina binder. The advantage of the KT-SS catalyst over the zeolitic KT-BS-1 is that the manufacture of the former uses conventional technology for producing zeolite-containing catalysts with a binder. As a result, the catalyst exhibits a developed secondary porous structure, which plays a transport role in the supply of reactants to the catalyst active centers as well as in the removal of reaction products. In addition, this catalyst can be produced in the required tonnage at any catalyst factory in Russia.

Thus, the advantages of the liquid-phase alkylation technology in the presence of contemporary highly active zeolite-containing catalysts make it the most preferable option in terms of minimal capital costs for construction as compared to other technologies for producing EB.

Authors' contributions

All authors contributed equally to the preparation of the article.

S.N. Potapova—analysis of the collected data, systematization of scientific literature, writing the text of the article.

L.A. Khakhin—planning the publication, writing and reviewing the article.

E.V. Korolev—data collection, preparing the tables, writing the text of the article.

S.M. Masoud—analysis of the collected data, data systematization, and preparing illustrations.

D.V. Svetikov—collecting the data, preparing the tables for the article.

The authors declare no conflicts of interest.

REFERENCES

1. Degnan Th.F.Jr., Smith C.M., Venkat Ch.R. Alkylation of aromatics with ethylene and propylene: recent developments in commercial processes. *Appl. Cat. A: Gen.* 2001;221(1-2): 283–294. http://doi.org/10.1016/S0926-860X(01)00807-9
2. Pavlov M.L., Basimova R.A., Alyabyev A.S. Alkylation of benzene with ethylene on a domestic zeolite-containing catalyst. *Neftegazovoe delo = Oil and Gas Business.* 2012;2:470–478 (in Russ.).
3. Ivashkina E.N., Koshkin S.A., Khlebnikova E.S. Modeling the operation of industrial ethylbenzene production plants. *Neftegaz* RU. 2019;9:82–87 (in Russ.).
4. Kosareva A.E., Kurakin M.E., Travkin M.E. Current state and prospective developments processes for obtaining ethylbenzene. Market overview and current state of processes obtaining ethylbenzene. *Vestnik Molodogo Uchenogo USNTU.* 2024;2:99–106 (in Russ.).
5. Popov S.V., Krymkin N.Yu., Khabibrakhmanova O.V., Papulovskikh E.N. Reconstruction of the hardware design for isopropylbenzene production for the production of ethylbenzene. *Vestnik Voronezhskogo gosudarstvennogo universiteta inzhenernykh tekhnologii = Proceedings of the Voronezh State University of Engineering Technologies.* 2021;83(2):184–190 (in Russ). https://doi.org/10.20914/2310-1202-2021-2-184-190
6. Pavlov M.L., Basimova R.A., Alyab'ev A.S., Khabibullin A.M., Glotov A.P., Zinnurov R.R. Ethylbenzene poduction at Gazprom Neftekhim Salavat. *Neftepererabotka i neftekhimiya = Oil Refining and Petrochemistry.* 2023;7-8:28–33 (in Russ.).
7. Pavlov M.L., Basimova R.A., Alyabyev A.S. *Method for Obtaining Catalyst and Method for Alkylating Benzene with Ethylene Using It*: RF Pat. 2755892C1 RU. Publ. 22.09.2021 (in Russ.).
8. Ponomareva O.A., Knyazeva E.E., Shkuropatov A.V., *et al.* Synthesis and catalytic properties of MWW structure zeolite in petrochemical processes. *Pet. Chem.* 2017;57(12): 1147–1150. https://doi.org/10.1134/S096554411706024X
[Original Russian Text: Ponomareva O.A., Knyazeva E.E., Shkuropatov A.V., Ivanova I.I., Gerzeliev I.M., Khadzhiev S.N. Synthesis and catalytic properties of MWW structure zeolite in petrochemical processes. *Neftekhimiya.* 2017;57(6):769–772 (in Russ.).]
9. Shavaleev D.A., Pavlov M.L., Basimova R.A., *et al.* Synthesis of modified catalyst for liquid phase alkylation of benzene with ethylene. *Pet. Chem.* 2020;60(9):1073–1079. https://doi.org/10.1134/S0965544120090182
[Original Russian Text: Shavaleev D.A., Pavlov M.L., Basimova R.A., Sadovnikov A.A., Sud'in V.V., Smirnova E.M., Demikhova N.R. Synthesis of modified catalyst for liquid phase alkylation of benzene with ethylene. *Neftekhimiya*. 2020;60(5): 686–692 (in Russ.). https://doi.org/10.31857/S0028242120050184]
10. Pavlov M.L., Basimova R.A., Shavaleev D.A., *et al.* Development of a catalyst and a process for liquid-phase benzene alkylation with ethylene and ethane-ethylene hydrocarbon pyrolysis fraction. *Pet. Chem.* 2019;59(7): 701–705. https://doi.org/10.1134/S0965544119070120
[Original Russian Text: Pavlov M.L., Basimova R.A., Shavaleev D.A., Ershtein A.S. Development of a catalyst and a process for liquid-phase benzene alkylation with ethylene and ethane-ethylene hydrocarbon pyrolysis fraction. *Neftekhimiya*. 2019;59(4): 417–422 (in Russ.). https://doi.org/10.1134/S0028242119040129]

СПИСОК ЛИТЕРАТУРЫ

1. Degnan Th.F.Jr., Smith C.M., Venkat Ch.R. Alkylation of aromatics with ethylene and propylene: recent developments in commercial processes. *Appl. Cat. A: Gen.* 2001;221(1-2): 283–294. http://doi.org/10.1016/S0926-860X(01)00807-9
2. Павлов М.Л., Басимова Р.А., Алябьев А.С. Алкилирование бензола этиленом на отечественном цеолитсодержащем катализаторе. *Нефтегазовое дело*. 2012;2: 470–478.
3. Ивашкина Е.Н., Кошкин С.А., Хлебникова Е.С. Моделирование работы промышленных установок получения этилбензола. *Neftegaz RU.* 2019;9:82–87.
4. Косарева А.Е, Куракин М.Е., Травкин М.Е. Современное состояние и перспективы развития процессов получения этилбензола. Обзор рынка и современное состояние процессов получения этилбензола. *Вестник молодого ученого УГНТУ.* 2024;2:99–106.
5. Попов С.В., Крымкин Н.Ю., Хабибрахманова О.В., Папуловских Е.Н. Реконструкция аппаратурного оформления производства изопропилбензола с целью выпуска этилбензола. *Вестник Воронежского государственного университета инженерных технологий.* 2021;83(2):184–190. https://doi.org/10.20914/2310-1202-2021-2-184-190
6. Павлов М.Л., Басимова Р.А., Алябьев А.С., Хабибуллин А.М., Глотов А.П., Зиннуров Р.Р. Производство этилбензола в ООО Газпром Нефтехим Салават. *Нефтепереработка и нефтехимия*. 2023;7-8:28–33.
7. Павлов М.Л., Басимова Р.А., Алябьев А.С. *Способ получения катализатора и способ алкилирования бензола этиленом с его использованием:* пат. 2755892C1 РФ. Заявка № 2020138987; заявл. 27.11.2020; опубл. 22.09.2021. Бюл. № 27.
8. Пономарева О.А., Князева Е.Е., Шкуропатов А.В., Иванова И.И., Герзелиев И.М., Хаджиев С.Н. Синтез и каталитические свойства цеолитов со структурой MWW в процессах нефтехимии (обзор). *Нефтехимия*. 2017;57(6):769–772.
9. Шавалеев Д.А., Павлов М.Л., Басимова Р.А., Садовников А.А., Судьин В.В., Смирнова Е.М., Демихова Н.Р. Синтез модифицированного катализатора для процесса жидкофазного алкилирования бензола этиленом. *Нефтехимия*. 2020;60(5):686–692. https://doi.org/10.31857/S0028242120050184
10. Павлов М.Л., Басимова Р.А., Шавалеев Д.А., Эрштейн А.С. Разработка катализатора и процесса жидкофазного алкилирования бензола этиленом и этан-этиленовой фракцией пиролиза углеводородов. *Нефтехимия*. 2019;59(4): 417–422. https://doi.org/10.1134/S0028242119040129
11. Рогов М.Н., Рахимов Х.Х., Ишмияров М.Х., Мячин С.И. *Способ приготовления цеолитсодержащего катализатора алкилирования бензола этиленом*: пат. 2265482 РФ. Заявка № 2004114845/04; заявл. 13.05.2004; опубл. 10.129.2005. Бюл. № 347.
12. Senderov E., Qureshi M.I. *Introduction of Mesoporosity into Zeolite Materials with Sequential Acid, Surfactant, and Base Treatment*: USA Pat. 9376324 US; Patent Publication Number 2013/0183231 A1. Publ. 18.07.2013.

11. Rogov M.N., Rakhimov Kh.Kh., Ishmiarov M.Kh., Myachin S.I. *Method of Preparating Zeolite-Containing Benzene-Ethylene Alkylation Catalyst*: RF Pat. 2265482 RU. Publ. 10.12.2005 (in Russ.).
12. Senderov E., Qureshi M.I. *Introduction of Mesoporosity into Zeolite Materials with Sequential Acid, Surfactant, and Base Treatment*: USA Pat. 9376324 US; Patent Publication Number 2013/0183231 A1. Publ. 18.07.2013.
13. Peters A.W., Knaeble W.J., Burton A.W., Johnson I.D., Oliveri C.G., Britto R.J. *Production of Alkylaromatic Compounds:* USA Pat. 11820723 US. Publ. 30.11.2023.
14. Khadzhiev S.N., Pavlov M.L., Basimova R.A., Gerzeliev I.M., Alyab'ev A.S., Kutepov B.I. *Catalyst, Method for Production Thereof and Method for Transalkylation of Benzene with Diethylbenzenes using Said Catalyst*: RF Pat. 2478429 C1 RU. Publ. 10.04.2013 (in Russ.).
15. Shavaleev D.A., Pavlov M.L., Basimova R.A., Shavaleeva N.N., Jershtejn A.S., Travkina O.S., Kutepov B.I. *Method of Producting Catalyst and Method for Transalkylation of Benzene with Diethylbenzenes Using Same:* RF Pat. 2553256 C1 RU. Publ. 10.06.2015 (in Russ.).
16. Woodle G.B., Cepla A. *Ethylbenzene Process Using Stacked Reactor Loading of Beta and Y Zeolites:* USA Pat. 5998687. Publ. 12.07.1999.
17. Lui G., Sundararaman R., Cao J. Ethylbenzene plant debottleneck with a high-activity transalkylation catalyst. *Hydrocarbon Processing*. 2021;6:51–54.
18. Pavlov M.L., Basimova R.A., Alyabyev A.S. *Catalyst, Method for its Preparation and Method for Transalkylation of Benzene with Diethylbenzenes Using It*: RF Pat. 2751336 C1. Publ. 13.07.2021 (in Russ.).
19. Degnan T.F., Smith C.M., Venkat C.R. Alkylation of aromatics with ethylene and propylene: recent developments in commercial processes. *Appl. Catal. A: Gen.* 2001;221(1-2): 283–294. https://doi.org/10.1016/S0926-860X(01)00807-9
20. Basimova R.A., Pavlov M.L., Prokopenko A.V., Mjachin S.I., Kajumov V.V., Musin A.R., Kozlova M.Ju., Kutepov B.I. *The main stages of development and the current state of the ethylbenzene production process*. *Neftepererabotka i neftekhimiya = Oil Refining and Petrochemistry.* 2009;2:24–28 (in Russ.).
21. Lee S. *Encyclopedia of Chemical Processing*. CRC Press; 2006. 3640 p.
22. Abrams M.L., Jeroro E., Moscoso J.G. *Process for Making Modified Small-Crystal Mordenite, Transalkilation Process Using Same, and Modified Small-Crystal Mordenite:* USA Pat. 11529615 B2. Publ. 20.12.2022.
23. Abrams M.L., Jeroro E., Moscoso J.G., Jan D.-Y., Cox P. *Process for Making Modified Small-Crystal Mordenite, Transalkilation Process Using Same, and Modified Small-Crystal Mordenite.* USA Pat. 2021/0187486 A1. Publ. 24.06.2021.
24. Jeroro E., Jan D-Y., Cox P., Moscoso J.G. *USM-54 and Transalkylation Process Using Same:* WO Pat. 2021/141870 A1. Publ. 15.07.2021.
25. Yang W., Wang Z., Sun H., Zhang B. Advances in development and industrial applications of ethylbenzene processes. *Chinese J. Catal*. 2016;37(1):16–26. https://doi.org/10.1016/S1872-2067(15)60965-2
13. Peters A.W., Knaeble W.J., Burton A.W., Johnson I.D., Oliveri C.G., Britto R.J. *Production of Alkylaromatic Compounds:* USA Pat. 11820723 US. Publ. 30.11.2023.
14. Хаджиев С.Н., Павлов М.Л., Басимова Р.А., Герзелиев И.М., Алябьев А.С., Кутепов Б.И. *Катализатор, способ его получения и способ трансалкилирования бензола диэтилбензолами с его использованием:* пат. 2478429 C1 РФ. Заявка № 2011131506/04; заявл. 28.07.2011; опубл. 10.04.2013. Бюл. № 10.
15. Шавалеев Д.А., Павлов М.Л., Басимова Р.А., Шавалеева Н.Н., Эрштейн А.С., Травкина О.С., Кутепов Б.И. *Способ получения катализатора и способ трансалкилирования бензола диэтилбензолами с его использованием:* пат. 2553256 C1 РФ. Заявка № 2014113800/04; заявл. 08.04.2014; опубл. 10.06.2015. Бюл. № 16.
16. Woodle G.B., Cepla A. *Ethylbenzene Process Using Stacked Reactor Loading of Beta and Y Zeolites:* USA Pat. 5998687. Publ. 12.07.1999.
17. Lui G., Sundararaman R., Cao J. Ethylbenzene plant debottleneck with a high-activity transalkylation catalyst. *Hydrocarbon Processing*. 2021;6:51–54.
18. Павлов М.Л., Басимова Р.А., Алябьев А.С. *Катализатор, способ его получения и способ трансалкилирования бензола диэтилбензолами с его использованием:* пат. 2751336 C1 РФ. Заявка № 2020132683; заявл. 02.10.2020; опубл. 13.07.2021. Бюл. № 20.
19. Degnan T.F., Smith C.M., Venkat C.R. Alkylation of aromatics with ethylene and propylene: recent developments in commercial processes. *Appl. Catal. A: Gen.* 2001;221(1-2):283–294. https://doi.org/10.1016/S0926-860X(01)00807-9
20. Басимова Р.А., Павлов М.Л., Прокопенко А.В., Мячин С.И., Каюмов В.В., Мусин А.Р., Козлова М.Ю., Кутепов Б.И. Основные этапы развития и современное состояние процесса получения этилбензола. *Нефтепереработка и нефтехимия*. 2009;2:24–28.
21. Lee S. *Encyclopedia of Chemical Processing*. CRC Press; 2006. 3640 p.
22. Abrams M.L., Jeroro E., Moscoso J.G. *Process for Making Modified Small-Crystal Mordenite, Transalkilation Process Using Same, and Modified Small-Crystal Mordenite:* USA Pat. 11529615 B2. Publ. 20.12.2022.
23. Abrams M.L., Jeroro E., Moscoso J.G., Jan D.-Y., Cox P. *Process for Making Modified Small-Crystal Mordenite, Transalkilation Process Using Same, and Modified Small-Crystal Mordenite.* USA Pat. 2021/0187486 A1. Publ. 24.06.2021.
24. Jeroro E., Jan D.-Y., Cox P., Moscoso J.G. *USM-54 and Transalkylation Process Using Same:* Pat. 2021/141870 A1 WO. Publ. 15.07.2021.
25. Yang W., Wang Z., Sun H., Zhang B. Advances in development and industrial applications of ethylbenzene processes. *Chinese J. Catal*. 2016;37(1):16–26. https://doi.org/10.1016/S1872-2067(15)60965-2
26. Meyers R. *Handbook of Petrochemicals Production Processes.* 2nd Ed. McGraw Hill.; 2018. 640 p.
27. Weitkamp J., Pupple L. *Catalysis and Zeolites: Fundamentals and Applications*. Springer Science & Business Media; 1999. 564 p.

26. Meyers R. *Handbook of Petrochemicals Production Processes.* 2nd Ed. McGraw Hill.; 2018. 640 p.
27. Weitkamp J., Pupple L. *Catalysis and Zeolites: Fundamentals and Applications*. Springer Science & Business Media; 1999. 564 p.
28. Girotti G., Cappeliazzo O. *Catalytic Composition and Process for the Alkylation or Transalkylation of Aromatic Compounds*: USA Pat. 6084143. Publ. 04.07.2000.
28. Girotti G., Cappeliazzo O. *Catalytic Composition and Process for the Alkylation or Transalkylation of Aromatic Compounds*: USA Pat. 6084143. Publ. 04.07.2000.

About the Authors

Leonid A. Khakhin, Cand. Sci. (Eng.), Head of the Laboratory of Polyalphaolefins, United Research and Development Center (55/1-2, Leninskii pr., Moscow, 119333, Russia). E-mail: KhakhinLA@rdc.rosneft.ru. RSCI SPIN-code 3653-9491, https://orcid.org/0009-0007-1120-8682

Svetlana N. Potapova, Cand. Sci. (Chem.), Leading Researcher, Laboratory of Polyalphaolefins, United Research and Development Center (55/1-2, Leninskii pr., Moscow, 119333, Russia). E-mail: PotapovaSN@rdc.rosneft.ru. RSCI SPIN-code 8015-3854, https://orcid.org/0009-0001-4580-0189

Evgeniy V. Korolev, Cand. Sci. (Eng.), Senior Researcher, Laboratory of Polyalphaolefins, United Research and Development Center (55/1-2, Leninskii pr., Moscow, 119333, Russia). E-mail: KorolevEV@rdc.rosneft.ru. https://orcid.org/0009-0001-3512-7736

Salekh M. Masoud, Cand. Sci. (Chem.), Researcher, Laboratory of Polyalphaolefins, United Research and Development Center (55/1-2, Leninskii pr., Moscow, 119333, Russia). E-mail: MasoudSM@rdc.rosneft.ru. Scopus Author ID 55327194000, ResearcherID J-8251-2018, https://orcid.org/0000-0003-2873-3612

Dmitry V. Svetikov, Senior Researcher, Laboratory of Polyalphaolefins, United Research and Development Center (55/1-2, Leninskii pr., Moscow, 119333, Russia). E-mail: SvetikovDV@rdc.rosneft.ru. https://orcid.org/0009-0002-0394-8895

Об авторах

Хахин Леонид Алексеевич, к.т.н., заведующий лабораторией полиальфаолефинов, ООО «Объединенный центр исследований и разработок» (ООО «РН-ЦИР») (119333, Россия, Москва, Ленинский пр-т, 55/1, стр. 2). E-mail: KhakhinLA@rdc.rosneft.ru. SPIN-код РИНЦ 3653-9491, https://orcid.org/0009-0007-1120-8682

Потапова Светлана Николаевна, к.х.н., ведущий научный сотрудник, лаборатория полиальфаолефинов, ООО «Объединенный центр исследований и разработок» (ООО «РН-ЦИР») (119333, Россия, Москва, Ленинский пр-т, 55/1, стр. 2). E-mail: PotapovaSN@rdc.rosneft.ru. SPIN-код РИНЦ 8015-3854, https://orcid.org/0009-0001-4580-0189

Королев Евгений Валерьевич, к.т.н., старший научный сотрудник, лаборатория полиальфаолефинов, ООО «Объединенный центр исследований и разработок» (ООО «РН-ЦИР») (119333, Россия, Москва, Ленинский пр-т, 55/1, стр. 2). E-mail: KorolevEV@rdc.rosneft.ru. https://orcid.org/0009-0001-3512-7736

Масоуд Салех Масоуд, к.х.н., научный сотрудник, лаборатория полиальфаолефинов, ООО «Объединенный центр исследований и разработок» (ООО «РН-ЦИР») (119333, Россия, Москва, Ленинский пр-т, 55/1, стр. 2). E-mail: MasoudSM@rdc.rosneft.ru. Scopus Author ID 55327194000, ResearcherID J-8251-2018, https://orcid.org/0000-0003-2873-3612

Светиков Дмитрий Викторович, старший научный сотрудник, лаборатория полиальфаолефинов, ООО «Объединенный центр исследований и разработок» (ООО «РН-ЦИР») (119333, Россия, Москва, Ленинский пр-т, 55/1, стр. 2). E-mail: SvetikovDV@rdc.rosneft.ru. https://orcid.org/0009-0002-0394-8895

Translated from Russian into English by M. Povorin
Edited for English language and spelling by Thomas A. Beavitt

Tonkie Khimicheskie Tekhnologii = Fine Chemical Technologies.
2025;20(5):516–524 ISSN 2686-7575 (Online)

UDC 669.018.6:620.193.3
https://doi.org/10.32362/2410-6593-2025-20-5-516-524
EDN RMXBKC

RESEARCH ARTICLE

Influence of equal channel angular pressing on the strength and corrosion properties of FeNiMnCr high-entropy alloy

Adham M.M. Abuayash✉, Konstantin M. Nesterov, Rinat K. Islamgaliev
Ufa University of Science and Technology, Ufa, Republic of Bashkortostan, 450076 Russia
✉ *Corresponding author, e-mail: adhamabuayash4@gmail.com*

Abstract

Objectives. High-entropy alloys (HEAs) represent a novel class of metallic materials known for their exceptional mechanical and corrosion-resistant properties. This study investigates the effects of equal channel angular pressing (ECAP) on the microstructure, tensile strength, and corrosion behavior of an equiatomic FeNiMnCr alloy.

Methods. The alloy was synthesized via arc melting, homogenized, and subjected to up to four ECAP passes at 400°C. Phase composition was analyzed using X-ray diffraction, while microstructural features were examined using scanning electron microscopy and transmission electron microscopy. Mechanical properties were evaluated based on Vickers microhardness and tensile testing, while corrosion resistance was assessed in a 3.5% NaCl solution using potentiodynamic polarization.

Results. The results indicate a significant grain refinement, an increased hardness and strength (by 1013 MPa), and an improved corrosion resistance of the alloy after ECAP processing.

Conclusions. The study demonstrates that ECAP is an effective method for enhancing the performance of FeNiMnCr HEAs. This makes it promising for use in nuclear energy, medicine, and aerospace industry.

Keywords

high-entropy alloy, equal channel angular pressing, strength, thermal stability, corrosion resistance

Submitted: 06.10.2024
Revised: 18.04.2025
Accepted: 11.09.2025

For citation

Abuayash A.M.M., Nesterov K.M., Islamgaliev R.K. Influence of equal channel angular pressing on the strength and corrosion properties of FeNiMnCr high-entropy alloy. *Tonk. Khim. Tekhnol. = Fine Chem. Technol.* 2025;20(5):516–524. https://doi.org/10.32362/2410-6593-2025-20-5-516-524

НАУЧНАЯ СТАТЬЯ

Влияние равноканального углового прессования на прочностные и коррозионные свойства высокоэнтропийного сплава FeNiMnCr

А.М.М. Абуайяш✉, К.М. Нестеров, Р.К. Исламгалиев

Уфимский университет науки и технологий, Уфа, Республика Башкортостан, 450076 Россия

✉ *Автор для переписки, e-mail: adhamabuayash4@gmail.com*

Аннотация

Цели. Исследовать влияние равноканального углового прессования (РКУП) на структуру, прочность и коррозионные свойства сплава FeNiMnCr.

Методы. Структурные характеристики изучались с помощью рентгенофазового анализа и электронной микроскопии (scanning electron microscopy, transmission electron microscopy). Механические свойства оценивались по микротвердости и испытаниям на растяжение, коррозионная стойкость — потенциодинамическим методом в 3.5% растворе NaCl.

Результаты. Установлено, что РКУП приводит к значительному измельчению зерна, увеличению прочности (до 1010 МПа) и снижению плотности коррозионного тока, что говорит об улучшении пассивирующих свойств поверхности.

Выводы. РКУП повышает прочность и коррозионную стойкость сплава, что делает его перспективным для применения в ядерной энергетике, медицине и авиационно-космической промышленности.

Ключевые слова

высокоэнтропийный сплав, равноканальное угловое прессование, прочность, термическая стабильность, коррозионная стойкость

Поступила: 06.10.2024
Доработана: 18.04.2025
Принята в печать: 11.09.2025

Для цитирования

Abuayash A.M.M., Nesterov K.M., Islamgaliev R.K. Influence of equal channel angular pressing on the strength and corrosion properties of FeNiMnCr high-entropy alloy. *Tonk. Khim. Tekhnol. = Fine Chem. Technol.* 2025;20(5):516–524. https://doi.org/10.32362/2410-6593-2025-20-5-516-524

INTRODUCTION

High-entropy alloys (HEAs) constitute a novel class of metallic materials characterized by the presence of five or more principal elements in near-equiatomic proportions [1–4]. This unique compositional strategy often results in exceptional mechanical strength and corrosion resistance, making HEAs a subject of extensive global research. Despite their promising properties, many HEAs suffer from limited strength, which restricts their practical applications. To overcome this limitation, various processing techniques can be employed to enhance the mechanical properties of such alloys.

The conventional approach to creating new structural materials involves selecting one main element as a matrix and its further alloying to obtain the desired combination of mechanical and/or technological properties. Recently, a new approach to creating multicomponent alloys containing several elements in nearly equiatomic concentrations has been proposed. In comparison with traditional alloys, these alloys are characterized by higher mixing entropy values, hence the name HEAs. The increased entropy in HEAs is explained by the maximum mixing entropy between dissolved components upon their equiatomic concentration. As a result, single-phase solid solutions with simple body-centered cubic (BCC) or face-centered cubic (FCC) lattices are formed in several HEAs. Depending on the chemical composition, HEAs can demonstrate enhanced functional properties, such as hardness, wear resistance, thermal stability, corrosion resistance, and superplasticity [5–10]. Meanwhile, methods of severe plastic deformation (SPD) offer additional possibilities for regulating the functional properties of metals and alloys by forming an ultrafine-grained structure. SPD methods are known to be capable of reducing the grain size to less than 300 nm in various metals and alloys [11], while the use of heat treatment (HT) on ultrafine-grained samples can further increase their strength and endurance limit. The high mixing entropy of elements in the alloy is considered a measure of the probability of maintaining their system in this state. This ensures an increased

thermal stability of the phase composition and structural state, along with the mechanical, physical, and chemical properties of the alloy. Thus, HEAs demonstrate the potential for forming and maintaining a multielement solid solution both immediately after crystallization and during subsequent thermomechanical treatment, acquiring unique combinations of characteristics [5–10].

A number of reviews [1–4, 12] present the research results on the structure and properties of HEAs; however, they mainly provide experimental data for coarse-grained and cast samples. One work reported the use of SPD for AlCrFeCoNiCu HEAs, but considered only structural-phase transformations during deformation processing.

The emerging interest in the application of SPD methods has not bypassed HEA materials, promising to enhance their functional properties. However, many HEAs contain Co in significant concentrations, which is undesirable for their use in nuclear reactors from the perspective of neutron activation and radiation waste management. Therefore, a new single-phase FeMnNiCr alloy with Co replaced by Mn, showing significant radiation resistance, has recently appeared [13]. Among HEAs, the FeNiMnCr system is known to form a stable FCC structure and to exhibit a good balance of strength, ductility, and corrosion resistance. However, further enhancement of its properties is essential for advanced engineering applications. Equal channel angular pressing (ECAP), a severe plastic deformation technique, offers a promising approach to improving the mechanical and corrosion characteristics of alloys without altering their chemical composition.

In this study, we aim to evaluate the influence of ECAP processing on the structural, mechanical, and corrosion properties of the FeNiMnCr alloy.

EXPERIMENTAL

The investigated HEA had a nominal composition of $Fe_{30}Ni_{30}Mn_{30}Cr_{10}$, which was selected due to its single-phase FCC structure as well as promising mechanical and corrosion properties. The alloy was synthesized by arc melting of high-purity elemental metals (purity ≥ 99.9%, University of Missouri, USA) in an argon atmosphere using a nonconsumable tungsten electrode (USA). To ensure chemical homogeneity, the ingot was remelted at least five times and flipped between each melting cycle. The final as-cast ingots were subjected to homogenization at 1100°C for 12 h in an evacuated quartz tube, followed by water quenching.

The billets (cylinders 20 mm in diameter and 100 mm in length) were processed via ECAP using a die with an internal channel angle of 120°, following the Bc route. Processing was conducted at 450°C for up to three passes to refine the microstructure and enhance strength. The deformation speed was approximately 1 mm/s.

The chemical composition of the alloy was confirmed by energy-dispersive X-ray spectroscopy (EDS). The phase composition was analyzed using X-ray diffraction (XRD) using a Bruker D2 Phaser diffractometer (*Bruker AXS GmbH*, Germany) with CuK_α radiation (0.154 nm) over a 2θ range of 20°–100°, both prior to and following ECAP. The analysis of XRD patterns was carried out using the Rietveld method implemented in the MAUD software package (University of Trento, Italy). The microstructure was studied using a TESCAN MIRA scanning electron microscope (SEM) (*TESCAN ORSAY HOLDING*, Czech Republic) and a JEM-2100 transmission electron microscope (*JEOL*, Japan) with an accelerating voltage of 200 kV, equipped with an attachment for EDS analysis, with special attention to grain size and phase distribution.

Mechanical properties were evaluated via microhardness testing by a Micromet 5101 device (*Buehler*, USA) (100 g load, 10 s dwell time) and tensile tests at room temperature (the range of 20–25°C (293–298 K)) with a strain rate of 10^{-3} (testing machine Instron 8801 — *Instron*, USA / United Kingdom). Corrosion resistance was assessed using potentiodynamic polarization in 3.5 wt % NaCl solution at 37°C using an R-5X electrochemical station (*Elins*, Russia). Electrode potential measurements were conducted for 2 h to achieve a steady-state value. Potentiodynamic polarization (PDP) was performed across the range from −600 to +400 mV relative to the open circuit potential at a scanning rate of 0.25 mV/s. A silver/silver chloride electrode filled with a 3.5 M KCl solution was used as a reference. The counter electrode was a graphite rod. PDP results were calculated using the Tafel method. Polarization resistance R_p was calculated from the slope of the polarization curve ±10 mV relative to the free corrosion potential.

RESULTS AND DISCUSSION

Figure 1a shows the alloy structure in the initial state, which is characterized by large grains with an average size of 290 μm. According to EDS analysis, the chemical composition of the alloy contains Fe = 30.93 wt %, Ni = 31.18 wt %, Mn = 29.57 wt %, and Cr = 8.32 wt %. In addition, segregations of Ni and Mn atoms near the grain boundaries are observed (Fig. 1). At the same time, there are also particles of NiMn precipitates in the grains, mainly of a globular shape with an average size of ~23 μm (Fig. 1b). EDS analysis showed that the content of Cr atoms in both triple junctions and particles was significantly lower, while the content of Mn and Ni was significantly higher, in comparison with the equilibrium content of these elements in the studied alloy Fe 30 wt %–Ni 30 wt %–Mn 30 wt %–Cr 10 wt % (points 1 and 2, Figs. 1b).

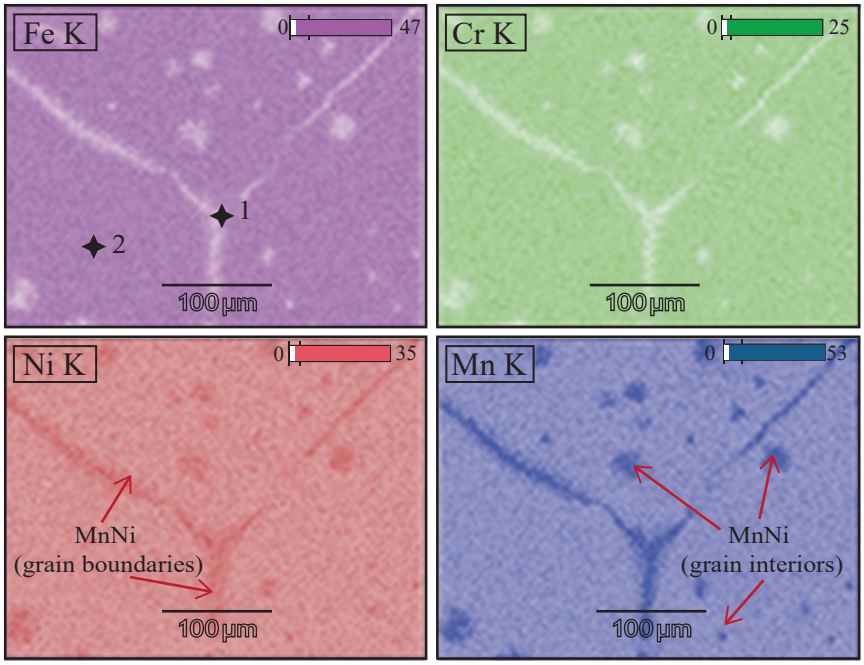

(a)

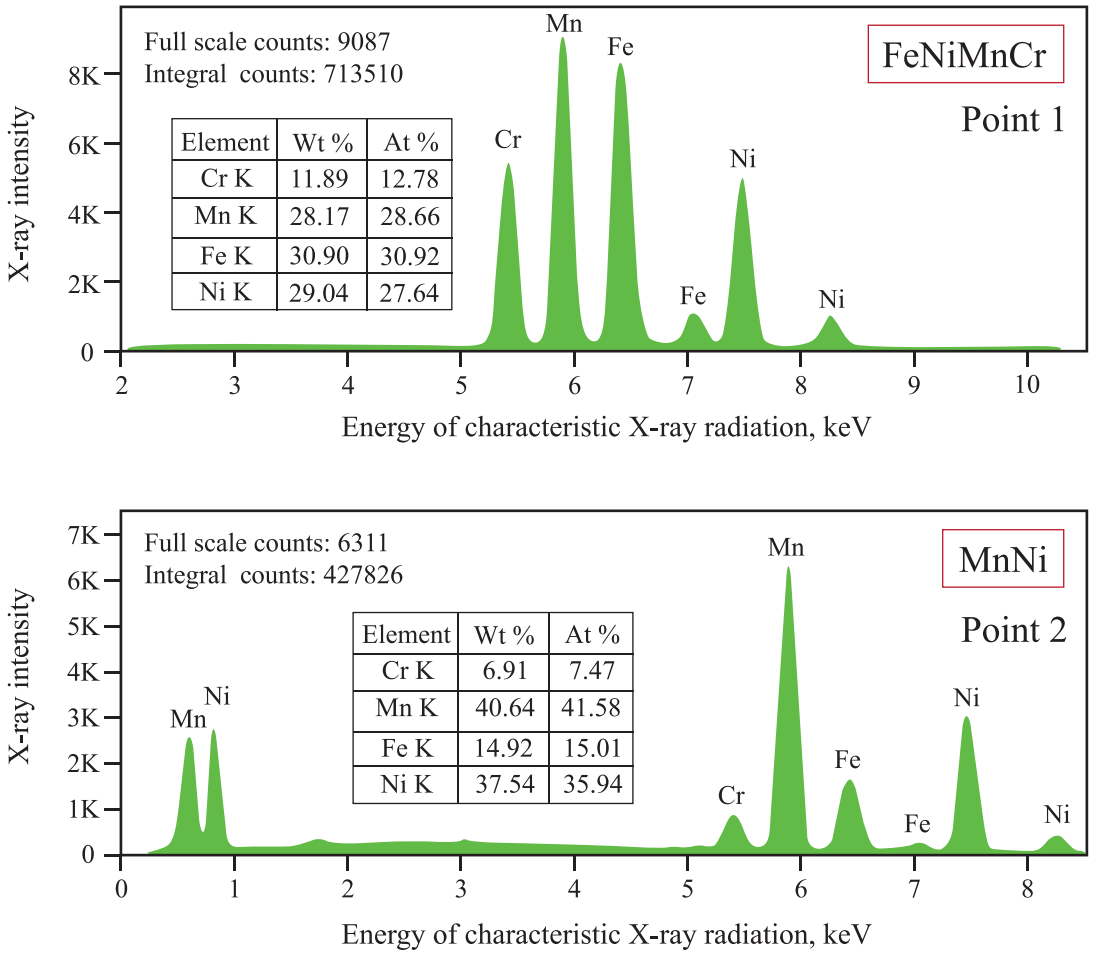

(b)

Fig. 1. EDS image of the initial alloy microstructure: (a) elemental distribution in the initial state; (b) elemental analysis at the triple junction (point 1) and in the MnNi particle (point 2)

Thermal stability studies showed the ECAP sample to exhibit the highest microhardness of 3500 MPa (Fig. 2), which was 80% higher than that of the sample in its initial state. The high thermal stability up to a temperature of 600°C is apparently due to conducting the ECAP deformation processing of the alloy at an elevated temperature of 450°C followed by annealing at 550°C (ECAP450°C+HT550°C).

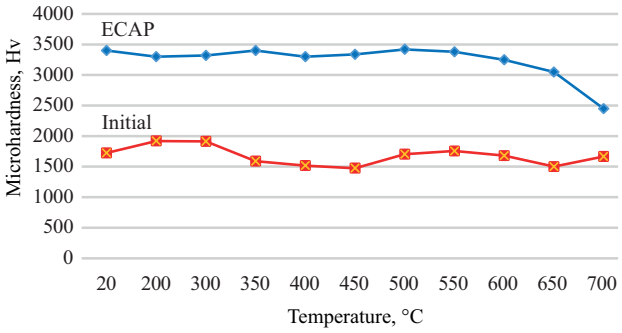

Fig. 2. Microhardness dependence on annealing temperature

In the sample subjected to ECAP+HT550°C processing, the transmission electron microscopy images revealed the presence of separate regions with elongated grains with a width of 0.3–0.5 μm and a length of 0.5–1.5 μm, within which an increased dislocation density was observed (Fig. 3).

X-ray diffraction (XRD) patterns of the FeNiMnCr alloy in the as-cast and ECAP-processed states are shown in Fig. 4. Their analysis showed that, both in the initial state and after the ECAP450°C+HT550°C treatment, the sample contains the FCC phase FeNiMnCr and the secondary phase MnNi (Fig. 4). The reflections of these phases are highlighted in Fig. 4 by blue rhombs and red squares at the bottom of the XRD patterns. After ECAP processing, the FCC phase remained dominant; however, the peaks became broader and slightly shifted. Peak broadening is associated with a significant grain refinement and the accumulation of internal lattice strain due to severe plastic deformation. No new phases or intermetallic compounds were

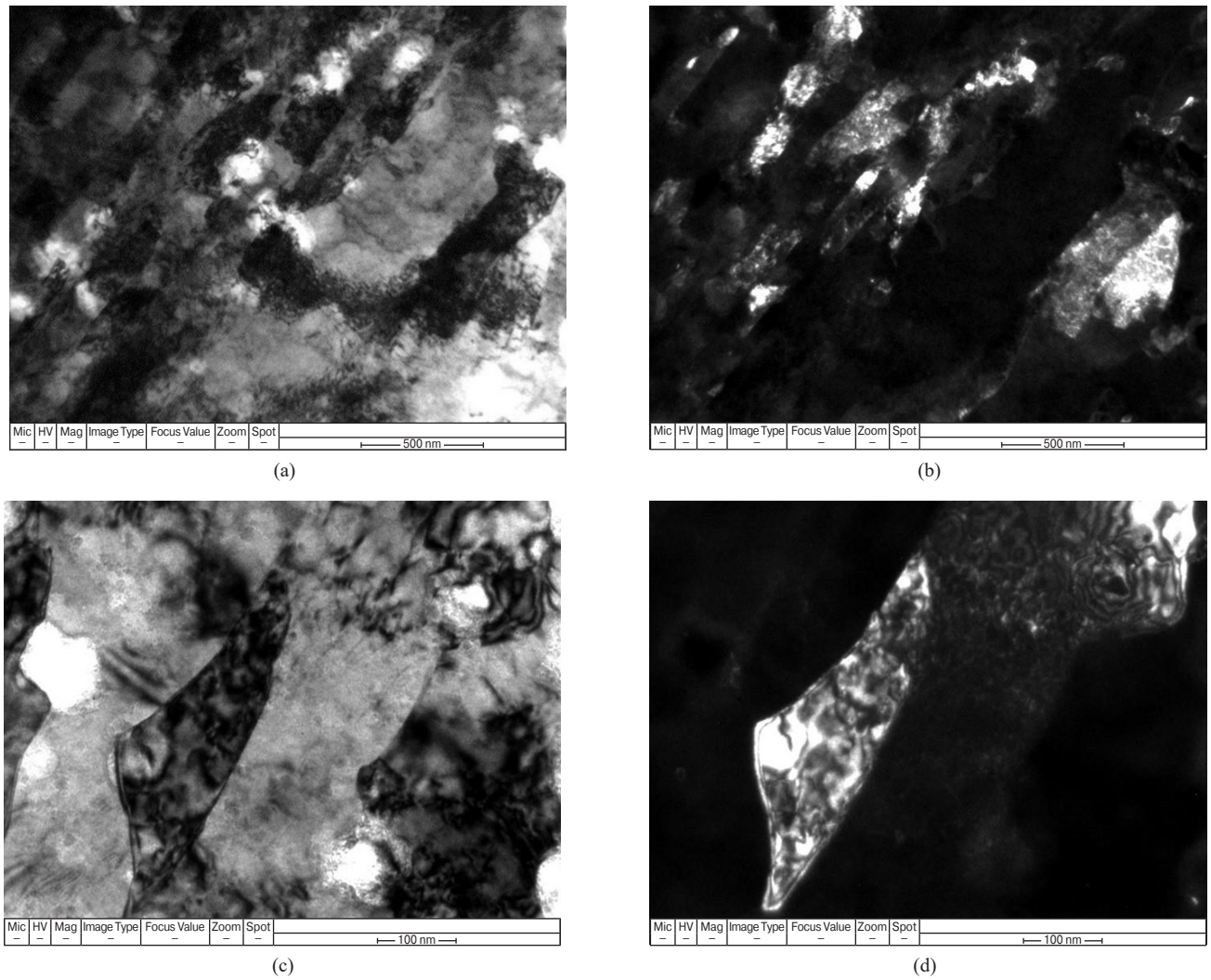

Fig. 3. Various regions in the alloy structure after ECAP+HT550°C, observed by a transmission electron microscope: (a, c) bright-field image; (b, d) dark-field image

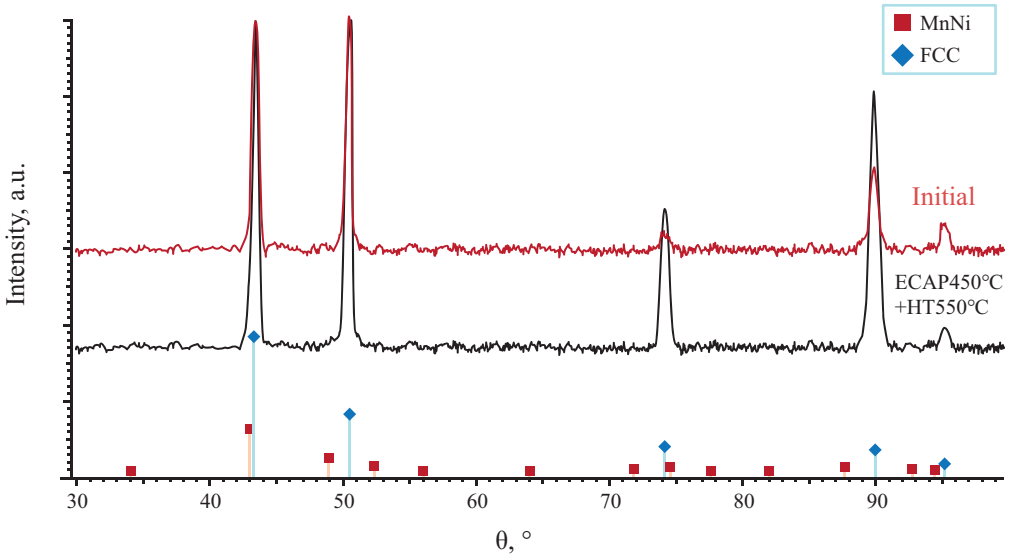

Fig. 4. X-ray diffraction patterns

detected, confirming the structural stability of the alloy under ECAP conditions.

The lattice parameter of the as-cast alloy (3.6158 Å) was calculated using the Bragg equation and was found to increase slightly after ECAP (3.6211 Å), which may be attributed to the redistribution of interatomic distances along numerous grain boundaries due to local strains.

The experimental data from tensile tests were used to construct graphs showing the dependence of strain on stress, as presented in Fig. 5. Prior to testing, the initial and ECAP samples were additionally annealed at temperatures of 450°C and 550°C, respectively, to relieve internal stresses. The tensile tests of the ECAP+550°C sample established the ultimate tensile strength to be 1013 MPa, which increased by more than 2.5-fold compared to that in the initial sample (377 MPa) annealed at 450°C. Meanwhile, the elongation of the initial sample was 63%, whereas it was much lower for the ECAP sample, at the level of 3.6%.

Figure 6 shows the results of electrochemical tests in the form of polarization curves.

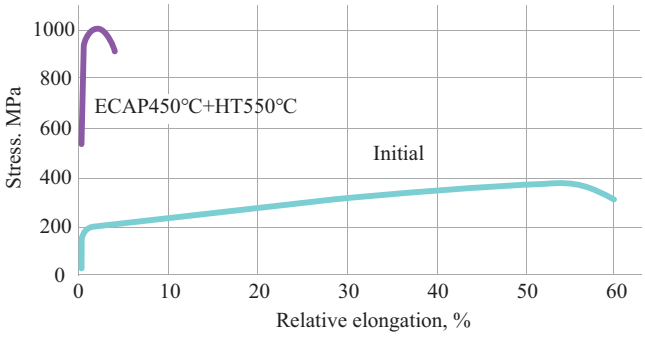

Fig. 5. Results of tensile tests

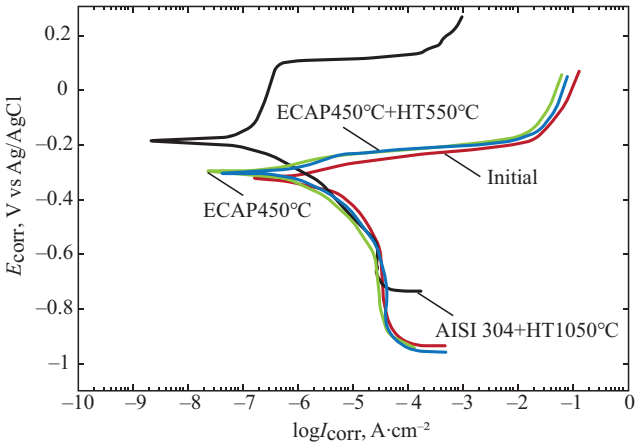

Fig. 6. Polarization curves obtained from electrochemical tests. E_{corr} is an open-circuit potential; I_{corr} is the lowest corrosion current

The table presents the corrosion parameters of the samples calculated based on electrochemical tests and corresponding polarization curves.

Table. Corrosion parameters

Sample	E_{corr}, V	I_{corr}, A/cm^2	R_p, Ohm·cm^2
Initial+450°C	−0.361 ± ± 0.12	$1.91 \cdot 10^{-6} \pm \pm 1.12 \cdot 10^{-7}$	$2.15 \cdot 10^{4} \pm \pm 0.23 \cdot 10^{4}$
ECAP450°C	−0.300 ± ± 0.01	$1.21 \cdot 10^{-6} \pm \pm 1.28 \cdot 10^{-7}$	$3.44 \cdot 10^{4} \pm \pm 0.41 \cdot 10^{4}$
ECAP450°C+HP550°C	−0.306 ± ± 0.01	$1.28 \cdot 10^{-6} \pm \pm 1.25 \cdot 10^{-7}$	$2.13 \cdot 10^{4} \pm \pm 0.11 \cdot 10^{4}$
AISI 304L	−0.190 ± ± 0.01	$0.15 \cdot 10^{-6} \pm \pm 1.24 \cdot 10^{-7}$	$23.3 \cdot 10^{4} \pm \pm 0.11 \cdot 10^{4}$

It can be seen from the table that processing conditions have a significant effect on the open-circuit potential (E_{corr}). A higher E_{corr} value indicates surface passivation, while a lower value indicates surface activation. Among the HEA samples, the ECAP sample showed the highest corrosion resistance (the lowest corrosion current I_{corr}). After additional annealing at 550°C (Table), the corrosion current slightly increased, although remaining lower than that in the initial state. The decrease in corrosion current and the increase in polarization resistance (R_p) after ECAP processing compared to the initial sample indicate better surface passivation in the ECAP samples during testing. Additional HT of the ECAP samples at 550°C led to the preservation of the corrosion current and open-circuit potential at the corrosion resistance level of the ECAP sample, and the maintenance of polarization resistance at the level of the initial samples. It can be assumed that the passive film formed on the surface of the ECAP HEA samples exhibits a greater adhesion to the crystal lattice defects in the form of grain boundaries with respect to the initial state. For comparison, Table also shows the corrosion parameters of AISI 304L stainless steel tested under identical conditions. This steel demonstrated a significantly lower corrosion current and a higher polarization resistance compared to the HEA samples, indicating a more passivated surface than the other samples. AISI 304L stainless steel was tested also under 3.5 wt % NaCl solution with potentiodynamic polarization in [14]. Overall, it should be noted that in the studied HEA, grain refinement by ECAP increases the ultimate tensile strength by more than 2.5 times, while maintaining corrosion resistance at the level of the initial samples.

In order to further understand the enhancing effect of ECAP on the mechanical and corrosion properties of the FeNiMnCr HEA, an additional analysis was conducted.

The increase in ultimate tensile strength and microhardness observed in ECAP+550°C samples is primarily attributed to the significant grain refinement resulting from severe plastic deformation. Transmission electron microscopy confirmed the presence of ultrafine elongated grains and high dislocation density, both of which contribute to strengthening via grain boundary strengthening and dislocation interaction mechanisms. The increased dislocation density enhances strain hardening and impedes dislocation motion, thus leading to elevated strength.

The corrosion behavior is also positively influenced by the ECAP process. The refinement of grain structure results in a higher density of grain boundaries, which are known to serve as preferential sites for passive film nucleation. This likely improves the adhesion and stability of the protective oxide layer, thereby reducing the corrosion current density and increasing polarization resistance. This is consistent with the results reported in recent studies [15, 16], which also observed improvements in corrosion resistance due to fine microstructural features.

Our findings align with [17], which emphasized the importance of phase composition and deformation-induced effects in enhancing the mechanical performance of HEAs. However, our study uniquely demonstrates these improvements in a cobalt-free FeNiMnCr system, which is particularly relevant for radiation-sensitive environments.

Improved characteristics of ECAP samples of HEA are of interest for the development of technologies for producing materials with optimal performance characteristics for operation under elevated temperatures and aggressive environments in nuclear power engineering, in the aerospace industry, for the manufacture of parts with high strength and thermal stability, as well as in medicine, due to good corrosion resistance and biocompatibility.

CONCLUSIONS

The $Fe_{30}Ni_{30}Mn_{30}Cr_{10}$ HEA demonstrates remarkable enhancements in both mechanical and corrosion properties when subjected to ECAP. The experimental results revealed that the ultimate tensile strength of the alloy increased from 377 MPa in its initial state to 1013 MPa after ECAP and subsequent HT, while its microhardness improved by 80%, reaching 3500 MPa. Additionally, the corrosion resistance of the alloy remained robust, with the ECAP samples exhibiting a lower corrosion current and higher polarization resistance compared to their initial state, indicating improved surface passivation.

These improvements are primarily attributed to the formation of an ultrafine-grained structure and increased dislocation density, which enhance strength through grain boundary and dislocation strengthening mechanisms. The refined grain structure also promotes the formation of a more stable and adherent passive film, contributing to improved corrosion resistance.

Furthermore, the cobalt-free composition of the alloy and its demonstrated stability under thermal and corrosive conditions render it a promising candidate for applications in the nuclear industry, chemical processing, and marine environments where high strength and corrosion resistance are critical under extreme conditions.

These results confirm that precise thermomechanical treatments of HEAs, such as FeNiMnCr, can enhance their performance for critical applications in industries

where materials are exposed to extreme conditions. Our findings emphasize the potential of tailored processing techniques in improving HEA properties for advanced engineering applications.

Authors' contribution

A.M.M. Abuayash — investigation of mechanical properties.

K.M. Nesterov — research of corrosion resistance.

R.K. Islamgaliev — structural investigations.

REFERENCES

1. Tsai M.H., Yeh J.W. High-Entropy Alloys: A Critical Review. *Mater. Res. Lett*. 2014;2(3):107–123. https://doi.org/10.1080/21663831.2014.912690
2. Miracle D.B., Senkov O.N. A critical review of high entropy alloys and related concepts. *Acta Mater.* 2017:122:448–511. https://doi.org/10.1016/j.actamat.2016.08.081
3. Shi Y., Yang B., Liaw P. Corrosion-Resistant High-Entropy Alloys: A Review. *Metals* (*Basel*). 2017;7(2):43. https://doi.org/10.3390/met7020043
4. Zhang Y., Zuo T.T., Tang Z., Gao M.C., Dahmen K.A., Liaw P.K., Lu Z.P. Microstructures and properties of high-entropy alloys. *Prog. Mater. Sci.* 2014;61:1–93. https://doi.org/10.1016/j.pmatsci.2013.10.001
5. Chen S.T., Tang W.Y., Kuo Y.F., Chen S.Y., Tsau C.H., Shun T.T., Yeh J.W. Microstructure and properties of age-hardenable $Al_xCrFe_{1.5}MnNi_{0.5}$ alloys. *Mater. Sci. Eng.: A.* 2010;527(21–22):5818–5825. https://doi.org/10.1016/j.msea.2010.05.052
6. Tong C.J., Chen M.R., Chen S.K., Yeh J.W., Shun T.T., Lin S.J., Chang S.Y. Mechanical performance of the $Al_xCoCrCuFeNi$ high-entropy alloy system with multiprincipal elements. *Metall. Mater. Trans. A.* 2005;36(5):1263–1271. https://doi.org/10.1007/s11661-005-0218-9
7. Vyrodova A.V. The influence of chemical composition on solid solution and strain hardening of single crystals of FCC high-entropy alloys. *Frontier Materials & Technologies*. 2022;1:15–23 (in Russ.). https://doi.org/10.18323/2782-4039-2022-1-15-23
8. Kourov N.I., Pushin V.G., Korolev A.V., Knyazev Yu.V., Kuranova N.N., Ivchenko M.V., Ustyugov Yu.M., Wanderka N. Structure and physical properties of the high-entropy AlCrFeCoNiCu alloy rapidly quenched from the melt. *Phys. Solid State.* 2015;57(8):1616–1626. https://doi.org/10.1134/S1063783415080144
9. Klimova M., Stepanov N., Shaysultanov D., Chernichenko R., Yurchenko N., Sanin V., Zherebtsov S. Microstructure and mechanical properties evolution of the Al, C-Containing CoCrFeNiMn-type high-entropy alloy during cold rolling. *Materials*. 2017;11(1):53. https://doi.org/10.3390/ma11010053
10. Gurtova D.Yu., Panchenko M.Yu., Melnikov E.V., Astapov D.O., Astafurova E.G. The influence of grain size on hydrogen embrittlement of a multicomponent (FeCrNiMnCo)99N1 alloy. *Frontier Materials & Technologies*. 2024;3:41–51. https://doi.org/10.18323/2782-4039-2024-3-69-4
11. Valiev R.Z., Zhilyaev A.P., Langdon T.J. Bulk Nanostructured Materials: Fundamentals and Applications. Wiley; 2013. 440 p. http://doi.org/10.1002/9781118742679
12. Kumar N.A.P.K., Li C., Leonard K.J., Bei H., Zinkle S.J. Microstructural stability and mechanical behavior of FeNiMnCr high entropy alloy under ion irradiation. *Acta Materialia*. 2016;113(Part 2):230–244. http://doi.org/10.1016/j.actamat.2016.05.007
13. Hoffman A., He L., Luebbe M., Pommerenke H., Duan J., Cao P., Sridharan K., Lu Z., Wen H. Effects of Al and Ti additions on irradiation behavior of FeMnNiCr multi-principal-element alloy. *JOM.* 2020;72(1):150–159. https://doi.org/10.1007/s11837-019-03871-4
14. Okonkwo B.O., Jeong Ch., Bae Lee H.L., Jang Ch., Rahimi E., Davoodi A. Development and optimization of trivalent chromium electrodeposit on 304L stainless steel to improve corrosion resistance in chloride-containing environment. *Heliyon*. 2023;9(12):e22538. https://doi.org/10.1016/j.heliyon.2023.e22538
15. Sun Z., Zhang M., Wang G., Yang X., Wang S. Wear and corrosion resistance analysis of $FeCoNiTiAl_x$ high-entropy alloy coatings prepared by laser cladding. *Coatings*. 2021;11(2):155. http://doi.org/10.3390/coatings11020155
16. Ding Z., Ding C., Yang Z., Zhang H., Wang F., Li H., Xu J., Shan D., Guo B. Ultra-high strength in FCC+BCC high-entropy alloy via different gradual morphology. *Materials*. 2024;17(18):4535. https://doi.org/10.3390/ma17184535
17. Osintsev K.A., Gromov V.E., Konovalov S.V., Ivanov Yu.F., Panchenko I.A. High-entropy alloys: Structure, mechanical properties, deformation mechanisms and application. *Izvestiya vysshikh uchebnykh zavedenii. Chernaya Metallurgiya = Izvestiya. Ferrous Metallurgy*. 2021;64(4):249–258 (in Russ.). https://doi.org/10.17073/0368-0797-2021-4-249-258

About the Authors

Adham Muhammad Musa Abuayash, Postgraduate Student, Ufa University of Science and Technology (32, Zaki Validi ul., Ufa, Republic of Bashkortostan, 450076, Russia). E-mail: adhamabuayash4@gmail.com. https://orcid.org/0000-0002-0319-0992

Konstantin M. Nesterov, Cand. Sci. (Phys.-Math.), Associate Professor, Materials Science and Metal Physics Department, Ufa University of Science and Technology (32, Zaki Validi ul., Ufa, Republic of Bashkortostan, 450076, Russia). E-mail: kmnesterov@mail.ru. Scopus Author ID 36521465900, RSCI SPIN-code 8244-3380, https://orcid.org/0000-0002-7053-3131

Rinat K. Islamgaliev, Dr. Sci. (Phys.-Math.), Professor, Materials Science and Metal Physics Department, Ufa University of Science and Technology (32, Zaki Validi ul., Ufa, Republic of Bashkortostan, 450076, Russia). E-mail: rinatis@mail.ru. Scopus Author ID 7004334546, RSCI SPIN-code 2609-3284, https://orcid.org/0000-0002-6234-7363

Об авторах

Абуайяш Адхам Мухаммад Муса, аспирант, ФГБОУ ВО «Уфимский университет науки и технологий» (450076, Россия, Приволжский федеральный округ, Республика Башкортостан, г. Уфа, ул. Заки Валиди, д. 32). E-mail: adhamabuayash4@gmail.com. https://orcid.org/0000-0002-0319-0992

Нестеров Константин Михайлович, к.ф.-м.н., доцент кафедры Материаловедения и физики металлов, ФГБОУ ВО «Уфимский университет науки и технологий» (450076, Россия, Приволжский федеральный округ, Республика Башкортостан, г. Уфа, ул. Заки Валиди, д. 32). E-mail: kmnesterov@mail.ru. Scopus Author ID 36521465900, SPIN-код РИНЦ 8244-3380, https://orcid.org/0000-0002-7053-3131

Исламгалиев Ринат Кадыханович, д.ф.-м.н., профессор кафедры Материаловедения и физики металлов, ФГБОУ ВО «Уфимский университет науки и технологий» (450076, Россия, Приволжский федеральный округ, Республика Башкортостан, г. Уфа, ул. Заки Валиди, д. 32). E-mail: rinatis@mail.ru. Scopus Author ID 7004334546, SPIN-код РИНЦ 2609-3284, https://orcid.org/0000-0002-6234-7363

The text was submitted by the authors in English
and edited for English language and spelling by Dr. David Mossop

MIREA – Russian Technological University
78, Vernadskogo pr., Moscow, 119454, Russian Federation.
Publication date *October 31, 2025.*
Not for sale

МИРЭА – Российский технологический университет
119454, РФ, Москва, пр-т Вернадского, д. 78.
Дата опубликования *31.10.2025 г.*
Не для продажи

www.finechem-mirea.ru